

**Effectiveness of Silane in Mitigating Alkali-Silica Reaction in the
Bibb Graves Bridge**

by

Darren Keith Johnson

A thesis submitted to the Graduate Faculty of
Auburn University
In partial fulfillment of the
Requirements for the Degree of
Master of Science

Auburn, Alabama
December 14, 2013

Keywords: Alkali-silica reaction, concrete, relative humidity,
strain, mitigation, silane

Copyright 2013 by Darren Keith Johnson

Approved by

Anton K. Schindler, Chair, Professor of Civil Engineering
Robert W. Barnes, James J. Mallett Associate Professor of Civil Engineering
James S. Davidson, Professor of Civil Engineering

Abstract

The Bibb Graves Bridge is in Wetumpka, Alabama, and it has severe damage caused by alkali-silica reaction (ASR) in two of its fourteen reinforced concrete arches. A silane-based, ASR mitigation procedure was developed and applied to the ASR-affected portions of the bridge by the Alabama Department of Transportation, the Federal Highway Administration, and Auburn University in 2010. The goal of this mitigation procedure was to lower the internal relative humidity of the ASR-affected concrete to below 80 percent so that continued ASR-related expansions cannot occur. After the application of the mitigation procedure, monitoring of the internal relative humidity, concrete expansion, and new crack development in the bridge was done for 34 months to evaluate the effectiveness of the mitigation procedure.

The two ASR-affected arches and one non-affected arch received the mitigation procedure, and all three of these arches along with another non-affected arch were monitored. Analysis of the 34 months of data revealed that there were few signs of decreasing relative humidity or slowed expansion rates in the ASR-affected concrete. Thus the silane sealer was ineffective, and alternative mitigation options should be considered. Other options could include covering or confining the concrete.

Acknowledgments

I would like to thank Dr. Schindler for providing me with this great opportunity, and for guiding me throughout the process of gaining my master's degree at Auburn University. I would like to thank my family for always encouraging me to follow my dreams, and I am thankful for my girlfriend, Liz Hammer, who was always there for me and kept me from procrastinating throughout this process.

Thanks to Les Warnock for beginning this research project and passing on countless amounts of data and guidance. I would also like to thank my committee members, Dr. Barnes and Dr. Davidson, for teaching me and reviewing and editing this thesis. A big thanks also goes out to all of the research assistants who helped collect data from the Bibb Graves Bridge: Zach Skinner, Tyler Neal, Patrick Koch, Chris Harrigan, Eric Miller, and Liz Hammer.

Lastly, I would like to thank the members of the Federal Highway Administration and the Alabama Department of Transportation that saw the need and provided funding for this unique project.

Table of Contents

Abstract	ii
Acknowledgments	iii
List of Tables	ix
List of Figures	xii
Chapter 1 Introduction	1
1.1 Background	1
1.2 Statement of Objectives	5
1.3 Research Methodology	5
1.4 Thesis Organization	7
Chapter 2 Literature Review	10
2.1 Introduction	10
2.2 ASR Overview	10
2.2.1 Occurrence of ASR	14
2.2.2 Mechanisms of the Reaction	14
2.3 Damage Caused by ASR	15
2.3.1 Microcracking	16
2.3.2 Surface Cracking	18
2.3.3 Surface Discoloration	20
2.3.4 Surface Deposits	20
2.3.5 Popouts	21
2.4 Effects of Exposure Conditions on ASR Damage	22

2.4.1	Wetting and Drying	22
2.4.2	Freezing and Thawing	23
2.5	Identification of ASR in Structures	23
2.5.1	Site Inspection	24
2.5.2	Core Sampling	28
2.5.3	Petrographic Analysis of ASR	29
2.6	Mitigation of ASR in Existing Structures	37
2.6.1	In-Situ Monitoring of ASR-Affected, Concrete Structures	38
2.6.2	Silane	39
2.6.3	Lithium	51
2.6.4	Crack Injection	56
2.6.5	Cladding	56
2.6.6	Confinement of Expansion	58
2.6.7	Slot-Cutting	65
2.6.8	Mitigation Summary	66
2.7	Predicted Time to Reach 80 Percent Relative Humidity in the Bibb Graves Bridge	68
2.8	Summary	72
Chapter 3	Bibb Graves Bridge	75
3.1	Background	75
3.2	Bridge Details and Construction	77
3.3	ASR in the Bibb Gravis Bridge	82
3.3.1	Petrography of Concrete	85
3.3.2	Examples of Distress from ASR	92
3.4	Summary	99
Chapter 4	ASR Mitigation Procedure	100

4.1	Introduction	100
4.2	Selection of Mitigation Procedure.....	100
4.2.1	Protocol Option A.....	101
4.2.2	Protocol Option B.....	101
4.2.3	Protocol Option C.....	102
4.2.4	Protocol Option D.....	103
4.3	Final ASR Mitigation Procedure	103
4.4	Installation of the ASR Mitigation Method.....	107
4.5	Summary.....	110
Chapter 5	Experimental Monitoring	111
5.1	Introduction	111
5.2	Crack Mapping	111
5.3	Relative Humidity Measurements.....	113
5.4	Strain Measurements	118
5.5	Summary.....	123
Chapter 6	Experimental Results and Discussion.....	124
6.1	Introduction	124
6.2	Crack Mapping	125
6.2.1	Pre-Mitigation State of Cracking	126
6.2.2	Post-Mitigation Crack Survey.....	133
6.2.3	Examples of Post-mitigation Cracking	140
6.2.4	Cracking Summary	148
6.3	Internal Relative Humidity	148
6.3.1	Relative Humidity Measurement Identification	150
6.3.2	Average Relative Humidity Data	151

6.3.3	3-inch Depth Analysis	165
6.3.4	Relative Humidity Data Analysis Summary	179
6.4	Concrete Strain Measurements.....	179
6.4.1	Strain Measurement Identification.....	180
6.4.2	Strain Adjustment for Temperature	181
6.4.3	Concrete Strain Data	182
6.4.4	Strain Data Analysis Summary	203
Chapter 7	Future Mitigation Considerations	205
7.1	Introduction	205
7.2	Covering Arches for Protection from Rain	206
7.2.1	Waterproof Fabric Cover.....	207
7.2.2	Ventilated Cladding.....	210
7.3	Cross-Sectional Confinement.....	216
7.3.1	CFRP Wrap	217
7.3.2	Post-Tensioned Confinement	218
7.4	Possible ASR in Locations other than Span 5.....	219
7.5	Summary.....	223
Chapter 8	Summary, Conclusions, and Recommendations	224
8.1	Project Summary.....	224
8.1.1	ASR Overview.....	224
8.1.2	Bibb Graves Bridge Overview	225
8.1.3	ASR Mitigation Procedure.....	225
8.1.4	Monitoring the Effectiveness of the Mitigation Procedure	226
8.2	Conclusions.....	227
8.3	Recommendations	227

References	230
Appendix A Coring Procedure and Samples	A-1
Appendix B Petrographic Analysis Report by The Transtec Group	B-1
Appendix C Petrographic Analysis Report by WJE	C-1
Appendix D Relative Humidity Survey Data	D-1
Appendix E Concrete Expansion Survey Data	E-1

List of Tables

Table 2.1. Mineral phases and corresponding rocks susceptible to ASR	12
Table 2.2. Potential AAR risk of features examined during site investigation	27
Table 2.3. Potential AAR risk of features from laboratory findings.....	36
Table 2.4. Features and weighting factors for damage rating index	37
Table 2.5. Average modulus of elasticity and compressive strength for directional cores taken out of blocks stressed in Y direction	62
Table 2.6. Summary of mitigation options for transportation structures	67
Table 3.1. Summary of petrographic observations on the cores.....	88
Table 5.1. Summary of strain measurement locations of spans 4 and 5	122
Table 6.1. RH survey dates and corresponding time since mitigation application	149
Table 6.2. 34-month average for 3-inch RH data and average RH data.....	172
Table 6.3. Concrete strain measurement survey dates	180
Table 6.4. Summary of prominent strain trends after mitigation	195
Table 6.5. Summary of prominent strain difference trends	202
Table A. 1. Information for 1A – South	A-8
Table A. 2. Information for Core 2A – South.....	A-9
Table A. 3. Information for Core 1B – South.....	A-10
Table A. 4. Information for Core 2B – South.....	A-11
Table A. 5. Information for 1A – North	A-12
Table A. 6. Information for 2A – North	A-13
Table A. 7. Information for Core 1B – North	A-14

Table A. 8. Information for Core 2B – North	A-15
Table A. 1. Information for 1A – South	8
Table A. 2. Information for Core 2A – South.....	9
Table A. 3. Information for Core 1B – South.....	10
Table A. 4. Information for Core 2B – South.....	11
Table A. 5. Information for 1A – North	12
Table A. 6. Information for 2A – North	13
Table A. 7. Information for Core 1B – North	14
Table A. 8. Information for Core 2B – North	15
Table D. 1. 4-S-WB monthly RH survey data	D-2
Table D. 2. 4-S-WT monthly RH survey data.....	D-3
Table D. 3. 4-S-EB monthly RH survey data	D-4
Table D. 4. 4-S-ET monthly RH survey data.....	D-5
Table D. 5. 4-N-WB monthly RH survey data	D-6
Table D. 6. 4-N-WT monthly RH survey data	D-7
Table D. 7. 4-N-EB monthly RH survey data	D-8
Table D. 8. 4-N-ET monthly RH survey data	D-9
Table D. 9. 5-S-WB monthly RH survey data	D-10
Table D. 10. 5-S-WT monthly RH survey data.....	D-11
Table D. 11. 5-S-EB monthly RH survey data	D-12
Table D. 12. 5-S-ET monthly RH survey data.....	D-13
Table D. 13. 5-N-WB monthly RH survey data	D-14
Table D. 14. 5-N-WT monthly RH survey data	D-15
Table D. 15. 5-N-EB monthly RH survey data	D-16
Table D. 16. 5-N-ET monthly RH survey data	D-17

Table D. 17. Average RH data for all readings	D-18
Table D. 18. 3-inch RH data for all readings.....	D-19
Table E. 1. Span 4 South gauge readings	E-2
Table E. 2. Span 4 North gauge readings	E-3
Table E. 3. Span 5 South gauge readings.....	E-4
Table E. 4. Span 5 North gauge readings	E-5
Table E. 5. Span 4 South change in strain	E-6
Table E. 6. Span 4 North change in strain.....	E-7
Table E. 7. Span 5 South change in strain	E-8
Table E. 8. Span 5 North change in strain.....	E-9
Table E. 9. Strain gauge readings for DEMEC studs installed in 2005.....	E-10
Table E. 10. Change in strain for locations dating back to 2005.....	E-10

List of Figures

Figure 1.1. The Bibb Graves Bridge in Wetumpka, Alabama	1
Figure 1.2. Surface deposits and ASR-induced cracking on 3/11/08.....	2
Figure 1.3. Measuring RH in Bibb Graves Bridge.....	4
Figure 1.4. Taking a strain reading on the Bibb Graves Bridge	4
Figure 2.1. RH threshold for expansion of ASR-affected mortar bars.....	13
Figure 2.2. Microcracking in aggregate due to ASR with (A) 0.066% and (B) 0.283% concrete expansion	17
Figure 2.3. Severe map-cracking and surface discoloration on a road barrier ...	19
Figure 2.4. Longitudinal cracking due to ASR in (A) a bridge deck soffit and (B) a precast, reinforced concrete beam	20
Figure 2.5. Efflorescence and exudations of alkali-silica gel on a foundation	21
Figure 2.6. Concrete popout caused by ASR	22
Figure 2.7. Dark rim around the perimeter of reactive aggregate particles	30
Figure 2.8. Topical application of 40% silane solution to ASR-affected barriers	40
Figure 2.9. Silanes basic structure and key chemistries.....	41
Figure 2.10. Silane's hydrophobic properties repelling water	42
Figure 2.11. (A) Expansion and (B) cumulative mass variation for air- entrained concrete cylinders subjected to exposure C5.....	46
Figure 2.12. (A) Unsealed and (B) silane-sealed air-entrained concrete cylinders subjected to exposure cycle C4, after 1.5 years	47
Figure 2.13. Comparison of unsealed versus silane-sealed, for 3 years, on highway median barriers in (A) Montmorency and (B) Sainte- Foy	49

Figure 2.14. Internal relative humidity from 3 to 6 years after silane-sealing highway median barriers in (A) Montmorency and (B) Sainte-Foy	50
Figure 2.15. Topical application of 30% lithium solution to concrete pavement..	52
Figure 2.16. Depth of lithium penetration with topical application on I-84.....	53
Figure 2.17. Depth of lithium penetration with vacuum impregnation on barrier.....	54
Figure 2.18. Depth of lithium penetration on columns with vacuum impregnation and electrochemical impregnation	55
Figure 2.19. Montrose New Bridge repair with confinement and cladding	58
Figure 2.20. Setup for concrete blocks being stressed in one direction.....	61
Figure 2.21. Longitudinal expansion of cores taken from bridge pier and submerged in tap water, (A) core free to expand and (B) uniaxial stress applied to cores	65
Figure 2.22. Arch cross section modeled in ANSYS.....	69
Figure 2.23. Multilinear approximation of the moisture diffusion coefficient.....	70
Figure 2.24. RH versus time for (A) silane only and (B) silane and epoxy.....	71
Figure 3.1. Alabama map with circle at Wetumpka.....	75
Figure 3.2. Covered bridge built in 1844.....	76
Figure 3.3. Iron bridge built in 1887	77
Figure 3.4. Northeast elevation view of the Bibb Graves Bridge	78
Figure 3.5. Concrete strengths used along arch.....	79
Figure 3.6. Elevation and plan view of Bibb Graves Bridge.....	80
Figure 3.7. Construction photos of the Bibb Graves Bridge.....	81
Figure 3.8. Construction of the Bibb Graves Bridge	81
Figure 3.9. ASR-induced cracking in the late 1990s on the (A) bottom and (B) top of a span 5 arch.....	83
Figure 3.10. (A) ASR-affected arch in March 2008 and (B) different non-distressed arch in August 2013	84

Figure 3.11. Core extraction layout.....	86
Figure 3.12. Example of reaction rim (RR) and severe cracking in core 2A-North	88
Figure 3.13. Example of severe cracking in polished section of core 2A-South .	89
Figure 3.14. Typical dark rim on chert coarse aggregate particle	91
Figure 3.15. Cracks with alkali-silica gel in peripheral region of chert and cracked cement paste containing white ettringite deposits	91
Figure 3.16. Severe distress due to ASR on span 5, south arch	93
Figure 3.17. Distress with surface deposits of efflorescence and alkali-silica gel on the eastern side of span 5 south	94
Figure 3.18. Closer view of longitudinal cracking and spalling on span 5 south on 3/11/08	95
Figure 3.19. Additional spalling on span 5 south from 3/11/08 to 12/14/09	96
Figure 3.20. Crack width close to 1/2 inch.....	96
Figure 3.21. Cracking and surface discoloration on the bottom of an arch.....	97
Figure 3.22. Cracking and surface deposits extending from arch to hanger.....	98
Figure 3.23. Map-cracking on an abutment of span 5	98
Figure 4.1. Span 4 and 5 of the Bibb Graves Bridge	104
Figure 4.2. Schematic of applied ASR mitigation procedure	106
Figure 4.3. Timeline of installation of ASR mitigation procedure in 2010.....	107
Figure 4.4. Arches that received the mitigation procedure	107
Figure 4.5. Span 5 after water-blasting.....	108
Figure 4.6. (A) Water-based silane sealant and (B) application of silane	109
Figure 4.7. (A) Applying flexible sealant and (B) smoothing sealant by hand...	109
Figure 5.1. Grid for crack survey	112
Figure 5.2. Grid spacing along arch.....	112
Figure 5.3. Using crack width gauge	113

Figure 5.4. Plastic tube with rubber plug installed in concrete	114
Figure 5.5. (A) Removing long rubber plug and (B) inserting probe into tube...	115
Figure 5.6. (A) Putting rubber plug around cable and (B) sliding it into tube	115
Figure 5.7. Placing protective cup and lid over tube	116
Figure 5.8. Measuring temperature and RH with indicator	116
Figure 5.9. Location and depth of RH measurements	117
Figure 5.10. DEMEC stud installed in the Bibb Graves Bridge	118
Figure 5.11. DEMEC strain gauge (A) field use and (B) dial reading 783.....	119
Figure 5.12. DEMEC stud locations on a typical arch.....	121
Figure 6.1. Crack mapping, November 2010, Span 4 – South Arch – Plan View	127
Figure 6.2. Crack mapping, November 2010, Span 4 – South Arch – Bottom View	128
Figure 6.3. Crack mapping, November 2010, Span 5 – North Arch – Plan View	129
Figure 6.4. Crack mapping, November 2010, Span 5 – North Arch – Bottom View	130
Figure 6.5. Crack mapping, November 2010, Span 5 – South Arch – Plan View	131
Figure 6.6. Crack mapping, November 2010, Span 5 – South Arch – Bottom View	132
Figure 6.7. Crack mapping, August 2013, Span 4 – South Arch – Plan View ..	134
Figure 6.8. Crack mapping, August 2013, Span 4 – South Arch – Bottom View	135
Figure 6.9. Crack mapping, August 2013, Span 5 – North Arch – Plan View ...	136
Figure 6.10. Crack mapping, August 2013, Span 5 – North Arch – Bottom View	137
Figure 6.11. Crack mapping, August 2013, Span 5 – South Arch – Plan View	138

Figure 6.12. Crack mapping, August 2013, Span 5 – South Arch – Bottom View	139
Figure 6.13. Widening and elongation of existing cracks in span 4 – south arch, (A) November 2010 and (B) August 2013	141
Figure 6.14. Additional cracking in span 5 – north arch, (A) November 2010 and (B) August 2013	142
Figure 6.15. Crack widening on span 5 – south arch, (A) November 2010 and (B) August 2013	143
Figure 6.16. Crack widening on span 5 – south arch, (A) November 2010 and (B) August 2013	144
Figure 6.17. New crack on span 5 – south arch, (A) November 2010 and (B) August 2013	145
Figure 6.18. Crack widening on span 5 – south arch, (A) November 2010 and (B) August 2013	146
Figure 6.19. Crack extending on span 5 – south arch, (A) November 2010 and (B) August 2013	147
Figure 6.20. Maxwell Air Force Base	150
Figure 6.21. RH measurements, West Bottom, average of all measurement depths	152
Figure 6.22. RH measurements, West Top, average of all measurement depths	153
Figure 6.23. RH measurements, East Bottom, average of all measurement depths	154
Figure 6.24. RH measurements, East Top, average of all measurement depths	155
Figure 6.25. RH difference for West Bottom average	160
Figure 6.26. RH difference for West Top average	161
Figure 6.27. RH difference for East Bottom average	162
Figure 6.28. RH difference for East Top average	163
Figure 6.29. RH measurements, West Bottom, 3-inch depth	166
Figure 6.30. RH measurements, West Top, 3-inch depth.....	167

Figure 6.31. RH measurements, East Bottom, 3-inch depth	168
Figure 6.32. RH measurements, East Top, 3-inch depth.....	169
Figure 6.33. Drying time predictions for silane and epoxy treated arch section	171
Figure 6.34. RH difference for West Bottom 3-inch depth	175
Figure 6.35. RH difference for West Top 3-inch depth	176
Figure 6.36. RH difference for East Bottom 3-inch depth	177
Figure 6.37. RH difference for East Top 3-inch depth	178
Figure 6.38. Change in concrete strain for Side Perpendicular since 2005	184
Figure 6.39. Change in concrete strain for Side Perpendicular since 2010	185
Figure 6.40. Change in concrete strain for Bottom Low since 2005	186
Figure 6.41. Change in concrete strain for Bottom Low since 2010	187
Figure 6.42. Change in concrete strain for Top Low since 2005	188
Figure 6.43. Change in concrete strain for Top Low since 2010	189
Figure 6.44. Change in concrete strain for Abutment since 2010	190
Figure 6.45. Change in concrete strain for Side Horizontal since 2010	191
Figure 6.46. Change in concrete strain for Bottom High since 2010.....	192
Figure 6.47. Change in concrete strain for Top High since 2010.....	193
Figure 6.48. Strain difference for Bottom Low at (A) west and (B) east.....	197
Figure 6.49. Strain difference for east, Top Low locations.....	198
Figure 6.50. Strain difference for west, Abutment locations	198
Figure 6.51. Strain difference for Side Horizontal at (A) west and (B) east	199
Figure 6.52. Strain difference for Bottom High at (A) west and (B) east	200
Figure 6.53. Strain difference for Top High at (A) west and (B) east	201
Figure 7.1. Fabric covered arch; top and side view	208
Figure 7.2. Cross section view of fabric covering	209

Figure 7.3. Bottom view of fabric secured around arch	210
Figure 7.4. Ventilated cladding layout on arch.....	211
Figure 7.5. First layer of side cladding.....	212
Figure 7.6. Outer side panels of cladding	213
Figure 7.7. Close-up view at the top of side panels	214
Figure 7.8. Close-up view at the bottom of side panels	214
Figure 7.9. Layered top panels	215
Figure 7.10. Examples of possible ASR in span 3.....	221
Figure 7.11. Examples of possible ASR in span 4.....	222
Figure A. 1. Use of ground penetrating radar to locate reinforcement	A-1
Figure A. 2. Close up of drilling set up.....	A-2
Figure A. 3. Drilling core sample.....	A-2
Figure A. 4. Close up of drilling process	A-3
Figure A. 5. Core holes left after drilling	A-3
Figure A. 6. Extraction of core samples.....	A-4
Figure A. 7. Labeling of core samples	A-4
Figure A. 8. Wrapping of core samples	A-5
Figure A. 9. Packing of core sample for (A) W.J.E. in Illinois and (B) Laval University in Canada	A-5
Figure A. 10. Map of core shipping.....	A-6
Figure A. 11. Core extraction layout	A-7
Figure A. 12. Core 1A – South.....	A-8
Figure A. 13. Core 2A – South.....	A-9
Figure A. 14. Core 1B – South.....	A-10
Figure A. 15. Core 2B – South.....	A-11
Figure A. 16. Core 1A – North	A-12

Figure A. 17. Core 2A – NorthA-13
Figure A. 18. Core 1B – NorthA-14
Figure A. 19. Core 2B – NorthA-15

Chapter 1

Introduction

1.1 Background

The Bibb Graves Bridge, pictured in Figure 1.1, was built in 1931, and it spans across the Coosa River in Wetumpka, Alabama. This is a reinforced concrete arch bridge with seven spans. The arches on each end of the bridge are completely under the deck, but the other five spans have the deck suspended from the arches at midheight of the arch.



Figure 1.1. The Bibb Graves Bridge in Wetumpka, Alabama

Most of this 82-year old structure is still in sound condition, but the concrete in both arches of the fifth span are severely distressed due to alkali-silica reaction (ASR). Examples of surface deposits and longitudinal cracking caused by ASR in the southern arch of span 5 can be seen in Figure 1.2.



Figure 1.2. Surface deposits and ASR-induced cracking on 3/11/08

The Alabama Department of Transportation (ALDOT) and the Federal Highway Administration (FHWA) began monitoring ASR-related expansions in the Bibb Graves Bridge in 2005.

Concrete expansion due to ASR will only occur when the internal relative humidity (RH) of the concrete is above 80 percent (Bérubé et al. 2002a and Stark 1991). Therefore, in an attempt to lower the relative humidity in the ASR-affected arches of span 5, in the Bibb Graves Bridge, an ASR mitigation procedure was developed by ALDOT, FHWA, and Auburn University in the summer of 2010. This mitigation procedure included cleaning the arches, applying a hydrophobic, penetrating sealer (silane), filling the wide cracks with a flexible sealant, and applying an epoxy flood coat to the top of the arches.

Auburn University assisted with the implementation and documentation of the ASR mitigation procedure that was applied to the bridge in October and November of 2010. The FHWA, ALDOT's Materials and Test Bureau, and Auburn University installed instrumentation for in-situ monitoring of the Bibb Graves Bridge. This instrumentation was installed at the same time as the ASR mitigation procedure, and it was used to collect monthly data pertaining to the internal relative humidity of the concrete and concrete strains. Examples of taking a relative humidity measurement and concrete strain measurement in the Bibb Graves Bridge can be seen in Figure 1.3 and Figure 1.4, respectively. In order to gauge how effective the mitigation procedure has been, relative humidity data were collected monthly from February of 2011 through August of 2013 and concrete strain data were collected monthly from November of 2010 through August of 2013.



Figure 1.3. Measuring RH in Bibb Graves Bridge (Warnock 2012)



Figure 1.4. Taking a strain reading on the Bibb Graves Bridge
(Warnock 2012)

1.2 Statement of Objectives

The primary objective of this research is to evaluate the effectiveness of the silane-based, ASR mitigation procedure that was applied to the Bibb Graves Bridge. In order for the mitigation procedure to be effective, it must show signs of lowering the internal relative humidity of the concrete, which will result in less ASR-related expansion. The secondary objectives of this project include

1. documenting the selection and installation of the ASR mitigation procedure,
2. monitoring and evaluating the internal relative humidity of the instrumented arches over time,
3. monitoring and evaluating the changes in concrete strain of the instrumented arches over time,
4. documenting existing cracking and development of new cracking after the application of the mitigation procedure, and
5. recommending alternative ASR mitigation methods in the event that mitigation of ASR with silane is ineffective.

1.3 Research Methodology

A four-stage research plan was developed to evaluate the effectiveness of the silane-based, ASR mitigation procedure. First, the selection of the ASR mitigation procedure, the initial damage on the Bibb Graves Bridge, and the installation of the ASR mitigation procedure and monitoring instrumentation were documented. The documentation of the ASR mitigation procedure included the materials and methods selected for the surface treatment, along with the order of application to

the bridge. The initial damage in the bridge was documented by performing a crack mapping survey on the top and bottom of both ASR-affected arches in span 5 and a control arch with little to no ASR in span 4. This survey recorded the length, width, and location of all cracks. The final documentation for the initial stages of this research project included the method of installation for the ASR mitigation procedure and the in-situ monitoring equipment used.

Second, the internal relative humidity and the concrete strains were monitored. Relative humidity and strain data were collected once per month from the bridge, weather permitting. Relative humidity was measured in four arches at a total of 48 locations. Two of these arches had little to no ASR deterioration, and two of them were severely cracked due to ASR. Concrete strain measurements were also taken from these same four arches at a total of 46 locations. The data collected each month were then plotted with all of the previous data and uploaded to a secure website for review by ALDOT and the FHWA.

Third, a follow-up crack mapping survey was performed on the same arches that had previously been surveyed. This follow-up survey was done near the end of the project, 33 months after the mitigation procedure was applied. The purpose of the follow-up survey was to document any new cracking that had occurred after the mitigation procedure was applied.

Lastly, the relative humidity and concrete strain data were analyzed. Of the two arches that were monitored but had very little signs of ASR, one arch received the mitigation procedure and one arch was left untreated for comparison purposes. All of the arches were analyzed independently for potential trends of

changing internal relative humidity and expansion. Then the three treated arches were compared to the non-treated control arch to identify any relative differences.

The last portion of this research addressed other ASR mitigation procedures that may be applicable to the Bibb Graves Bridge if the silane-based mitigation procedure is ineffective.

1.4 Thesis Organization

Chapter 2 of this thesis is a literature review with a main focus on ASR mechanisms, damage caused by ASR, identifying ASR in structures, and ASR mitigation techniques. The chapter begins with an overview of ASR that includes the three essential ingredients for the reaction and a brief history of ASR. The mechanisms of the reaction are explained in more detail next, followed by damage caused in concrete by ASR. Effects of different exposure conditions on ASR such as wetting and drying, and freezing and thawing are discussed in the next section. The next major section in Chapter 2 pertains to identifying ASR in structures. This section is broken down into two main steps: recognizing ASR-related symptoms during field surveys and confirming the presence of ASR in cores with petrographic analysis. Next, methods of mitigating ASR are covered in this literature review. The first two methods are the use of silane and lithium. These two methods are heavily discussed here because they are the most documented mitigation methods, and because silane was used on the Bibb Graves Bridge. Other mitigation methods discussed are crack injection, cladding, confinement of expansion, and slot-cutting. Confinement of expansion is also discussed more than some of the techniques here because it could be a viable

option for the bridge. The last section in Chapter 2 covers moisture diffusion modeling that was done by Warnock (2012) on a cross section of an arch in the Bibb Graves Bridge.

Chapter 3 of this thesis provides a detailed overview of the Bibb Graves Bridge. The chapter begins with background information about the bridge such as location and history of the bridge. Next, more details about the size and construction of the bridge are discussed. The occurrence of ASR in the bridge is then covered, followed by summaries of the petrographic reports for concrete cores taken from the arches. Last, examples of ASR-related distress in the bridge are presented.

The ASR mitigation procedure is discussed in Chapter 4. This chapter begins with a presentation of all of the potential mitigation procedures for the Bibb Graves Bridge. Next, the ASR mitigation procedure that was selected for the bridge is discussed, and the chapter ends with a summary of the mitigation procedure application.

The methods and instrumentation for in-situ monitoring of the Bibb Graves Bridge are presented in Chapter 5. The procedure for performing the crack mapping survey is first discussed. After that, the instrumentation and procedure for measuring relative humidity are presented. Lastly, the instrumentation and procedure for measuring concrete strains are explained.

The results and discussion for the in-situ monitoring are in Chapter 6. The chapter begins with the initial and follow-up cracks surveys. Examples are shown of new cracks forming after the application of the mitigation procedure. The

results from 34 months of data collection are then presented and discussed. The relative humidity data are shown first, and then the concrete strain data are reviewed.

Future mitigation methods that could be used on the Bibb Graves Bridge are covered in Chapter 7.

A summary of the important information, conclusions, and recommendations is covered in Chapter 8.

A summary of the process where ALDOT extracted cores from the Bibb Graves and sent them to The Transtec Group and WJE for petrographic analysis to determine if ASR was the cause of the deterioration is covered in Appendix A. Appendices B and C contain the petrographic analysis reports from The Transtec Group and WJE, respectively. The measured relative humidity data are presented in Appendix D, and the measured DEMEC data with corresponding change in strain values are presented in Appendix E.

Chapter 2

Literature Review

2.1 Introduction

The main topics covered in this literature review on alkali-silica reaction include essential ingredients for ASR, reaction mechanisms, resulting damage, and how ASR-affected concrete responds to different exposure conditions. Techniques for identifying ASR in concrete, along with various mitigation methods to possibly lower or eliminate the continuation of deleterious effects in concrete caused by ASR, are covered in this chapter as well.

2.2 ASR Overview

ASR is one of two types of alkali-aggregate reaction (AAR), the other being alkali-carbonate reaction (ACR). CSA (2000) defines AAR as

a chemical reaction in either mortar or concrete between the hydroxyl ions associated with the alkalis, sodium and potassium, from portland cement or other sources, with certain mineral phases that may be present in the coarse or fine aggregate.

Deleterious expansion of the concrete or mortar may result from AAR if certain conditions are met. ASR is associated with various reactive silica minerals, and ACR occurs with certain types of dolomitic rocks (Fournier et al. 2010).

A simplified overview of the ASR process is that alkalis from the cement react with silica from the reactive aggregates in the concrete to form gel reaction products (alkali-silica gel), and this gel will expand in the presence of sufficient amounts of moisture (Fournier and Bérubé 2000). This swelling will cause detrimental effects, such as cracking, throughout the ASR-affected concrete.

There are three requirements that must be met in the concrete in order for ASR to form and continue expanding (Fournier and Bérubé 2000):

1. Reactive forms of silica in the aggregate
2. Sufficient alkali, primarily from the cement
3. Sufficient amounts of moisture in the concrete

There are many recognized forms of reactive, siliceous aggregates.

Table 2.1 was adapted from CSA (2000), and it lists the mineral phases and corresponding rock types that are potentially susceptible to ASR.

The main source of alkalis in concrete is the portland cement; therefore, one of the best ways to lower the alkali content is with the use of low-alkali portland cement. CSA (2000) reports that alkali contents of 5.1 lb/yd³ (3.0 kg/m³) Na₂O equivalent or less for mass concrete will prevent the onset of ASR when reactive aggregates are present. Na₂O equivalent is the percentage of Na₂O + 0.658 K₂O. Another technique for lowering the alkali content is the use of supplementary cementing materials (SCMs), such as blast-furnace slag, fly ash, or silica fume. This will be effective in mitigating ASR if a sufficient amount of portland cement is replaced with SCMs (CSA 2000).

Table 2.1. Mineral phases and corresponding rocks susceptible to ASR

(Adapted from CSA 2000)

(a) Alkali-reactive poorly crystalline or metastable silica minerals and volcanic or artificial glasses (classic alkali-silica reaction)	
Reactants:	Opal, tridymite, cristobalite; acid, intermediate, and basic volcanic glasses; artificial glasses; beekite
Rocks:	Rock types containing opal, such as shales, sandstones, silicified carbonate rocks, some cherts, flints, and diatomite Vitrophyric volcanic rocks: acid, intermediate, and basic, such as rhyolites, dacites, latites, andesites and their tuffs; perlites and obsidians; all varieties with a glassy groundmass; some basalts
(b) Alkali-reactive quartz-bearing rocks	
Reactants:	Chalcedony; cryptocrystalline to microcrystalline quartz; quartz with deformed crystal lattice, rich in inclusions, intensively fractured or granulated; poorly crystalline quartz at grains boundaries; quartz cement overgrowths (in sandstones)
Rocks:	Cherts, flints, quartz veins, quartzites, quartz-arenites, quartzitic sandstones that contain microcrystalline to cryptocrystalline quartz or chalcedony or both Volcanic rocks such as those listed in (b) but with devitrified, crypto- to microcrystalline groundmass Micro- to macrogranular silicate rocks of various origins that contain microcrystalline to cryptocrystalline quartz: <ul style="list-style-type: none"> • Metamorphic rocks: gneisses, quartz-mica schists, quartzites, hornfelses, phyllites, argillites, slates; • Igneous rocks; granites, granodiorites, charnockites; and • Sedimentary rocks: sandstones, greywackes, siltstones, shales, siliceous limestones, arenites, arkoses Sedimentary rocks (sandstones) with epitaxial quartz cement overgrowths

The last requirement for ASR expansion to take place is that sufficient amounts of moisture must be present. Bérubé et al. (2002a) and Stark (1991),

among others, have found that an internal relative humidity (RH) of greater than 80 percent is necessary for alkali-silica gel to expand. The study from Bérubé et al. (2002a) will be discussed later in the silane section, but they found that a reactive cylinder did not expand with an internal relative humidity of 81 to 86 percent while a reactive cylinder at 95 percent relative humidity did expand. Stark (1991) studied expansions of mortar bars made with reactive aggregate and the results are presented in Figure 2.1. It can be seen that expansions in the reactive mortar bars only took place when the relative humidity was greater than 80 percent. The length contraction shown in Figure 2.1 was attributed to the fact that the bars shrank relative to an already expanded condition: "that is, alkali-silica gel reaction products, as well as cement paste matrix, shrank progressively in response to more severe drying conditions" (Stark 1991).

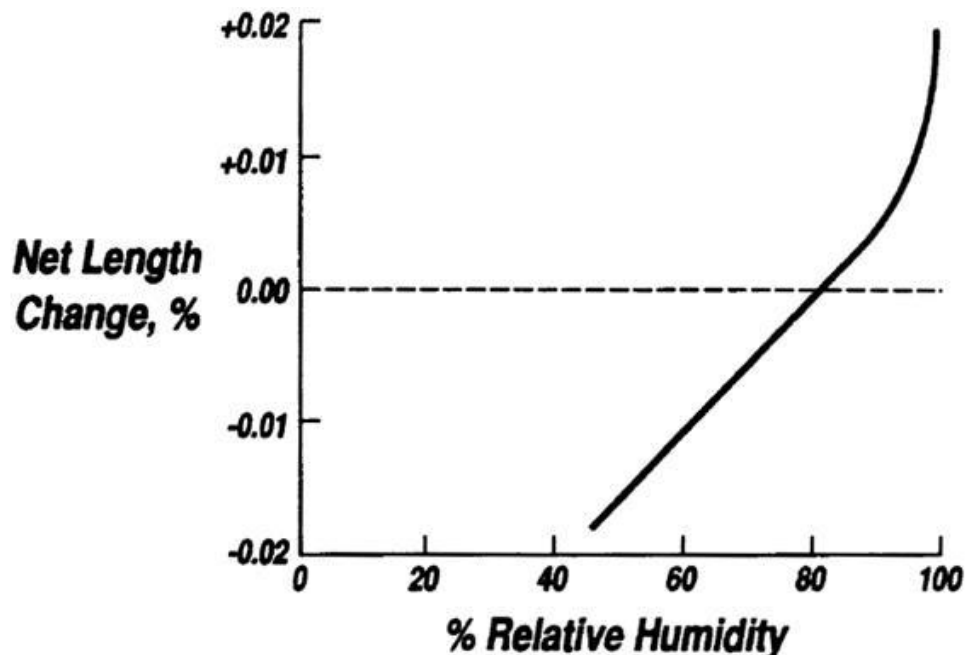


Figure 2.1. RH threshold for expansion of ASR-affected mortar bars

(Stark 1991)

2.2.1 Occurrence of ASR

AAR-related problems in concrete were first discovered in California in the 1940s (Fournier and Bérubé 2000), and have since been recognized in over 47 countries worldwide (Fournier and Bérubé 2000; Institution of Structural Engineers 2010). There are indications that only a few countries may be free of AAR, and the risk of AAR spreading throughout the world is increasing with the growth in international trade of cementitious materials and aggregates (Institution of Structural Engineers 2010). ASR is the most common form of AAR in the world, and has been found in concretes with aggregates having a variety of compositions and textures (Fournier et al. 2004).

2.2.2 Mechanisms of the Reaction

Fournier et al. (2004) describe the ASR reaction as follows:

ASR refers to chemical reactions between alkali hydroxides (Na^+ , K^+ , OH^-) in the concrete pore fluid and certain siliceous phases present in the aggregate materials. The reaction results in the formation of a secondary calcium-rich alkali-silica gel which has a strong affinity with water. As the gel absorbs water, internal swelling pressure develops causing volume change and fracturing of the reacting aggregate particles, cracking of the surrounding cement paste and subsequent deterioration of the concrete, which in turn can result in a significant reduction in the service life of affected concrete structures.

The alkali-silica gel is typically made up of silica, alkalis (sodium and potassium) and calcium, and this gel lines or fills the voids and fractured surfaces of the cement paste and aggregate particles. The amount of gel present is not necessarily indicative of how much expansion or cracking the element has suffered. Large amounts of gel have been seen in concrete elements without extensive cracking and large expansion, and very little gel has been seen in concrete with extensive cracking and large expansions (CSA 2000; Fournier et al. 2004).

2.3 Damage Caused by ASR

Wood (2008) states the best way to determine the expansion potential, influence of temperature and moisture on expansion, and how the reinforcement stress will contain expansion, is to monitor the structure and evaluate the results over time, not rely solely on literature to predict the structure's response to ASR. Monitoring the structure for two or three years will account for seasonal affects and show overall trends of damage development and expansion that are reliable for predicting long-term damage and useful remedial actions (Fournier et al. 2010; Wood 2008). Wood (2008) says "unless there is a change in the water availability to the structure, the rate of AAR damage and crack growth, once cracking has initiated, is steady and roughly linear with time."

The rate and extent of ASR-induced concrete deterioration depends on several conditions as listed by Fournier et al. (2004):

1. The proportion and inherent reactivity of the siliceous phases in the aggregates

2. The pH of the concrete pore solution, which in turn is related to the internal and external sources of alkalis
3. The availability of moisture
4. The temperature and thermal gradients
5. The configuration of structural restraint provided to the concrete structure or element

When discussing factors that affect how concrete will behave under the influence of AAR, Fournier and Bérubé (2000) list all five of the previously mentioned items along with the type and composition of cement, water-to-cement ratio, and the use of SCMs. The major forms of concrete damage caused by ASR are discussed in the following sections, and they include microcracking, surface cracking, surface discoloration, surface deposits, and popouts.

2.3.1 Microcracking

Microcracking in concrete due to ASR is caused by the internal forces in the concrete that are created from the expanding aggregate particles or expansion of the alkali-silica gel within and around the boundaries of the reacting aggregate particles (Fournier and Bérubé 2000; Fournier et al. 2004). Microcracking will initially be in the reactive aggregates and at their interface with the cement paste, as shown in Figure 2.2 (A). Once the ASR reaction and expansion have progressed, microcracks will extend farther into the cement paste and into more aggregates as shown in Figure 2.2 (B). The alkali-silica gel will be found in the microcracks in the aggregates and cement paste. Microcracking may even

spread through nonreactive aggregate particles if the concrete cracking is severe enough. (CSA 2000; Fournier et al. 2004)

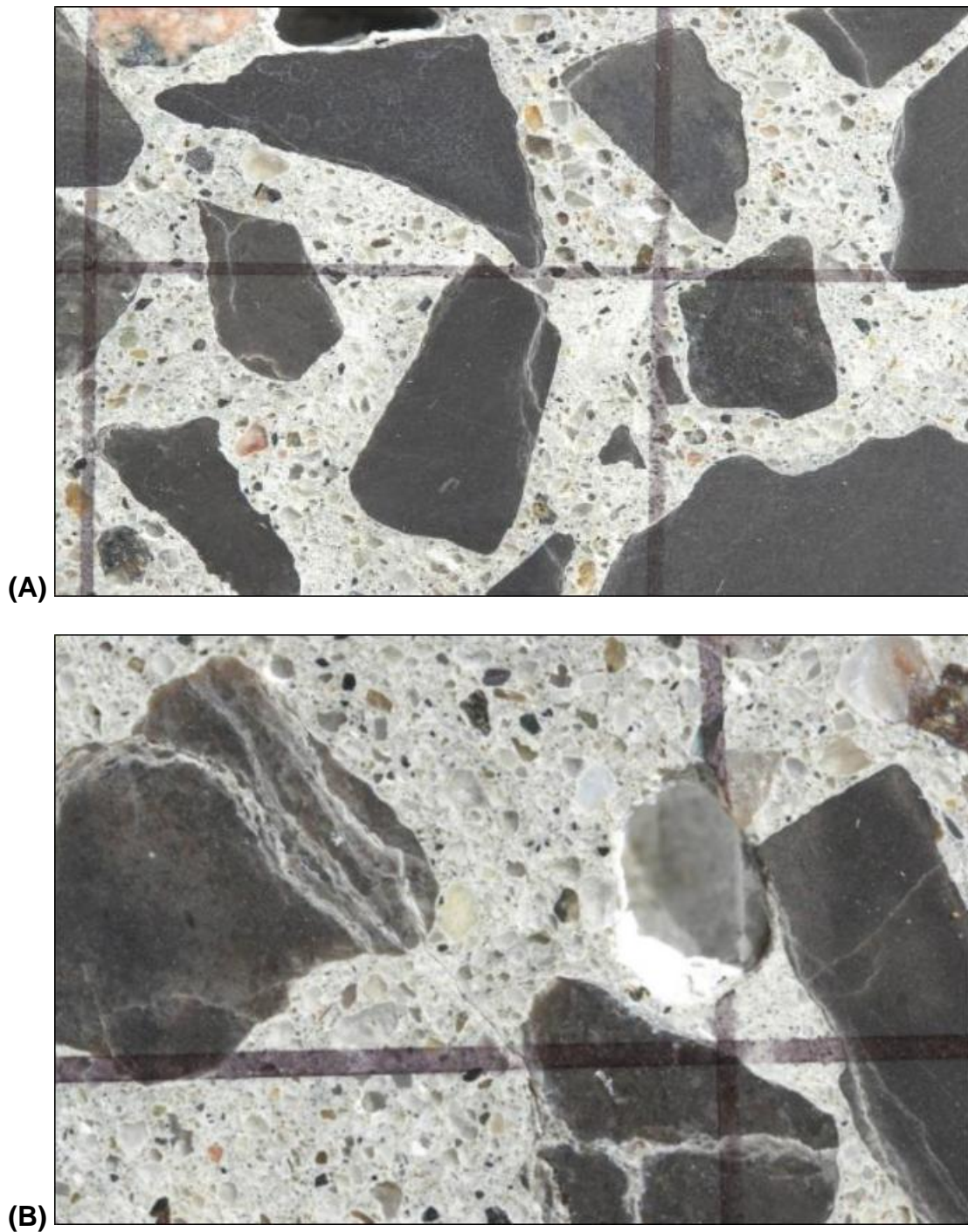


Figure 2.2. Microcracking in aggregate due to ASR with (A) 0.066% and (B) 0.283% concrete expansion (Fournier et al. 2010)

2.3.2 Surface Cracking

Surface macrocracks due to ASR are generally in the range of 0.004 to 0.4 inches (0.1 to 10 mm) wide and penetrate 1 to 2 inches (25 to 50 mm) deep before they convert into microcracks. Severe surface macrocracks can penetrate to depths of 4 inches (100 mm) and beyond. Concrete members experiencing ASR that are exposed to sun, moisture, and frost-action typically have more cracking and deterioration (CSA 2000; Fournier and Bérubé 2000; Fournier et al. 2004). The mechanisms driving surface cracking in concrete members exposed to the elements are described by Fournier et al. (2004) as follows:

In the case of concrete members undergoing internal expansion due to ASR and subjected to wetting and drying cycles (cyclic exposure to sun, rain, wind, or portions of concrete piles in tidal zones, etc.), the concrete often shows surface cracking because of induced tension cracking in the “less expansive” surface layer (because of variable humidity conditions and leaching of alkalis) under the expansive thrust of the inner concrete core (with more constant humidity and pH conditions).

Map, or pattern, cracking is often visible on the surface of concrete members affected by ASR that have little to no major stress or restraint. Figure 2.3 is an example of map cracking on a highway barrier. In reinforced concrete members or members subjected to loading stresses, the ASR crack patterns will typically follow the direction of the primary reinforcing steel or the direction of the major stress fields, respectively, as shown in Figure 2.4, (BCA 1988; CSA 2000;

Fournier and Bérubé 2000; Fournier et al. 2004). When a compressive stress field is present, the concrete will have greater net expansive strains, due to ASR expansion and Poisson's effect, in the transverse directions. Thus, if there is any cracking, it will be parallel to the major compressive stress field. The opposite is true for applied major tension stress fields. The tension and ASR-related strains are acting in conjunction with each other; therefore, greater expansive strains will occur parallel to the tension field and cause cracking perpendicular to the tension (Courtier 1990).



Figure 2.3. Severe map-cracking and surface discoloration on a road barrier
(Fournier et al. 2010)

Not only is surface cracking due to ASR deteriorating the concrete, but it may accelerate deterioration due to inducing corrosion of the reinforcement, freezing and thawing action, and sulfate attack. Conversely, ASR may be induced if the previously mentioned deterioration mechanisms are already present and they cause cracking in the concrete that is made with reactive aggregates (Fournier and Bérubé 2000).

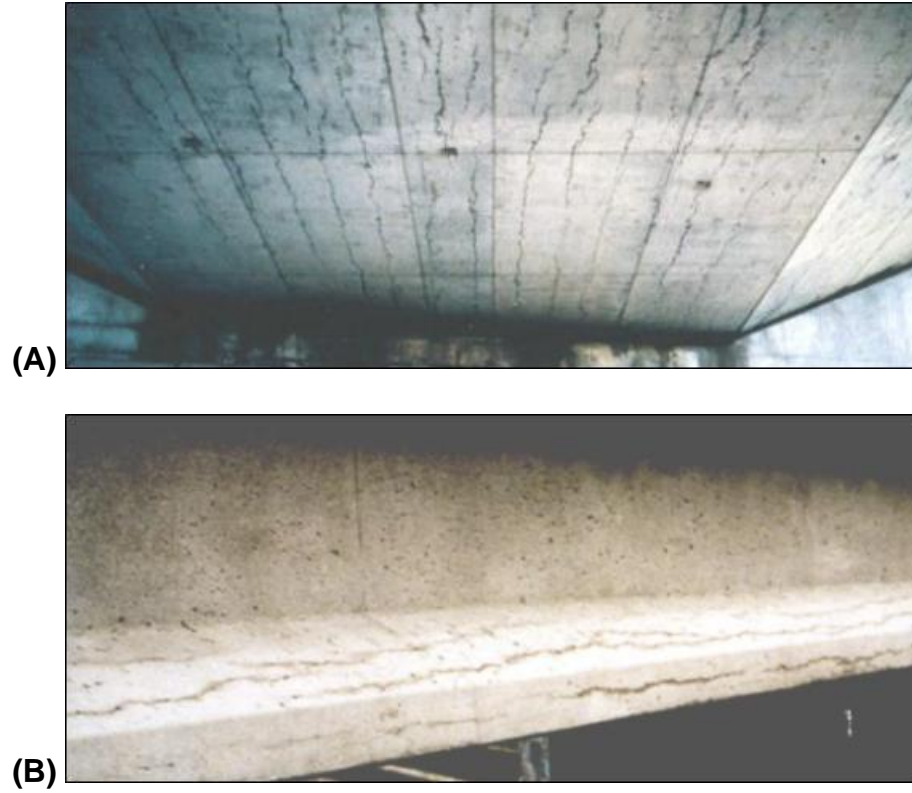


Figure 2.4. Longitudinal cracking due to ASR in (A) a bridge deck soffit and (B) a precast, reinforced concrete beam (Fournier et al. 2010)

2.3.3 Surface Discoloration

Broad brownish zones appearing to be damp often border surface cracking in concrete caused by ASR (BCA 1988; CSA 2000; Fournier and Bérubé 2000; Fournier et al. 2004). These surface discoloration zones are clearly shown in Figure 2.3 and Figure 2.4.

2.3.4 Surface Deposits

Surface deposits of efflorescence (leaching of carbonated lime) on concrete may be due to ASR or a number of other things, such as the migration of water through cracks in the concrete or frost action (CSA 2000, Fournier et al. 2004).

An example of efflorescence and alkali-silica gel on the surface of a foundation is presented in Figure 2.5. It is important to survey the extent, location, color, texture, dampness, and hardness of the surface deposit. Along with a survey, X-ray and chemical analysis of deposit samples are helpful in determining if alkali-silica gel is present (Fournier et al. 2004).



Figure 2.5. Efflorescence and exudations of alkali-silica gel on a foundation
(Fournier et al. 2010)

2.3.5 Popouts

The main cause of popouts is expansion of frost-susceptible aggregates and individual unsound aggregate particles, but ASR may also be a cause of popouts when reactive aggregates are present. If alkali-silica reactive aggregates expand enough near the surface, conical portions of the concrete surface may detach from the member leaving a portion of the fractured aggregate in the bottom of the hole (BCA 1988; CSA 2000; Fournier et al. 2004). Figure 2.6 is an example of a popout due to ASR.



Figure 2.6. Concrete popout caused by ASR (Fournier et al. 2004)

2.4 Effects of Exposure Conditions on ASR Damage

Concrete expansion and cracking due to ASR are generally most severe in elements subjected to an external supply of moisture. The surfaces of elements affected by ASR usually have more cracking and deterioration when exposed to sun, wetting and drying cycles, freezing and thawing, and deicing salt (Fournier et al. 2004; Bérubé et al. 2002a).

2.4.1 Wetting and Drying

The effects of wetting and drying of concrete suffering from ASR were observed in experiments performed by Bérubé et al. (2002a); this study is discussed in more detail in section 2.6.2.6. For this experiment, ASR-affected concrete cylinders were subjected to different 14-day exposure cycles that consisted of varied combinations of the following: humid air curing, drying, immersion in tap or salt water, and freezing and thawing cycles. The cylinders that had four days of drying in their cycle experienced 40 percent less expansion than the cylinders

continuously exposed to high humidity over the two-year period. However, the cylinders exposed to the wetting and drying cycles experienced more map cracking on the surface. This was due to higher tension stresses near the surface, because ASR-favorable conditions were not always present in this region due to alkali leaching during wetting and lower humidity during drying (Bérubé et al. 2002a).

2.4.2 Freezing and Thawing

If ASR-related cracking is present in concrete, freezing and thawing cycles may accelerate the deterioration of concrete. This is because the cracks generated through ASR will allow more water into the concrete; therefore, more expansion will occur when the additional water freezes (Bérubé et al. 2002a).

On the other hand, concrete cracking generated through freezing and thawing cycles may accelerate ASR-related deterioration. This is because moisture, an essential ingredient for ASR expansion, will penetrate into the concrete easier, and because the concrete is less able to withstand the expansive forces generated from the ASR, due to the concrete being previously weakened from freezing and thawing action (Bérubé et al. 2002a).

2.5 Identification of ASR in Structures

When investigating concrete structures that are cracked or otherwise deteriorated, one should approach it with a completely open mind and not jump to conclusions too fast. BCA 1988 says one should ask “‘What has caused the deterioration?’ , rather than ‘Is this a case of ASR?’” Misdiagnosing the cause of damage may result in misleading, costly, or dangerous circumstances if

inadequate or unnecessary remedial work is done. BCA (1988) gives basic guidelines when beginning an investigation:

1. At the start of an investigation, every mechanism that could cause concrete deterioration should be considered as a possibility.
2. No single possible cause should be eliminated until the investigation has shown clearly that it could not have contributed to the deterioration.
3. Evidence of alkali-silica reaction may be found in concrete where siliceous material form a portion of or all of the aggregates, whether the concrete has cracked or not.

BCA (1988) also offers a logical sequence to follow when investigating a structure:

1. Examine records, inspect site, and assess results to establish whether laboratory work or in-situ testing or monitoring is required and what tests should be undertaken.
2. Take samples for testing in the laboratory.
3. Commence site testing and monitoring.
4. Do laboratory tests.
5. Assess results of laboratory tests in conjunction with the results and observations from the site.

2.5.1 Site Inspection

The site investigation alone is not enough to confirm or deny the existence of ASR in the concrete with any certainty; sampling and testing will also be necessary to correctly identify the cause of damage and deterioration to the

structure. The main purpose of the site inspection is to identify whether or not the structure exhibits any features that are consistent with ASR-related damage and to identify features that may be due to another deleterious mechanism (BCA 1988; CSA 2000).

There are several factors and ASR-related signs to look for and take note of when performing a site inspection. Here are a few things BCA (1988) and CSA (2000) say to look for, most of which were described previously in the damage section:

1. Environmental conditions — Several environmental factors should be noted such as: degree and frequency of wetting and drying, the reason for wetting, if salt solutions have been in contact with the surface from seawater or deicing salts, and if elements of the structure are vulnerable to frost action.
2. Cracking — Position, nature, and pattern of the cracks should be recorded and/or photographed, and major cracks should be plotted to scale with regards to length, width, apparent depth, continuity, and path.
3. Discoloration — Distinctive surface discoloration along cracks may be a sign of ASR.
4. Efflorescence — Position, extent and quantity of efflorescence should be recorded, and the color, texture, dampness and hardness of the deposit described. Samples of this should also be taken.
5. Popouts — Number, size and distribution of any popouts should be recorded along with the type of aggregate exposed at the base. Any

surface deposits associated with these should also be recorded and possibly sampled.

6. Structural Movements — Significant structural movements may occur due to ASR. Any evidence of differential movement, such as the closing of joints, relative displacement of adjacent sections, excessive deflection and twisting or bulging of originally flat surfaces, should be noted.

CSA (2000) has listed the probability of AAR being the cause of concrete deterioration based on the apparent damage that the structure has experienced and if that damage is consistent with AAR. The probability of AAR is listed in Table 2.2 as low, medium, or high, based on the features present during the site investigation.

Table 2.2. Potential AAR risk of features examined during site investigation (Adapted from CSA 2000)

Feature	Probability of AAR		
	Low	Medium	High
Expansion and/or displacement of elements	None	Some	Structure shows symptoms of increase in concrete volume leading to displacement and misalignment of elements
Cracking and crack pattern	None	Some cracking patterns typical of AAR (i.e., map-cracking or cracks aligned with major reinforcement or stress)	Extensive map-cracking or cracking aligned with major reinforcement or stress
Surface discoloration	None	Slight surface discoloration associated with some cracks	Line of crack having dark discoloration with an adjacent zone of light-colored concrete
Exudations	None	White exudations around some cracks	Colorless, jelly-like exudations readily identifiable as ASR gel associated with some cracks
Environment	Dry and sheltered	Outdoor exposure but sheltered from wetting	Parts of component frequently exposed to moisture, e.g., rain, groundwater, water due to natural function of the structure (hydraulic dam)

2.5.2 Core Sampling

The number of concrete core samples required for a given structure depends on the type and complexity of the structure. The sample should be representative of the elements in the structure; it is ideal to take samples from three areas in each element that represent: sound, typical, and poor concrete. In general, better assessment results will be obtained from single tests on multiple samples rather than multiple tests on single samples. But the deciding factor for sample numbers usually comes down to element access limitations and economics (BCA 1988).

Coring is the only sampling technique that meets the needs of most laboratory analysis and testing. Core diameters of 4 inches (100 mm) are preferred, but smaller or larger diameter cores are often necessary because of reinforcement spacing or aggregate size. Cores should be as long as feasibly possible, because even though the major cracking and distress due to ASR are typically in the outer cover, microcracking can occur throughout the depth of the concrete member. Last, it is essential that care be taken when drilling the cores so that the sides are smooth and parallel, and so that additional cracks are not added to the sample (BCA 1988; CSA 2000; Fournier et al. 2010).

Detailed records of all sampling should be made on site. The following list of information and tasks to be recorded and performed on site is adapted from CSA (2000) and Fournier et al. (2010):

1. Sketch showing location of core
2. Photograph of core location
3. Size (diameter and total length) and orientation

4. Record of any features that may be indicative of ASR, such as damp patches on core surfaces, gel in cracks and voids, or reaction rims around the aggregate particles.

Cores should also be immediately labeled and wrapped after removal.

They can be “wrapped and sealed in heavy-duty shrink wrap, polyethylene sheeting, aluminum foil, or polyethylene bags, to limit moisture loss during subsequent transport and storage” (CSA 2000).

2.5.3 Petrographic Analysis of ASR

Petrographical examination of concrete samples is the best technique for confirming or denying the presence of gel and microcracking (BCA 1988). The main petrographic features related to ASR that should be noted and, if possible, characterized by their extent and distributions are listed as follows by CSA (2000):

1. Microcracks in and around aggregate particles and in the cement paste, with some of these cracks filled to various extents with secondary reaction products.
2. Reaction rims around aggregate particles.
3. Distribution of reaction products in voids or pores of the cement paste, impregnating cement paste around reacted aggregate particles, etc.

2.5.3.1 Microcracks

Microcracks are generally limited to the reactive aggregate particles and the cement paste-aggregate interface during the early stages of AAR. As the reaction/expansion process continues, pre-existing or AAR-induced microcracks

will extend from the aggregate particles into the cement paste. Secondary reaction products are often found filling these cracks, and in badly cracked specimens, cracks, possibly filled with gel, may even run through nonreactive aggregate particles (CSA 2000; Fournier et al. 2004).

2.5.3.2 Reaction Rims

When examining cut sections of concrete samples affected by ASR, dark reaction rims like the ones shown in Figure 2.7 are often visible around the reactive aggregates. Care must be taken not to confuse these reaction rims with weathered edges that may be preexisting (before concrete mixing) on the aggregates (CSA 2000; Fournier et al. 2004; Fournier and Bérubé 2000).



Figure 2.7. Dark rim around the perimeter of reactive aggregate particles

(Fournier et al. 2010)

2.5.3.3 Reaction Products

The alkali-silica gel is typically made up of silica, alkalis (sodium and potassium) and calcium; this gel lines or fills the voids and fractured surfaces of the cement paste and aggregate particles. The amount of gel present is not necessarily indicative of how much expansion or cracking the element has suffered (CSA 2000; Fournier et al. 2004).

The alkali-silica gel is often seen when examining cracks on sawn, polished, or thin sections of concrete affected by ASR. Relatively low magnification (up to 50x) with a petrographic microscope, stereobinocular, or scanning electron microscope is all that is necessary to observe the alkali-silica gel (CSA 2000).

2.5.3.4 ASTM C856 Standard Practice for Petrographic Examination of Hardened Concrete

ASTM C856 outlines the procedure for petrographic examination of samples of hardened concrete. This outline is applicable to all types of hardened hydraulic-cement mixtures, including concrete, mortar, grout, plaster, stucco, terrazzo, and the like from concrete constructions in natural environments, or simulated service conditions, or laboratory test specimens (ASTM C856 2011).

In order to obtain accurate and reliable results from a petrographic examination, ASTM C856 (2011) says that “All petrographic examinations of hardened concrete described in this practice shall be performed by or under the technical direction of a full time supervising petrographer with at least 5 years experience in petrographic examinations of concrete and concrete-making

materials.” It is also important to have core samples that are truly representative of the structure. The minimum sample size is at least one core, preferably 6 inches in diameter and 1 foot long, for each mixture, condition, or category of concrete. Smaller cores may be necessary due to economic or other limitations; if this is the case, the diameter of the core should still be at least twice as big as the maximum aggregate size, preferably three times bigger (ASTM C856 2011).

The purpose for petrographic examination of concrete from constructions with emphasis on ASR is listed below from (ASTM C856 2011).

1. Determination in detail of the condition of concrete in a construction
2. Determination of the causes of inferior quality, distress, or deterioration of concrete in a construction
3. Determination of the probable future performance of the concrete
4. Description of the cementitious matrix, including qualitative determination of the kind of hydraulic binder used, degree of hydration, degree of carbonation if present, evidence of unsoundness of the cement, presence of a mineral admixture, the nature of the hydration products, adequacy of curing, and unusually high water-cement ratio of the paste
5. Determination whether alkali-silica or alkali-carbonate reactions, or cement-aggregate reactions, or reactions between contaminants and the matrix have taken place, and their effects upon the concrete

The petrographic examination of concrete should begin with a review of all of the information available about the specimens followed by a visual examination of each sample. The following is summarized from a table in ASTM

C856 (2011) that gives guidelines on what to look for during the visual examination of concrete.

1. Coarse Aggregate
 - a. Composition, percentage of volume, shape, distribution, packing, and grading
2. Fine Aggregate
 - a. Type, distribution, particle shape, grading, and preferred orientation
3. Matrix
 - a. Color and color distribution
4. Air
 - a. More than three percent total, predominantly in spherical voids?
 - b. Less than three percent total, abundant nonspherical voids?
 - c. Color differences between voids and mortar?
 - d. Voids empty, filled, lined, or partly filled?
 - e. Shape, distribution, and grading
5. Embedded Items
 - a. Type, size, location, kinds of metal, and other items
 - b. Clean or corroded, and cracks associated with embedded items?
6. Condition
 - a. Can one break it with one's fingers? Cracked and how are the cracks distributed? Cracks through or around coarse aggregate? Aggregate tear during drilling or sawing? Crack filling? Surface deposits? Wet or dry looking areas? And rims on the aggregate?

Once the visual examination has taken place, the sample should then be examined with a stereomicroscope. This examination will be similar to the visual examination but reveals more detail about microcracking. In some cases, a report can be prepared at this point, but other cases may require additional stereomicroscope study, more detailed examination using the petrographic or metallographic microscopes, X-ray diffraction, other instrumental methods, and/or chemical or physical tests (ASTM C856 2011).

Another useful technique associated with petrographic analysis is the examination of “thin sections”. For this, the concrete is ideally sliced into 1/16 inch sections if it is strong enough. Weaker concrete and/or sections containing fragile deposits of alkali-silica gel in voids may be thicker. The thin slices of concrete are then mounted to a glass slide and ground down to between 20 and 30 μm thick with progressively finer abrasives. When examining ASR-affected concrete, the thin section areas should be taken so that the cracked coarse aggregate is visible. ASTM C856 (2011) also gives guidelines of what to look for during the examination of ASR-affected, concrete thin sections.

Does the aggregate contain particles of types known to be reactive (chert, novaculite, acid volcanic glass, cristobalite, tridymite, opal, bottle glass)? If quartzite, metamorphosed subgraywacke, argillite, phyllite, or any of those listed in the sentence above, are there internal cracks inside the periphery of the aggregate? Has the aggregate been gelatinized so that it has pulled off during sectioning leaving only a peripheral hull bonded to the mortar?

(This last phenomenon also occurs in concrete with air-cooled slag aggregate, where it indicates reaction between cement and slag.)

Cracks that appear to be tensile and to narrow from the center toward the border or the particle are also evidence of alkali-silica reaction.

One limitation to the examination of thin sections is they will not provide evidence of the extent or rate of deterioration (BCA 1988).

Lastly, ASTM C856 ANNEX A1 explains the technique for detecting alkali-silica gel by treating the surface of conditioned concrete with a solution of uranyl-acetate. Once the surface treatment is complete, the specimen is viewed by dampening the surface and exposing it to short-wave ultraviolet (UV) light; “alkali-silica gel will fluoresce bright greenish-yellow, and usually occur in and around aggregate particles, in voids, and in cracks” (ASTM C856 2011). Ettringite and a few materials will also fluoresce similar to alkali-silica gel; therefore, the presence of alkali-silica gel found using this technique must be confirmed with other petrographic analysis techniques.

2.5.3.5 Probability of AAR Based on Laboratory Findings

The presence of alkali-silica gel and sites of expansive reaction are all that is needed to positively diagnose the presence of ASR in polished surfaces or thin sections. There are many other features consistent with AAR, but these features alone are not sufficient to reliably diagnose AAR, as they may be a result of another mechanism (CSA 2000). Table 2.3 gives guidelines for the probability of AAR being present based on features found during the laboratory investigation.

Table 2.3. Potential AAR risk of features from laboratory findings

(Adapted from CSA 2000)

Probability of AAR	Nature and extent of features
Low	No gel present, no sites of expansive reaction, presence of other indicative features rarely found
Medium	Presence of some or all of features generally consistent with AAR, such as <ol style="list-style-type: none">1. Cracking and microcracking (especially when associated with known reactive aggregates)2. Presence of potentially reactive aggregates3. Internal fracturing of known reactive aggregates4. Darkening of cement paste around aggregate particles, cracks, or voids5. Presence of reaction rims around internal periphery of reactive aggregate particles6. Presence of damp patches on core surfaces
High	Presence of features such as <ol style="list-style-type: none">1. Evidence of sites of expansive reaction, i.e., locations within the concrete where evidence of reaction and emanation of swelling pressure can be positively identified2. Presence of alkali-silica gel in cracks and voids associated with reactive particles and readily visible to normal or corrected-to-normal vision under low magnification

2.5.3.6 Damage Rating Index

The damage rating index (DRI) is a procedure to quantify the degree of deterioration of a concrete specimen affected by AAR. For this test, a concrete sample, either extracted from a structure or collected after completion of laboratory testing, is generally cut in two. The cut surface is then polished and sectioned into a grid of 0.4 by 0.4 in. squares; in general, at least 200 squares are needed for a valid test. These grid sections are then individually viewed

under a stereomicroscope at 16-times magnification for the petrographic features listed in Table 2.4. These features are then counted and multiplied by their weighting factors to signify their importance. Lastly, the totals of each of the weighted defects are summed and normalized for an area of 16 square inches. This normalized value is the DRI (Thomas 2010). Thomas (2010) also describes the interpretation of the results as follows: “although there is no arbitrary value which will indicate whether the concrete suffers deterioration due to ASR, nor its severity, DRI values above 500 are generally suggestive of significant damage due to ASR.”

Table 2.4. Features and weighting factors for damage rating index

(Adapted from Thomas 2010)

Features	Abbreviation	Weighting Factor
Cracks in coarse aggregates	CCA	X 0.75
Cracks in coarse aggregates + gel	C+GCA	X 2.0
Open cracks in coarse aggregate	OCCA	X 4.0
Coarse aggregates debonded	CAD	X 3.0
Reaction rims	RR	X 0.5
Cracks in the cement paste	CCP	X 2.0
Cracks + gel in the cement paste	C+GCP	X 4.0
Gel in air voids	GAV	X 0.5

2.6 Mitigation of ASR in Existing Structures

AAR has been and will always be a major concern because there is currently no way to completely cure the problem before it stops on its own, which may take decades and cause extensive damage in the meantime (Fournier and Bérubé

2000). The Institute of Structural Engineers (2010) says mitigation measures must be taken to lower the moisture in concrete affected by ASR; otherwise, there is expected to be a trend of steady growth and expansion of the concrete. Once measures are taken to dry the concrete, the expansive reaction may slow, but it is very important to maintain the waterproofing because any increase in moisture later on will accelerate the damage (Institution of Structural Engineers 2010).

2.6.1 In-Situ Monitoring of ASR-Affected, Concrete Structures

Both severely ASR-damaged structures and structures that are not yet damaged severely enough to require immediate intervention should be periodically monitored to check expansions and displacements if applicable. The data collected may be analyzed to determine the rate of expansion and the potential for future expansion (BCA 1988; Fournier et al. 2004). "However, considering the seasonal and thermal effects, it will generally take a minimum of 2 and preferably 3 years to obtain reliable data" (Fournier et al. 2010). Fournier et al. (2004) says "the management of concrete structures affected by ASR involves overall interpretation of the results of both field and laboratory investigations. This is essential to develop long-term monitoring programs, and to determine the nature and the extent of the repair program required."

The following types of in-situ monitoring were adapted from a list in Fournier et al. (2010):

1. Installation of probes for temperature and humidity measurements

2. Installation of DEMEC points for expansion or relative movement measurements
3. Stress measurements (if required) in the steel reinforcement or in the concrete

2.6.2 Silane

Coatings or sealers have the potential to effectively reduce ASR in concrete because they can lower the internal relative humidity of the concrete by preventing external water from penetrating the surface and allowing internal water vapor to escape (Fournier et al. 2010). As long as sealers penetrate into the concrete sufficiently and remain stable in the voids, they can be very effective at preventing water infiltration into the concrete. But it is important to repair any cracks before sealing because chemical penetrating sealers are not capable of bridging cracks (CSA 2000; Fournier et al. 2010). CSA (2000) also lists essential characteristics for an effective sealer:

1. Be resistant to water absorption
2. Penetrate to a measurable depth
3. Resist deterioration from UV radiation
4. Possess long-term stability in an alkaline environment
5. Be of low health and environmental risk
6. Allow vapor transmission

Silicon-based water repelling products, such as silane, are very advantageous to use because they meet all of the previously mentioned effective sealer requirements and are easy to work with. Silanes are easily applied

through a low pressure sprayer, such as the garden sprayer used in Figure 2.8, and they will cure enough to withstand weathering and traffic within 24 hours (Selley 2010). One side effect of silane is it is not believed to be a permanent fix with a single application because its effectiveness will dissipate over time due to abrasion and UV exposure. Reapplying silane every 5 years or so is generally thought to be prudent (Fournier et al. 2010).



Figure 2.8. Topical application of 40% silane solution to ASR-affected barriers (Fournier et al. 2010)

2.6.2.1 Chemistry of Silane

Silane is a functional monomeric silicon compound with four chemical attachments. Figure 2.9 is a basic representation of the chemistry and make-up of a silane particle (Selley 2010). There are a variety of silanes available; the variations are primarily the concentration of silane in the formulation (20 to close to 100 percent) and the type of carrier the silane is combined with (water-based or solvent-based) (Fournier et al. 2010).

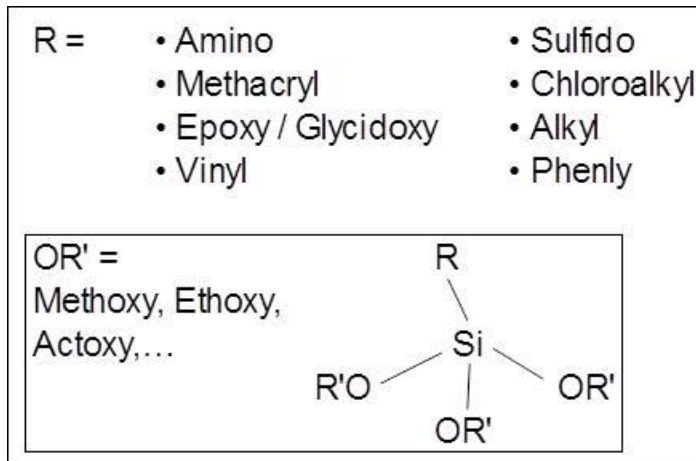


Figure 2.9. Silanes basic structure and key chemistries

(Adapted from Selley 2010)

2.6.2.2 Penetration and Water Repellency of Silane

Silanes are effective water repellents because they are able to easily penetrate into concrete, masonry, and stone structures. They are capable of easy surface penetration because they start out as a very low viscosity, low molecular weight, and low surface tension fluid (Selley 2010). Concrete characteristics such as porosity, moisture and silica content, and pH also have an influence on the penetration depth of silane (Engstrom 1994). Along with penetration, “durable water repellency is achieved through being able to anchor to the substrate, and silanes do this by first reacting with water (from the atmosphere) and then chemically bonding to the substrate” (Selley 2010).

Selley (2010) describes how the silane reacts with the concrete and forms a hydrophobic layer and gives a visual representation of how water beads on the surface in Figure 2.10:

When silanes have a longer hydrophobic alkyl tail—such as a butyl (4 carbon) or octyl (8 carbon) group—they tend to orient

themselves such that this tail is pointed out towards the air. The effect is to impart a low surface energy to the substrate. Water, of course, has high surface energy (surface tension). The difference between these energies causes water to be more attracted to itself than to the substrate, and so the water has a tendency to stay in spherical droplet shape. This is why water “beads” on a hydrophobic surface. Water beading is not an absolute measure of the ability to keep out water, but because the water does not “wet-out” on a surface, the tendency for water to find and flow into small cracks in the surface is substantially reduced.

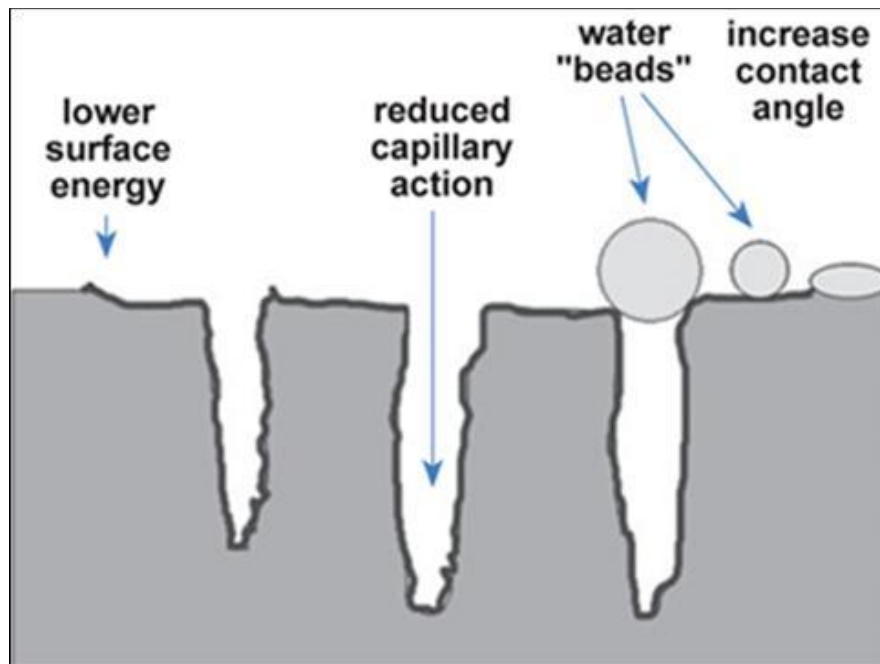


Figure 2.10. Silane’s hydrophobic properties repelling water (Selley 2010)

2.6.2.3 Resistance of Silane

Silane is resistant to degradation from oxidation and in many cases, pH extremes. Silane's surface penetration also makes it resistant to friction, abrasion, and degradation due to UV radiation (Engstrom 1994; Selley 2010).

2.6.2.4 Health and Environmental Risk of Silane

BASF (2007) warns that direct contact or inhalation of silane may cause skin, eye, or respiratory irritation. They suggest flushing eyes with water and washing skin with soap and water, and if irritation persists afterwards, seeking medical attention.

Silane formulation has evolved along with stricter regulations on volatile organic compounds (VOCs). Silane formulations are using either water-based or solvent-based with more silane concentrations (thus lower solvent content) in order to lower their VOC content to meet regulations (Fournier et al. 2010).

2.6.2.5 Vapor Permeability of Silane

Water repellency is not enough alone for a sealer to be effective in reducing ASR symptoms because the concrete must also be able to release some of the moisture already present in order to get below 80 percent relative humidity; therefore, it is important for the sealer to also be water vapor permeable. Silanes and silicones are water vapor permeable “due to the fact that the siloxane bond is quite long (on an atomic scale), so the spaces between the silicone and attached oxygen are actually larger than the size of individual water molecules. This allows water vapor to pass through the polymer or network” (Selley 2010).

2.6.2.6 Laboratory Testing of Silane on Cylinders

Bérubé et al. (2002a) conducted experiments to evaluate the effectiveness of various sealers for controlling the deleterious effects of ASR on exposed concrete cylinders with diameters of 10 inches (255 mm). There were five sealers used for this study: silane, oligosiloxane, polysiloxane, epoxy resin, and linseed oil. Four types of concrete were also used: plain/low-alkali, plain/high-alkali, air-entrained/low-alkali, and air-entrained/high-alkali. Each of the sealers was applied in two applications with about 10 minutes between applications.

The cylinders were subjected to various 14-day exposure cycles (listed in Table 1 of Bérubé et al. 2002a) for up to a year or more. The worst of the exposure cycles, C5, was (i) 7 days at over 95 percent relative humidity and 100 °F (38 °C), with the cylinders placed above water in sealed plastic pails, (ii) 4 days of air drying at 100 °F and 30 percent relative humidity, (iii) 30 minutes of submersion in 3 percent NaCl solution at 100 °F, and (iv) 3 days of freezing and thawing cycling in humid air, one cycle per day.

Many of the cylinders were sealed before the exposure cycles began with one of the sealers previously listed after 28 days of curing. This was done in order to test the effectiveness of the sealer in preventing excessive expansion of the concrete due to ASR. Other cylinders were left unsealed and subjected to the exposure cycles for 1 year (plain concrete) and 1.5 years (air-entrained concrete) before they were sealed. This was done in order to determine the effectiveness of the sealers on severely ASR-affected concrete. A number of other cylinders were also subjected to 105 or 119 consecutive freezing and thawing cycles, one

per day, to see the effect of freezing and thawing on ASR-affected concrete (unsealed cylinders), and to evaluate the frost-susceptibility of sealers applied at early ages. All of the specimens were then returned to their respective exposure cycles for the duration of testing.

Because exposure cycle C5 was the most severe, the results from it are plotted in Figure 2.11. It is apparent from this figure that silane is the best sealer for all three scenarios here: late sealing, early sealing, and low-alkali cement. There is a noticeable trend of decreased expansion once the silane is applied for the late application. The early silane treated, low-alkali cement cylinder not only had decreased expansion for this whole exposure condition and time; it had decreased expansion for all of the exposure cycles and testing periods. All of the cylinders that were treated early with silane also did not have any map-cracking (Bérubé et al. 2002a). There was a net moisture weight loss in the specimens after the silane was applied, whether it was late or early application, as shown in Figure 2.11 (B).

A visual comparison of an unsealed cylinder versus a silane-sealed cylinder after 1.5 years of exposure cycle C4 is shown in Figure 2.12. It is very apparent from this figure that the silane prevented damage to the cylinder.

Bérubé et al. (2002a) also found that the internal humidity after one year of a silane-sealed and non-expansive specimen was 86 percent relative humidity in the center and 81 percent near the surface versus a 95 percent relative humidity at the center and 96 percent relative humidity near the surface of an unsealed and expansive cylinder in the same exposure conditions. "This

suggests in turn that "internal" humidity conditions over 80 to 85 percent are necessary for ASR expansion" (Bérubé et al. 2002a).

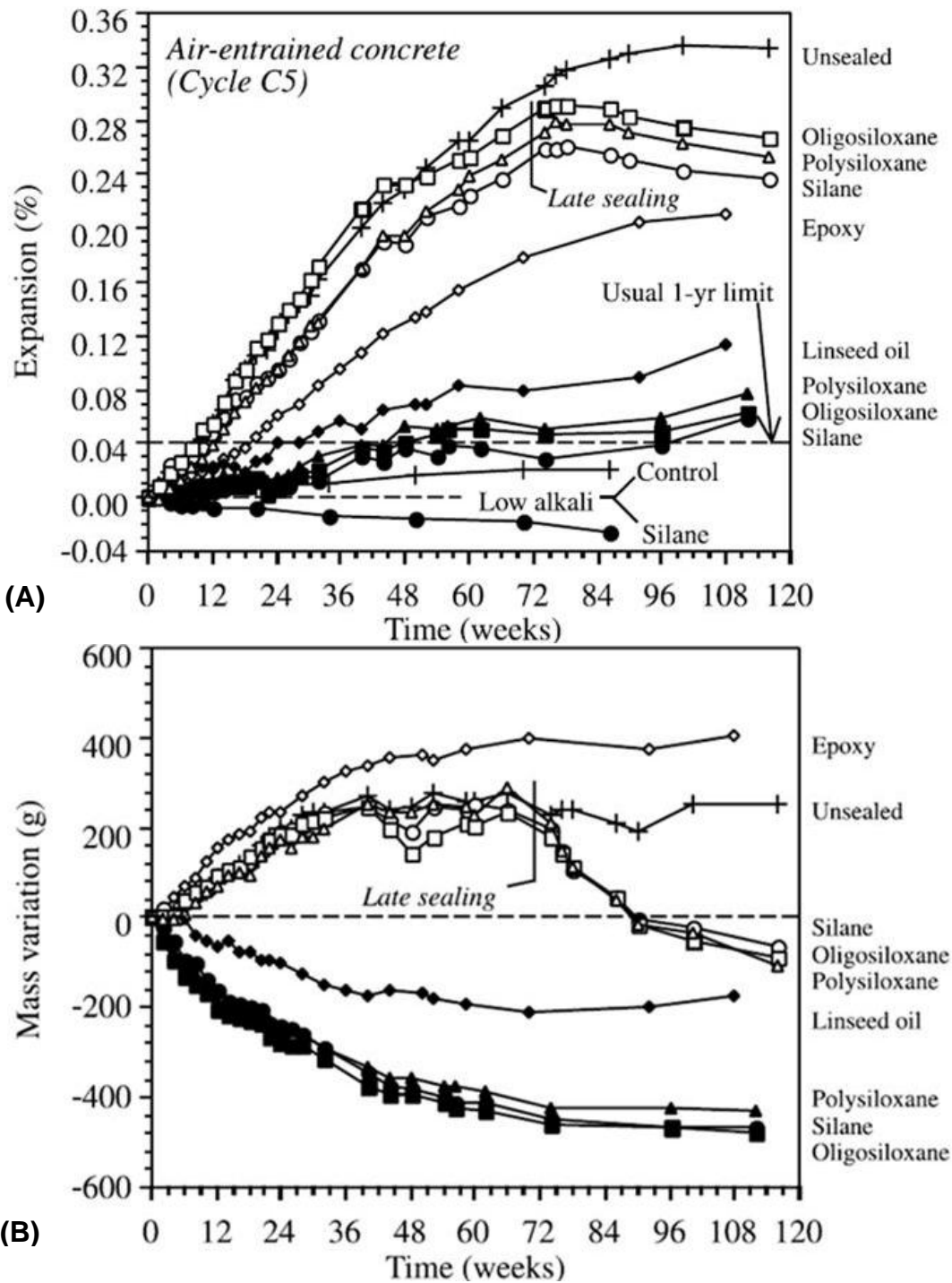


Figure 2.11. (A) Expansion and (B) cumulative mass variation for air-entrained concrete cylinders subjected to exposure C5 (Bérubé et al. 2002a)



Figure 2.12. (A) Unsealed and (B) silane-sealed air-entrained concrete cylinders subjected to exposure cycle C4, after 1.5 years

(Adapted from Bérubé et al. 2002a)

This test has proven that the use of silane and other sealers is capable of preventing and mitigating ASR effects in thin, 10 inch (255 mm) for this test, concrete members subjected to very severe environmental exposure conditions. Good sealers should work even better in preventing ASR damage in thinner concrete members because the members are more permeable and have more deficient air void systems. But Bérubé et al. (2002a) say that "it is unlikely that a good sealer can reduce ASR expansion of massive concrete members; however, it should reduce the development of cracking on the surface of such members, by reducing the deleterious effects of all exposure conditions such as wetting and drying cycles, freezing and thawing cycles, sea water and deicing salt."

2.6.2.7 Effectiveness of Silane for Mitigation of ASR in Highway Barriers

A follow-up study to the previously discussed sealer testing on concrete cylinders subjected to various exposure conditions, in section 2.6.2.6, was done. This follow-up used the three best sealers from the cylinder testing: silane, oligosiloxane, and polysiloxane, and applied them to highway median barriers that had different degrees of ASR-related deterioration. These barriers naturally experienced different exposure conditions such as wetting and drying, freezing and thawing, and, deicing salt (Bérubé et al. 2002b).

As with the previous study with cylinders, the silane performed the best on the highway median barriers. The effectiveness of the silane at preventing map-cracking on the barrier surface is shown in Figure 2.13, and the relative humidity for each barrier from three to six years after sealing with silane is graphed in Figure 2.14.

It is clear from Figure 2.14 that the silane-sealed concrete sections have a much lower relative humidity than the unsealed sections. The humidity in the sealed concrete section converged with the unsealed section at Montmorency, as shown in Figure 2.14 (A); this would indicate that the maximum effectiveness of the silane was within the first three years after sealing. But the graph for Sainte-Foy in Figure 2.14 (B) has a diverging trend, indicating that the silane's maximum effectiveness still had not been reached at the end of six years after sealing. The maximum effectiveness time ranges for the two locations may be justified by the fact that the concrete at Montmorency was initially deteriorated much worse than at Sainte-Foy (Bérubé et al. 2002b).

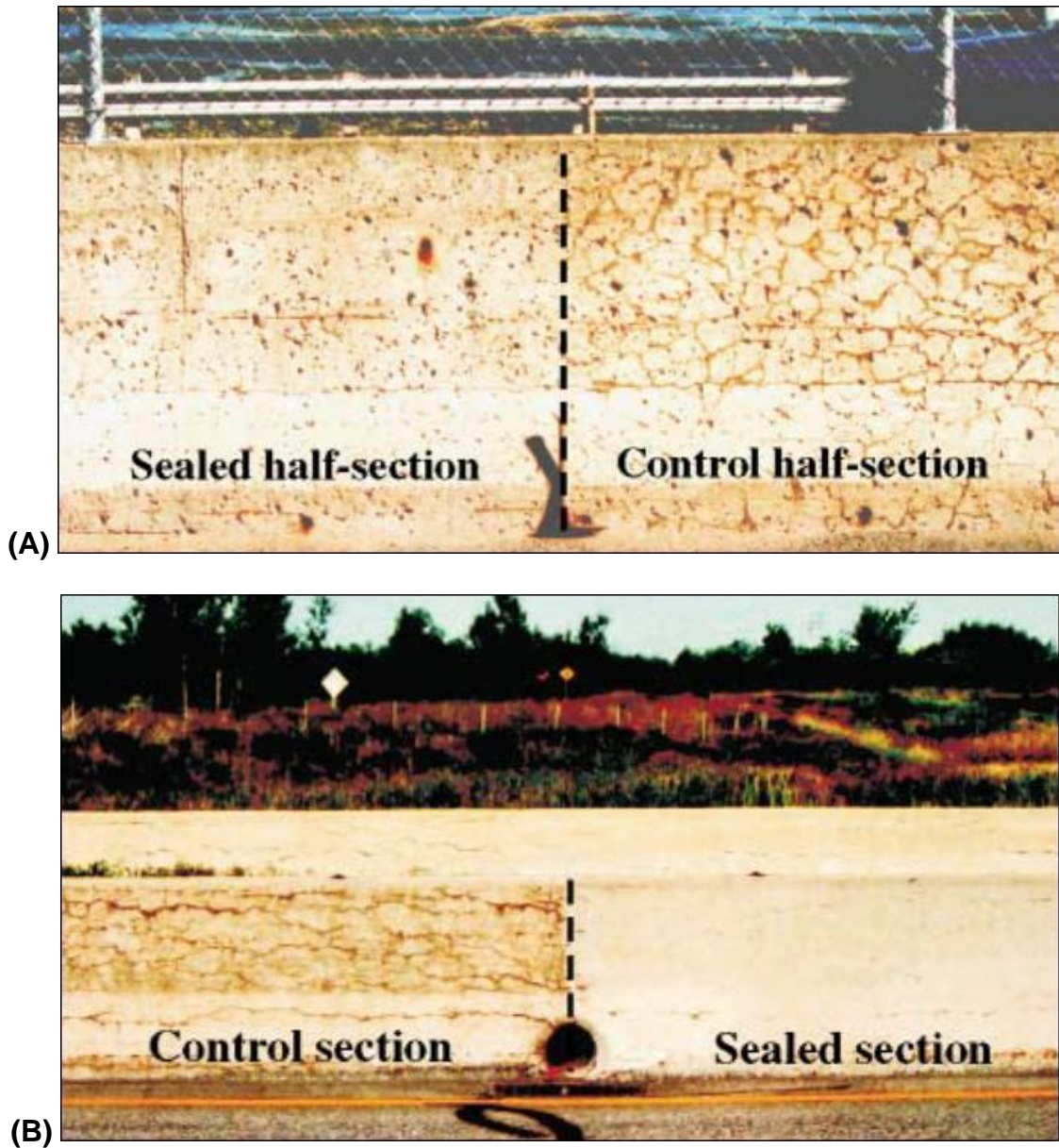
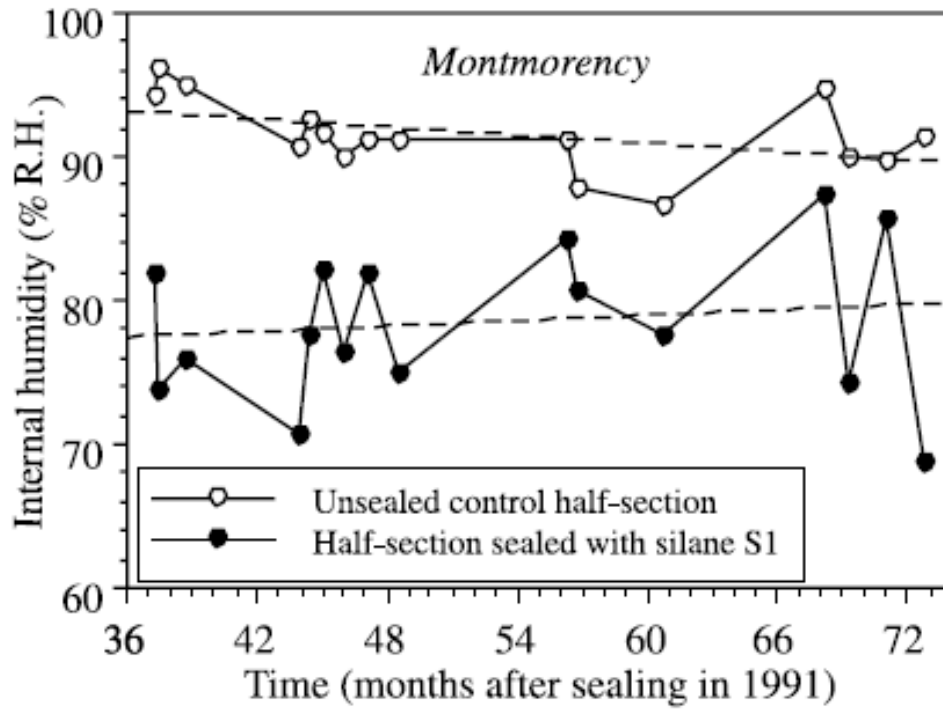
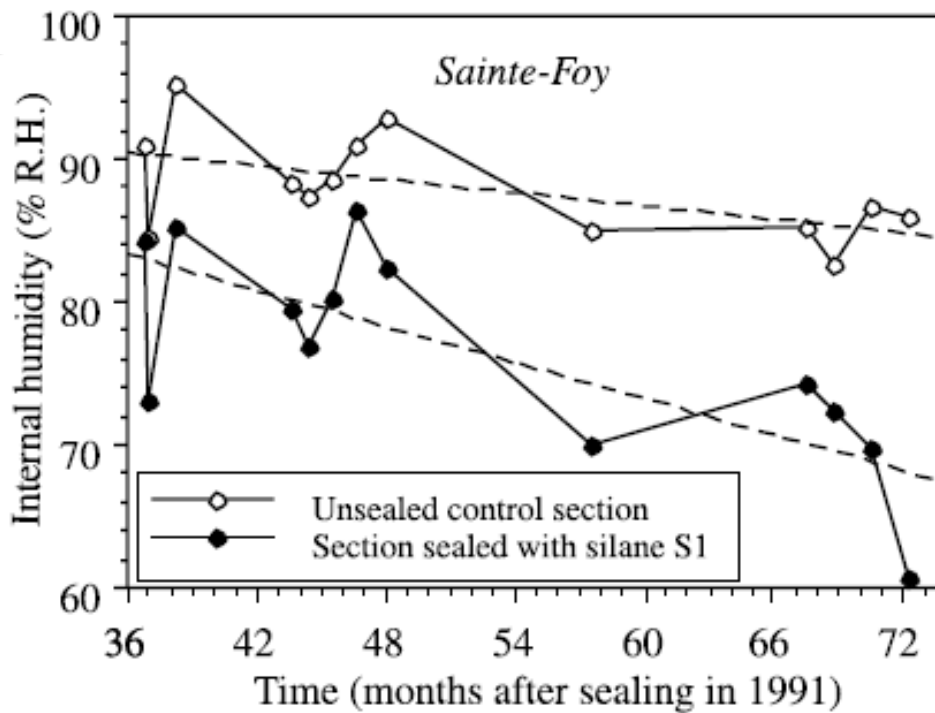


Figure 2.13. Comparison of unsealed versus silane-sealed, for 3 years, on highway median barriers in (A) Montmorency and (B) Sainte-Foy

(Bérubé et al. 2002b)



(A)



(B)

Figure 2.14. Internal relative humidity from 3 to 6 years after silane-sealing highway median barriers in (A) Montmorency and (B) Sainte-Foy

(Bérubé et al. 2002b)

Bérubé et al. (2002b) draw the conclusion that “the higher the degree of deterioration due to ASR at the time of sealing, the shorter seems to be the period of maximum effectiveness of a good sealer.” It was also concluded that silane greatly improved the aesthetics of the barriers for the 10-year study, and the silane was able to stop concrete expansion and even cause contraction for at least six years (Bérubé et al. 2002b).

2.6.2.8 Ineffectiveness of Silane on Piers of the Hanshin Expressway

Silane was applied to the severely cracked piers of the Hanshin Expressway in Japan. The cracks were first pressure injected with epoxy resin. Second, coatings of either an epoxy resin or silane were applied; followed by a coating of polymer cement paste for cosmetic reasons. After four years of monitoring, it was determined that the repair was not successful in controlling the expansion of the piers due to observations of additional crack widening (Hobbs 1988).

2.6.3 Lithium

Early treatment of ASR with lithium used lithium hydroxide, but lithium nitrate solutions are now preferred due to their neutral pH, ease of handling, and better penetration rates. Topical application of lithium, shown in Figure 2.15, has been the most common method of application, especially in pavements and bridge decks. The application rate is important to prevent runoff and ponding that may evaporate; an application rate of 4 to 10 gallons per 1000 square feet is optimal for most cases. (Fournier et al. 2004)

Research on the penetration depths of sufficient amounts of lithium with various application techniques has been performed and documented by Folliard

et al. (2009). They determined that a concentration of 100 ppm in pore solution would approximately be sufficient to suppress excessive expansion due to ASR. The mechanism for lithium suppression of ASR is not fully understood, but “it is generally believed that lithium compounds enter into the existing gel and change the nature and behavior of the gel from expansive to essentially non-expansive” (Fournier et al. 2010). There are three different application techniques for lithium used: topical application, vacuum impregnation, and electrochemical impregnation; the latter two methods are aimed at increased penetration depths (Folliard et al. 2009; Fournier et al. 2010).



Figure 2.15. Topical application of 30% lithium solution to concrete pavement
(Folliard et al. 2009)

2.6.3.1 Topical Application of Lithium Nitrate

Folliard et al. (2009) tested the lithium penetration depths using topical applications, as shown in Figure 2.15, of 30 percent lithium nitrate solution with up to three coatings on I-84 outside of Boise, Idaho. In order to determine the penetration depth, cores were taken from the pavement and increments of 0.04 in. (1 mm) sections were removed from the top of the core at a time to be tested

for their lithium concentration. It was found that only the upper 0.16 in. (4 mm) contained sufficient amounts of lithium, over 100 ppm, to suppress ASR expansion, and this was consistent with laboratory treatments of pavement sections from the same location and laboratory-produced concrete. Figure 2.16 contains a graphical representation of the lithium concentrations versus depth, and it can be seen in this figure that concentrations of greater than 100 ppm are only within the top 0.16 inches of the concrete. Because of only reaching a few millimeters into the concrete, topical applications of lithium nitrate do not appear to be sufficient enough to suppress future expansion and cracking caused by ASR (Folliard et al. 2009).

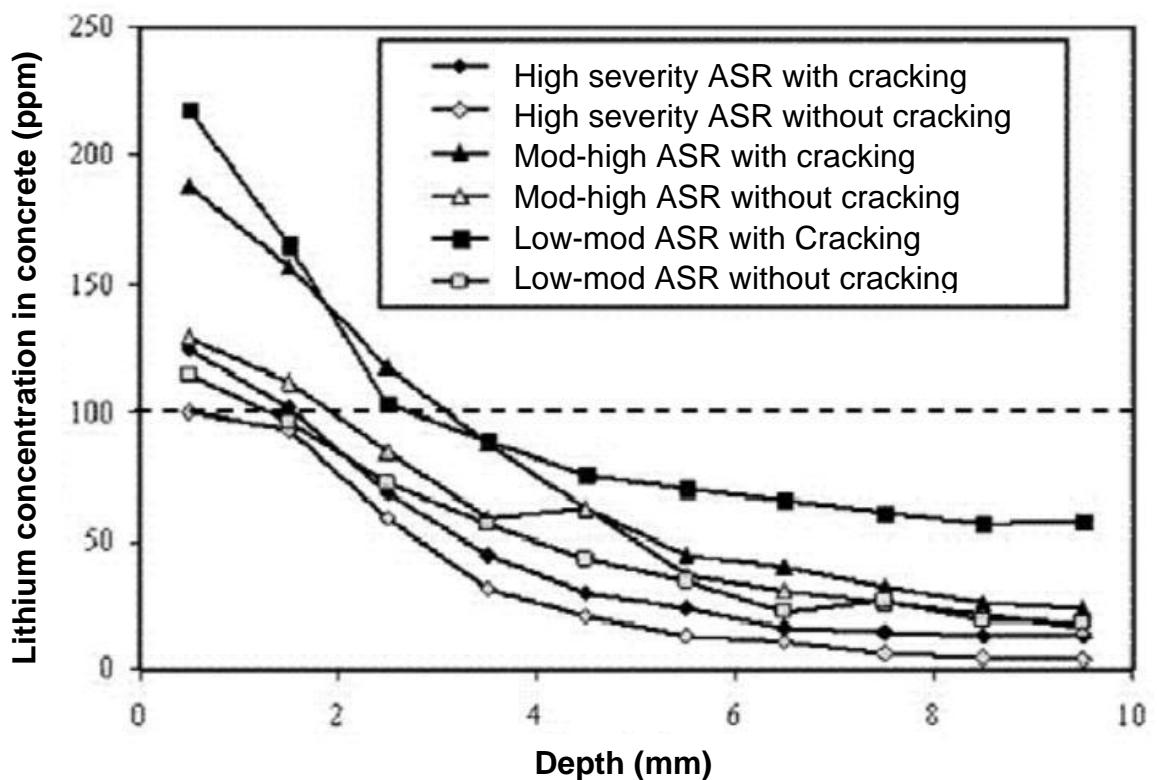


Figure 2.16. Depth of lithium penetration with topical application on I-84

(Adapted from Folliard et al. 2009)

2.6.3.2 Vacuum Impregnation of Lithium Nitrate

ASR-affected highway barriers outside of Boston, Massachusetts and Bridge Columns in Houston, Texas were chosen for testing the penetration depths of lithium applied via vacuum impregnation. Cores were taken from both of the structures and tested in the same manner as the pavement cores from I-84 discussed in the previous section. The penetration depths of sufficient amounts of lithium in the barriers and columns were 0.08 to 0.16 in. (2 to 4 mm) and 0.31 to 0.39 in. (8 to 10 mm), respectively. These depths are graphed in Figure 2.17 and Figure 2.18. Although these depths are greater than topical application, it is not yet known if these depths are deep enough to help mitigate ASR effects, and if the additional costs and complexity in vacuum impregnation are justified (Folliard et al. 2009).

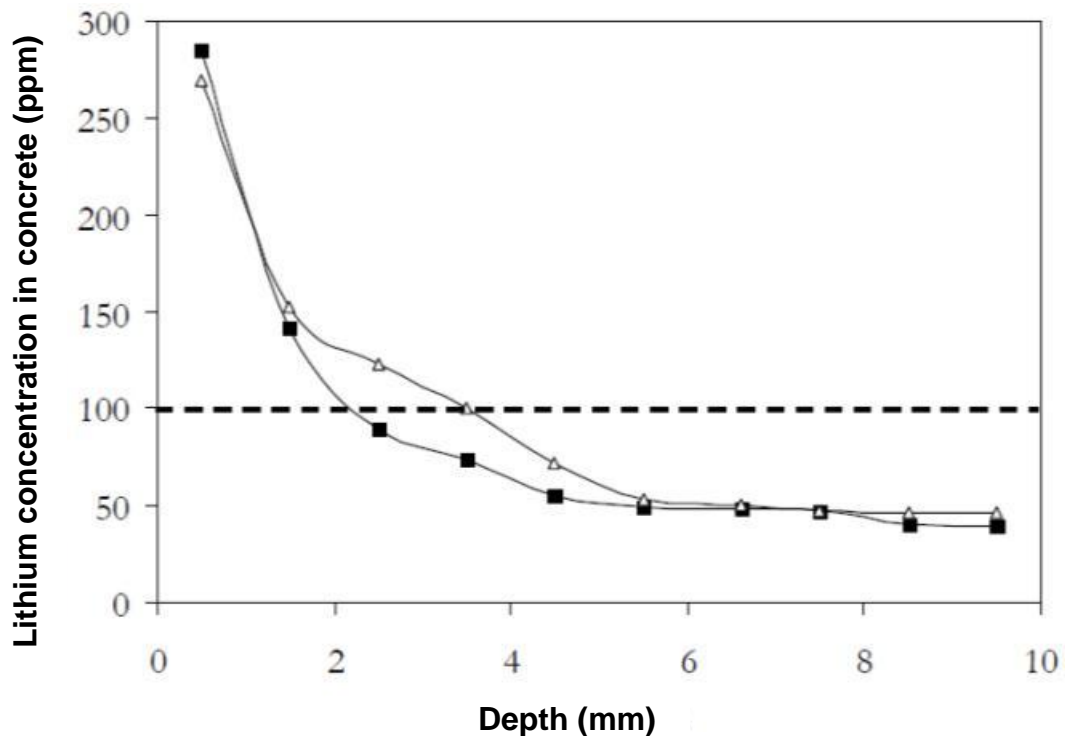


Figure 2.17. Depth of lithium penetration with vacuum impregnation on barrier

(Adapted from Folliard et al. 2009)

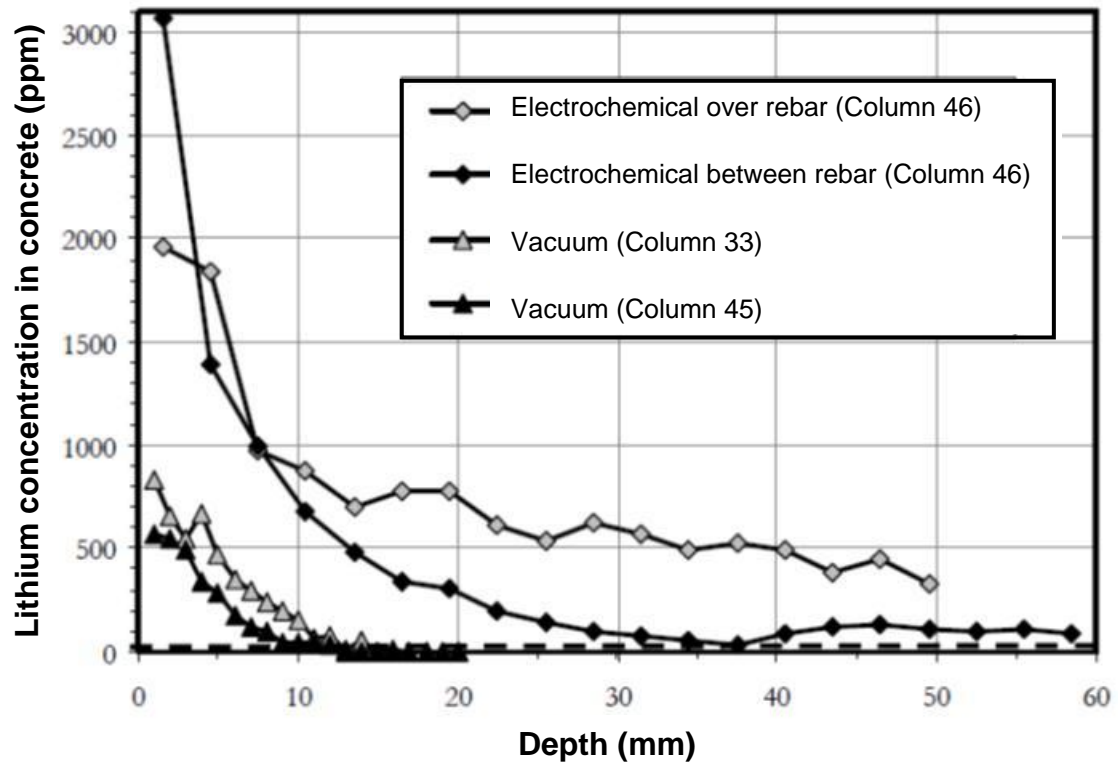


Figure 2.18. Depth of lithium penetration on columns with vacuum impregnation and electrochemical impregnation (adapted from Folliard et al. 2009)

2.6.3.3 Electrochemical Impregnation of Lithium Nitrate

Electrochemical impregnation of lithium shows the most promise for mitigating ASR of all the application methods tested. As shown in Figure 2.18, sufficient lithium concentration depths are reaching the reinforcement steel at 2 inches (50 mm) and beyond. A side effect of using electrochemical impregnation of lithium to suppress ASR is that it has the potential to increase ASR around the reinforcing steel as explained in the following by Folliard et al. (2009):

It was also found that internal alkalis (sodium and potassium) were drawn to the surface of the steel because the steel serves as a

cathode in the electrochemical process, resulting in the formation of hydroxyl ions. As such, it is possible that ASR may be exacerbated in the concrete adjacent to the reinforcing steel, due to the local increase in hydroxyl, sodium, and potassium concentrations. More research is needed to determine if the potential benefits of increased lithium penetration outweigh the potential negative effects of increased pore solution pH near the imbedded reinforcing steel.

2.6.4 Crack Injection

Cracks in ASR-affected concrete members are often filled with a cement grout or epoxy resin to prevent water from easily penetrating into the member; this is commonly done before applying a waterproofing or water repellent agent. Fournier et al. (2004) and (2010) stated that the injection of a flexible grout or caulk may be more effective than rigid epoxy resins for preventing leakage through cracks in concrete that are still expanding due to AAR.

2.6.5 Cladding

Fournier and Bérubé (2000) stated that improved drainage with the use of ventilated cladding can drain water away from the affected concrete and may reduce moisture ingress in small cross sections, thus allowing the concrete to dry. It is still important to realize that the moisture within the concrete will continue to supply the reaction; therefore, the potential for differential growth between the ASR-affected concrete and integral cladding must be accounted for (CSA 2000).

Cladding was one of the elements applied to the Montrose New Bridge in Montrose, Scotland in an attempt improve drainage and mitigate ASR.

Construction of the bridge was completed in 1930, and the ASR mitigation and repair work was done in 1994. Wood and Angus (1995) explain the cladding portion of the mitigation procedure as follows:

To reduce frost action and slow the rate of further AAR damage, the larger cracks in the tower top area were sealed with epoxy, and covers were fitted over the tower top and top chord to provide ventilated cladding, which minimizes water ingress and permits the drying of concrete, unlike coatings which can trap moisture.

Figure 2.19 is a picture of the repair done on the Montrose New Bridge.

This image shows the cladding on the top chords along with confining straps and plates at the top of the tower. However, it is important to know that the Montrose New Bridge was removed in 2004 due to continued problems caused by internal decay (Canmore 2013).



Figure 2.19. Montrose New Bridge repair with confinement and cladding
(Fournier et al. 2004)

2.6.6 Confinement of Expansion

Numerous studies and field trials show that physically restraining concrete will significantly reduce the deleterious expansion caused by ASR. The restraint may be applied by encapsulation of the affected member by a nonreactive concrete, applied stress in one or two dimensions with post-tensioning, or reinforcement (Fournier et al. 2004). No firm guidelines are available for the process of confining a structure because every structure is different; therefore, structural engineers are required for the process. Fournier et al. (2010) explains the necessity for a structural engineer to be involved in the process of confining a structure:

Because of the unique nature of this mitigation approach and the fact that the structural response is impacted, it is imperative that a structural engineer play the leading role in specifically designing the

methodology for a given ASR-affected structure. A detailed structural evaluation is essential, and care must be taken to select and implement this type of mitigation option.

Along with cladding that was discussed earlier, the Montrose New Bridge also required strengthening. The bridge was effectively strengthened and confined in the ASR-affected regions by reinforcing straps and steel plates with tensioned through bolts as shown in Figure 2.19 (Wood and Angus 1995). It is important that sufficient reinforcement is used with encapsulation to control the stresses due to ASR expansion. Without sufficient reinforcement, the main benefit from the encapsulation may be to limit moisture ingress (CSA 2000).

CSA (2000) states that "confinement of concrete, by post-tensioning in one or two dimensions or by encasement by conventional reinforced concrete, probably must be restricted to small masses of structural concrete, because of the high range of potential expansive pressures that characterizes the alkali-silica reaction." Pressures in the order of 500 to 580 psi (3.5 to 4.0 MPa) have been suggested for confining of ASR in concrete, but up to 2030 psi (14 MPa) have been measured in high-alkali mortars (CSA 2000).

2.6.6.1 Confining ASR Expansion with Carbon Fiber Reinforced Polymer

The benefits of using carbon fiber reinforced polymer (CFRP) over traditional methods of adding additional reinforcement and strength to structures are explained in the following by Yang et al. (2010):

Externally bonded CFRP composites are an excellent tensile reinforcement for structural repairs, strengthening, and

rehabilitation of concrete bridge members. They offer exceptional mechanical properties, simplicity and flexibility of installation. CFRP composites can reduce user costs, measured in terms of road closures and delays, which traditional reinforcement and repair methods cannot offer.

The Texas Department of Transportation (TxDOT) applied CFRP wraps to circular columns of a bridge that were experiencing high levels of expansion and cracking due to ASR. Yang et al. (2010) explains the process of mitigating the columns with CFRP wraps and cost associated with this procedure. This project was the first time that TxDOT used CFRP to confine ASR expansion, and the petrography reports indicated that the ASR could generate swelling pressures of up to 500 psi. CFRP was applied to the columns in two directions to confine the expansion and strengthen the member. Circumferential CFRP wraps were used to provide the primary hoop confinement, and vertical strips were used to provide secondary longitudinal reinforcing. This project took 45 days to complete in 2003 and cost \$258,868 to confine 6,225 square feet of concrete with CFRP. The bridge was closely monitored in the following years, and there was no sign of new cracking as of 2009 (Yang et al. 2010).

2.6.6.2 Study of Applied Stress in One Direction

Research was conducted at the University of London to study the effects of stressing concrete blocks affected by ASR at different stress levels (Rigden et al. 1992). For this study, three unreinforced concrete blocks, 19.7 inches (Y) by 19.7 inches (Z) by 7.87 inches (X) (500 mm by 500 mm by 200 mm), were made and

stressed in the Y direction with oversized, end plates and external, threaded rods to 1160, 580, and 0 psi (8, 4, and 0 MPa). A schematic of the post-tensioning setup is shown in Figure 2.20. These blocks were then placed in water at 100 °F (38 °C) for one year in order to accelerate the expansion and cracking due to ASR, and the rods were tightened throughout this period to account for creep effects.

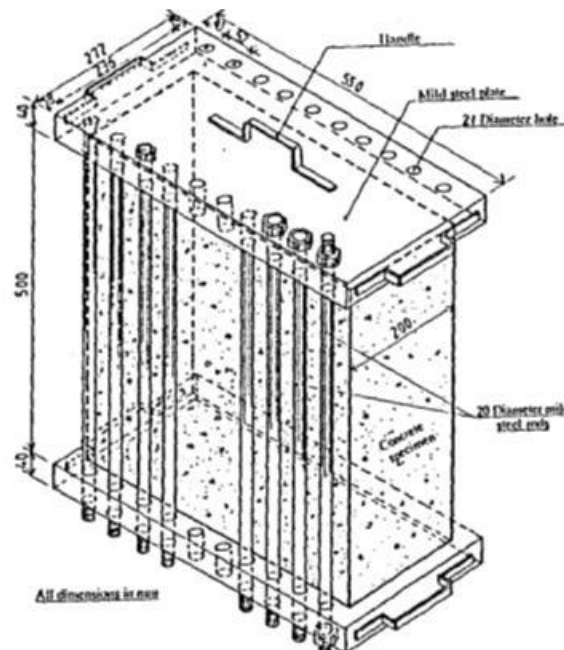


Figure 2.20. Setup for concrete blocks being stressed in one direction
(Rigden et al. 1992)

The cracking that formed in the concrete had similar crack patterns as described previously in the surface cracking section of this literature review. The block without any stress exhibited map cracking as expected, and the 2 blocks that were stressed had crack patterns that were parallel to the direction of applied stress, with the 1160 psi block having more closely spaced cracks. Expansions of the concrete were also measured, and it was found that the unstressed block had roughly equal expansions in all directions. The stressed

blocks had significantly less expansion in the direction of stress when compared to the Y-axis of the unstressed block and to the other directions of the stressed blocks. The 1160 psi stress direction had the least expansion, and the most expansion was in the narrower dimension perpendicular to the stress. The modulus of elasticity and compressive strength of the concrete also varied depending on the stress level and the orientation of the concrete sample with respect to the direction of stress as shown in Table 2.5.

Table 2.5. Average modulus of elasticity and compressive strength for directional cores taken out of blocks stressed in Y direction

(Adapted from Rigden et al. 1992)

	1160 psi Block			580 psi Block			Unstressed Block		
Core Direction	Y	X	Z	Y	X	Z	Y	X	Z
E (ksi)	3340	2120	1650	3100	2510	2290	2760	2490	2220
E (GPa)	(23.0)	(14.6)	(11.4)	(21.4)	(17.3)	(15.8)	(19.0)	(17.2)	(15.3)
f_c (psi)	4050	2990	2700	3860	3380	3340	3710	3630	3440
f_c (MPa)	(27.9)	(20.6)	(18.6)	(26.6)	(23.3)	(23.0)	(25.6)	(25.0)	(23.7)

The modulus of elasticity and the compressive strength of the concrete affected by ASR increased in the direction of stressing as the stress magnitude was increased, but compressive strength of the cores went down as much as 21 percent in the directions orthogonal to the applied stress as the stress magnitude increased. Unlike the compressive strength, the modulus of elasticity was only detrimentally affected in the orthogonal directions for the 1160 psi stress block;

the 580 psi stress block and unstressed block had almost identical elasticities in the X and Z directions.

From this study, it was concluded that "high levels of preload will increase the amount of damage recorded in the directions perpendicular to the uniaxial stress direction and decrease the amount of damage recorded in the direction of the uniaxial stress" (Rigden et al. 1992). Pantazopoulou and Thomas (1999), speaking in regards to this study, say that a concrete member must be restrained in three-dimensions; otherwise, any unrestrained directions will expand so as to maintain the overall volume of free expansion.

2.6.6.3 Prestressing of Bridge Piers Suffering from AAR

Le Roux et al. (1992) discussed experimental testing on cores taken from AAR-affected bridge piers, located near Paris, France, and how different levels of prestressing will affect the expansion of the concrete. The piers were experiencing horizontal deformations of 400 μ strains/year (0.4 mm/m/year), and transverse prestressing of the members was considered as a viable option to stop expansion. In order to determine the level of prestressing required, testing was performed on suitably oriented cores taken from the piers and stressed to 0, 145, 435, and 725 psi (0, 1, 3, and 5 MPa).

Surface cracking due to AAR was present on the piers. With this being a reinforced and loaded structure, the main cracking followed the longitudinal reinforcement and load direction. The vertical cracks ranged from 0.01 to 0.12 inches (0.3 to 3 mm) in width and the horizontal cracks were much smaller, with a maximum crack width of 0.02 inches (0.6 mm).

For the experimental testing, the cores were uniaxially stressed to the desired levels previously stated, and then submerged in tap water at about 68 °F (20 °C) for 378 days; expansion readings were taken at various time intervals during this period. The expansion results for the cores are shown in Figure 2.21, and it is clear that confining the ASR-affected concrete greatly reduced the expansion compared to the unconfined concrete. A uniaxial stress of 725 psi (5 MPa) was sufficient for eliminating most of the longitudinal expansion in the ASR-affected concrete core.

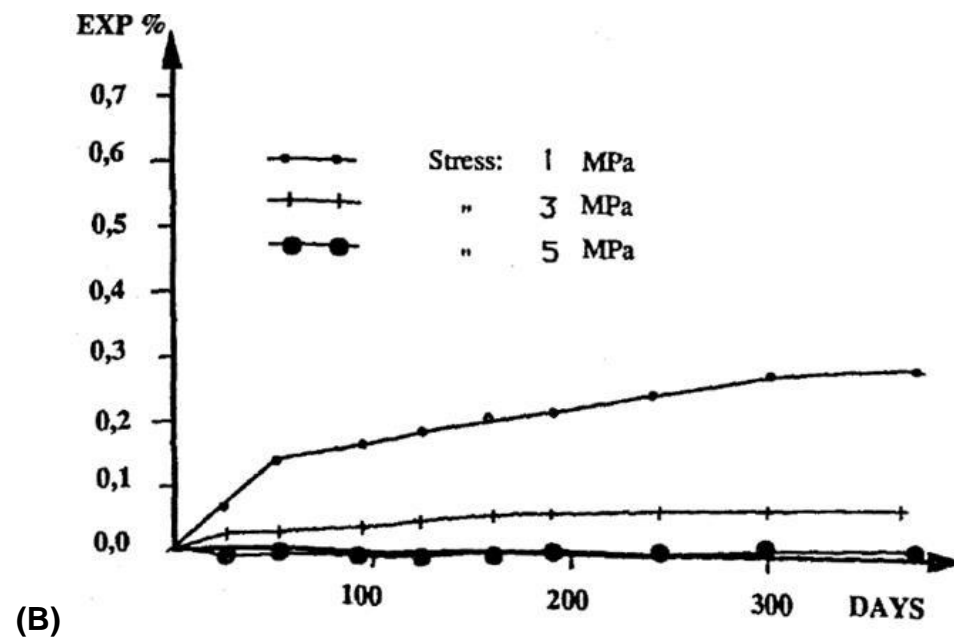
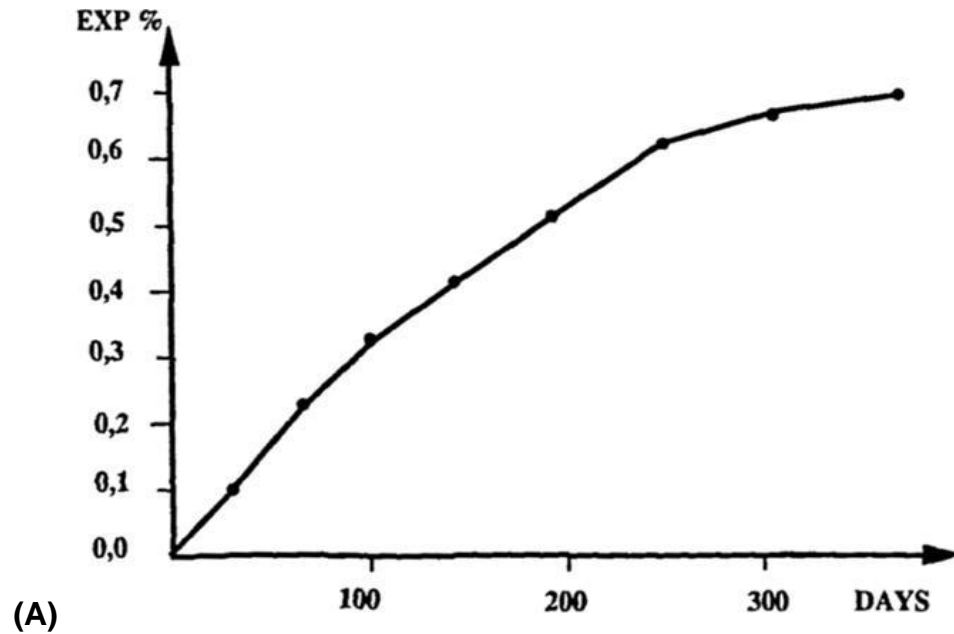


Figure 2.21. Longitudinal expansion of cores taken from bridge pier and submerged in tap water, (A) core free to expand and (B) uniaxial stress applied to cores (Le Roux et al. 1992)

2.6.7 Slot-Cutting

Slot-cutting is an approach that relieves stress buildup due to ASR, but this may only be a temporary solution for structures where ASR expansion has not

terminated. Slot-cutting provides space for future expansion and this temporarily relieves the development of stress due to ASR. Re-cutting may be necessary as ASR expansion continues further, thus increasing the rehabilitation costs. It is also important to note that slot-cutting will change the internal stress distributions; therefore, additional reinforcement may be required (Fournier et al. 2004).

2.6.8 Mitigation Summary

Fournier et al. (2010) provides a table that summarizes all of the mitigation procedures previously discussed in this literature review; an adapted version of this table is shown in Table 2.6.

Table 2.6. Summary of mitigation options for transportation structures (Adapted from Fournier et al. 2010)

Mitigation Measure	Applicability to Specific Structure	Positive Attributes of Mitigation Measure	Negative Attributes of Mitigation Measure	Other Relevant Information
Improved drainage and enhanced maintenance	All structures benefit from less contact with water. Obvious benefits where drainage problems exists.	Water is essential to ASR expansion. RH below 80% stops ASR expansion.	May not be effective when source of moisture is below or behind structure.	Should be included in overall management strategy, due to high benefit/cost ratio.
Application of penetrating sealers (silanes, etc.)	Most applicable to bridge structures, highway barriers, etc.	Proven to reduce RH in lab and field tests. Best when element is easily accessible and not in direct contact with moisture.	Benefits may not be seen when element is directly or permanently exposed to moisture. (Need dry cycles for RH to decrease).	Must apply to dry surface. Typically need to re-apply every 5 years, possibly sooner. Sealer must be breathable.
Application of cladding	Applicable to certain bridge elements.	Can be effective in reducing ASR if concrete below is not saturated and able to sustain ASR.	Can trap moisture and difficult to inspect element underneath cladding.	Should take measures to dry out concrete before applying cladding.
Application of lithium compounds	Applicable to certain bridge elements and pavements	Has suppressed ASR in small lab specimens. Electrochemical methods increase penetration depth.	Effectiveness in topical and vacuum application is minimal, due to lack of penetration. Electrochemical methods cause K^+ and Na^+ to migrate to steel, possibly exacerbating ASR there.	Although optimistic results have been found in lab, it remains experimental in field applications, due to lack of monitoring/documentation proving its long-term efficacy.
Crack filling	Applicable to most structures	Flexible caulking or crack fillers work best. Can be effective in reducing ingress of water and Cl.	Only provides benefit in slowing ingress of water, chlorides, etc. No restoration of structural integrity.	Flexible caulking is especially beneficial when crack widths are large and the structure is still expanding.
Application of restraint to confine/strengthen structure	Most applicable to columns (especially circular).	Sufficient confinement can help manage stress generated by ASR. Can use FRP, internal/external reinforcement, etc.	Difficult to confine many structural elements (e.g., square columns). Qualified structural engineer required to design and implement.	Qualified structural engineer must design and implement, and they must monitor subsequent strains to ensure mitigation is safe and effective.
Saw cutting/slot cutting	Most applicable to pavements and bridge decks (at joints)	Can help accommodate stresses and joint-related failures.	Does not address cases of ASR, and in fact, allows it to continue unimpeded.	Must ensure proper joint details when removing concrete near joints of pavements or decks.

2.7 Predicted Time to Reach 80 Percent Relative Humidity in the Bibb Graves Bridge

Times required for the relative humidity in the Bibb Graves Bridge to decrease to 80 percent were predicted with the use of finite element analysis by Warnock (2012). The moisture diffusion analysis was actually performed as a heat transfer analysis by relating the following moisture and thermal properties: diffusion coefficient as the isotropic conductivity, specific gravity of water as the density, and saturated moisture content of the concrete as the specific heat.

The finite element analysis was done using ANSYS 12.0 on a 24 by 48 inch concrete arch cross section that was made of 1 inch by 1 inch four-node elements, as shown in Figure 2.22. This analysis was performed with an upper and lower concrete strength of 3,250 and 2,000 psi in compression. These two strengths were chosen based on the in-situ concrete strengths that were determined for this bridge, as discussed in Chapter 3. The models with both of these compressive strength values were run twice to simulate (a) a silane only treated section and (b) a silane plus epoxy flood coat treated section. Because the model does not simulate rain effects, the silane only section did not have any modifications made to the surface of the concrete in the model. Additionally, to simulate the epoxy flood coat, the top boundary condition was defined so that no moisture could diffuse out of it.

1
ELEMENTS
MAT NUM

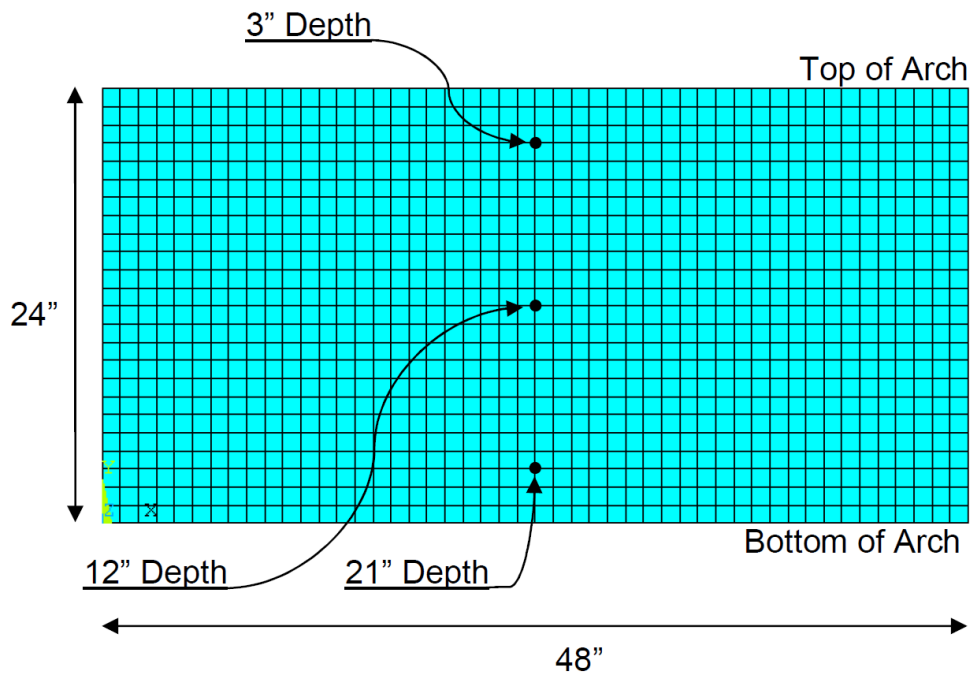


Figure 2.22. Arch cross section modeled in ANSYS (Warnock 2012)

The moisture diffusion coefficients for the different concrete strengths are not constant. These coefficients are highly dependent on the internal relative humidity of the concrete among other variables, as shown in Figure 2.23. The ambient relative humidity, which is the driving force for the diffusion process, was also varied monthly in the modeling based on a 30-year monthly average for Montgomery, Alabama.

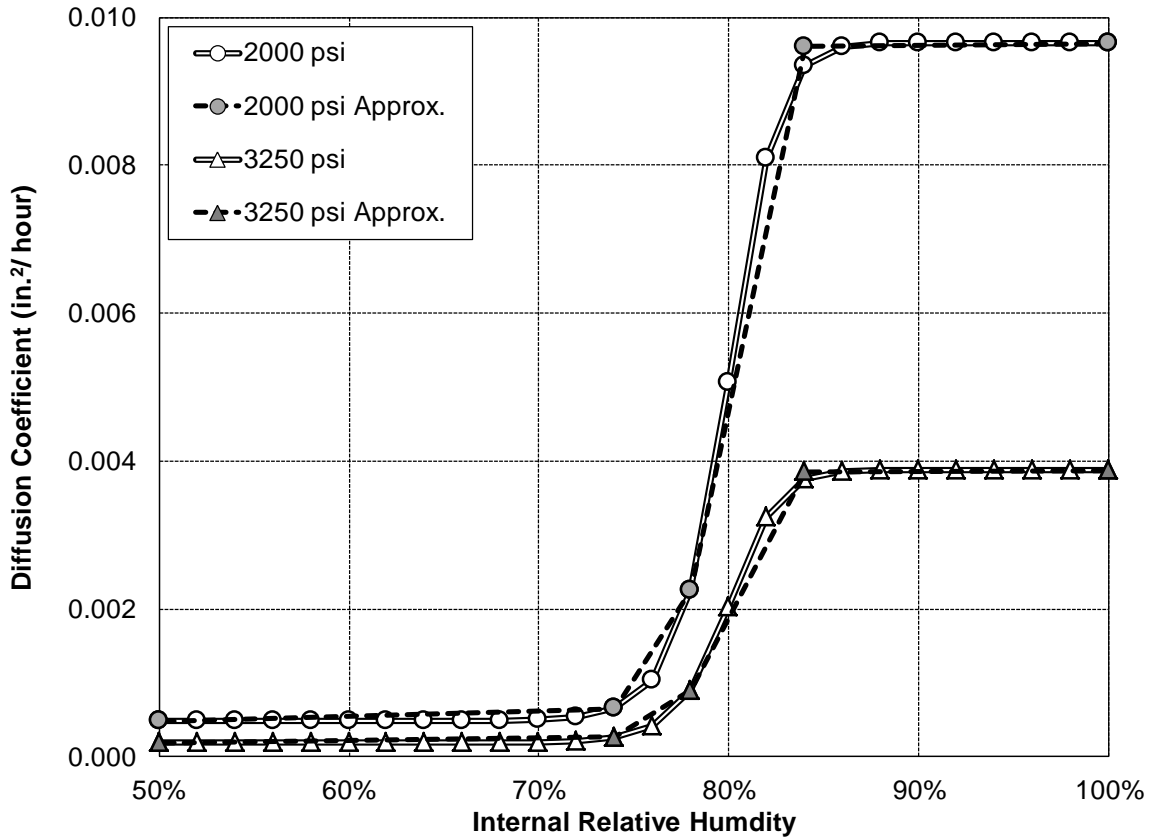


Figure 2.23. Multilinear approximation of the moisture diffusion coefficient
(Adapted from Warnock 2012)

The finite element analysis of the moisture diffusion started at 95 percent relative humidity and was carried out to 14 years with automatic time steps. A minimum step of 24 hours and maximum step of 1 week were assigned to the model. The results of the moisture diffusion model are shown in Figure 2.24. Figure 2.24 (A) is for the section that represented silane only, and Figure 2.24 (B) is for the section that had top boundary conditions to simulate epoxy by not allowing diffusion through that side. The depths shown in these figures are taken from the top of the 24-inch thick cross section.

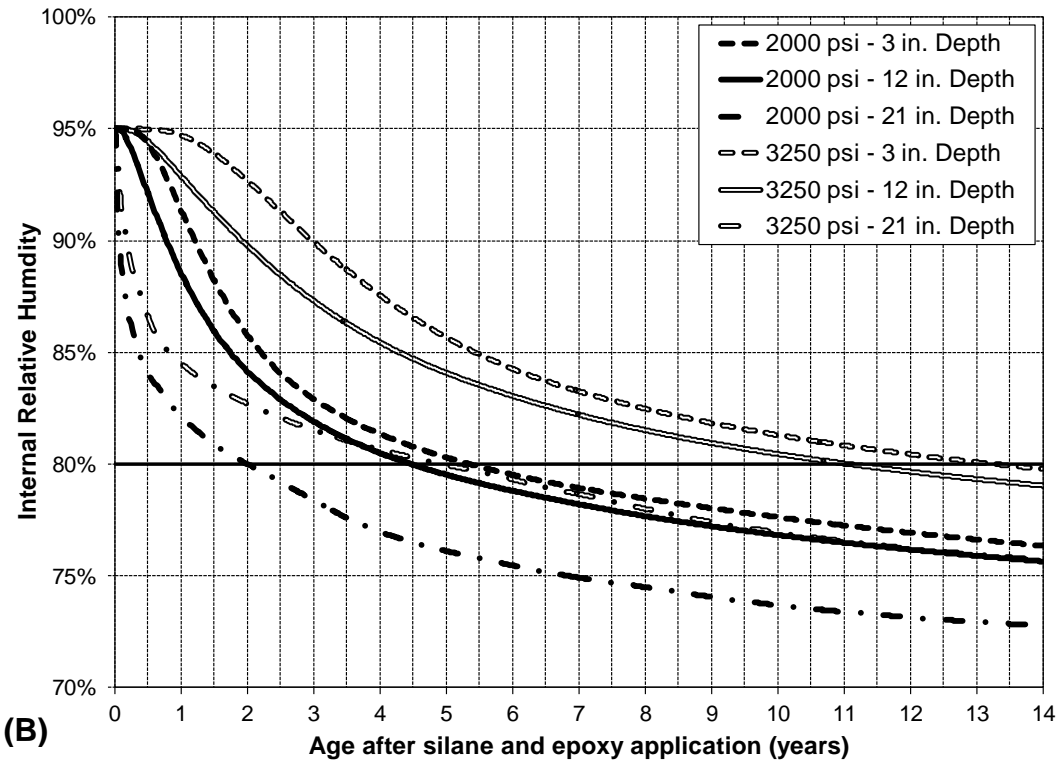
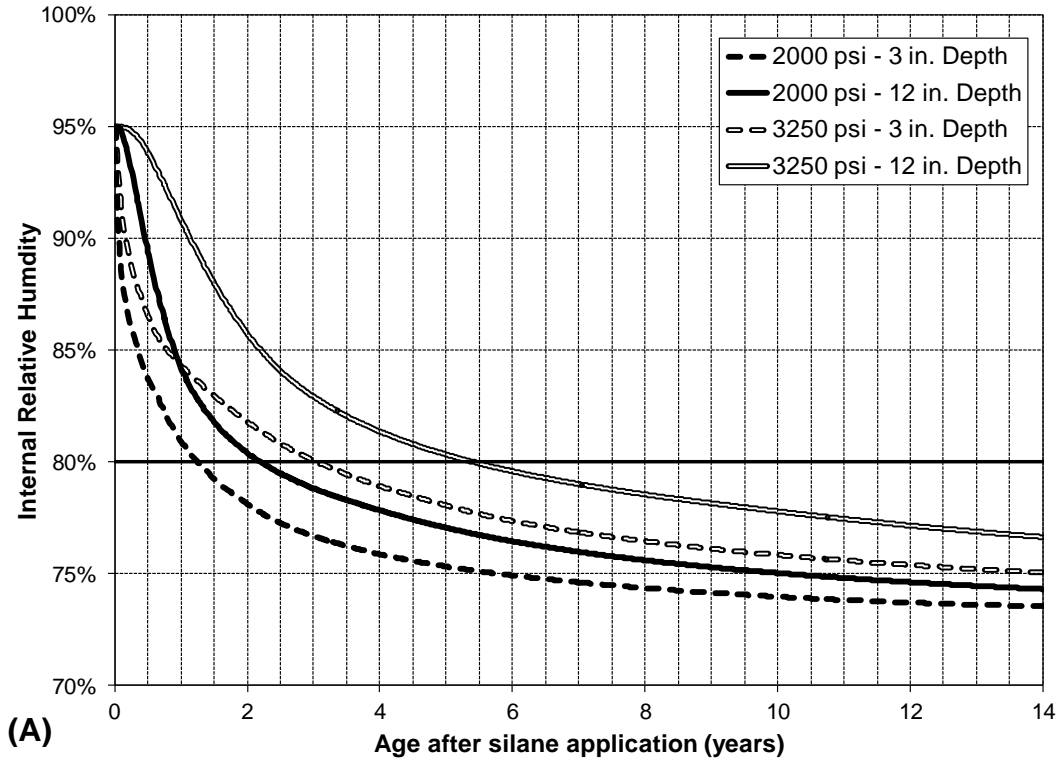


Figure 2.24. RH versus time for (A) silane only and (B) silane and epoxy

(Adapted from Warnock 2012)

For the silane only model, the relative humidity should be below the 80 percent threshold for the 3-inch depths within three years, as shown in Figure 2.24 (A). And the relative humidity will be below 80 percent for the center of the 3,250 psi section after five and a half years. These results should be below the actual drying times seen in the field because of the epoxy flood coat on the top of the arches. When the epoxy was applied to the model, the arches dried out from the bottom up; therefore, the bottom of the arch is the first to reach 80 percent humidity and the top of the arch is the last to reach 80 percent humidity, as shown in Figure 2.24 (B). In this graph, the bottom of the low strength concrete will reach 80 percent humidity in 2 years, and the top of the 3,250 psi concrete will not reach 80 percent humidity until almost 14 years.

2.8 Summary

In review, ASR is a form of AAR and it is a deleterious chemical reaction that can cause expansion within concrete having the following conditions (Fournier and Bérubé 2000):

1. Reactive forms of silica in the aggregate
2. Sufficient alkali, primarily from the cement
3. Sufficient amounts of moisture in the concrete.

The ASR reaction occurs when reactive silica from the aggregate and alkalis such as sodium and potassium, mostly from cement, react to form alkali-silica gel. This gel has a strong affinity with water and will swell if the internal relative humidity of the concrete is above 80 percent. The swelling in turn creates several deleterious mechanisms within the concrete.

Cracking is the main form of damage associated with ASR. Surface cracking will vary depending on the loading and reinforcement of the structure. Low stress and lightly reinforced members will typically exhibit map cracking; while stressed or highly reinforced structures will have cracking that follows the compressive stress or reinforcement direction. The extent of surface cracking is also greatly affected by exposure conditions such as wetting and drying and freezing and thawing. Surface cracks are generally less than 0.4 inches wide and between 1 and 2 inches deep; below this depth, the cracking is typically microcracks. Microcracks begin in the reactive aggregates and spread throughout the surrounding cement paste and possibly even through nonreactive aggregates as expansion continues. Microcracks are also where the alkali-silica gel will be found.

Properly diagnosing structures suffering from ASR is very important. Other detrimental mechanisms should not be ruled out until it is known for sure that they do not exist. Diagnosing structures will begin with a thorough site investigation that looks into all possible distress mechanisms, and then samples will be sent for petrographic analysis to confirm or deny the presence of alkali-silica gel. Petrographic analysis must be performed under the supervision of an experienced petrographer, ASTM C856 outlines testing procedures. The damage rating index will also be determined by the petrographer; this test quantifies the extent of deterioration in the sample caused by ASR.

Mitigation options for ASR-affected concrete may be targeted at lowering the relative humidity, changing the chemistry with lithium, or countering the

expansive stress of a structure. Silane and/or cladding have been proposed to lower the internal relative humidity below 80 percent to stop expansion. Silane has proven to be effective on thin elements, such as test cylinders and highway barriers, but not mass structures thus far. Changing the chemistry with lithium has proven to effectively mitigate ASR in small laboratory testing, but lack of penetration depth on actual structures has shown lithium to be ineffective in most cases. Electrochemical impregnation of lithium is the only application technique with sufficient penetration, and it is feared that this drives alkalis to the reinforcement and worsens ASR there. Three-dimensional confinement may be used to overcome the expansion generated through ASR. This process is challenging because every structure is different and requires different amounts of compensative stress to stop expansion; therefore, a structural engineer is required to design and monitor this process.

Lastly, finite element analysis was carried out on concrete cross sections representing those of the Bibb Graves Bridge. This was a moisture diffusion analysis that predicts the time required for the relative humidity to reach 80 percent in the concrete. The analysis with an impermeable layer on the top of the section estimated a time 5 to 14 years for all parts of the arches to reach 80 percent humidity. These time intervals are based on 2,000 and 3,250 psi concrete strengths.

Chapter 3

Bibb Graves Bridge

3.1 Background

The Bibb Graves Bridge is located in Wetumpka, Alabama, about 13 miles northeast of Montgomery. Wetumpka is pointed out on the map in Figure 3.1.

This bridge is the fifth one built to cross the Coosa River at this location (Blackburn 1997).

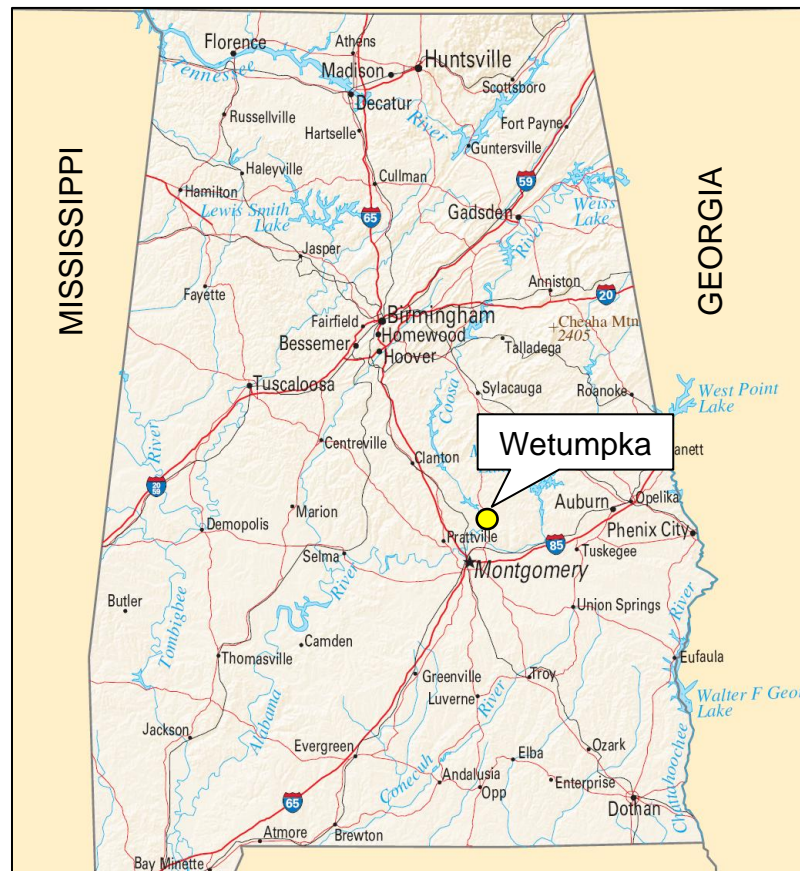


Figure 3.1. Alabama map with circle at Wetumpka (Wikimedia Commons 2006)

All of the history of the five bridges in this section is from Blackburn (1997). The first bridge on record spanning the Coosa River in Wetumpka was constructed in 1830, but no information is available about the fate of the bridge. In 1834, the Wetumpka Bridge Company built a toll bridge, but this bridge was destroyed in a flood in 1844. After the flood, the bridge company was required to ferry people across the river at the same rate as the bridge toll until a new bridge was built.

The third bridge built to span the river in Wetumpka was built later in the same year of 1844, under the supervision of a slave named Horace King, an accomplished bridge builder in the region. This was a covered bridge, pictured in Figure 3.2, and it lasted until the “Great Flood of 1866” washed it away.



Figure 3.2. Covered bridge built in 1844 (Blackburn 1997)

An iron bridge was built in 1887 by the Southern Bridge Company of Birmingham. This bridge is pictured in Figure 3.3. In 1908, the Wetumpka Bridge Company was bought by the county commission, and the toll fee was dropped for good. The iron bridge had a service life of 40 years, much longer than any of the former bridges at this location. By 1927, the bridge was in need of extensive and costly maintenance. Because of this, the commissioners determined that it

would be more effective to build a new bridge instead of repairing and maintaining the iron one.



Figure 3.3. Iron bridge built in 1887 (Blackburn 1997)

Alabama Governor Bibb Graves and the county commissioners debated whether a new bridge should be constructed of steel or reinforced concrete. Governor Graves eventually agreed with the commission that reinforced concrete was the best option. The total estimated cost for the new bridge was \$177,400, and it was split equally between the state and county. The Bibb Graves Memorial Bridge was designed by Edward Houk, the State Bridge Engineer, and construction was completed in 1931. This structure is one of only a couple of bridges south of the Mason-Dixon Line that are suspended from reinforced concrete arches. To this day, the bridge is still the most unique landmark in the city of Wetumpka, and it has become the emblem used in connection with most local organizations.

3.2 Bridge Details and Construction

The Bibb Graves Bridge spans AL 111 across the Coosa River in order to join the two halves of Wetumpka. As of 2009, Holth (2010) gave an average daily

traffic count of 9180. The current appearance of the bridge is shown in Figure 3.4 with a photo that was taken from the northeast side of the bridge.



Figure 3.4. Northeast elevation view of the Bibb Graves Bridge

The Bibb Graves Bridge is 700-feet long with a 24-foot wide roadway. This bridge consists of seven arches, five of which the road deck is suspended from. These arches are 2-feet thick by 4-feet wide, and they have horizontal span lengths of 40, 117, 128, 132, 128, 117, and 40 feet between the piers, from east to west. Each of the main arches consists of approximately 38,000 pounds of steel and 30 cubic yards of concrete. The arches also have different grades of concrete at various locations as shown in Figure 3.5. This was done in order to expedite form removal and decrease the overall construction time (Taylor 1930).

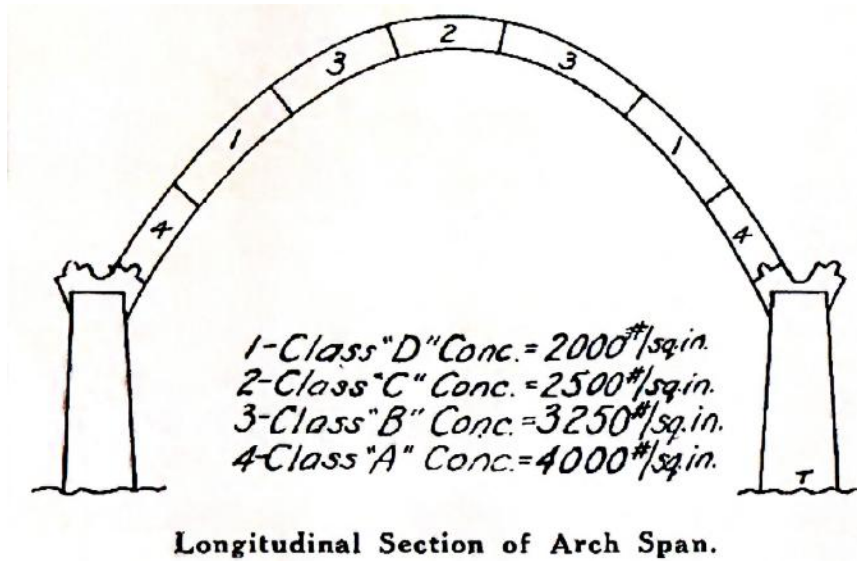


Figure 3.5. Concrete strengths used along arch (Taylor 1930)

The road deck is a series of reinforced concrete slabs suspended from the arches at midheight. The deck was placed before the hangers were encapsulated with concrete. This ensured that the steel would carry all of the deck weight and not elongate after encapsulation, as this would crack the concrete. All of the bridge weight is transferred into bedrock through massive tapered piers. These piers are set 8 to 10 feet in solid rock, and they have average dimensions of 40-feet long and 10-feet wide (Taylor 1930).

Elevation and plan views of the Bibb Graves Bridge with important locations and directions are in Figure 3.6.

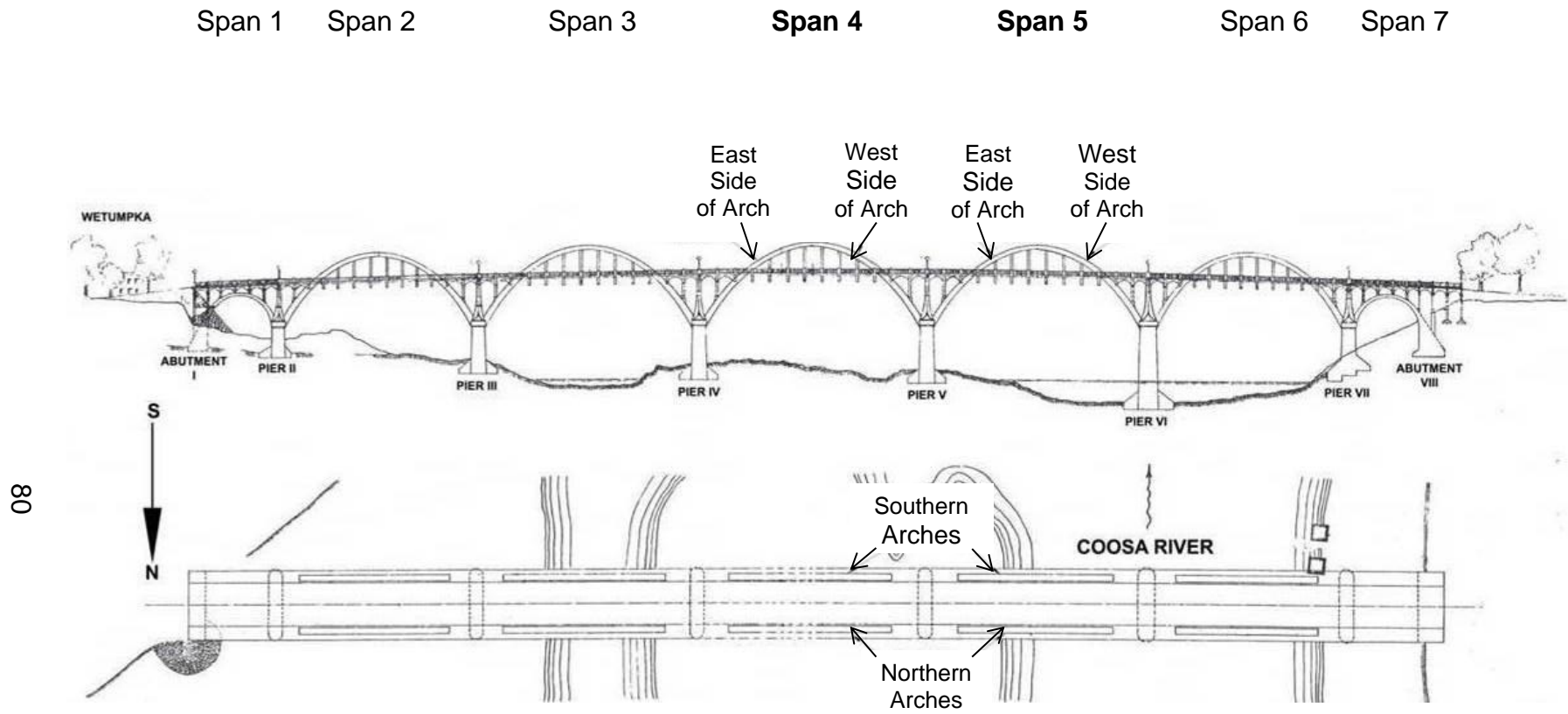


Figure 3.6. Elevation and plan view of Bibb Graves Bridge (Adapted from ALDOT 2010)

Figure 3.7 and Figure 3.8 give a few images of the construction process used in the early 1930's on this particular bridge.

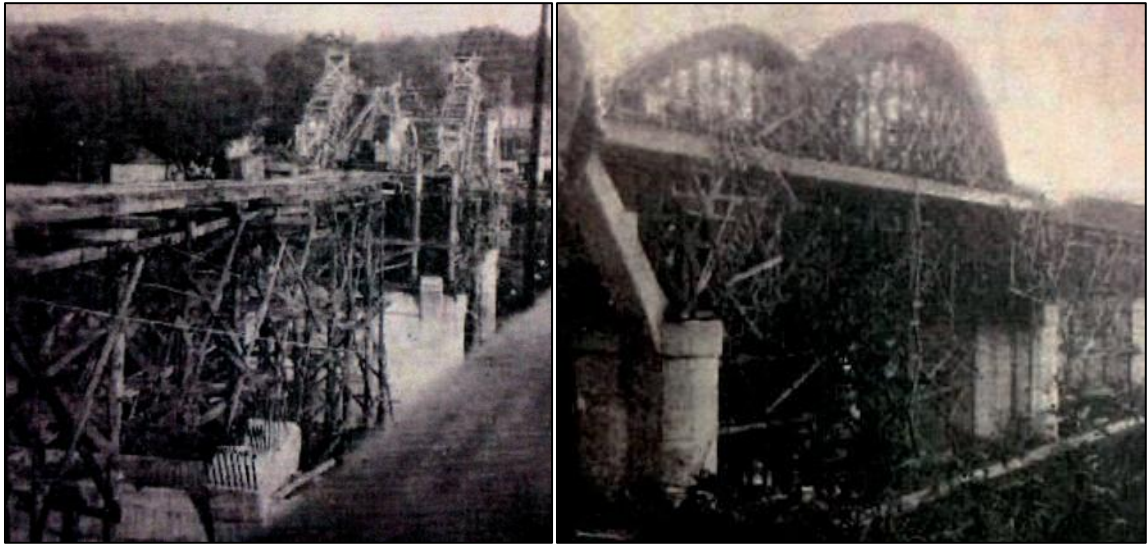


Figure 3.7. Construction photos of the Bibb Graves Bridge (Taylor 1930)

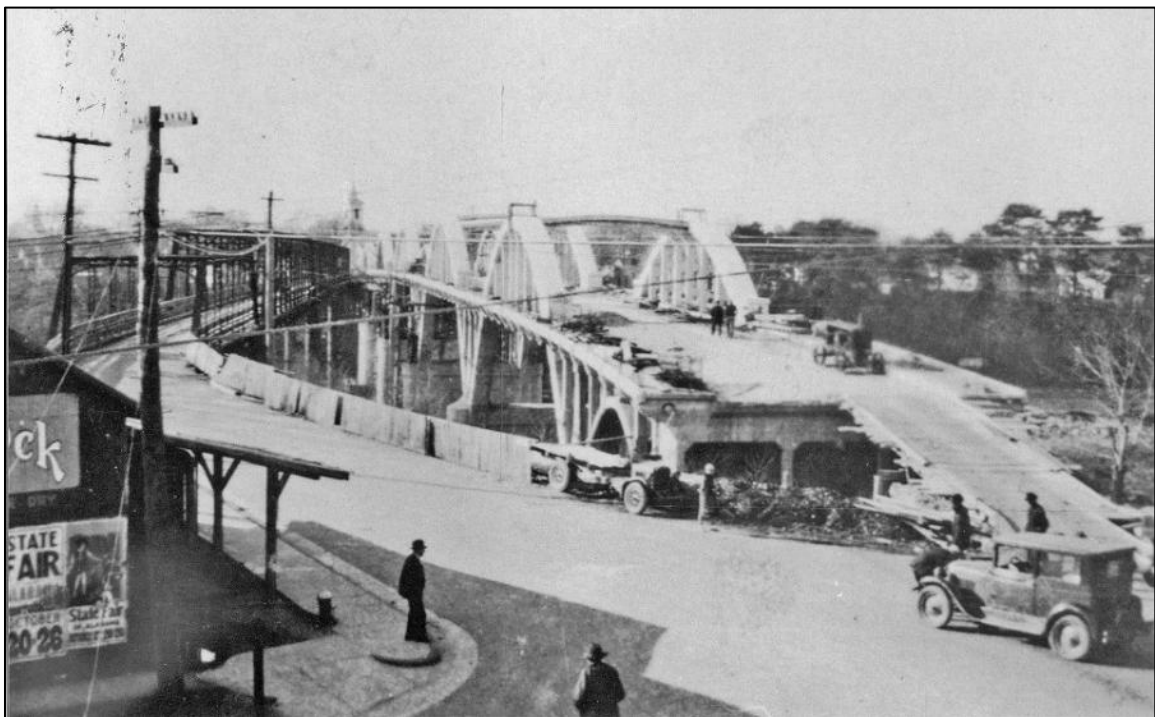


Figure 3.8. Construction of the Bibb Graves Bridge

(Photo courtesy of Sergio Rodriguez)

3.3 ASR in the Bibb Gravis Bridge

Of the seven spans in the Bibb Graves Bridge, only span 5 exhibits severe distress from ASR. Severe cracking and surface deposits due to ASR are present on both arches above the road deck in this span. The presence of ASR in the Bibb Graves Bridge was first noted in the 1956 ALDOT report by Hester and Smith, and significant distress was first noticed in 1993 by Sergio Rodriguez, who was ALDOT's Concrete Engineer at the time. Sergio Rodriguez also took photographs of the distress in the late 1990s and a couple of these pictures are shown in Figure 3.9. Figure 3.10 (A) is a photo at the same location as Figure 3.9 (B), but it was taken in March of 2008 and exhibits much more cracking and spalling. Figure 3.10 (B) is a picture of a non-distressed portion of an arch taken in August of 2013.

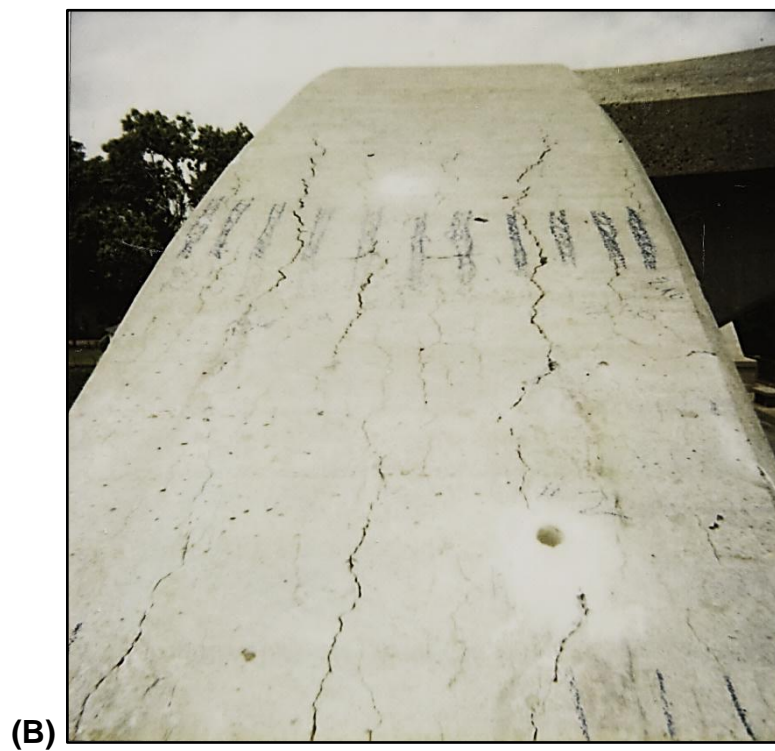
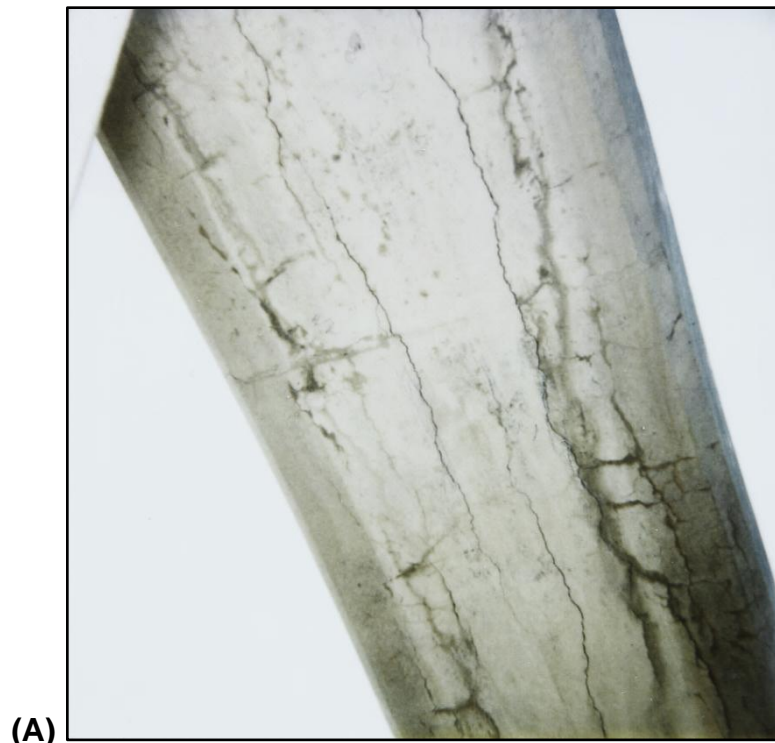


Figure 3.9. ASR-induced cracking in the late 1990s on the (A) bottom and (B) top of a span 5 arch

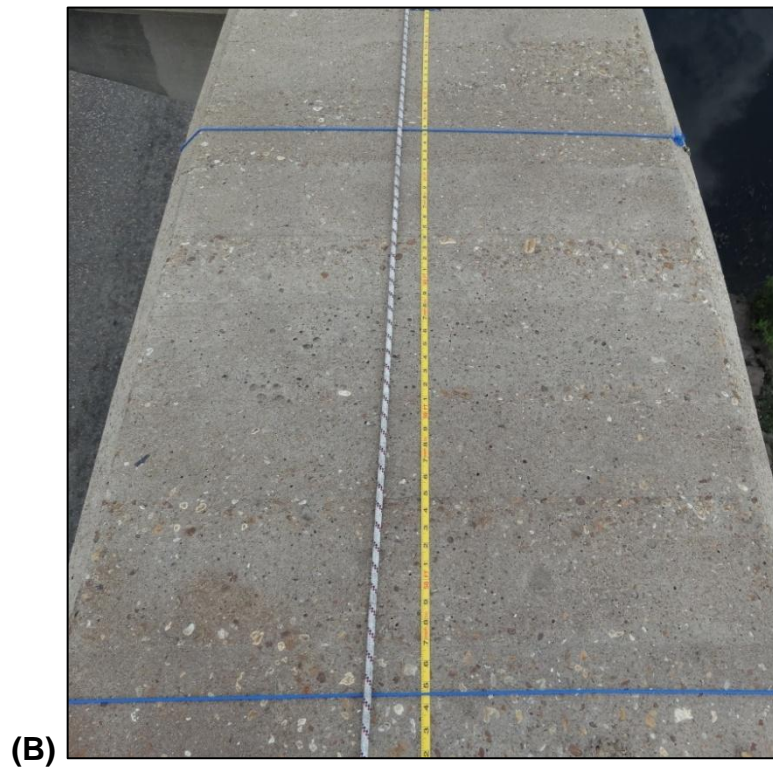


Figure 3.10. (A) ASR-affected arch in March 2008 and (B) different non-distressed arch in August 2013

3.3.1 Petrography of Concrete

Cores were taken from spans 4 and 5 of the Bibb Graves Bridge in January of 2010 by ALDOT for evaluation by The Transtec Group, through Dr. Benoit Fournier in Canada, and Wiss, Janney, Elstner Associates, Inc. (WJE), Illinois, to determine the cause of distress.

3.3.1.1 Coring Layout and Details

The coring process, which involved locating reinforcement, drilling, extracting, labeling, wrapping, packing, and shipping to Illinois and Canada, is shown in Appendix A through Figures A.1, A.2-A.4, A.5 and A.6, A.7, A.8, A.9, and A.10, respectively. Figure 3.11 is a schematic of the core extraction locations on the Bibb Graves Bridge. Each of the four locations shown here had two 3-inch diameter cores taken from them, one for The Transtec Group and one for WJE. Appendix A also has figures of each core along with an extraction location and brief description of the core.

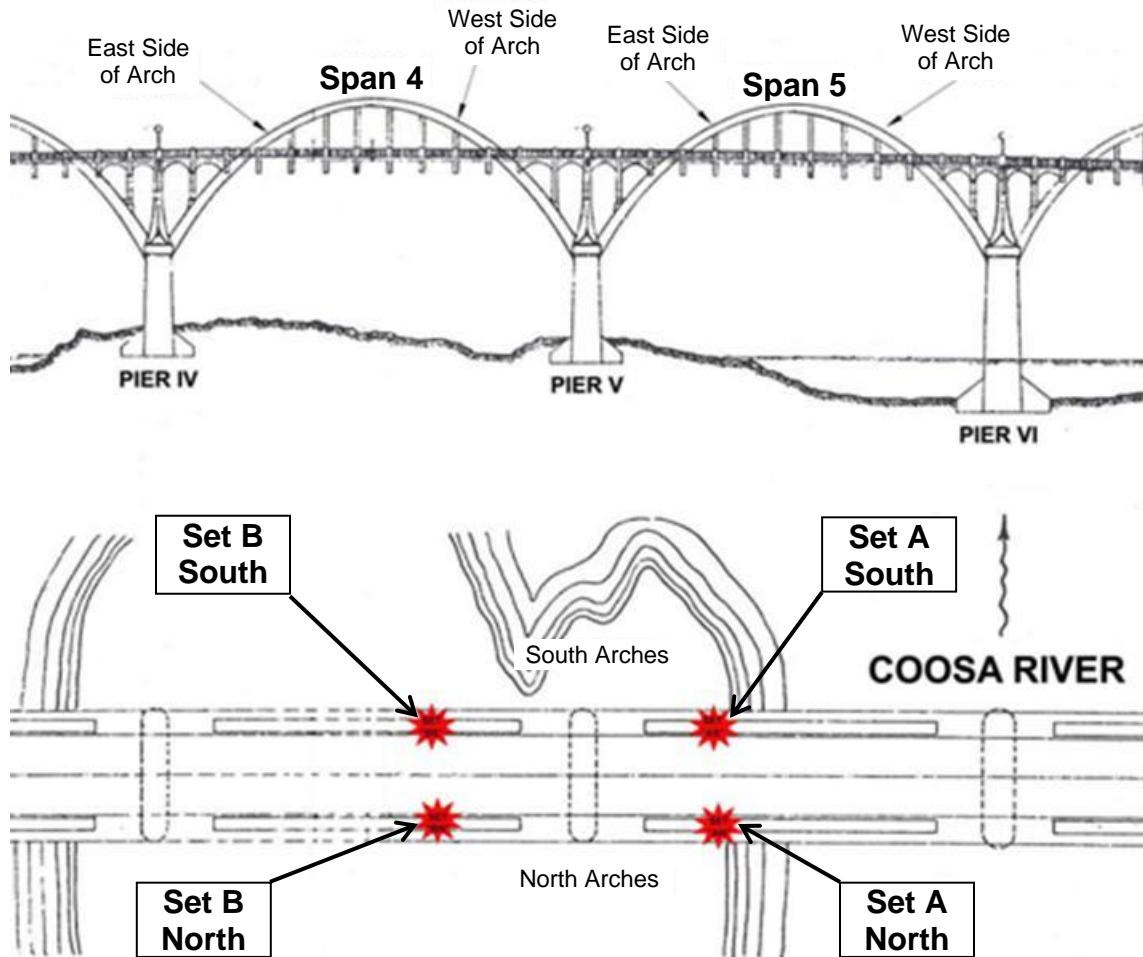


Figure 3.11. Core extraction layout (Adapted from ALDOT 2010)

3.3.1.2 The Transtec Group's Petrographic Analysis Results

The information presented in this section was adapted from The Transtec Group (2010), the body of their report along with pictures are presented in Appendix B. The Transtec Group performed a petrographic analysis on four cores from the Bibb Graves Bridge: 2A-South, 2A-North, 2B-South, and 2B-North. The evaluation consisted mainly of the Damage Rating Index (DRI); refer to Chapter 2 for specifics of this ASR evaluation method. An explanation for how the DRI value relates to the extent of ASR damage is presented below from The Transtec Group (2010).

There is currently no rating system for the DRI values that correspond to concrete affected to a low, moderate or severe degree by ASR. However, our experience is such that values below 200-250 are indicative of a low degree of reaction / deterioration, DRIs in excess of about 500-600 represent a high to very high (DRI > 1000) degree of ASR. It is important to mention, however, that since the DRI is not a standardized method, values can vary significantly from one petrographer to another.

The Transtec Group summarized their results for each core, and this summary is presented in Table 3.1. Both cores from span 5, 2A-South and 2A-North, exhibit very high degrees of ASR with DRI values of over 1000 each. These cores also had reaction rims, secondary reaction products (consisting of ettringite and alkali-silica gel), and cracks reaching up to 0.04 inches (1 mm) in width. Figure 3.12 contains an image of a polished section from core 2A-North, and Figure 3.13 contains a polished section from core 2A-South. Reaction rims around aggregate particles, ettringite, and severe cracking due to ASR are shown in these images. There is also a square drawn on the concrete in each of these images with dimensions of 0.4 by 0.4 inches (1 by 1 cm).

Table 3.1. Summary of petrographic observations on the cores
(The Transtec Group 2010)

Sample	DRI	Typical crack width in the concrete (mm)	Extent of ASR	Reactive aggregates in the polished sections
2A-South	1430	Extensive cracking in the cement paste and the aggregate particles; cracks were found to reach 1 mm in width (mainly 0.1 to 0.3 mm)	Very high degree of ASR	Quartzite and chert
2A-North	1081	Extensive cracking in the cement paste and the aggregate particles; cracks were found to reach 1 mm in width (mainly 0.1 to 0.2 mm; several very fine cracks of < 0.05 mm in size are filled with compacted ettringite)	High degree of ASR	Quartzite and chert
2B-South	141	No significant cracking in the cement paste (i.e. at the 16x magnification used for the DRI)	No significant ASR	Same type of aggregates as in 2A series
2B-North	205	No significant cracking in the cement paste (i.e. at the 16x magnification used for the DRI)	No significant ASR	as in 2A series but no signs of ASR

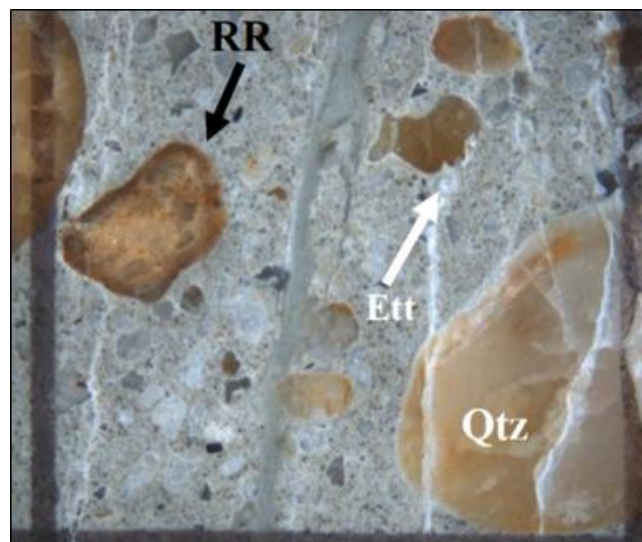


Figure 3.12. Example of reaction rim (RR) and severe cracking in core 2A-North

(The Transtec Group 2010)

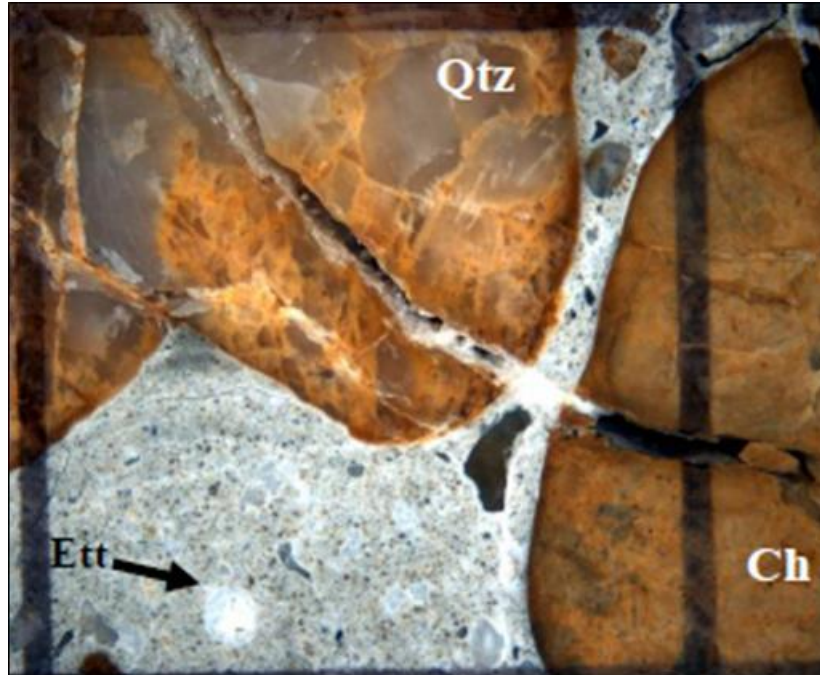


Figure 3.13. Example of severe cracking in polished section of core 2A-South

(The Transtec Group 2010)

3.3.1.2.1 The Transtec Group's Conclusions and Recommendations

With the use of petrographic analysis and the DRI, The Transtec Group found that cores from span 4 had very little signs of ASR and cores from span 5 were severely affected by ASR. It was recommended that the affected arches be cleaned by sandblasting and larger cracks be filled with a flexible sealant, and then to apply a hydrophobic sealer, such as silane, to the surface.

3.3.1.1 WJE's Petrographic Analysis Results

Wiss, Janney, Elstner Associates, Inc. also performed a petrographic analysis on four cores from the Bibb Grave Bridge, and the information presented in this section was adapted from their report (WJE 2010), the body of this report is

presented in Appendix C. The four cores evaluated by WJE were 1A-South, 1A-North, 1B-South, and 1B-North.

3.3.1.1.1 Concrete Composition

WJE (2010) states:

The cores represent visually similar concrete that consists of siliceous gravel coarse aggregate and predominantly siliceous natural sand fine aggregate dispersed in a non-air-entrained portland cement paste. The aggregate is poorly graded. Aggregate top size was 3/4 inch in some cores and 1 1/2 inches in others. Coarse aggregate volume was low in one core. The coarse aggregates were typically non-uniformly distributed. Overall, the concrete was well consolidated and appeared to have been placed with a moderate (Cores 1B-N and 1B-S) to moderately high (Cores 1A-N and 1A-S) water-cement ratio. Paste volume was somewhat high, suggesting that the cement content was also moderate.

3.3.1.1.2 Summary of WJE's Findings

It was common for thin, dark, glassy rims to be seen on the coarse aggregate particles and even some on the fine aggregate particles. An example of these dark rims is shown in Figure 3.14. Figure 3.15 has examples of alkali-silica gel in the cracks of the chert aggregate particle and white deposits of ettringite following the cracks in the cement paste.

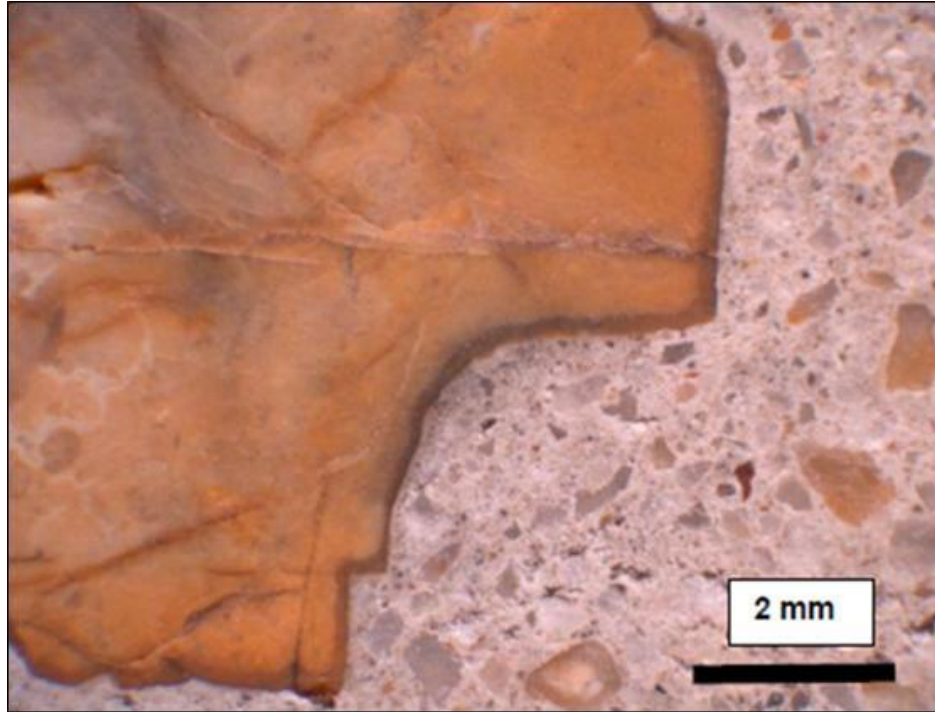


Figure 3.14. Typical dark rim on chert coarse aggregate particle (WJE 2010)



Figure 3.15. Cracks with alkali-silica gel in peripheral region of chert and cracked cement paste containing white ettringite deposits (WJE 2010)

The following statements are from the summary given by WJE (2010):

Cores 1A-S and 1A-N exhibit significant cracking and microcracking attributed to alkali-silica reaction involving quartzite and chert coarse aggregate particles. Cracks caused by ASR were observed throughout the depth represented by these cores. ASR gel was most commonly observed in cracks within the outer portion of aggregate particles. Occasional patches of crystalline material, possibly okenite, were observed within the gel suggesting that the gel is relatively old. Overall, ASR gel is less common than ettringite, which is abundant on all crack surfaces. ASR distress was possibly exacerbated by the formation of major amounts of ettringite.

Cores 1B-S and 1B-N did not exhibit visible distress although minor evidence of alkali-silica reaction was observed. It is possible that this concrete was made with cement that had lower alkali content than the cement used in the concrete represented by cores 1A-S and 1A-N. Comparison of the alkali contents of these cores could be conducted with further analysis.

3.3.2 Examples of Distress from ASR

There are several photographic examples of distress caused mainly by ASR in the Bibb Graves Bridge presented in this section. Figure 3.16 contains an

example of severe longitudinal cracking and surface deposits of efflorescence and alkali-silica on the south side of the southern arch in span 5.



Figure 3.16. Severe distress due to ASR on span 5, south arch

Figure 3.17 is a view of distress and surface deposits on the eastern top side of span 5 south. Figure 3.18 is a closer view of the high end of the arch shown in Figure 3.17. Figure 3.18 was taken in March of 2008 and exhibits severe spalling and longitudinal cracking. The following image, Figure 3.19, is the same location, but was taken in December of 2009. More spalling has occurred since the 2008 photo.



Figure 3.17. Distress with surface deposits of efflorescence and alkali-silica gel on the eastern side of span 5 south



Figure 3.18. Closer view of longitudinal cracking and spalling on span 5 south on

3/11/08



Figure 3.19. Additional spalling on span 5 south from 3/11/08 to 12/14/09

Crack widths in this structure range from hairline up to half an inch, as shown in Figure 3.20, and a full crack distribution is shown in Chapter 6.



Figure 3.20. Crack width close to 1/2 inch

The next two images are examples of distress on the bottom of the arches. Wide longitudinal cracking and a lot of surface discoloration are shown in Figure 3.21. Figure 3.22 has cracks and surface deposits that run from the bottom of the arch to the hanger that supports the bridge deck. The Bibb Graves Bridge also has cracking and surface discoloration in map patterns in low stress and low reinforcement regions. An example of this type of cracking and surface discoloration is shown on an abutment in Figure 3.23.



Figure 3.21. Cracking and surface discoloration on the bottom of an arch



Figure 3.22. Cracking and surface deposits extending from arch to hanger



Figure 3.23. Map-cracking on an abutment of span 5

3.4 Summary

Construction of the Bibb Graves Bridge in Wetumpka, Alabama was completed in 1931. This is a reinforced concrete bridge that is 700-feet long and has a 24-foot wide roadway. The bridge consists of seven arched spans with the roadway suspended at midheight from all but the two end span arches, the roadway runs over the arches on the end spans, as shown in Figure 3.6.

Core samples from spans 4 and 5 were sent to The Transtec Group and WJE for petrographic examination to determine the cause of distress. Even though it was determined that all of the cores had a similar composition, the cores from span 5 exhibited significantly more distress, and the cause of distress was determined to be ASR. Several photographs of the distressed concrete are also shown in section 3.3.2 of this chapter.

Chapter 4

ASR Mitigation Procedure

4.1 Introduction

All of the information presented in this chapter about developing and implementing an ASR mitigation procedure was documented by former Auburn University graduate research assistant Robert Warnock; therefore, the information presented in this chapter is adapted from Warnock (2012).

Due to the continuation of severe cracking and distress in span 5 of the Bibb Graves Bridge, it is imperative that a mitigation procedure be applied to slow or stop the expansion due to ASR. During the summer of 2010, ALDOT, FHWA, and Auburn University determined this procedure should include the following:

1. A water repelling silane sealer on all exposed concrete of the arches
2. A flexible silicone sealant in the wide cracks of the ASR-affected arches
3. An epoxy flood coat on the top surface of the arches to seal all intermediate to narrow cracks

4.2 Selection of Mitigation Procedure

Due to the severity of the concrete's deterioration, typical manufacturer's instructions for the application of silane could not be used. There were four mitigation options developed and considered by the FHWA, Auburn University,

ALDOT's Materials and Test Bureau, and ALDOT's Maintenance Bureau. The main differences between the options were methods of application, order of application, and practicality of application. The following four options were considered:

4.2.1 Protocol Option A

1. Water-blast all concrete surfaces to clean concrete surfaces and remove loose impediments, efflorescence, alkali-silica gel, algae, etc.
2. Seal all cracks 0.04 inches and wider with a UV-resistant, flexible sealant.
3. Apply silane to all surfaces.
4. Apply an epoxy flood coat to the top arch surface to seal the unsealed cracks on this surface.
5. Install instrumentation for monitoring.

Crack widths of 0.04 inches were chosen because ALDOT's Maintenance Bureau said this was the smallest crack they would be able to fill with a flexible sealant without having to rout it out. The use of an epoxy flood coat did raise a concern of whether it would prevent the top of the arches from drying and thus exacerbate ASR more in this region than it would help.

4.2.2 Protocol Option B

1. Water-blast all concrete surfaces to clean concrete surfaces and remove loose impediments, efflorescence, alkali-silica gel, algae, etc.
2. Temporarily tape all cracks 0.04 inches and wider on the top arch surface.
3. Apply an epoxy flood coat to the top arch surface to seal the un-taped cracks on this surface.

4. Water-blast the top arch surface to remove the excess epoxy from the concrete surface.
5. Remove tape from the arch.
6. Seal all cracks 0.04 inches and wider with a UV-resistant, flexible sealant.
7. Apply silane to all surfaces.
8. Install instrumentation for monitoring.

This option was believed to have the best results due to having minimal amounts of epoxy on the top surface, but the detail and labor intenseness along with the uncertainty of epoxy penetration depth of this protocol make it unpractical. There are also environmental concerns associated with water-blasting the excess epoxy into the river below.

4.2.3 Protocol Option C

1. Water-blast all concrete surfaces to clean concrete surfaces and remove loose impediments, efflorescence, alkali-silica gel, algae, etc.
2. Apply silane to all surfaces.
3. Seal all cracks 0.01 inches and wider with a UV-resistant, flexible sealant.
4. Install instrumentation for monitoring.

The benefit of this option is the top surface would be expected to allow moisture movement through it for drying without the epoxy flood coat, but this protocol option has a couple drawbacks. One of which is silane is not capable of bridging cracks, and water can migrate into cracks smaller than 0.01 inches. The second drawback to this is the intense amount of time and labor required to rout

all of the cracks smaller than 0.04 inches to achieve a sufficient bond with the silicone.

4.2.4 Protocol Option D

1. Water-blast all concrete surfaces to clean concrete surfaces and remove loose impediments, efflorescence, alkali-silica gel, algae, etc.
2. Seal all cracks 0.01 inches and wider with a UV-resistant, flexible sealant.
3. Apply an epoxy flood coat to the top arch surface to seal the unsealed cracks on this surface.
4. Apply silane to all remaining surfaces.
5. Install instrumentation for monitoring.

This protocol option was similar to C, but included the addition of an epoxy flood coat, and moved the application of silane to the last step. This procedure was deemed ineffective by all parties due to concerns about silane's ability to bond to the epoxy and having to rout small cracks.

4.3 Final ASR Mitigation Procedure

Following a conference call between the FHWA, ALDOT, and Auburn University, the following ASR mitigation procedure was chosen:

1. Water-blast all concrete surfaces to clean concrete surfaces and remove loose impediments, efflorescence, alkali-silica gel, algae, etc.
2. Apply silane to all surfaces.
3. Seal all cracks 0.04 inches and wider with a UV-resistant, flexible sealant.
4. Apply an epoxy flood coat to the top arch surface to seal the cracks on this surface.

5. Install instrumentation for monitoring.

The mitigation procedure was applied to both ASR-affected arches of span 5, and the south arch of span 4, in order to have a treated control, as shown in Figure 4.1. A schematic of the ASR mitigation method applied is shown in Figure 4.2. Cleaning the concrete arches with water-blasting was the first step in the procedure before any products could be applied to the concrete. Next, a hydrophobic layer was created with silane. The silane was applied first so that it could penetrate the concrete surface as much as possible before the flexible sealant and epoxy flood coat sealed the pores of the concrete.

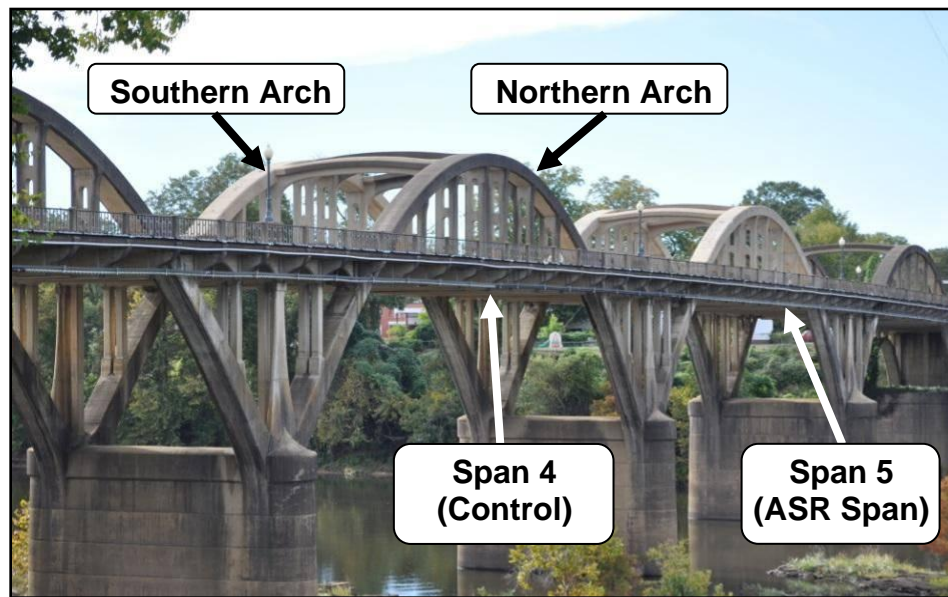


Figure 4.1. Span 4 and 5 of the Bibb Graves Bridge

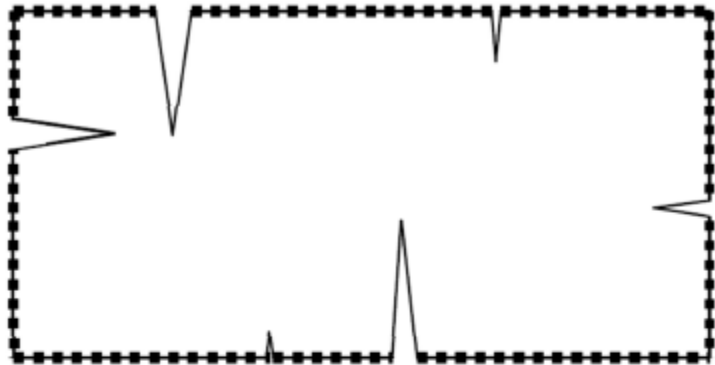
(Adapted form Warnock 2012)

The third step in the process was filling the all of the cracks that were 0.04 inches and wider with a UV-resistant, flexible sealant. This crack size was chosen because it is the smallest width that ALDOT could seal without routing. The flexible sealant is essential in the large cracks because the silane cannot

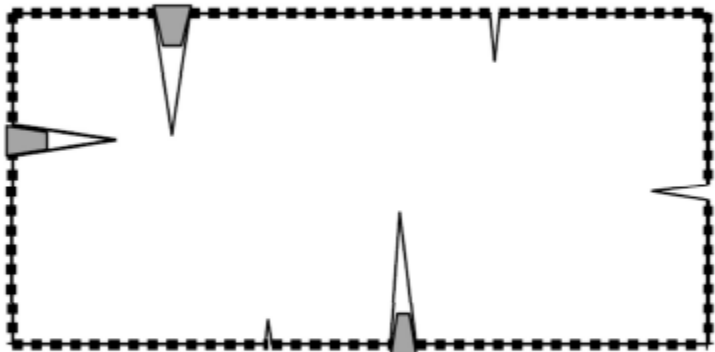
bridge gaps and the concrete is constantly expanding and contracting due to ASR and temperature.

The last step in the mitigation process was the application of an epoxy flood coat to the top of the arches. Even though the epoxy will theoretically prevent drying through the top surface, it is necessary to seal all of the cracks smaller than 0.04 inches, because they would otherwise allow rainwater to enter the structure. Crack widths up to 0.04 inches are still exposed on the other three surface of the arch, but this was deemed insignificant because these surfaces will not have standing water on them.

1. Arch after silane application only

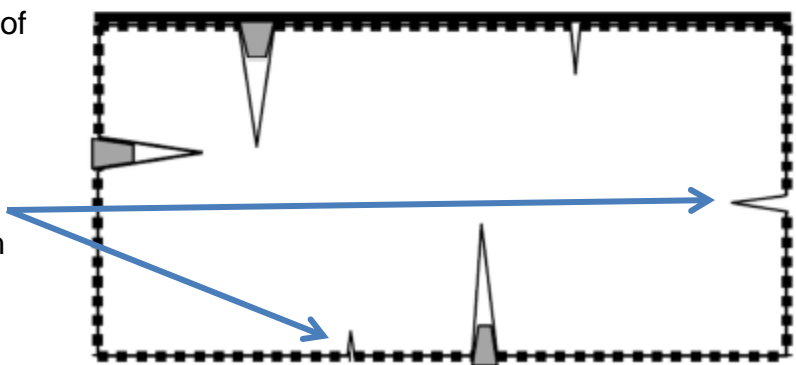


2. Arch after application of flexible sealant



3. Arch after application of epoxy flood coat

Note: Small cracks on bottom and sides of arch are left unsealed



Legend

-  Large Crack (≥ 0.04 in.)
-  Small Crack (< 0.04 in.)
-  Silane Sealant
-  Flexible Sealant
-  Epoxy Flood Coat

Figure 4.2. Schematic of applied ASR mitigation procedure

(Adapted from Warnock 2012)

4.4 Installation of the ASR Mitigation Method

The chosen mitigation procedure was implemented during October and November of 2010. The order and date of each step in the procedure are shown on the timeline in Figure 4.3. As previously stated, both arches in span 5 and the south arch in span 4 received the ASR mitigation procedure, as shown in Figure 4.4. All four arches in spans 4 and 5 received instrumentation for monitoring future relative humidity and expansion.

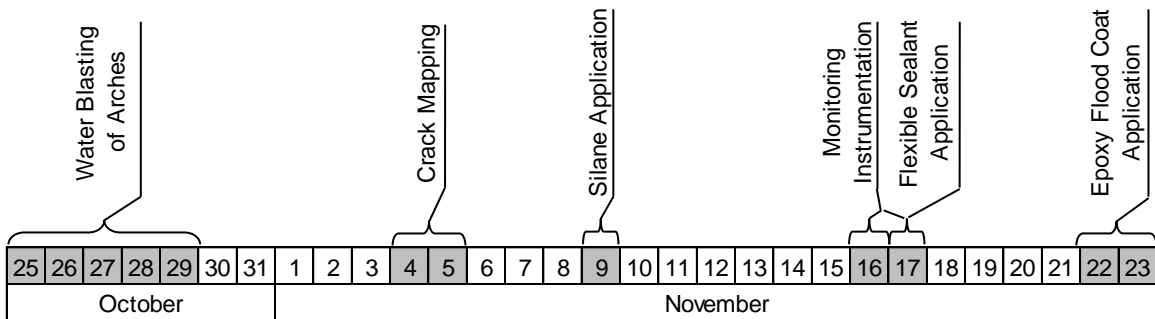


Figure 4.3. Timeline of installation of ASR mitigation procedure in 2010

(Warnock 2012)

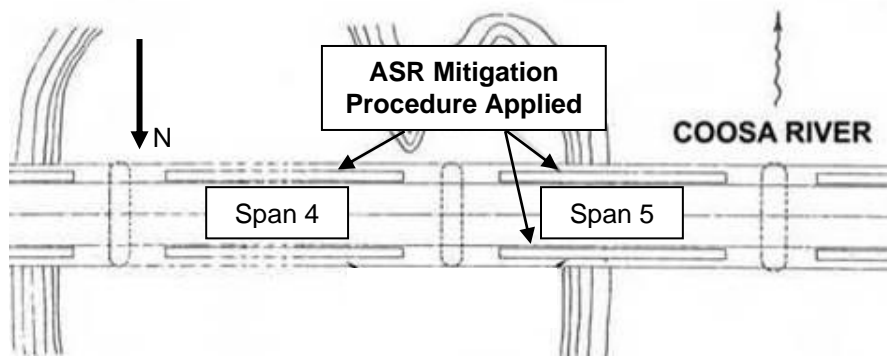


Figure 4.4. Arches that received the mitigation procedure

(Adapted from Warnock 2012)

The three arches to be treated were water-blasted from October 25th through the 29th to clean the concrete surfaces and remove loose impediments,

efflorescence, alkali-silica gel, algae, etc. Figure 4.5 shows the cleaned arches of span 5 prepared for silane application. A 72-hour drying period was required before the silane membrane could be sprayed on.



Figure 4.5. Span 5 after water-blasting (Warnock 2012)

The silane was applied to the bridge on November 9, 2010. The silane chosen for this project was Enviroseal 40, pictured in Figure 4.6 (A). Enviroseal 40 is a water-based, 40 percent silane penetrating sealer. The silane was applied to the bridge with a low-pressure garden sprayer that produces a fine mist, as shown in Figure 4.6 (B). When silane is wet, it has a white color, but it dries clear.

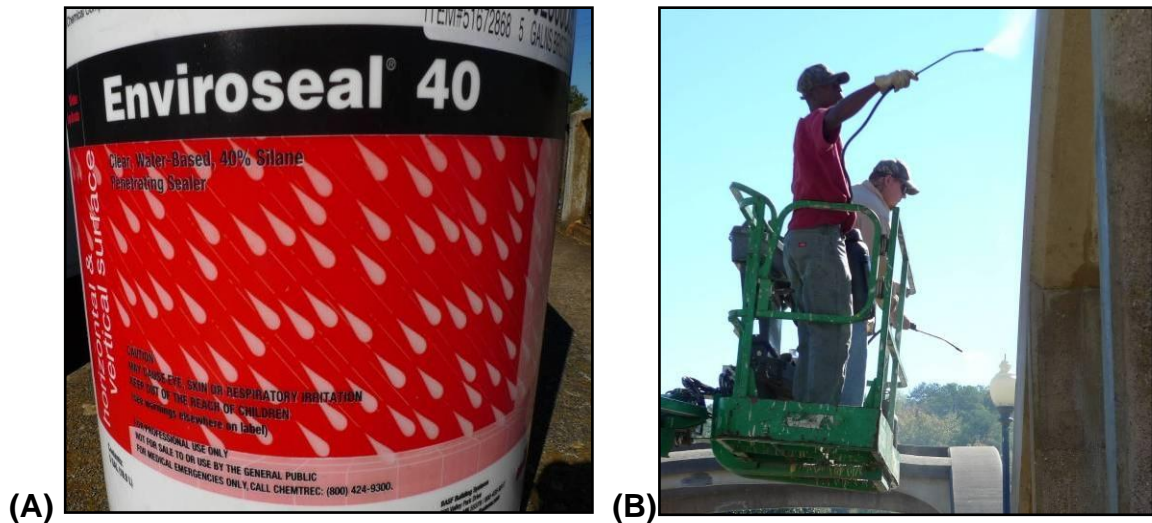


Figure 4.6. (A) Water-based silane sealant and (B) application of silane
(Warnock 2012)

Next, all of the cracks greater than or equal to 0.04-inches wide were sealed with a flexible sealant to prevent water penetration. The flexible sealant used was Pecora 895NST, Structural Silicone Glazing & Weatherproofing Sealant. This silicone was applied with a caulk gun, shown in Figure 4.7 (A), and then forced into the crack and smoothed by hand, as shown in Figure 4.7 (B).



Figure 4.7. (A) Applying flexible sealant and (B) smoothing sealant by hand
(Warnock 2012)

The last step in the ASR mitigation process was applying an epoxy flood coat to the top of the arches to prevent rainfall from entering the cracks that were not filled with the flexible sealant. The epoxy used was Dayton Superior Sure Seal™ LV/LM. This is a two-part epoxy that is combined with a 1:1 ratio. The two parts were mixed together for three minutes and then applied to the concrete with a paint roller.

4.5 Summary

The following is the final ASR mitigation procedure chosen for the Bibb Graves Bridge by the FHWA, ALDOT, and Auburn University:

1. Water-blast all concrete surfaces to clean concrete surfaces and remove loose impediments, efflorescence, alkali-silica gel, algae, etc.
2. Apply silane to all surfaces.
3. Seal all cracks 0.04 inches and wider with a UV-resistant, flexible sealant.
4. Apply an epoxy flood coat to the top arch surface to seal the cracks on this surface.
5. Installation of instrumentation for monitoring.

This procedure was implemented in the given order during October and November of 2010. Both arches in span 5 and the southern arch of span 4 received the mitigation treatment. The arches of span 4 are being used as control arches in this project; therefore, both of them have the instrumentation for monitoring, as do the affected arches of span 5. Span 4 north is an untreated control arch, and span 4 south is a treated control arch.

Chapter 5

Experimental Monitoring

5.1 Introduction

This chapter documents the installation and use of the equipment used to monitor the effectiveness of the ASR mitigation procedure. Data collected with this equipment is presented and discussed in the next chapter.

Temporary gridlines were installed to monitor cracking, and permanent instrumentation was installed on the bridge to monitor the relative humidity and expansion/contraction of the concrete. The installation of the permanent instrumentation was performed by personnel from the FHWA, Auburn University, and ALDOT's Materials and Test Bureau on November 16th and 17th of 2010.

5.2 Crack Mapping

Crack mapping was performed prior to the application of the mitigation procedure in November of 2010 and again in August of 2013 to determine the extent of cracking and assess the effectiveness of the ASR mitigation procedure. These surveys were carried out on both arches of span 5 and on the southern arch of span 4, control arch.

A temporary reference grid was installed on the arches, as shown in Figure 5.1, and used in conjunction with grids on paper to roughly hand-sketch the cracks to scale. The reference grid consisted of a 100-foot tape measure laid

longitudinally across the arch and colored string wrapped around the arch every three or four feet, as shown in Figure 5.2. Bungees were used to connect the two ends of sting on the side of the arches.



Figure 5.1. Grid for crack survey

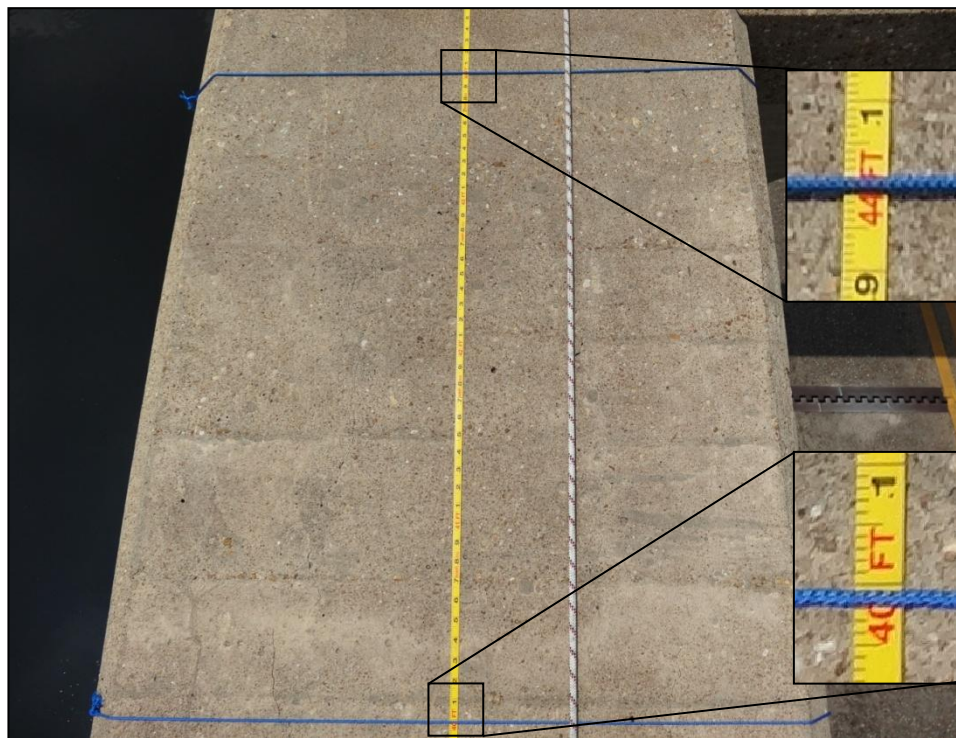


Figure 5.2. Grid spacing along arch

The crack widths were measured with the use of a crack width gauge, as shown in Figure 5.3. For this process, cracks were measured at their widest point, and the values were recorded.



Figure 5.3. Using crack width gauge

5.3 Relative Humidity Measurements

The relative humidity of the concrete was measured with Vaisala's HM44 Structural Humidity Measurement Kit. This kit includes the following:

1. HMI41 indicator
2. HMP44 relative humidity and temperature probes
3. Protective orange cups with lids
4. Plastic tubes
5. Rubber plugs
6. Long rubber plugs

The plastic tubes were permanently installed in the concrete at depths of 1, 2, and 3 inches. For this, the concrete was drilled to the desired depth with a 5/8-inch diameter bit, and the holes were cleaned with compressed air for good

bonding. The plastic tubes were then epoxied into the holes and sealed at the base with silicon. Next, the long rubber plugs were inserted into the tubes and sealed with a flexible silicone sealant to prevent atmospheric moisture from entering the tubes. An installed and sealed tube and plug assemble is shown in Figure 5.4



Figure 5.4. Plastic tube with rubber plug installed in concrete

Relative humidity readings are taken by removing the long rubber plug and inserting a relative humidity and temperature probe into the tube. These probes have an accuracy of ± 2 percent relative humidity for relative humidity ranges of 0 to 90 percent and an accuracy of ± 3 percent relative humidity for relative humidity ranges of 90 to 100 percent (Vaisala 1998). The process of removing the plug and inserting the probe is shown in Figure 5.5. The probe goes all the way to the bottom of the tube where it snaps into place. Next, a small rubber plug is placed around the cord and pushed down into the top of the tube to seal it off, as depicted in Figure 5.6. A protective cup is then slid down over the tube assemble and capped, shown in Figure 5.7, while the probe equilibrates with the internal conditions of the concrete for at least one hour. Once the probe

has reached equilibrium, its cord is plugged into the indicator to take temperature and humidity readings. The indicator is pictured in Figure 5.8 while taking readings from probe number 4.

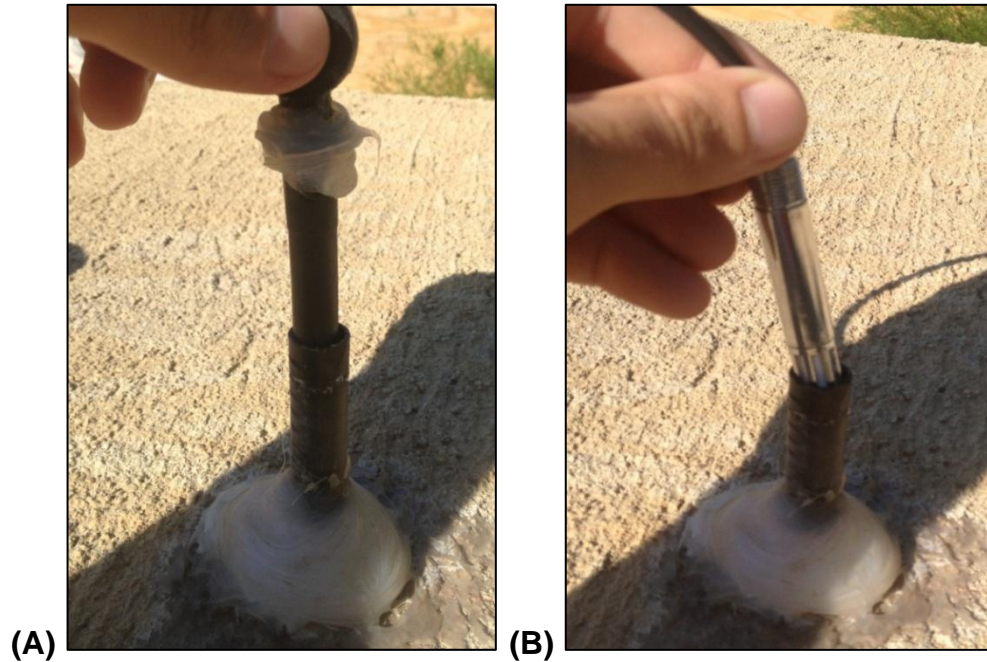


Figure 5.5. (A) Removing long rubber plug and (B) inserting probe into tube

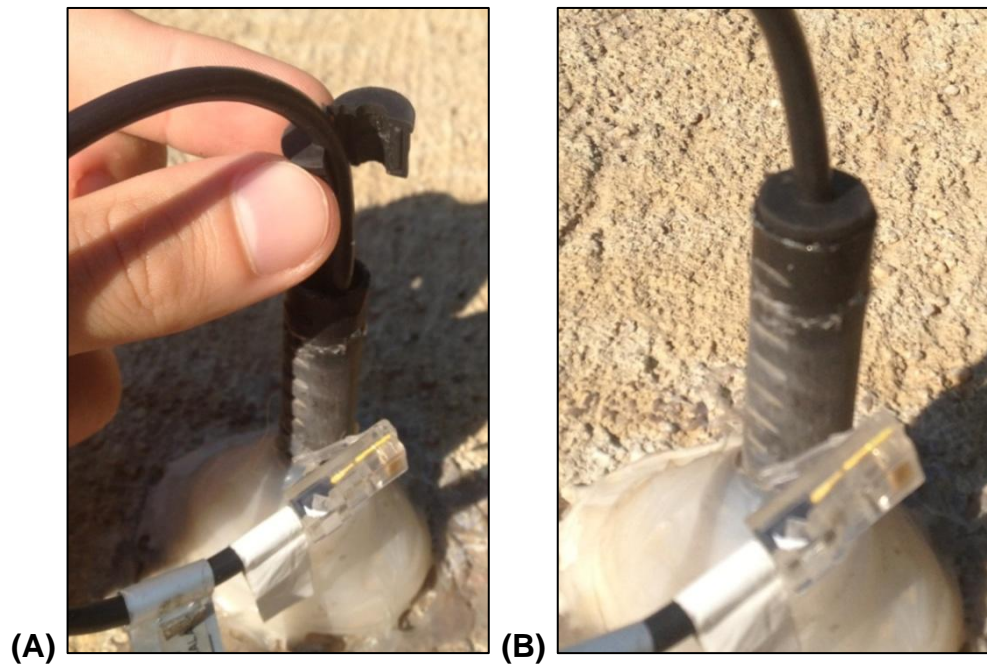


Figure 5.6. (A) Putting rubber plug around cable and (B) sliding it into tube



Figure 5.7. Placing protective cup and lid over tube



Figure 5.8. Measuring temperature and RH with indicator

Each arch of spans 4 and 5 has four locations where the relative humidity and temperature are measured at a depth of 1, 2, and 3 inches. These locations are west top, west bottom, east top, and east bottom. The top and bottom measurement locations are shown in Figure 5.9 on one end of a generic arch. There are a total of 48 measurement points, 4 arches with 4 locations each and 3 depths per location.

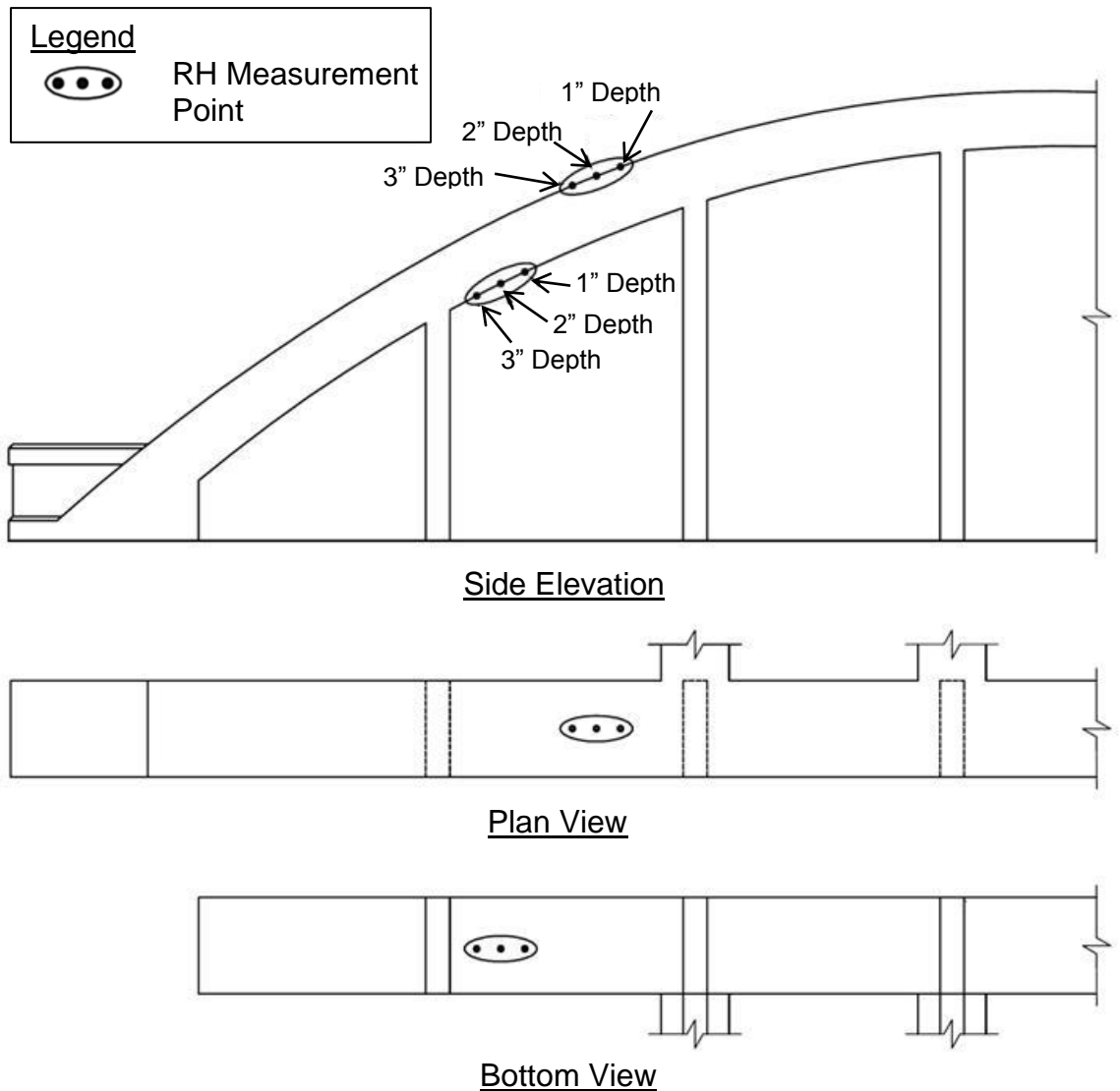


Figure 5.9. Location and depth of RH measurements

(Adapted from Warnock 2012)

5.4 Strain Measurements

Concrete strains in the bridge were measured with a Mayes demountable mechanical (DEMEC) concrete strain gauge. This gauge consists of one fixed point and one movable point on a lever arm connected to a dial for reading strains. The two points on the gauge are spaced 19.69 inches (500 mm) apart on a beam, and two punched DEMEC studs are permanently attached to the structure with the same spacing. The DEMEC studs are installed in the concrete by drilling holes with a slightly bigger diameter than the stud and epoxying the stud into the hole. The surface of the stud sits flush with the concrete surface, as shown in Figure 5.10, and concrete strains are determined by taking DEMEC readings on the studs at different times to see a relative distance change between the studs. The accuracy of the DEMEC strain gauge is $\pm 5 \times 10^{-6}$ in/in. (Mayes Instruments Limited, n.d.). There is an example of someone using this gauge in the field along with a close-up view of the dial shown in Figure 5.11.



Figure 5.10. DEMEC stud installed in the Bibb Graves Bridge

(Warnock 2012)

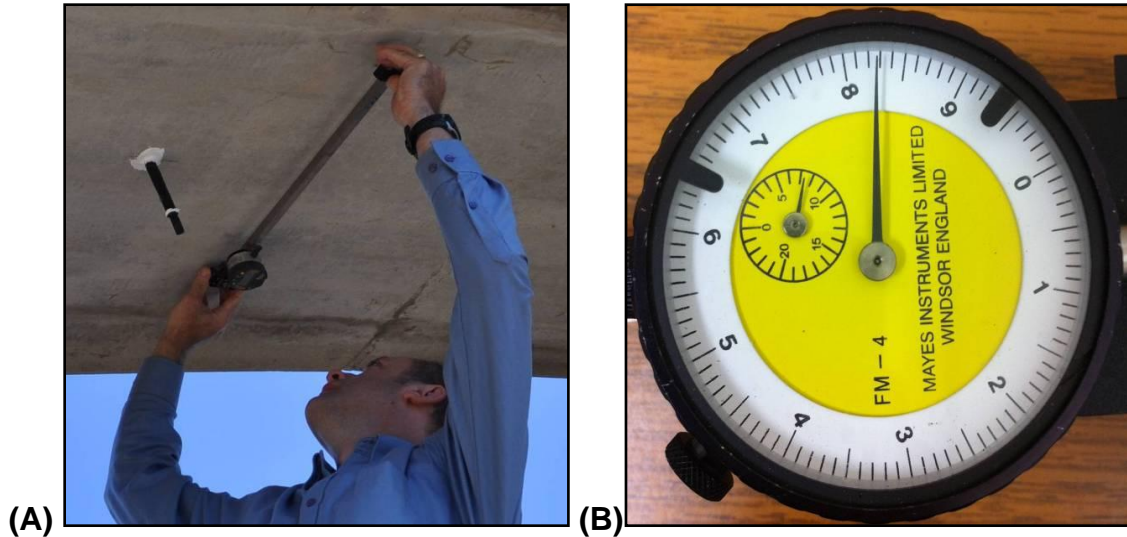


Figure 5.11. DEMEC strain gauge (A) field use and (B) dial reading 783

(Adapted from Warnock 2012)

DEMEC readings are taken and converted into strains with the following procedure:

1. Take a reference bar reading.
 - a. Insert the movable point on the DEMEC gauge into the punched point at one end of the reference bar.
 - b. Insert the fixed point on the DEMEC gauge into the punched point at the other end of the reference bar.
 - c. Apply a slight downward pressure to the gauge and read the number on the smaller dial followed by the number on the larger dial, e.g.

Figure 5.11 (B) has a small dial reading of 7 and a large dial reading of 83; therefore, the DEMEC reading is 783.

2. Take a reading on the studs in the concrete, as shown in Figure 5.11 (A), with the same procedure as step 1.
3. Subtract the reference bar reading from the DEMEC stud reading.

4. Multiply the difference of the readings by the gauge factor (unique to each gauge) to convert the DEMEC readings into strains. The gauge factor for the DEMEC strain gauge used in this project is 3.235×10^{-6} in./in./dial number.
5. The difference in strain measurements at different times is the actual strain in the structure over that time period.

The DEMEC studs were installed at specific locations on each of the four arches to measure strains. These locations are shown in Figure 5.12, but not every arch has studs installed at every location. And not all of the installed studs are measurable due to the spacing of the studs not being close enough to the spacing of the DEMEC gauge points. There were ten studs installed by the FHWA in 2005, and 41 more studs installed in 2010 by the FHWA, ALDOT's Maintenance Bureau, and Auburn University. Table 5.1 is a summary of which stud locations were utilized on each arch, what year the studs were installed, and if the installed studs are measurable. Each of the locations in Figure 5.12 and Table 5.1 are abbreviated as follows:

- AB - Abutment
- SH - Side Horizontal
- SP - Side Perpendicular
- BL - Bottom Low
- BH - Bottom High
- TL - Top Low
- TH - Top High

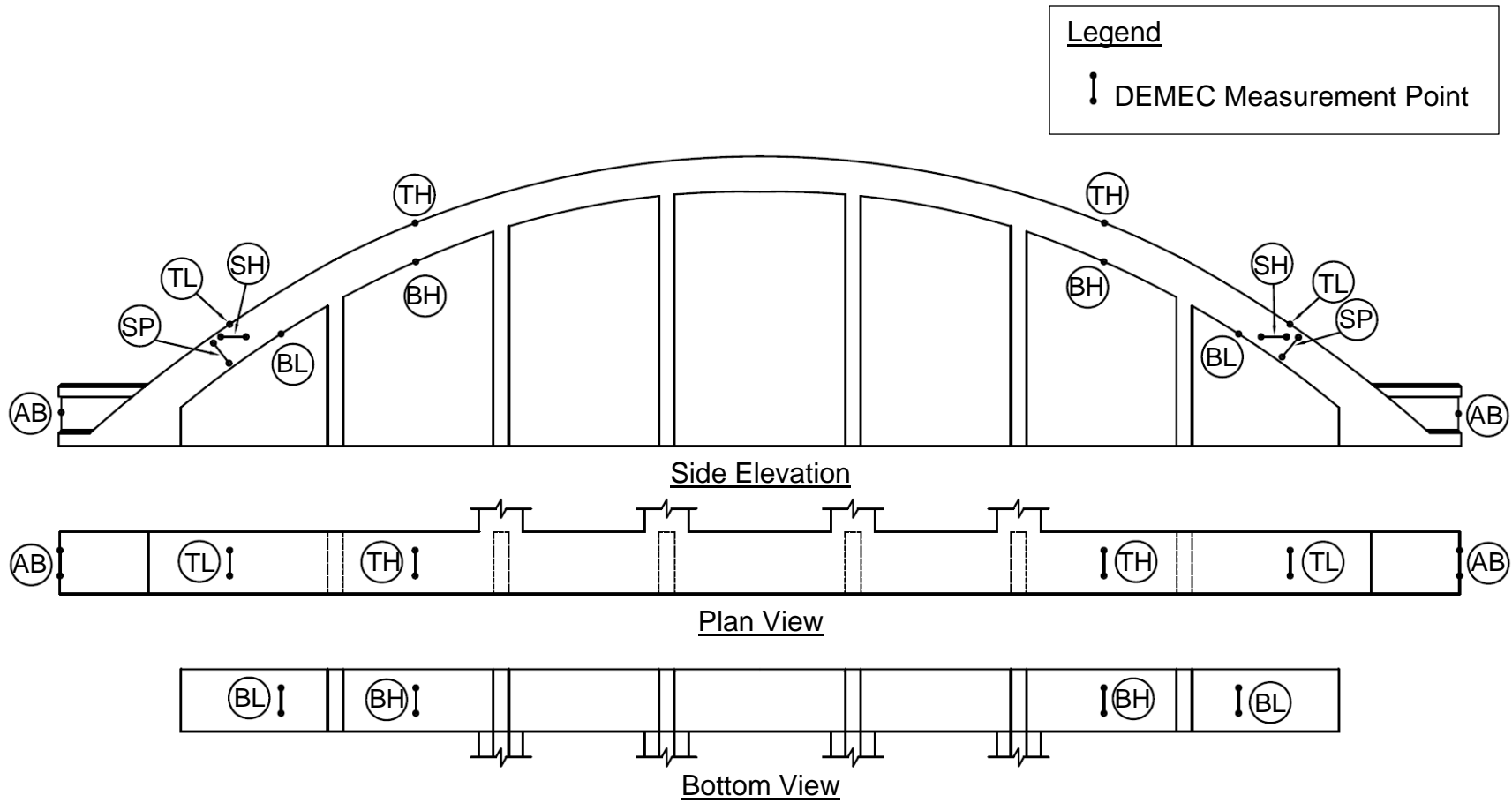


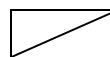
Figure 5.12. DEMEC stud locations on a typical arch

Table 5.1. Summary of strain measurement locations of spans 4 and 5

Span 4				Span 5					
Arch Location		Location on Arch	Installed		Arch Location		Installed		
			2005	2010			2005	2010	
South	West	AB		X	South	West	AB		X
		SH		X			SH		
		SP	X				SP	X	
		BL	X				BL	X	
		BH		X			BH		X
		TL	X				TL	X	
		TH		X			TH		X
	East	AB		X		East	AB	X	
		SH		X			SH		X
		SP					SP	X	
		BL		X			BL	X	
		BH		X			BH		X
		TL		X			TL	X	
		TH		X			TH		X
North	West	AB		X	North	West	AB		X
		SH		X			SH		X
		SP					SP		
		BL		X			BL		X
		BH		X			BH		X
		TL		X			TL		X
		TH		X			TH		X
	East	AB		X		East	AB		X
		SH		X			SH		X
		SP					SP		X
		BL		X			BL		X
		BH		X			BH		X
		TL		X			TL		X
		TH		X			TH		X



Cannot Measure



Studs Not Installed

5.5 Summary

Permanent instrumentation was installed on the Bibb Graves Bridge on November 16th and 17th of 2010 by the FHWA, ALDOT's Materials and Test Bureau, and Auburn University to monitor the effectiveness of the ASR mitigation procedure. This permanent instrumentation is for measuring the relative humidity and expansion of the concrete. A temporary grid system was also set up a couple of times to map the cracks in the concrete.

Crack mapping was performed with the help of a reference grid, pictured in Figure 5.1, prior to the application of the mitigation procedure in November of 2010 and again in August of 2013. This crack mapping survey was done on both arches of span 5 and on the southern arch of span 4.

Relative humidity was monitored in the concrete with the use of Vaisala's HM44 Structural Humidity Measurement Kit. All four arches were instrumented for relative humidity monitoring at specific locations: west top, west bottom, east top, and east bottom. Each of these locations has tubes installed at 1, 2, and 3-inch depths; for a total of 48 relative humidity measurement points on the bridge.

The concrete's expansion and contraction were also monitored at several locations in spans 4 and 5. These locations are shown and listed in Figure 5.12 and Table 5.1. The locations are where studs were installed to measure the concrete strain with a Mayes DEMEC concrete strain gauge.

Chapter 6

Experimental Results and Discussion

6.1 Introduction

The experimental monitoring data results for the Bibb Graves Bridge are presented in this chapter. Data pertaining to concrete cracking, internal relative humidity, and expansion were collected by Auburn University during a 34-month period from November 2010 to September 2013. There were also additional concrete strain measurements taken by the FHWA at ten locations in 2005 and 2009, that are included in this chapter.

For all types of analysis, span 4 serves as a control because it has little to no signs of ASR. The northern arch of span 4 was left untreated and used as a comparison to judge the effectiveness of the mitigation procedure on other arches. Span 4 south received the full mitigation procedure and was analyzed to determine the effectiveness of the mitigation procedure on non-distressed concrete. Both arches in span 5 are severely distressed due to ASR and received the mitigation procedure.

Crack mapping was performed just prior to the application of the mitigation procedure in November of 2010 and again in August of 2013. These crack surveys were performed on the three arches that were treated with the mitigation procedure only. The first crack survey was used to assess the state of cracking in

the arches prior to mitigation, and the latter survey was used to help evaluate the effectiveness of the mitigation procedure.

The relative humidity data are presented after the crack mapping. The goal of the mitigation procedure is to reduce the internal relative humidity of the concrete to below 80 percent, because ASR expansion should not occur below this moisture level (Bérubé et al. 2002a; Stark 1991). Therefore, the relative humidity results are presented before the expansion results, and they are the best indication of how effective the mitigation procedure has been. The raw relative humidity data and the “relative humidity difference” data are analyzed for any trends that may confirm drying in the arches. The “relative humidity difference” is simply the difference in data between any location on a treated arch and the corresponding location on the untreated arch in span 4 north.

Concrete strain data are presented in this chapter after the relative humidity results. The strains for all of the data are adjusted to a normalized temperature of 73 °F in order to isolate the ASR-related strains as much as possible. The raw change in strain data and “strain difference” data are presented and analyzed with linear regression. Because the concrete in all of the monitored arches has nearly identical material compositions (The Transtec Group 2010; WJE 2010), the “strain difference” will eliminate environmental factors that affect the data even more than just adjusting for temperature.

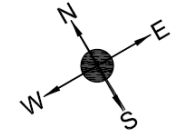
6.2 Crack Mapping





Crack surveys of the Bibb Graves Bridge were performed on November 4th and 5th of 2010, prior to the ASR mitigation procedure application. This survey was

taken on both arches of span 5 and the southern arch of span 4, and was used to visualize the state of cracking in the ASR-affected arches. Another survey was taken on August 6th and 7th of 2013 to see how much additional cracking has occurred since the mitigation procedure was applied. A detailed explanation of how these surveys were performed is presented in section 5.2 of this thesis.


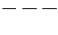
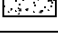
6.2.1 Pre-Mitigation State of Cracking

As previously stated, an initial crack survey was performed just prior to the application of the mitigation procedure in November of 2010, and the results of this survey are presented in this section. The first two surveyed locations presented, Figure 6.1 and Figure 6.2, are for the top and bottom of span 4 south, respectively. Crack surveys from span 5 are presented in the next four figures, Figure 6.3 through Figure 6.6. It is very clear from comparing these six crack maps that span 5 is experiencing much more severe cracking due to ASR than span 4. Span 4 only has a few red cracks (crack widths between 0.04 and 0.1 inches) and no blue cracks (cracks widths above 0.1 inches), but approximately half of the documented cracks in the arches of span 5 have widths greater than 0.04 inches, several of these are above 0.1 inches. The largest measured crack widths were in span 5 south, and they measured up to 3/8 of an inch; several examples of these larger cracks are shown in the figures presented in section 3.3.2.



Crack Width (CW) Legend	
	CW \leq 0.01 in.
	0.01 < CW \leq 0.04 in.
	0.04 < CW \leq 0.10 in.
	CW > 0.10 in.

Scale
0' 5'

Common Features Legend	
	Spalling
	Hidden Feature
	Cross Cut Section

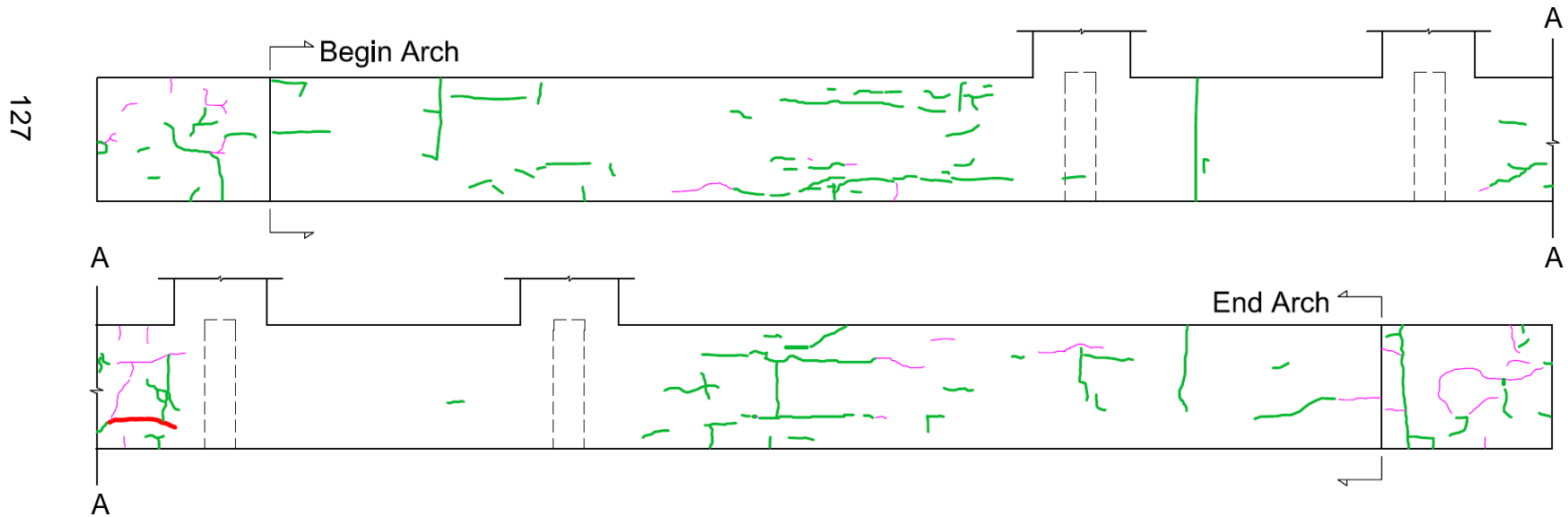


Figure 6.1. Crack mapping, November 2010, Span 4 – South Arch – Plan View

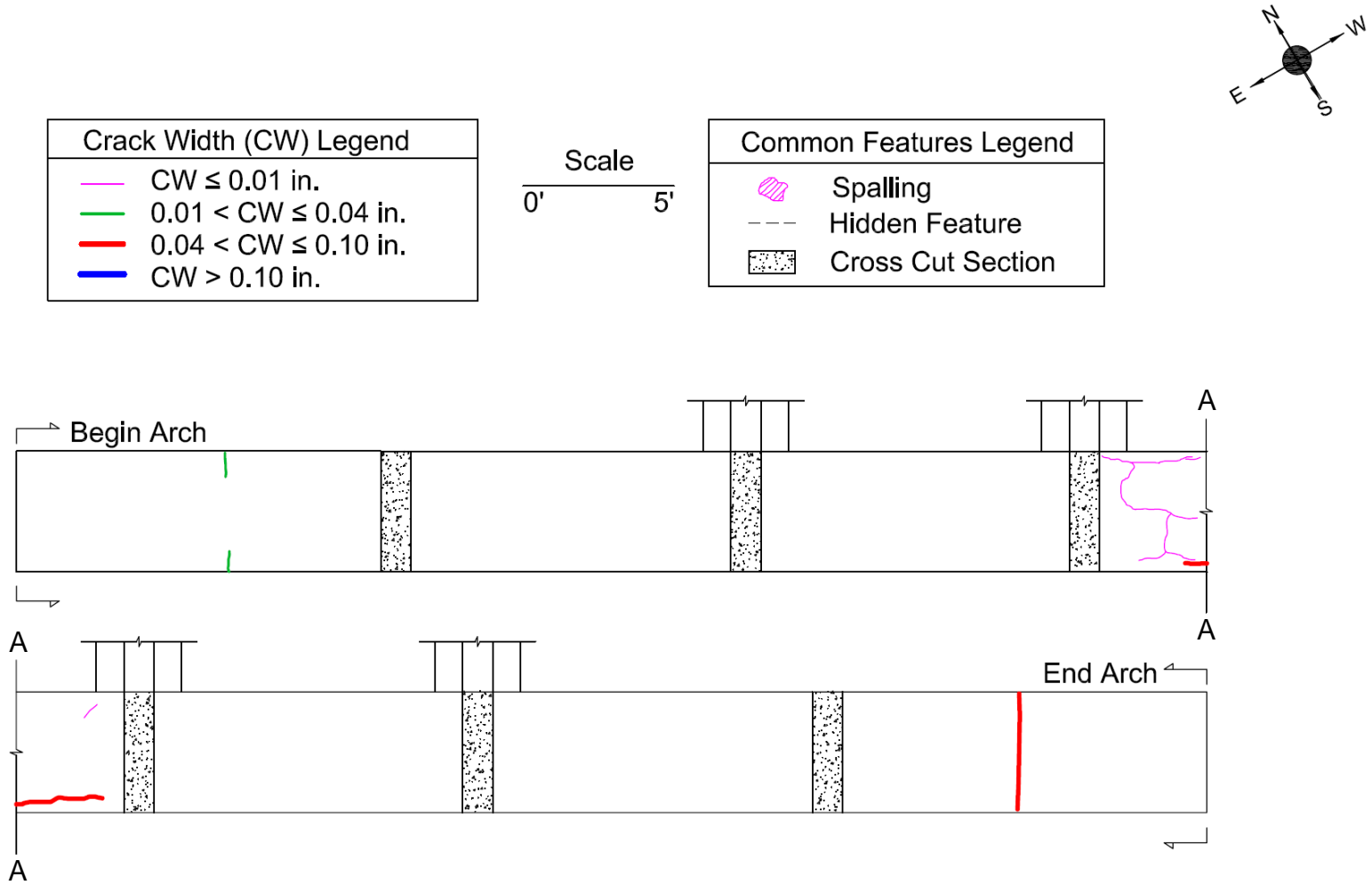
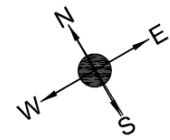


Figure 6.2. Crack mapping, November 2010, Span 4 – South Arch – Bottom View



Crack Width (CW) Legend	
	CW \leq 0.01 in.
	0.01 < CW \leq 0.04 in.
	0.04 < CW \leq 0.10 in.
	CW > 0.10 in.

Scale
0' 5'

Common Features Legend	
	Spalling
	Hidden Feature
	Cross Cut Section

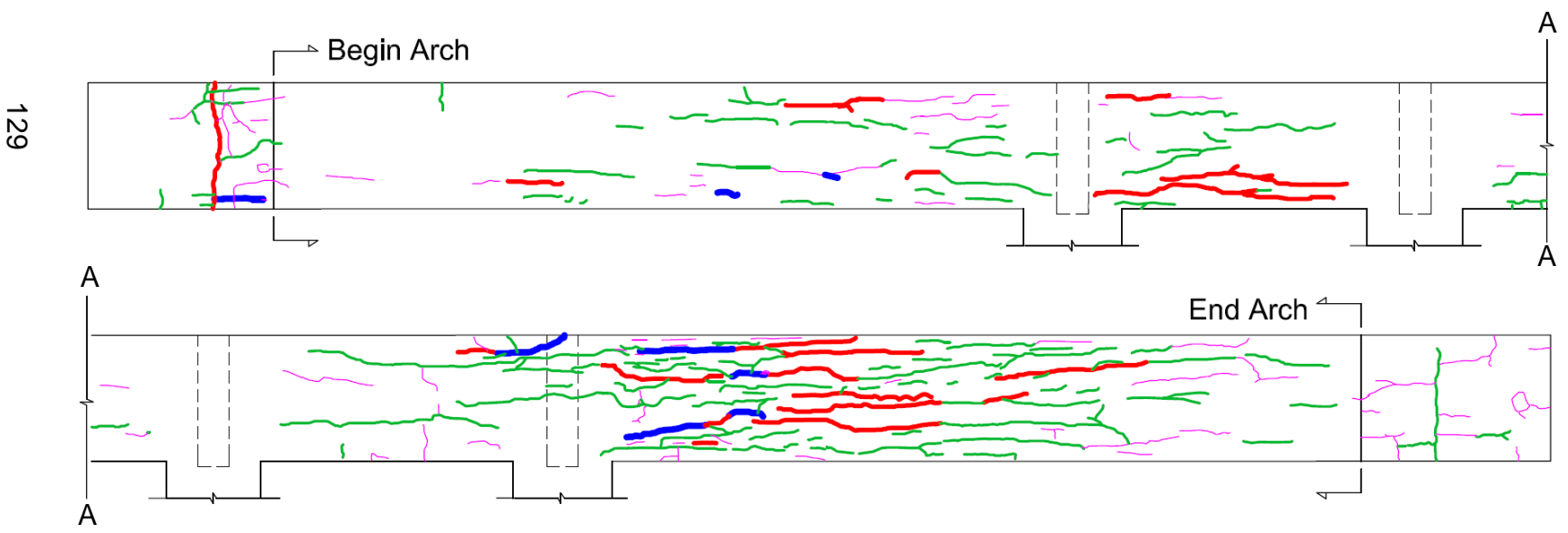
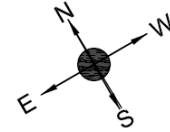


Figure 6.3. Crack mapping, November 2010, Span 5 – North Arch – Plan View



Crack Width (CW) Legend	
—	CW ≤ 0.01 in.
—	0.01 < CW ≤ 0.04 in.
—	0.04 < CW ≤ 0.10 in.
—	CW > 0.10 in.

Scale
 0' ————— 5'

Common Features Legend	
	Spalling
	Hidden Feature
	Cross Cut Section

130

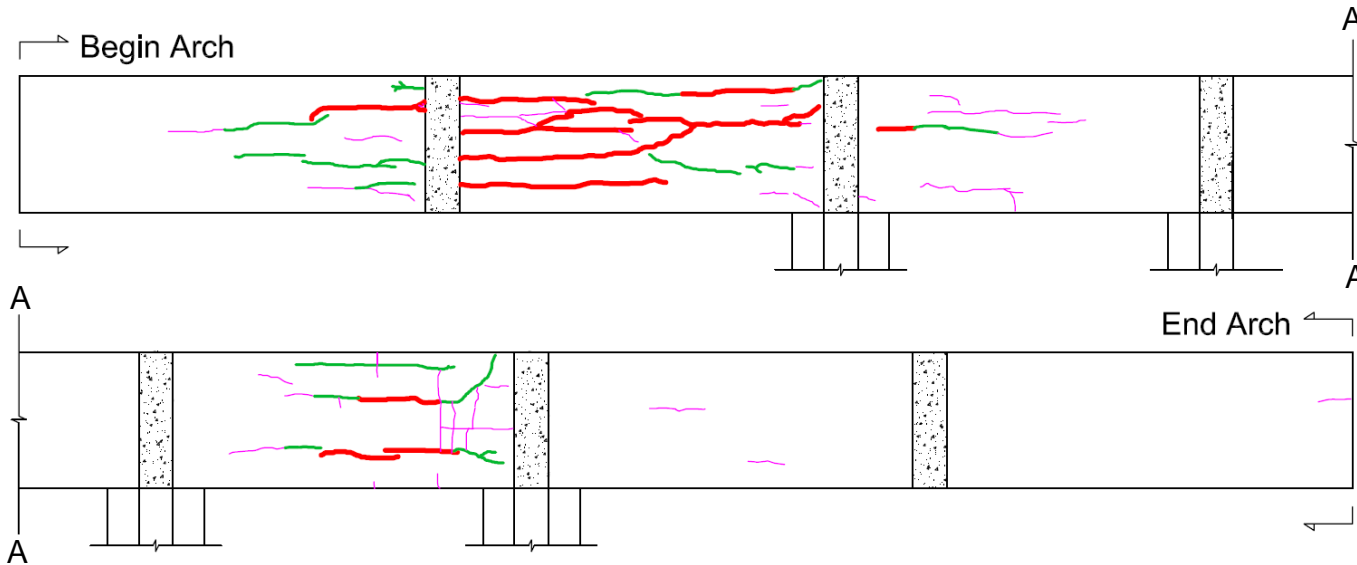
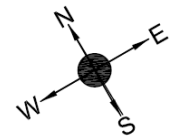


Figure 6.4. Crack mapping, November 2010, Span 5 – North Arch – Bottom View



Crack Width (CW) Legend	
	CW ≤ 0.01 in.
	0.01 < CW ≤ 0.04 in.
	0.04 < CW ≤ 0.10 in.
	CW > 0.10 in.

Scale
0' 5'

Common Features Legend	
	Spalling
	Hidden Feature
	Cross Cut Section

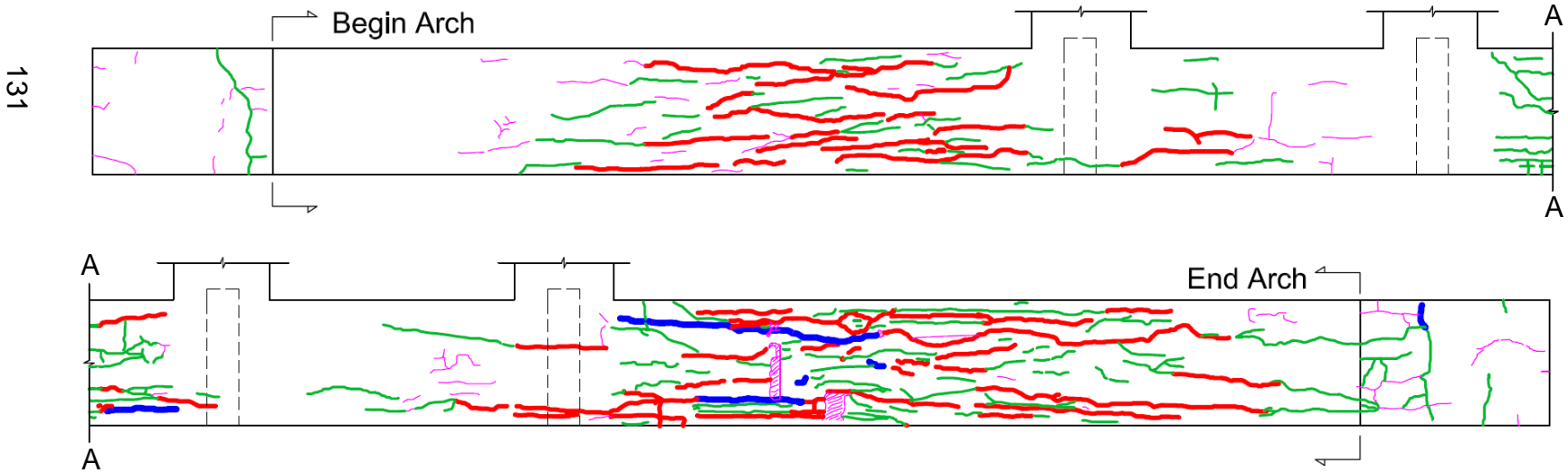
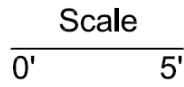


Figure 6.5. Crack mapping, November 2010, Span 5 – South Arch – Plan View

Crack Width (CW) Legend	
	CW ≤ 0.01 in.
	0.01 < CW ≤ 0.04 in.
	0.04 < CW ≤ 0.10 in.
	CW > 0.10 in.



Common Features Legend	
	Spalling
	Hidden Feature
	Cross Cut Section

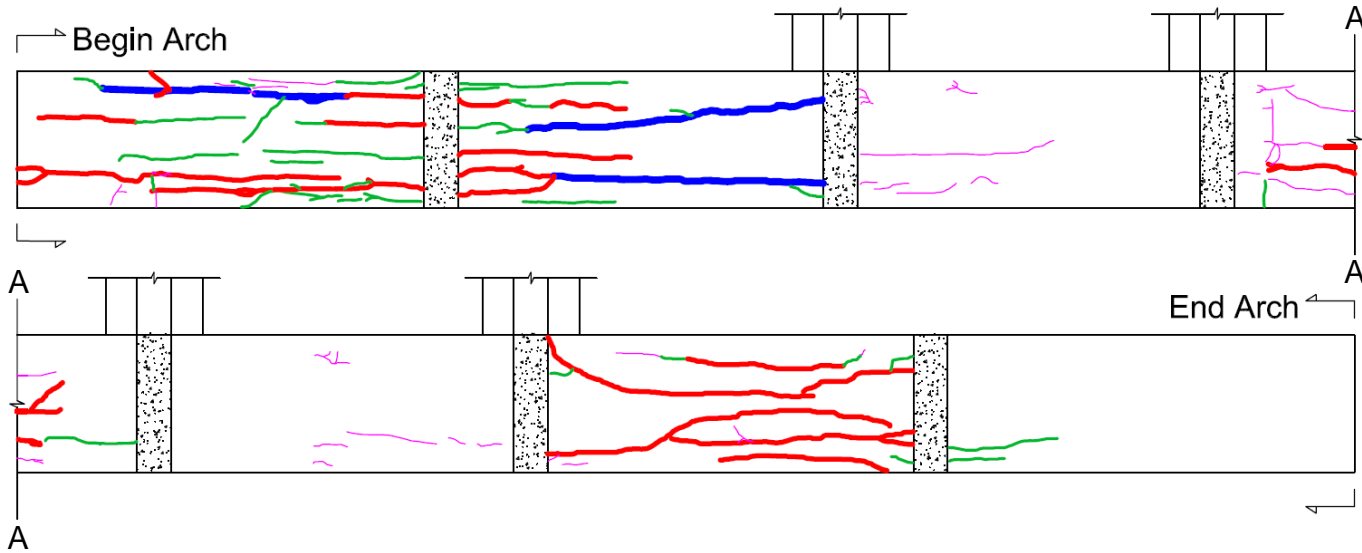
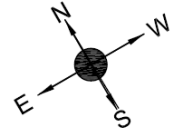


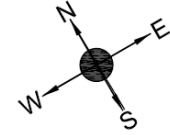
Figure 6.6. Crack mapping, November 2010, Span 5 – South Arch – Bottom View

6.2.2 Post-Mitigation Crack Survey

This section contains figures that were drawn from the follow-up crack survey performed in August of 2013. These figures also have the cracks that were present before the mitigation procedure, but they are all the same line weight and colored gray on the plots, regardless of their actual size.

As shown by all of the figures in this section, all of the new cracking is below 0.04 inches wide, and most are below 0.01 inches wide. However, it is important to keep in mind that pre-mitigation cracks were not re-measured due to them being sealed, and it is likely that these cracks widened, especially in the locations where the concrete is still expanding due to ASR. The addition of several new cracks in all of the arches shows that the concrete is still expanding, and the ASR mitigation procedure, discussed in detail in Chapter 4, has not been effective thus far.

The addition of new cracking also emphasizes the importance of maintaining the mitigation procedure by sealing new cracks as they form. Otherwise, all of the new cracks are paths for water to penetrate directly into the concrete and feed the ASR-expansion process. It should also be understood that cracking and expansion can still occur in large concrete sections after mitigation, even if all water is directed away from the concrete. This is because large cross sections of concrete may take several years to reach the 80 percent relative humidity mark, and the expansion process can still occur until this happens.



Crack Width (CW) Legend	
—	Pre-repair Cracks
—	New CW \leq 0.01 in.
—	0.01 < New CW \leq 0.04 in.
—	0.04 < New CW \leq 0.10 in.
—	New CW > 0.10 in.

Scale
0' 5'

Common Features Legend	
	Pre-repair Spalling
	New Spalling
- - -	Hidden Feature
	Cross Cut Section

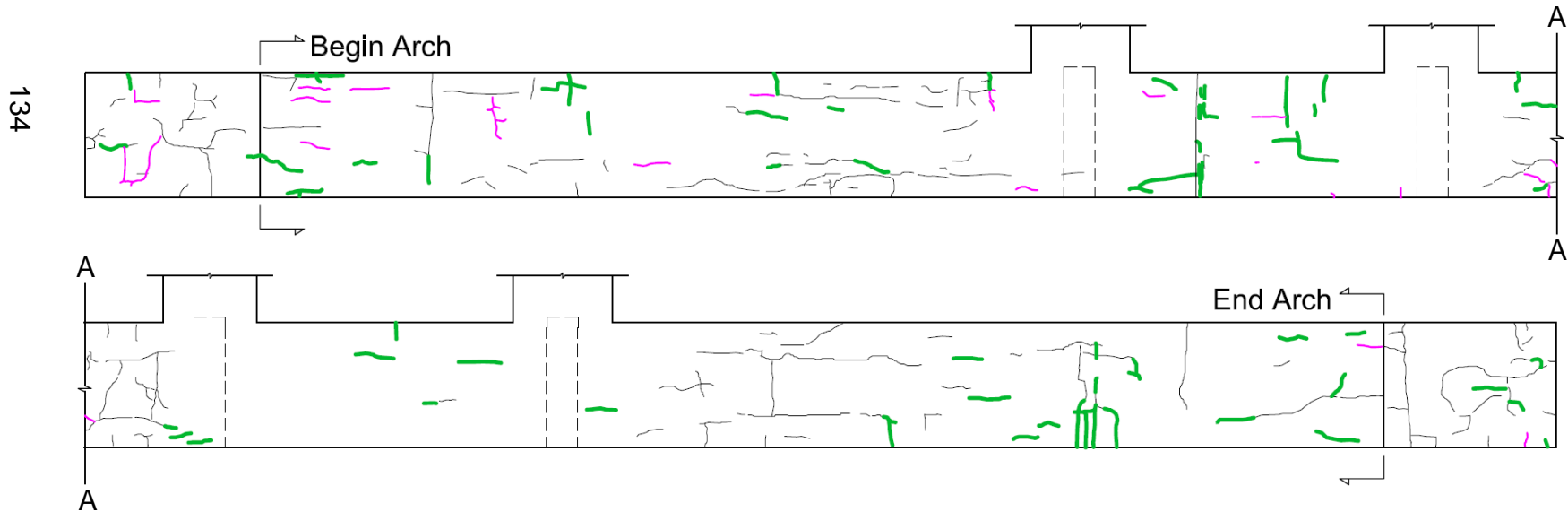
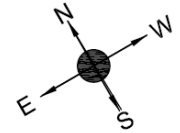
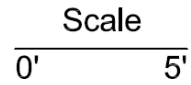


Figure 6.7. Crack mapping, August 2013, Span 4 – South Arch – Plan View



Crack Width (CW) Legend	
	Pre-repair Cracks
	New CW ≤ 0.01 in.
	0.01 < New CW ≤ 0.04 in.
	0.04 < New CW ≤ 0.10 in.
	New CW > 0.10 in.



Common Features Legend	
	Pre-repair Spalling
	New Spalling
	Hidden Feature
	Cross Cut Section

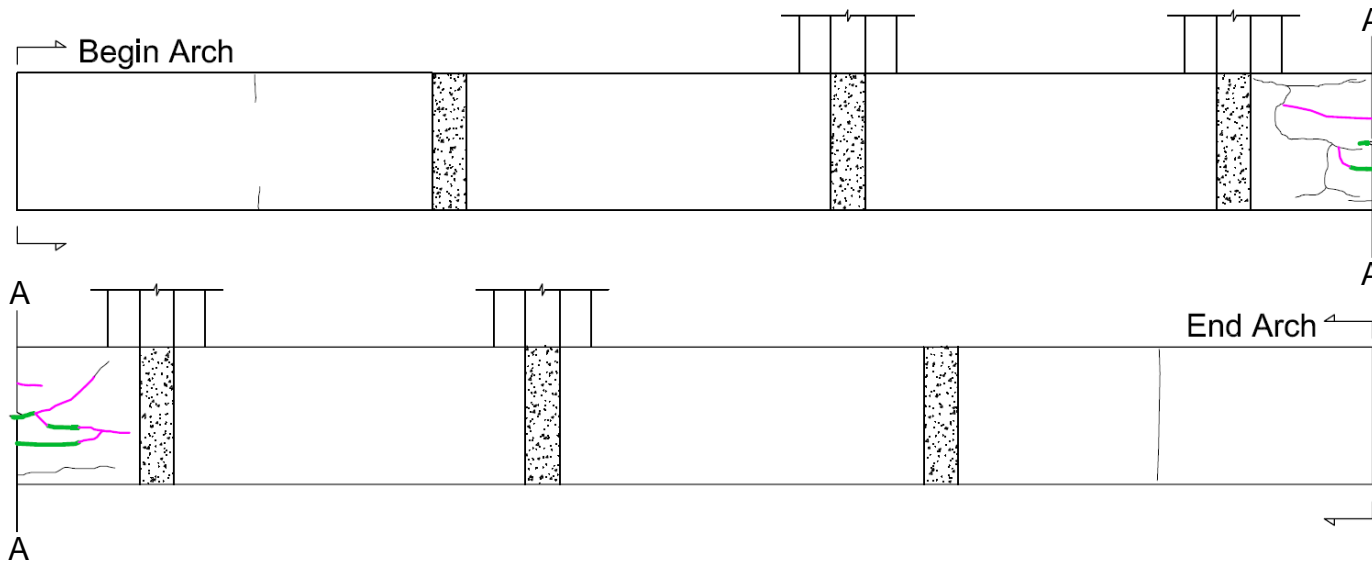
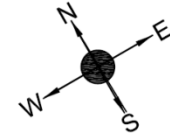
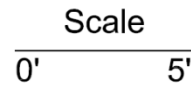


Figure 6.8. Crack mapping, August 2013, Span 4 – South Arch – Bottom View



Crack Width (CW) Legend	
—	Pre-repair Cracks
—	New CW ≤ 0.01 in.
—	$0.01 < \text{New CW} \leq 0.04$ in.
—	$0.04 < \text{New CW} \leq 0.10$ in.
—	New CW > 0.10 in.



Common Features Legend	
	Pre-repair Spalling
	New Spalling
- - -	Hidden Feature
	Cross Cut Section

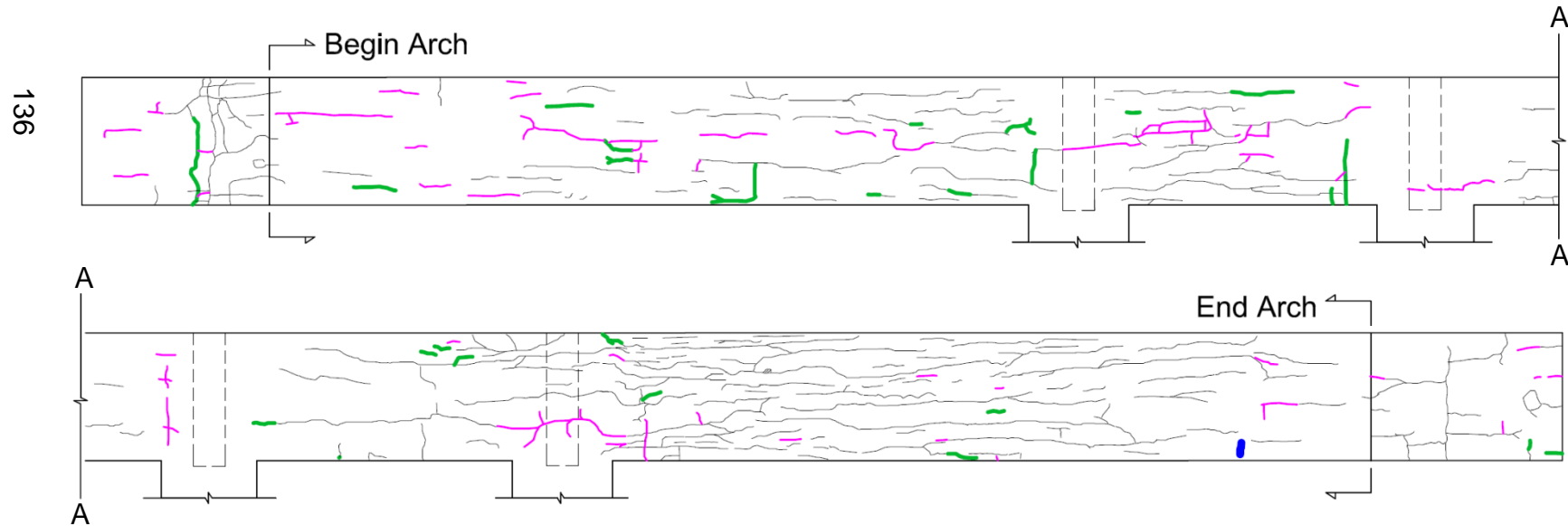
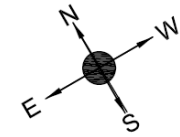
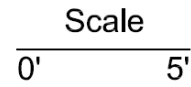


Figure 6.9. Crack mapping, August 2013, Span 5 – North Arch – Plan View



Crack Width (CW) Legend	
—	Pre-repair Cracks
—	New CW ≤ 0.01 in.
—	0.01 < New CW ≤ 0.04 in.
—	0.04 < New CW ≤ 0.10 in.
—	New CW > 0.10 in.



Common Features Legend	
	Pre-repair Spalling
	New Spalling
---	Hidden Feature
	Cross Cut Section

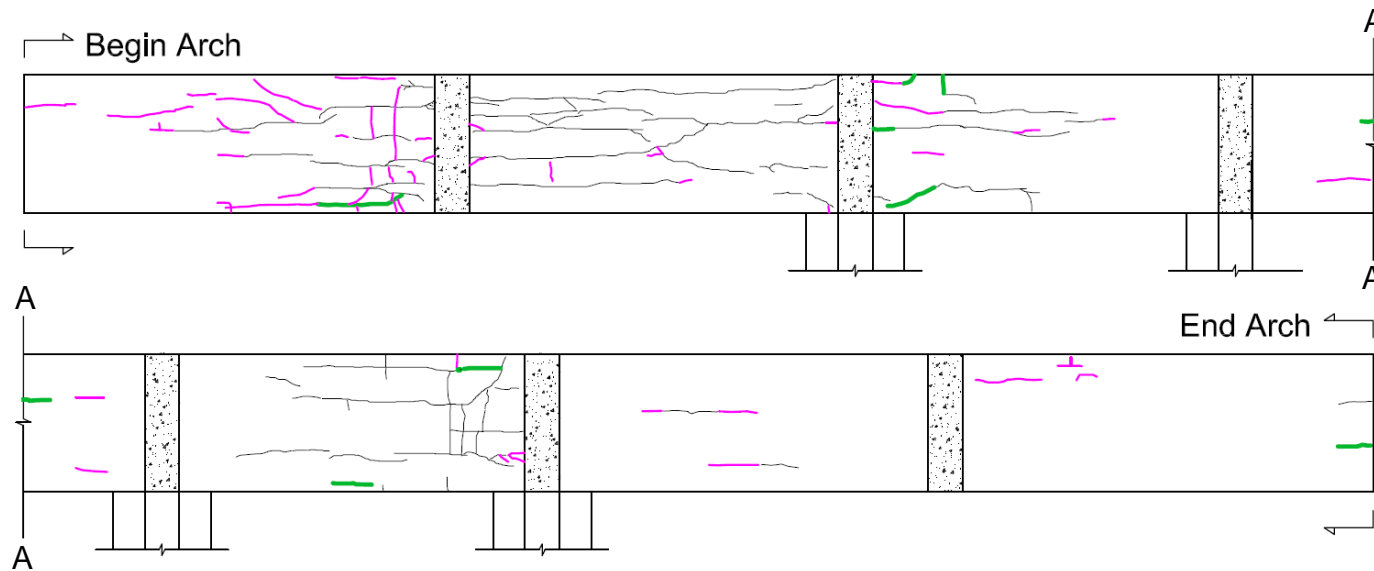
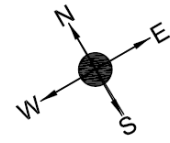
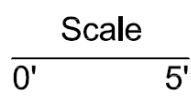


Figure 6.10. Crack mapping, August 2013, Span 5 – North Arch – Bottom View



Crack Width (CW) Legend	
—	Pre-repair Cracks
—	New CW \leq 0.01 in.
—	0.01 < New CW \leq 0.04 in.
—	0.04 < New CW \leq 0.10 in.
—	New CW > 0.10 in.



Common Features Legend	
	Pre-repair Spalling
	New Spalling
- - -	Hidden Feature
	Cross Cut Section

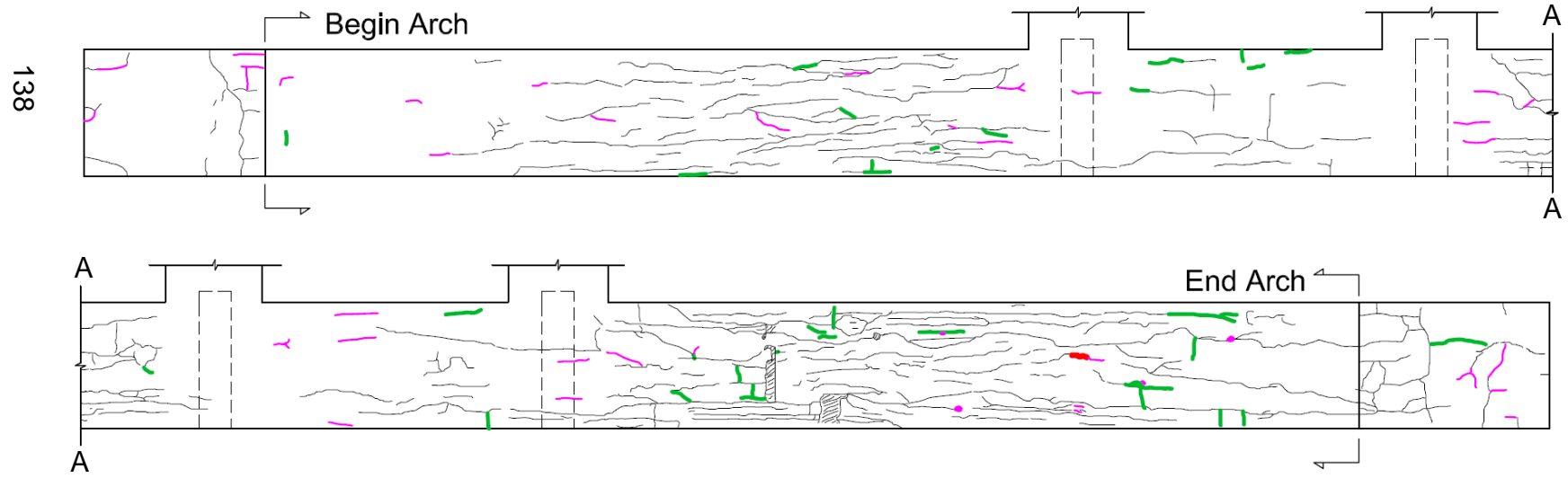
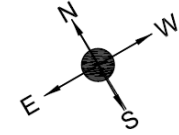


Figure 6.11. Crack mapping, August 2013, Span 5 – South Arch – Plan View



Crack Width (CW) Legend	
—	Pre-repair Cracks
—	New CW \leq 0.01 in.
—	0.01 < New CW \leq 0.04 in.
—	0.04 < New CW \leq 0.10 in.
—	New CW > 0.10 in.

Scale
0' 5'

Common Features Legend	
	Pre-repair Spalling
	New Spalling
---	Hidden Feature
	Cross Cut Section

139

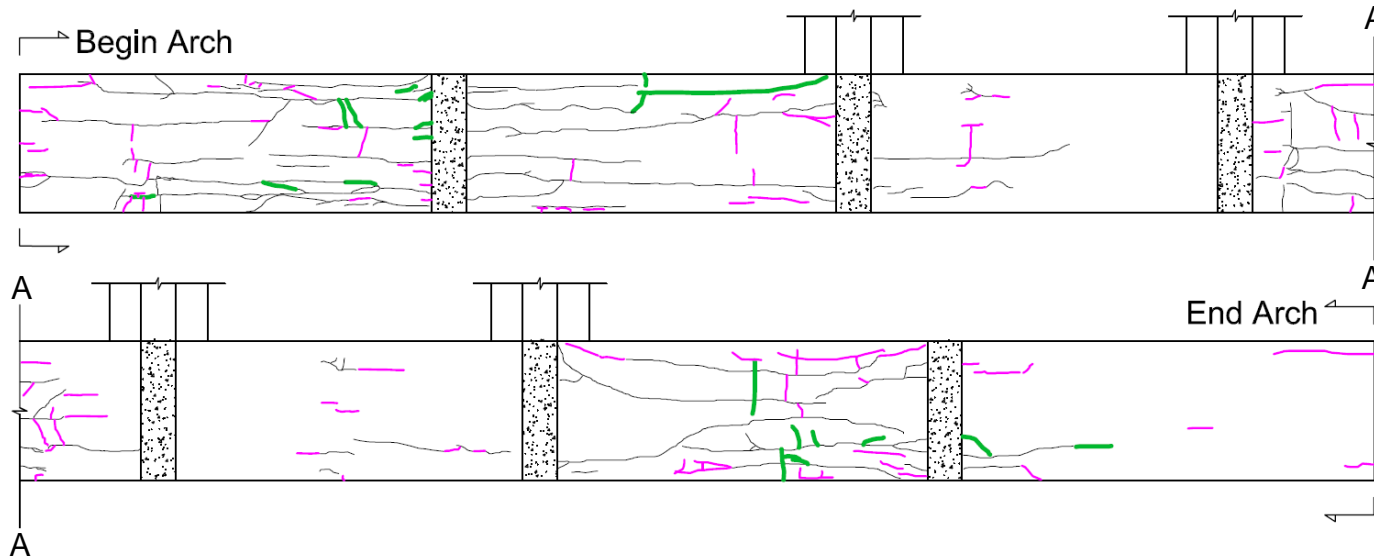


Figure 6.12. Crack mapping, August 2013, Span 5 – South Arch – Bottom View

6.2.3 Examples of Post-mitigation Cracking

This section contains photographs taken while performing the crack mapping surveys. All of the figures have a part (A), picture taken during November 2010 survey, and a part (B), picture taken during August 2013 survey. These images show widening and elongation of existing cracks, and/or additional new cracking. Some of these images appear to be skewed between (A) and (B). This occurs when the pictures were taken from opposite ends of the grid, and thus have different camera angles.

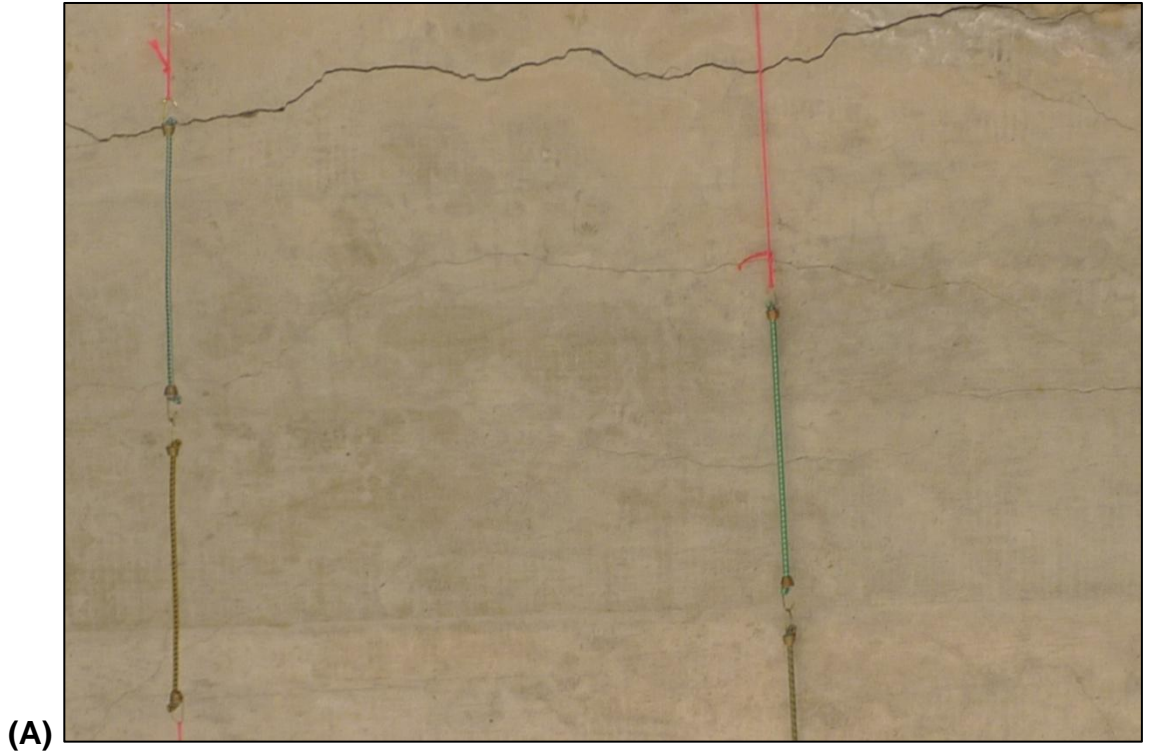


Figure 6.13. Widening and elongation of existing cracks in span 4 – south arch,
(A) November 2010 and (B) August 2013



Figure 6.14. Additional cracking in span 5 – north arch, (A) November 2010 and
(B) August 2013

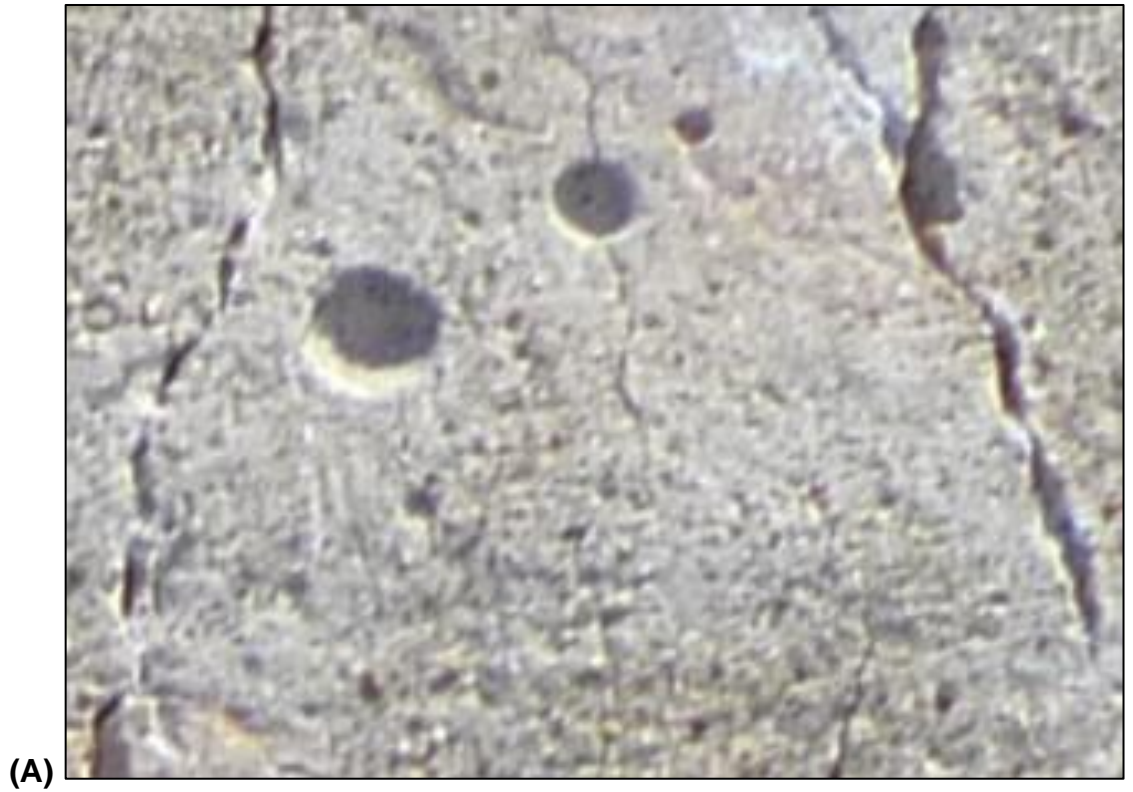


Figure 6.15. Crack widening on span 5 – south arch, (A) November 2010 and (B) August 2013

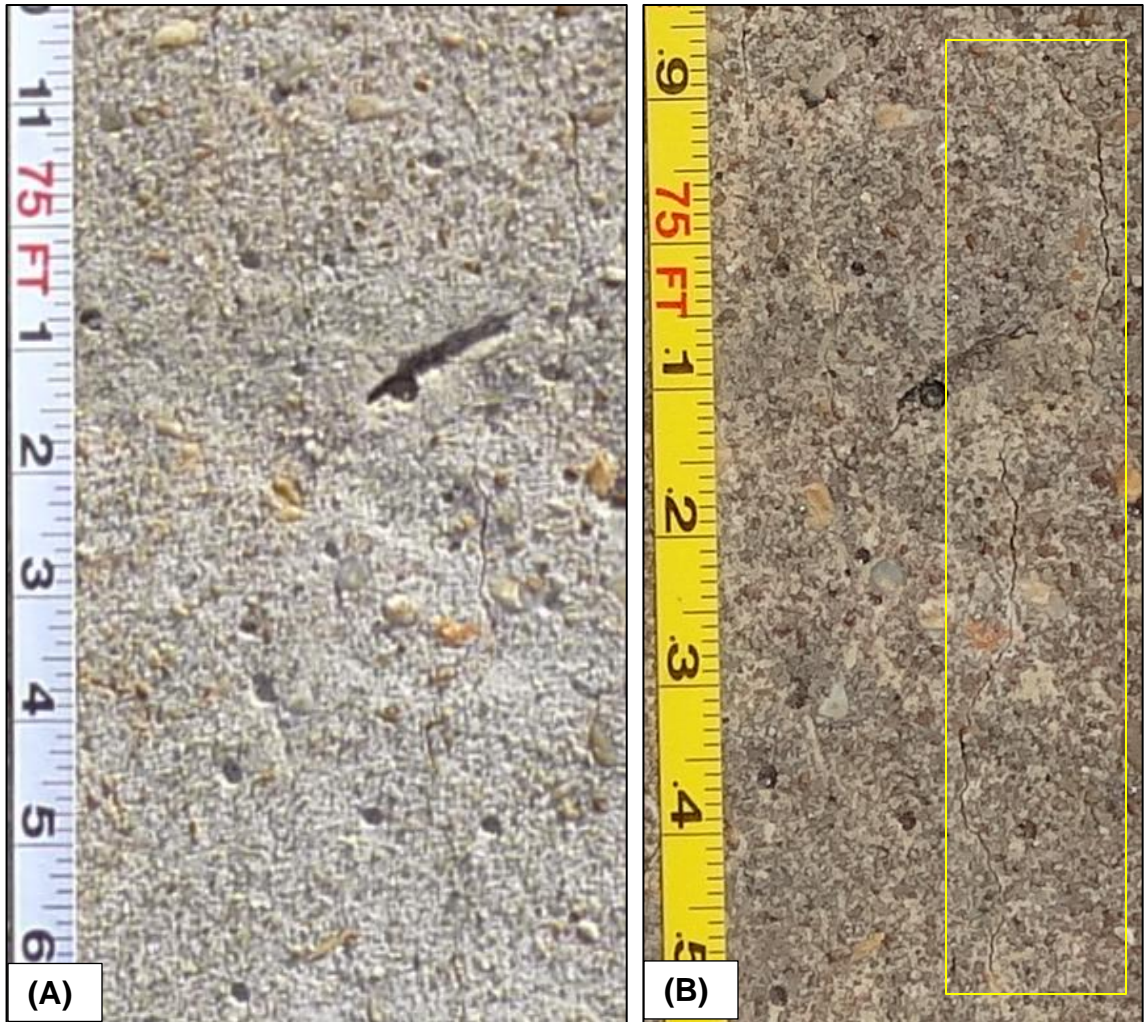


Figure 6.16. Crack widening on span 5 – south arch, (A) November 2010 and (B) August 2013

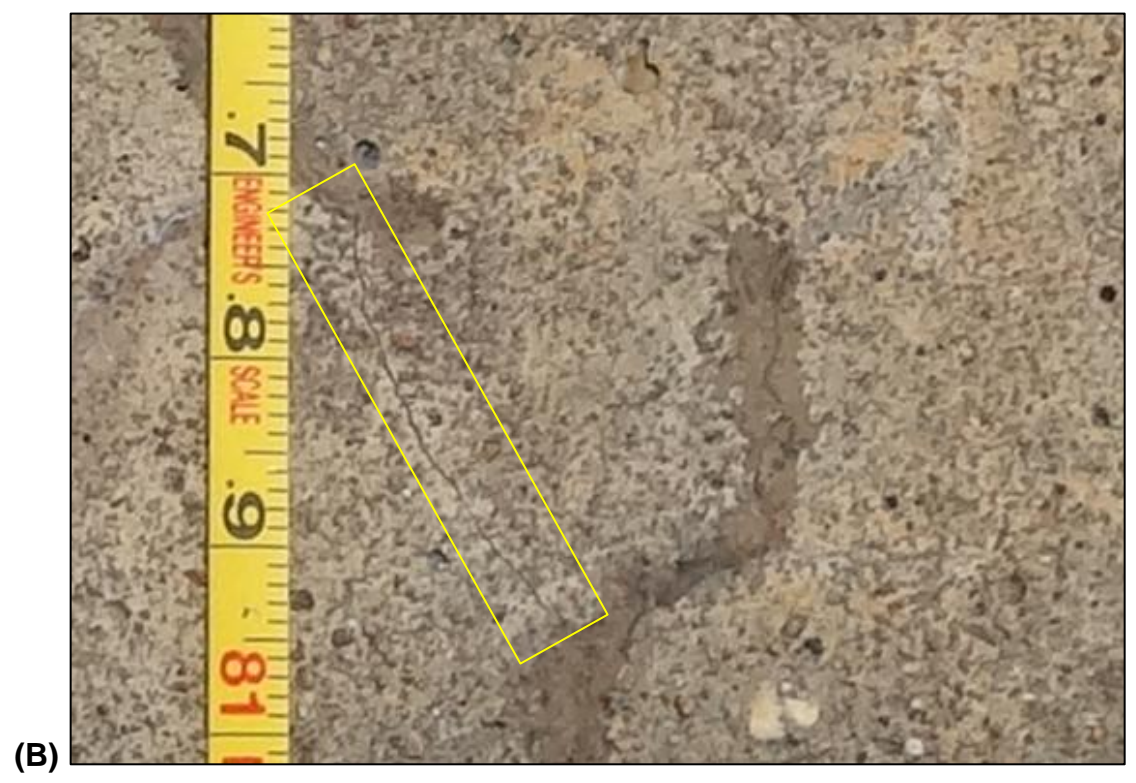


Figure 6.17. New crack on span 5 – south arch, (A) November 2010 and (B) August 2013

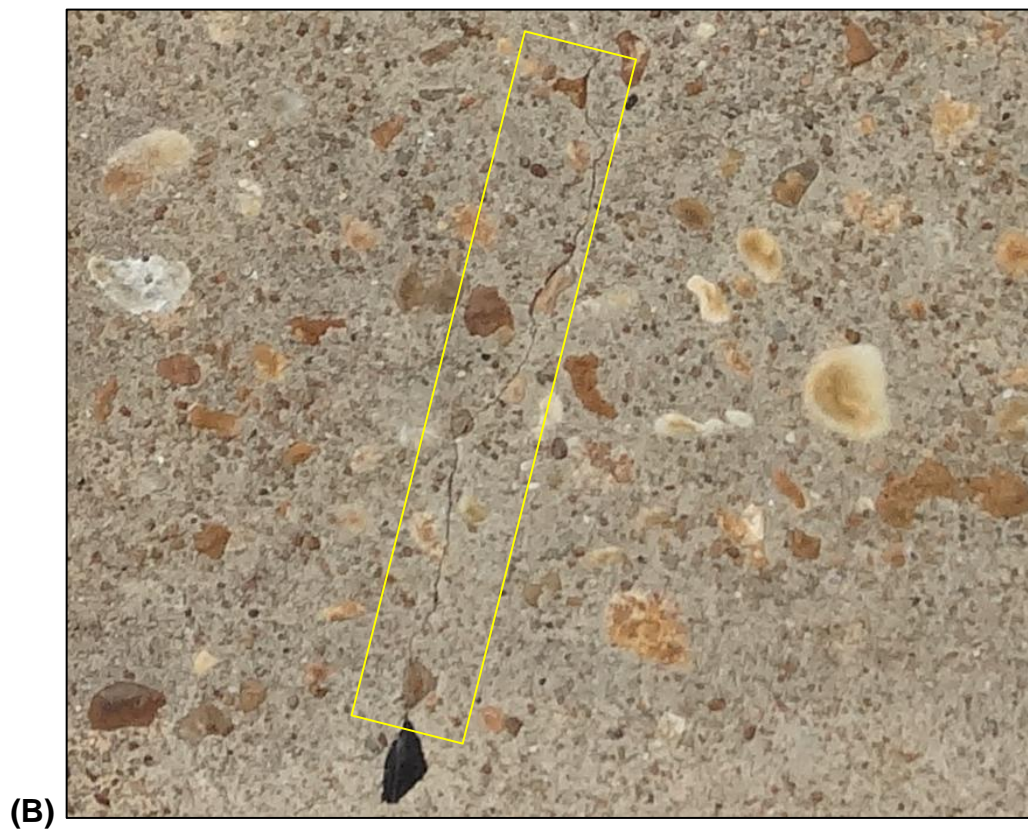
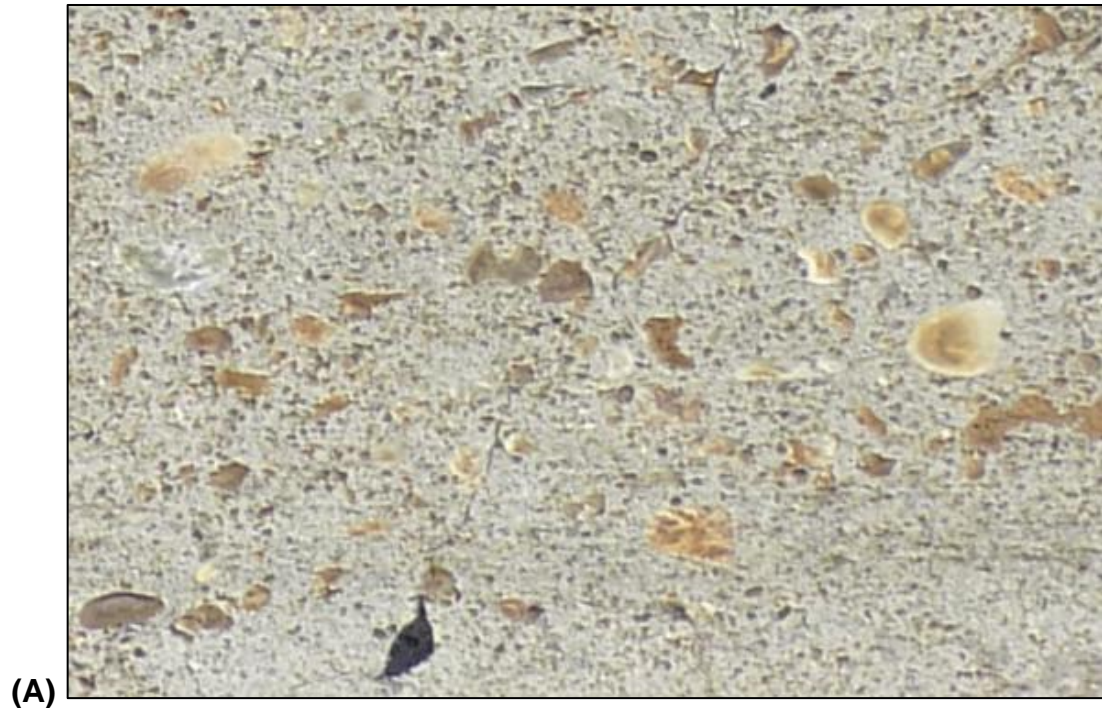


Figure 6.18. Crack widening on span 5 – south arch, (A) November 2010 and (B) August 2013

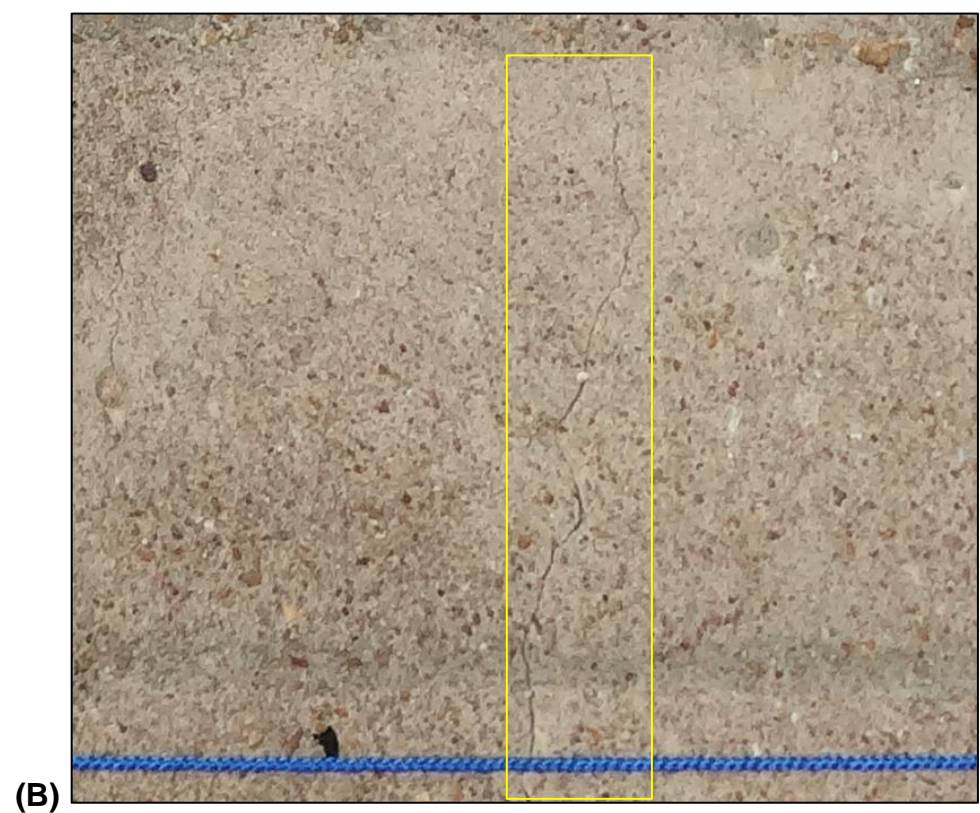


Figure 6.19. Crack extending on span 5 – south arch, (A) November 2010 and
(B) August 2013

6.2.4 Cracking Summary

Crack surveys were taken on the Bibb Graves Bridge before and after the mitigation procedure was applied, November 2010 and August 2013, respectively. These surveys were performed on both arches of span 5 and the southern arch of span 4. Cracks were found on all three of the arches prior to application of the mitigation procedure, and additional cracking was seen on all of these arches three years later, as shown in Figure 6.7 through Figure 6.12.

New cracking along with the widening of older hair-line cracks were found in the second survey and suggest that the ASR mitigation procedure has not been effective thus far. New cracks also provide routes for water to enter the concrete, even though the concrete was sealed before, and drive the ASR-expansion process. Therefore, it is important to seal any new cracks as soon as possible.

6.3 Internal Relative Humidity

A summary of the relative humidity survey dates along with the corresponding time since the application of the ASR mitigation procedure, in mid-November of 2010, is given in Table 6.1. Relative humidity data were collected monthly, weather permitting, from 3 months after the application of the mitigation procedure to 34 months after.

The relative humidity survey results are presented before expansion results because ASR-related expansions will continue until the internal relative humidity of the concrete is below 80 percent. This threshold of 80 percent is also plotted with a bold line on all of the humidity plots along with the 28-day running

average, ambient relative humidity. The ambient humidity conditions were collected from Maxwell Air Force Base in Montgomery, Alabama; which is about 13 miles from the Bibb Graves Bridge and is shown in Figure 6.20. All of the relative humidity data collected from the bridge are presented in Appendix D.

Table 6.1. RH survey dates and corresponding time since mitigation application

RH Measurement Survey Dates			
Survey Date	Months After Mitigation	Survey Date	Months After Mitigation
02/15/11	3.0	07/16/12	20.0
04/07/11	4.7	08/13/12	20.9
05/05/11	5.6	09/13/12	21.9
06/03/11	6.5	10/14/12	22.9
07/07/11	7.7	11/19/12	24.1
08/10/11	8.8	12/06/12	24.7
09/15/11	10.0	01/08/13	25.8
10/18/11	11.0	02/05/13	26.7
11/08/11	11.7	03/14/13	27.9
12/14/11	12.9	04/09/13	28.8
01/31/12	14.5	05/14/13	29.9
03/08/12	15.7	07/17/13	32.0
04/12/12	16.8	08/05/13	32.6
05/17/12	18.0	09/10/13	33.8
06/08/12	18.7		



Figure 6.20. Maxwell Air Force Base (Adapted from Bing Maps 2013)

6.3.1 Relative Humidity Measurement Identification

Each arch in spans 4 and 5 has four locations where relative humidity measurements were taken at 1, 2, and 3-inch depths, for a total of 48 individual points. A summary of how the data were collected along with a schematic of these locations can be found in section 5.3. For figures, tables, and the discussion of data and analysis in this chapter, the following simplified identification system for measurement locations is used:

Span Number - Arch Location - Measurement Location - Measurement Depth

4	South (S)	West Top (WT)	1"
5	North (N)	West Bottom (WB)	2"
		East Top (ET)	3"
		East Bottom (EB)	Average (AVG)

Example: 4-N-ET-AVG is the average of all three measurement depths at the east top location, on the northern arch of span 4.

6.3.2 Average Relative Humidity Data

The average of the relative humidity measurement data at all three depths per location (four locations per arch) along with the 28-day running average of the ambient relative humidity are presented in next four figures. The data for the west bottom locations are graphed in Figure 6.21, and west top data are presented in Figure 6.22. The relative humidity data for the east bottom and east top measurement locations are graphed in Figure 6.23 and Figure 6.24, respectively.

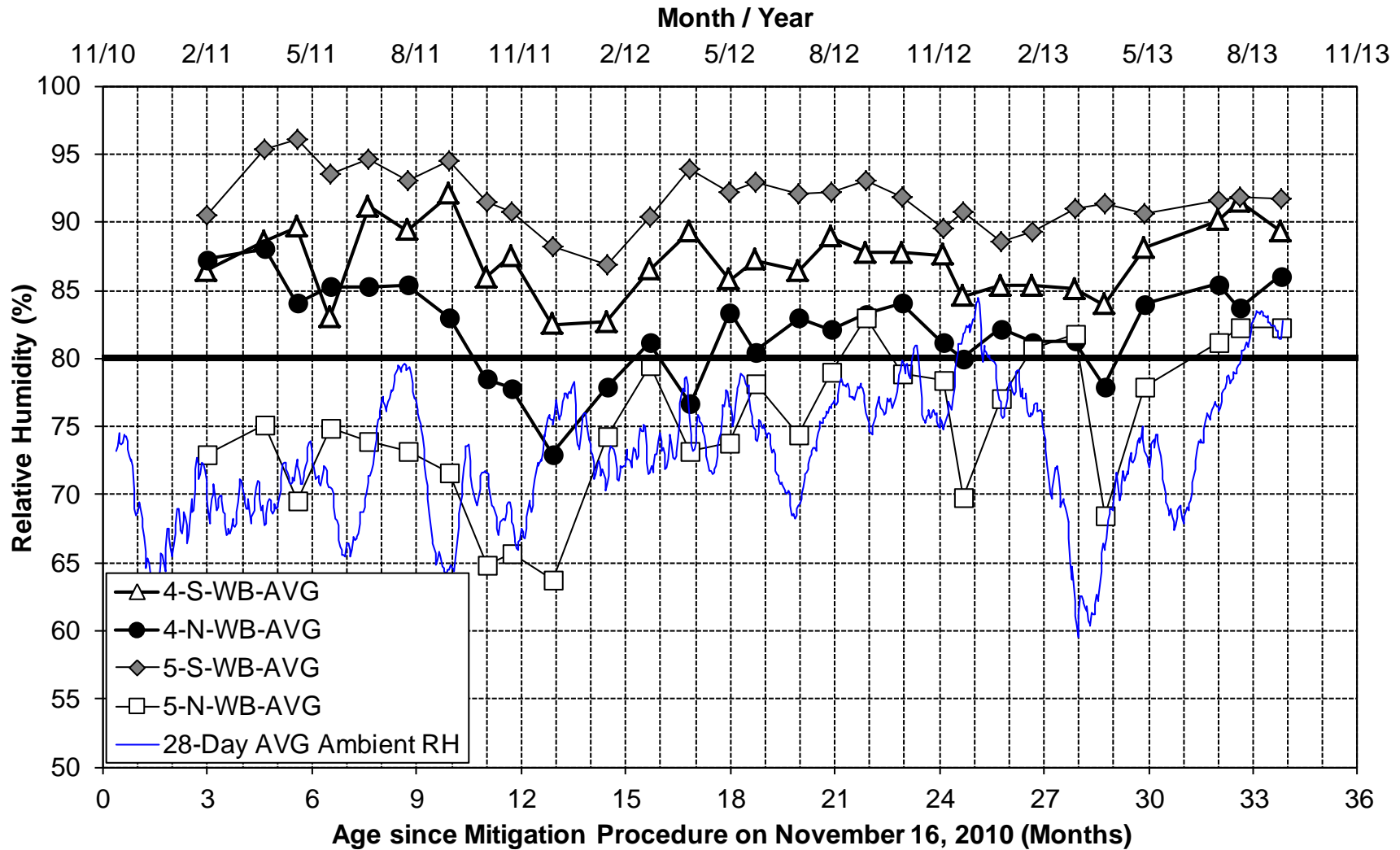


Figure 6.21. RH measurements, West Bottom, average of all measurement depths

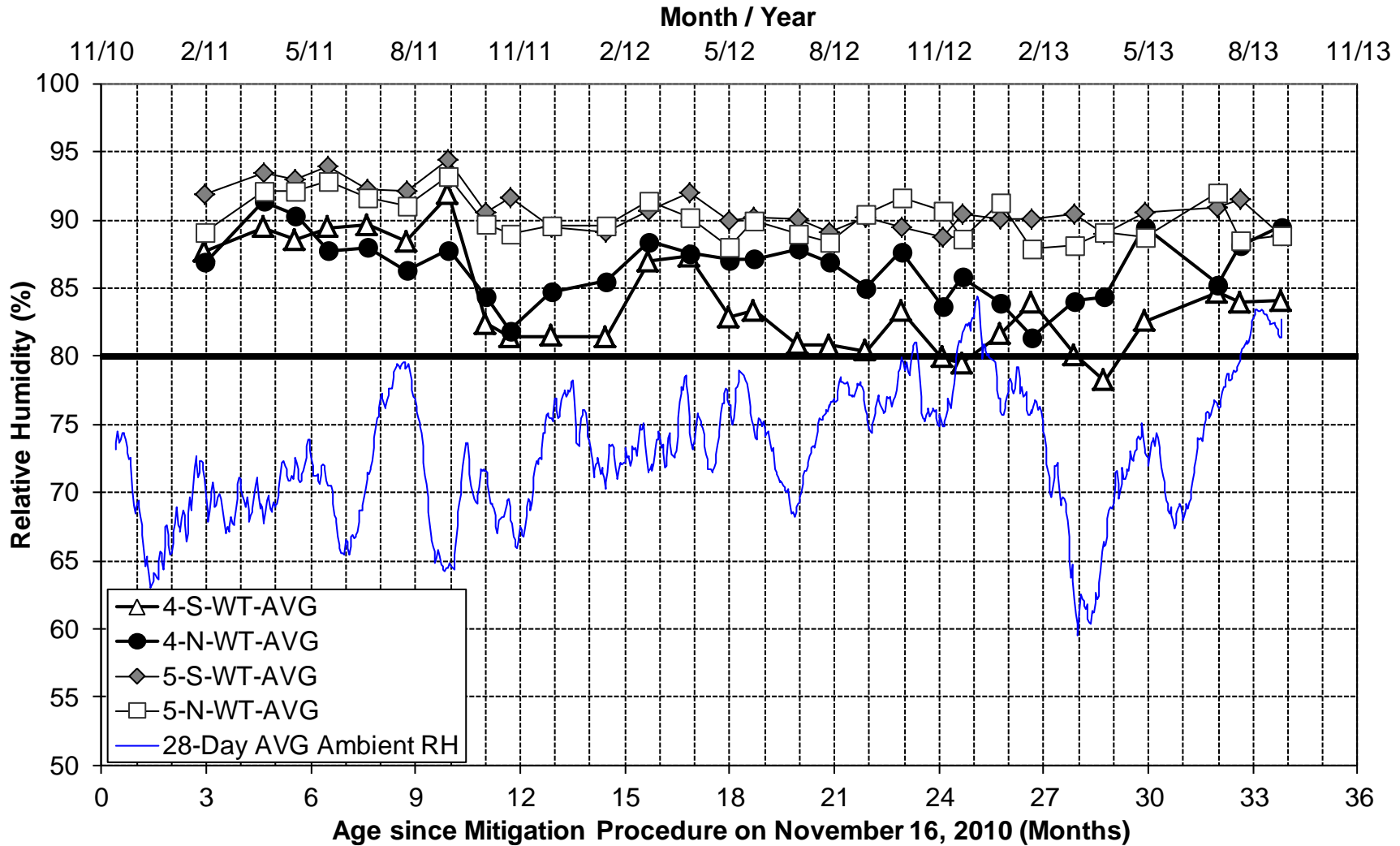


Figure 6.22. RH measurements, West Top, average of all measurement depths

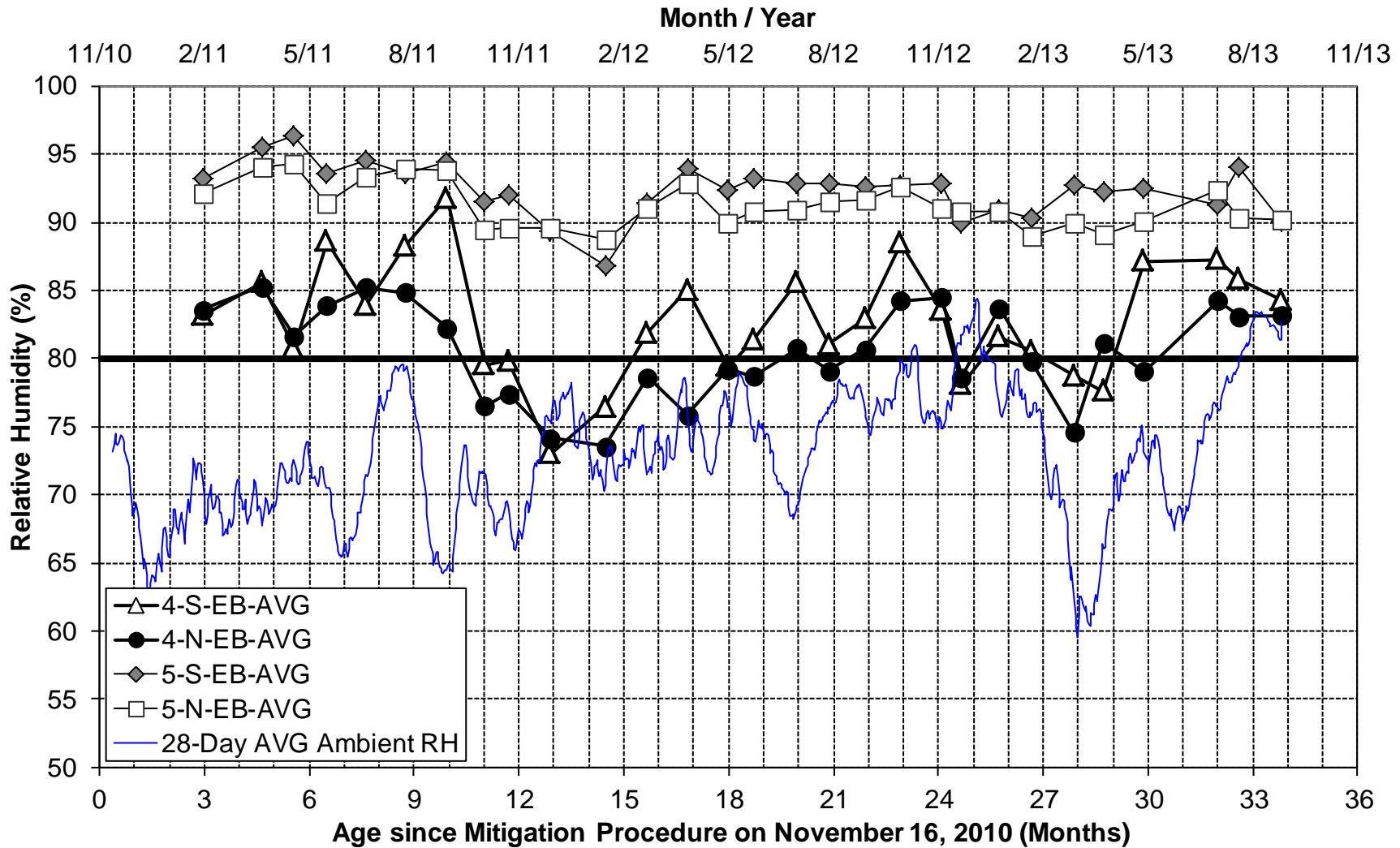


Figure 6.23. RH measurements, East Bottom, average of all measurement depths

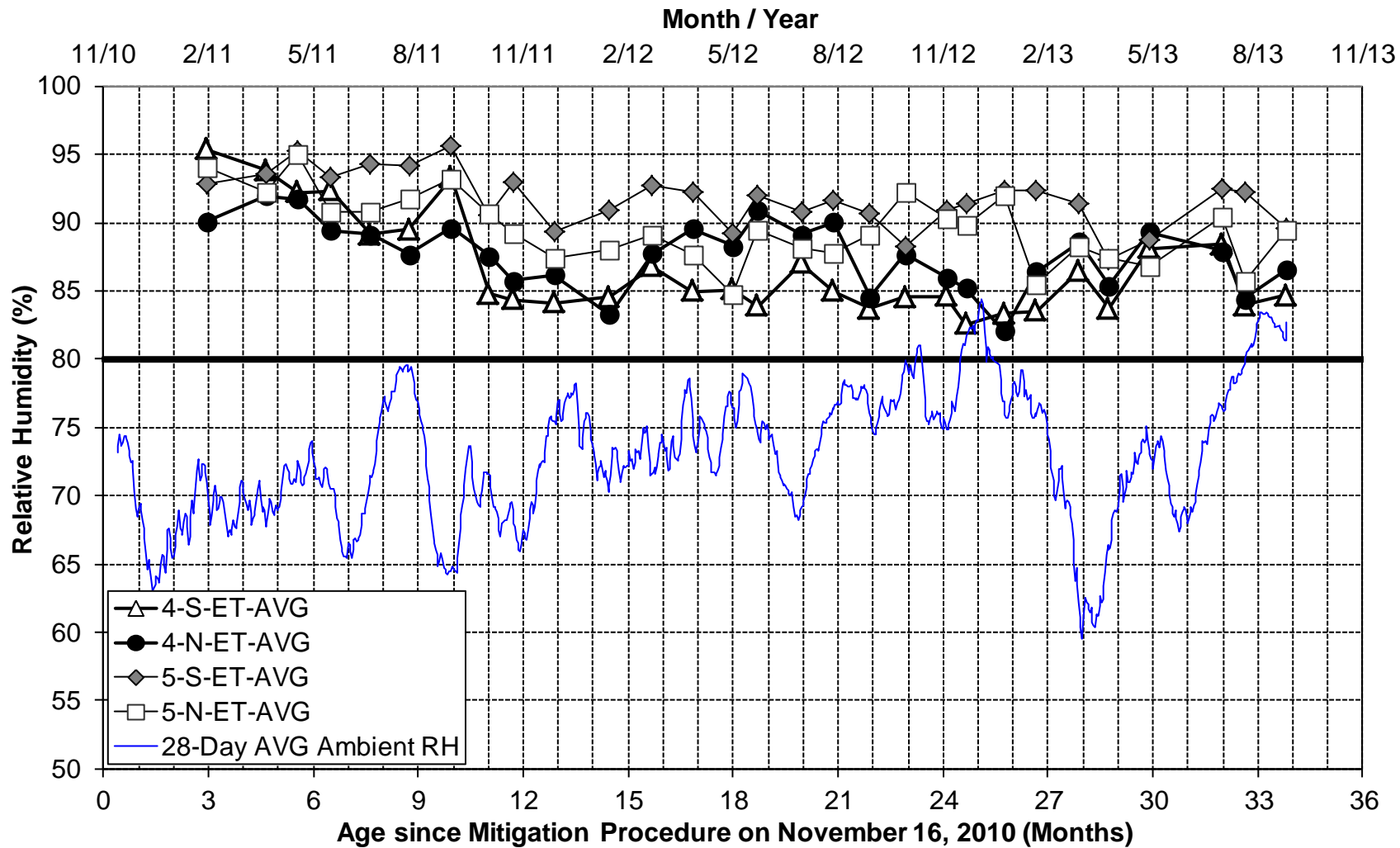


Figure 6.24. RH measurements, East Top, average of all measurement depths

Upon looking at the relative humidity data presented in Figure 6.21 through Figure 6.24, it is very apparent that the humidity in the arches of span 4 is typically lower than the humidity in span 5, with the exception of 5-N-WB-AVG. 5-N-WB-AVG has had relative humidity measurements below the 80 percent goal for most of the monitoring period, and visual inspection of this location reveals that this concrete is very sound and does not have any signs of ASR. For the most part, the data in Figure 6.22 through Figure 6.24 (west top, east bottom, and east top locations) seems to form a group for span 4 and a group for span 5; they are not divided between treated and non-treated as one would expect if the silane was effective. It is also notable that the data for each respective arch location tend to respond to ambient conditions similarly; meaning most of the data in each graph rise and fall together over time.

Figure 6.21 is the graph of the relative humidity data for the west bottom locations. As previously stated, 5-N-WB-AVG has the lowest data, but it is followed closely by 4-N-WB-AVG in the latter half of the monitoring time period. The sharp rise in relative humidity at 5-N-WB-AVG may be explained by the fact that 5-N-WT-AVG, which is directly above 5-N-WB-AVG, has a 15 percent higher humidity than 5-N-WB-AVG, as shown later in Table 6.2. The plots for 5-S-WB-AVG and 4-S-WB-AVG are mostly in the low ninety and upper eighty percent relative humidity ranges, respectively, and both are well above 4-N-WB-AVG. The combination of all of these findings suggests that the ASR mitigation procedure has not had any effect at the west bottom locations.

The relative humidity data for the west top locations are presented in Figure 6.22. The plotted humidity measurements for both arches of span 5 are very similar and hover around the 90 percent relative humidity mark for a vast majority of the readings. The span 4 data have the most variability between readings for the west top locations. 4-S-WT-AVG has the lowest humidity at this typical location for a majority of the readings, but it will take further analysis to determine if there is any drying relative to the untreated arch location, 4-N-WT-AVG. However, it is also very apparent in Figure 6.22 that the mitigation procedure has not had any effect on lowering the moisture content in span 5.

The largest separation of humidity data between spans 4 and 5 is at the east bottom locations as shown in Figure 6.23. Once again, the ASR-affected locations 5-N-EB-AVG and 5-S-EB-AVG have the highest humidity with measurements constantly in the lower ninety percent relative humidity range. 4-N-EB-AVG has the lowest humidity for most of the readings, and it fluctuates between 75 and 85 percent relative humidity. The lack of lowered humidity over time nor when compared to compared to the control arch confirms that the mitigation procedure was not effective at the east bottom locations either.

The east top locations shown in Figure 6.24 have the most similar relative humidity data for all of the arches. The readings for both arches in span 5 dropped few percent within the first year of monitoring, but they have remained around the 90 percent relative humidity line since. 4-S-ET-AVG had the highest overall drop in relative humidity at the east top location, down to about 85 percent, but this was also within the first year. Regression analysis will be

necessary to determine if there is any statistical evidence of drying in the arches that may suggest the mitigation procedure has had a positive effect; especially when comparing the results of the treated arches to the untreated arches.

All of the previously presented relative humidity data were analyzed with regression trends to see if there was any evidence of drying within the concrete arches. The coefficient of determination (r^2) value was used to determine if the trends were statistically significant. An r^2 threshold of at least 0.5 was used to denote a significant trend. With the use of this analysis technique, it was determined that none of the average relative humidity data at the 16 locations had any strong evidence of drying. These findings helped confirm the already mentioned notion that the ASR mitigation procedure applied to three of the four monitored arches was not effective in lowering the moisture content in the concrete.

6.3.2.1 Relative Humidity Difference Analysis

Another analysis technique used to evaluate the effectiveness of the mitigation procedure is referred to as the “relative humidity difference” analysis. This analysis takes the difference between the measured data in the treated arches relative to the data in the untreated, control arch. The benefit of this type of procedure is that it directly compares the relative humidity of the concrete treated with the mitigation procedure to the untreated concrete. This technique is viable because measurement locations are at the same relative position on each arch and these locations should have similar concrete compositions.

The relative humidity difference analysis results for the average humidity at the four typical locations are presented in Figure 6.25 through Figure 6.28. All of these plots have trend lines on the data, but only strong trends with r^2 values above 0.5 have the equation for the trend line displayed.

The first relative humidity difference plot presented, Figure 6.25, is for the west bottom locations. This location is the only one that has a statistically relevant trend out of the four locations, but this trend for 5-N-WB-AVG is increasing at a rate of 0.366 percent relative humidity per month, which indicates that this location is gaining moisture compared to 4-N-WB-AVG. Even though 5-N-WB-AVG is increasing in humidity when compared to the control arch, it still had the lowest humidity of any of the 16 locations throughout monitoring, and it does not have any signs of ASR at this time. The other two locations in this plot, 4-S-WB-AVG and 5-S-WB-AVG, do not have any signs of behaving differently than the control arch.

Figure 6.26 is the relative humidity difference plots for the west top locations. It is clear that the two span 5 locations do not have any diverging humidity trends when compared to span 4 north, but 4-S-WT-AVG appears to be drying relative to the untreated arch. This apparent decreasing trend could be used to reason that the mitigation procedure might have had a little effect on the top of the un-distressed arch. But upon further investigation into the 4-S-WT-AVG data, it had an r^2 value of 0.314 and it reached its maximum difference with 4-N-WT-AVG over a year before the end of monitoring. Only time will tell if this downward trend will gain strength or continue to weaken.

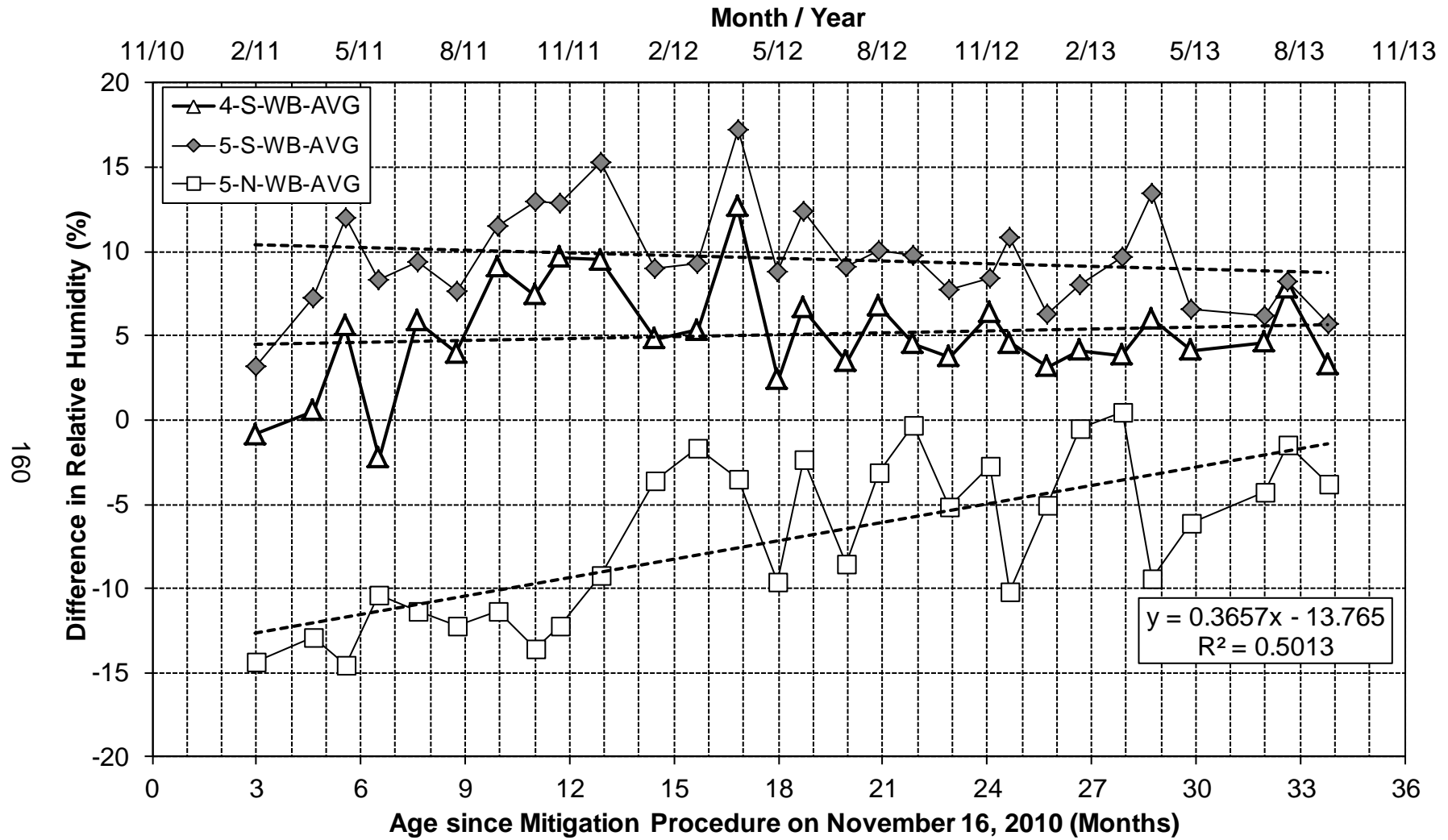


Figure 6.25. RH difference for West Bottom average

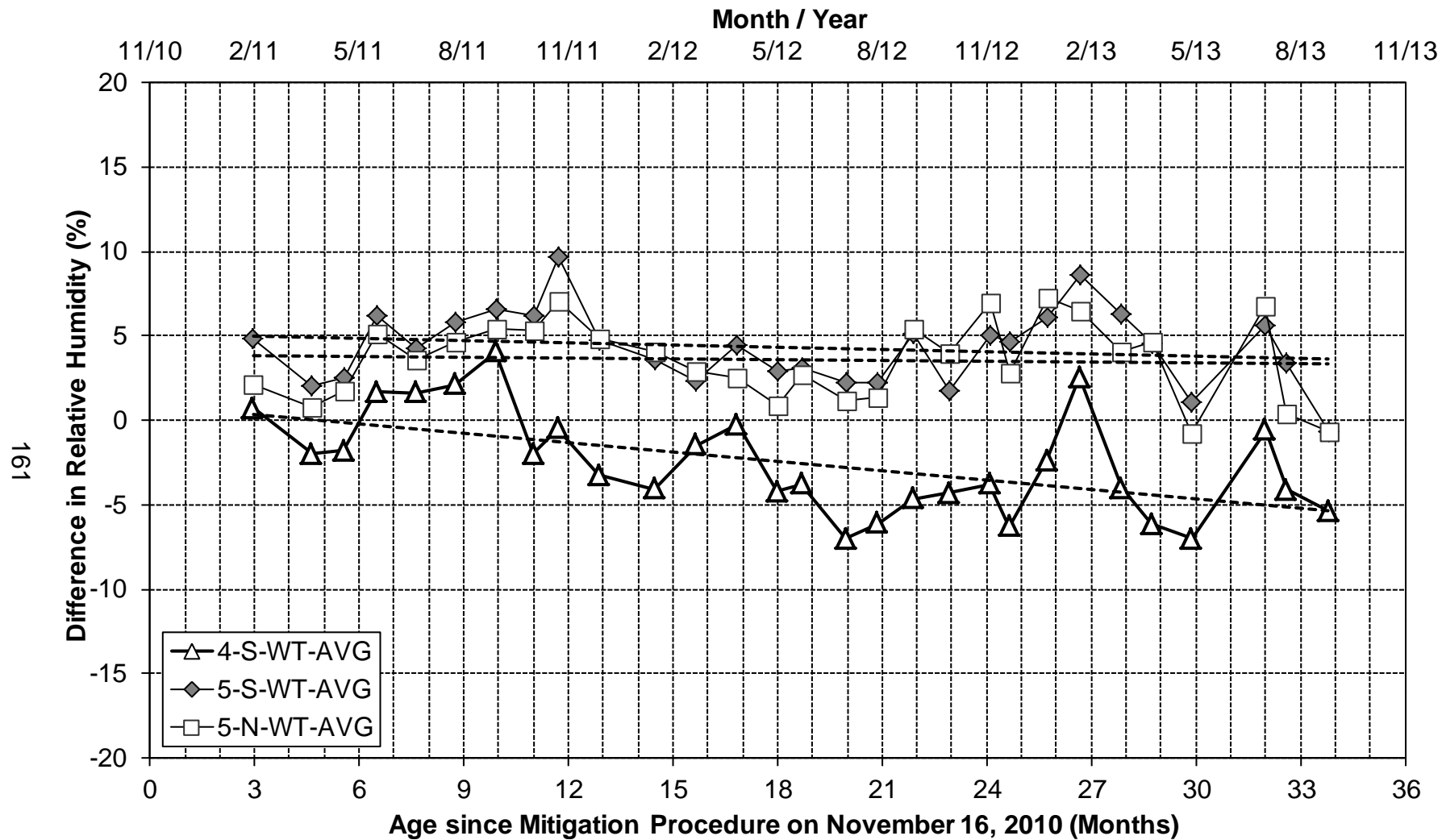


Figure 6.26. RH difference for West Top average

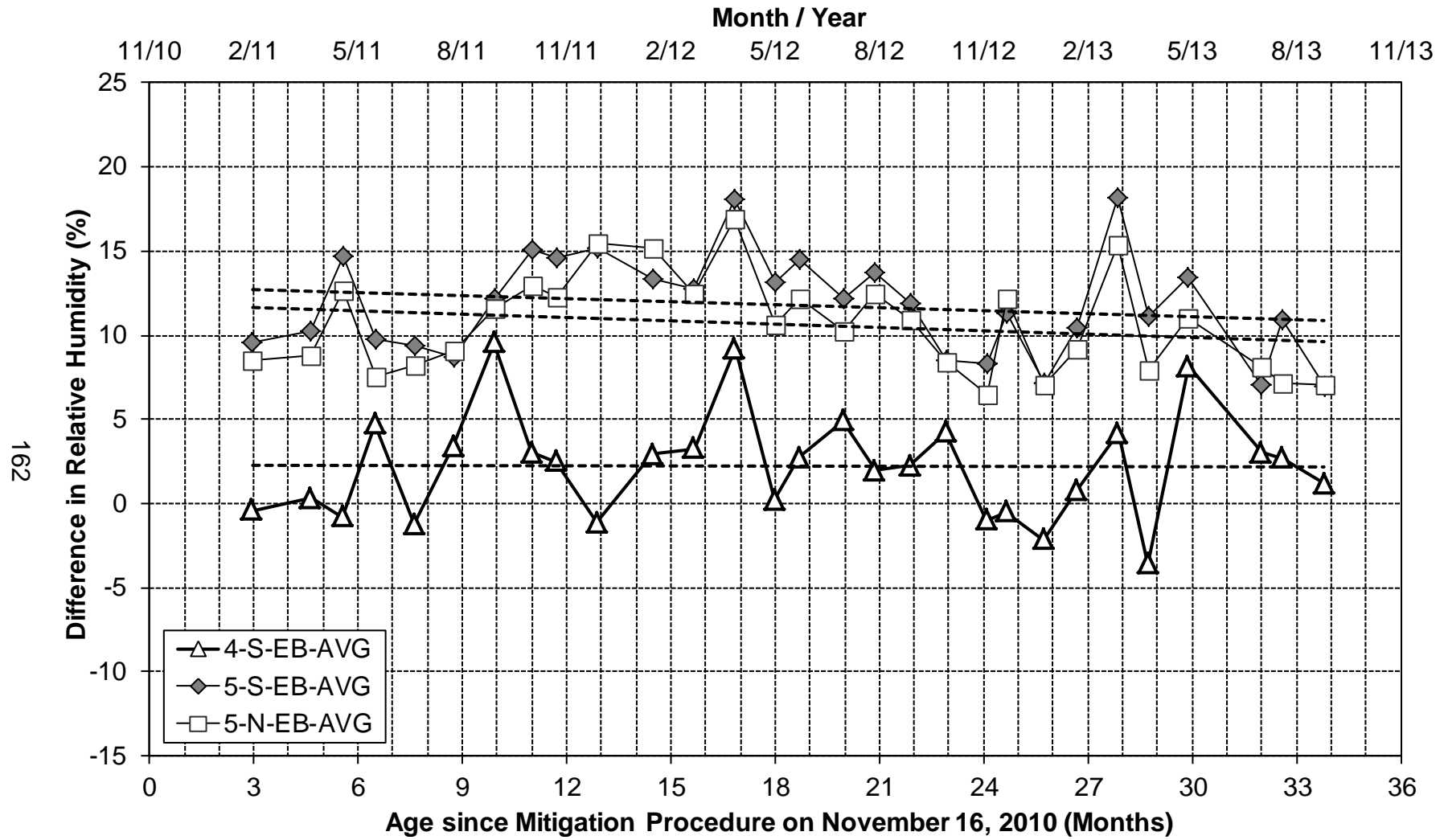


Figure 6.27. RH difference for East Bottom average

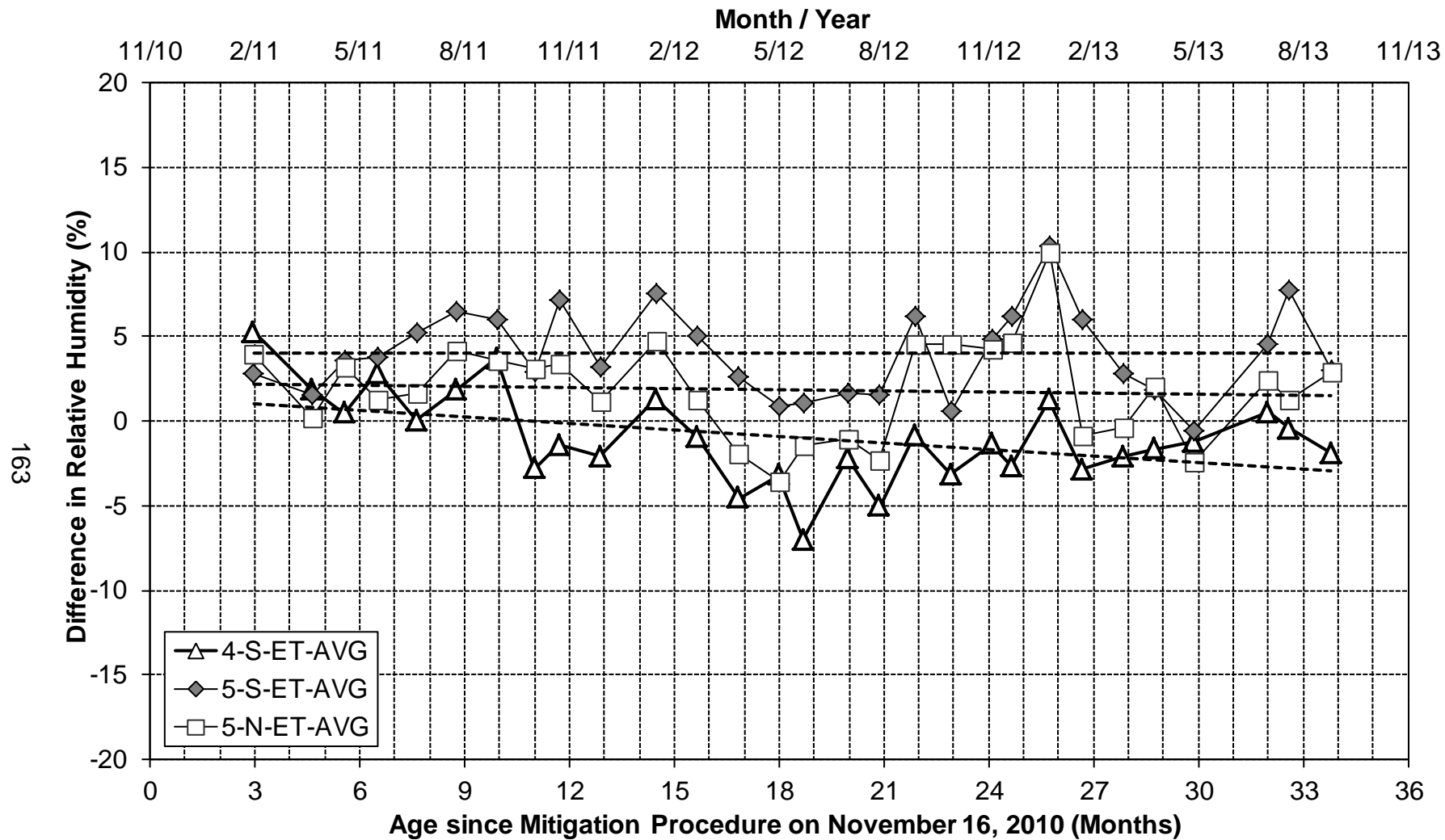


Figure 6.28. RH difference for East Top average

The relative humidity difference analysis results are presented for the average east bottom locations in Figure 6.27. The trend for 4-S-EB-AVG is completely flat, indicating that there is not any drying at this location compared to the 4-N-EB-AVG. Both arches in span 5 are showing a slight drying trend for the east bottom location, but there is not enough correlation of the data to support the conclusion that the mitigation procedure is working at this location.

Figure 6.28 is the difference analysis results for the east top locations. Like with the west top locations, span 5 does not have any drying relative to the control, but span 4 is showing some downward trend. 4-S-ET-AVG also reached its maximum differential drying compared to the control over a year before the conclusion of monitoring the same as 4-S-WT-AVG did. However, instead of staying at a roughly constant difference once reaching the peak difference, 4-S-ET-AVG has been converging back towards the state of drying of the control arch. Further monitoring is required to assess if the mitigation procedure has had a positive effect on 4-S-ET-AVG, but there is sufficient results to conclude that the mitigation procedure had no effect on the east top locations of span 5.

After analyzing all of the results from the relative humidity difference analysis, it can be concluded that the ASR mitigation procedure has not had any positive effects on drying the distressed concrete in span 5 nor the bottom of span 4 south when compared to the untreated control arch, span 4 north. The top of span 4 south, which has virtually no signs of ASR, has shown potential signs of drying compared to the control arch, especially in the first 18 months after

treatment. Continued monitoring may reveal that silane can be effective when applied in the early stages of ASR development or as a preventative measure.

6.3.3 3-inch Depth Analysis

An analysis of only the 3-inch relative humidity data was also performed in order to see if there are more prominent trends when not including the data from the outer couple inches of concrete. There is a possibility that the relative humidity near the surface of the concrete does not accurately represent the moisture state in the bridge at the time of measuring.

The same analysis techniques were used on the 3-inch data as the average relative humidity data. Figure 6.29 and Figure 6.30 are the west bottom and west top measured relative humidity data at the 3-inch depth, respectively, and Figure 6.31 and Figure 6.32 are the east bottom and east top 3-inch data, respectively.

When comparing the 3-inch depth raw data to the average data, most of the locations exhibit similar relative humidity patterns, with the exception of 4-N-WT. 4-N-WT-3" (Figure 6.30) not only had a different pattern over time than 4-N-WT-AVG (Figure 6.22), but it also had a much higher overall humidity than 4-N-WT-AVG.

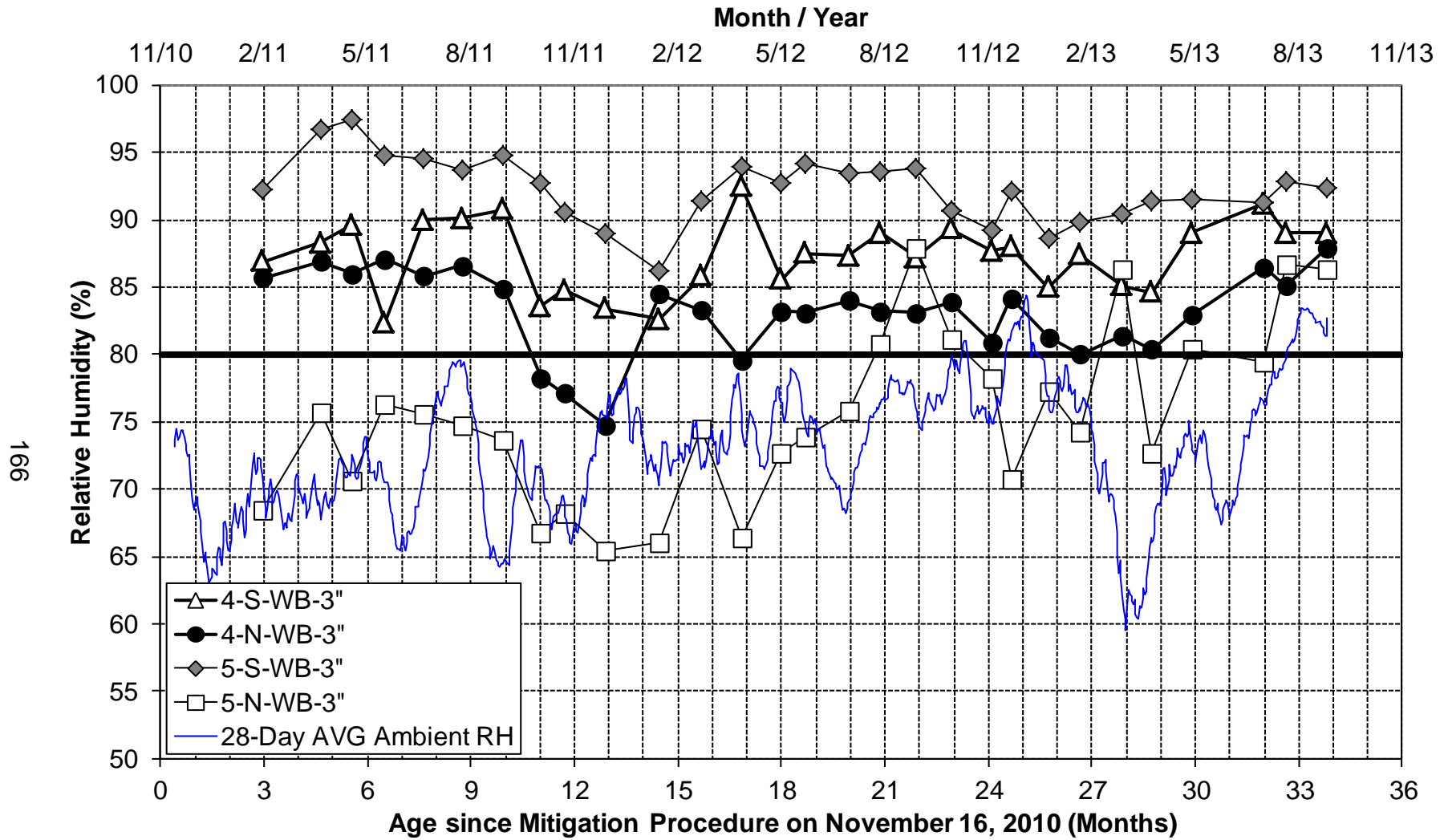


Figure 6.29. RH measurements, West Bottom, 3-inch depth

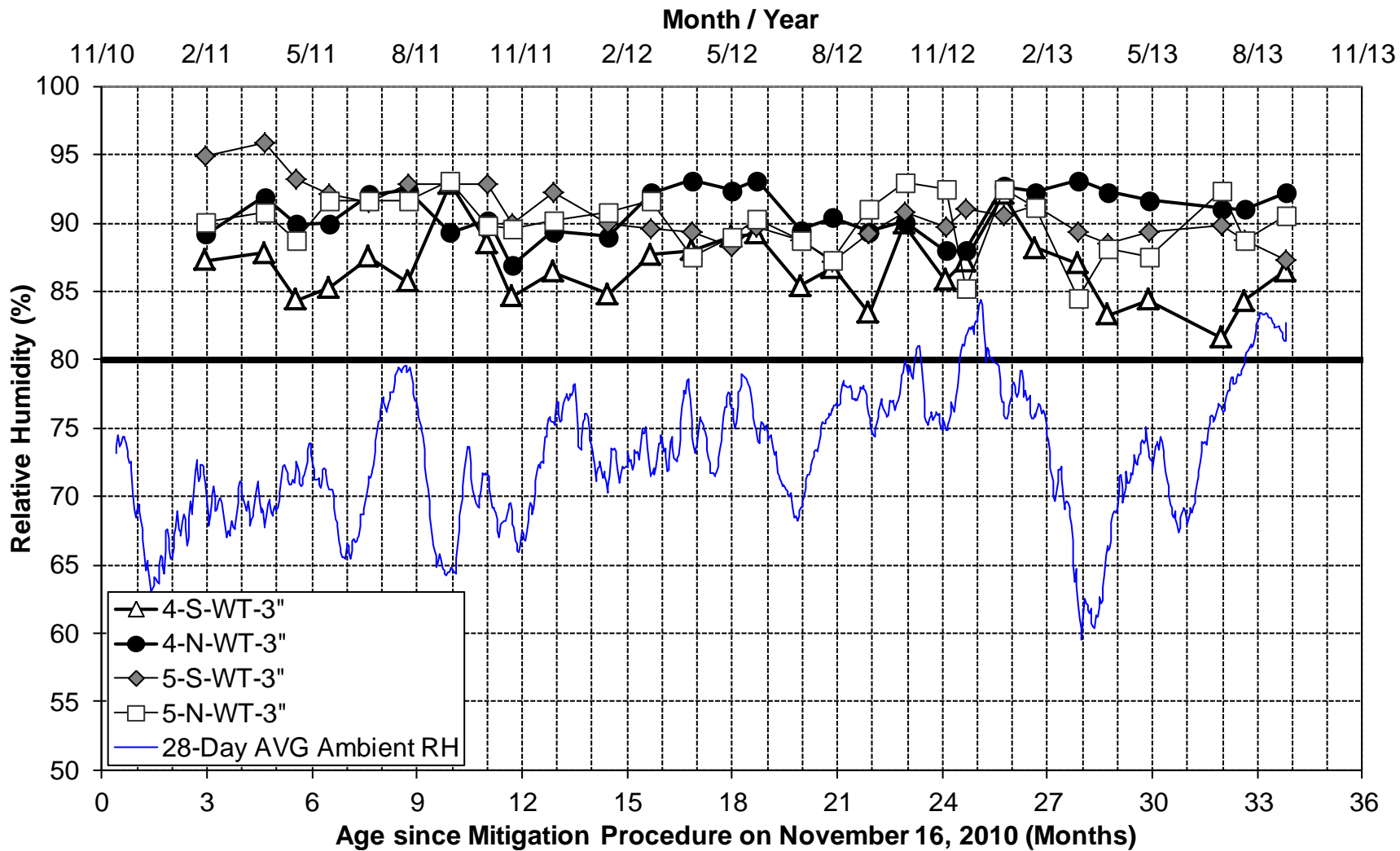


Figure 6.30. RH measurements, West Top, 3-inch depth

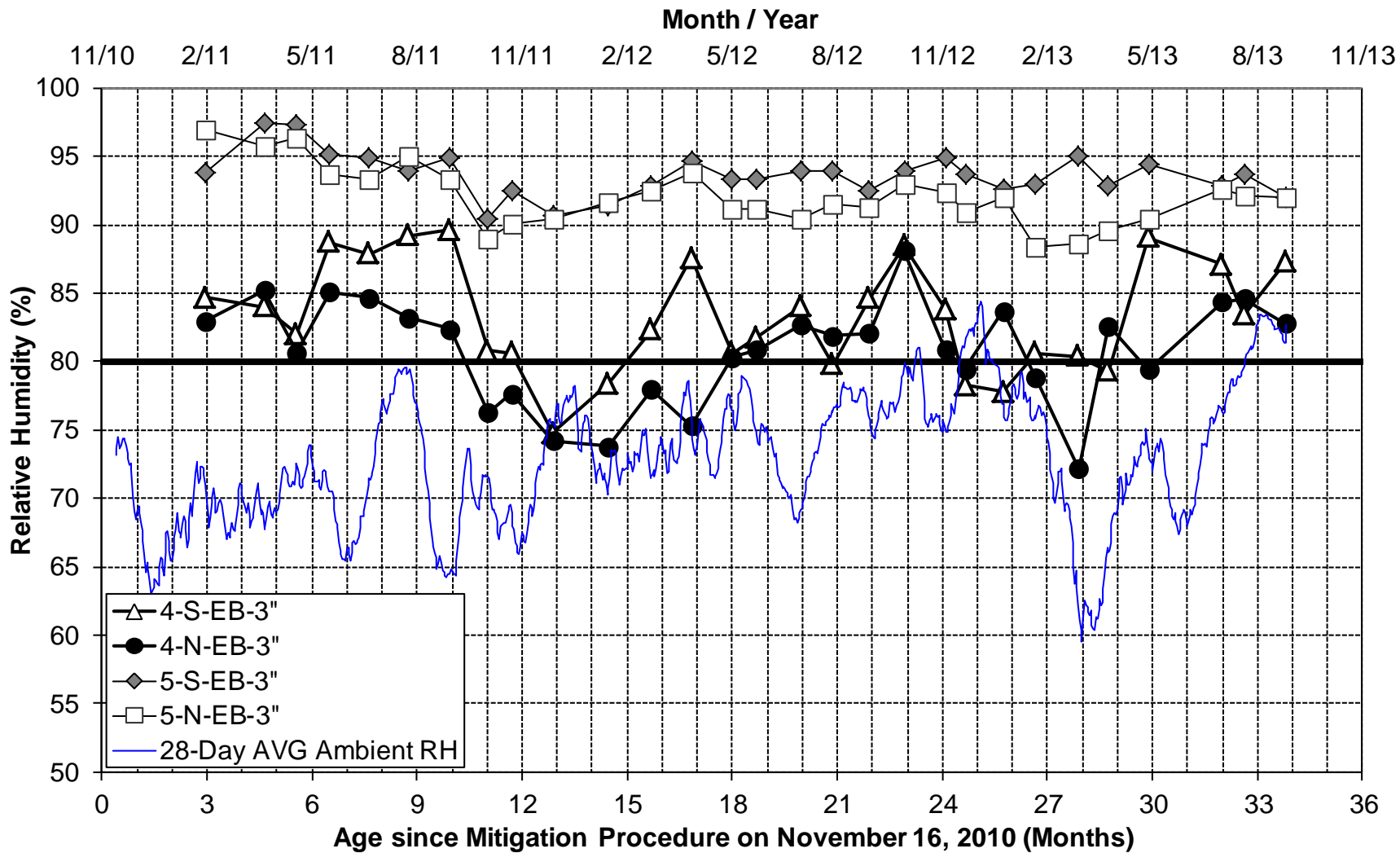


Figure 6.31. RH measurements, East Bottom, 3-inch depth

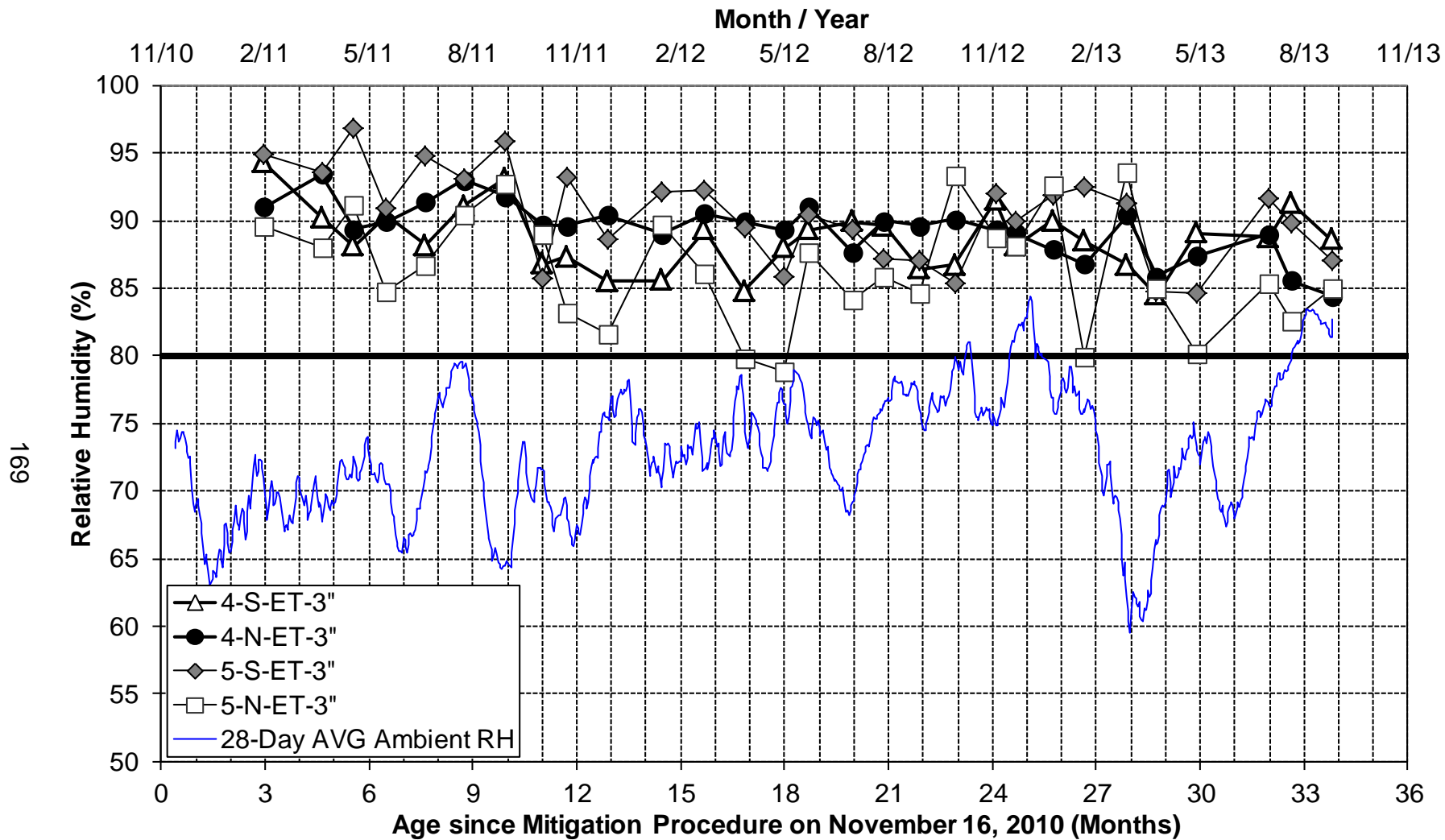


Figure 6.32. RH measurements, East Top, 3-inch depth

Linear regression trends were also inspected for the 3-inch data to determine if there is any statistical evidence of relative humidity changes. Only two locations had an r^2 value above 0.5, one of which was the untreated control arch at the east top location with a trend line slope of -0.166 percent relative humidity per month. The other significant trend was 5-S-WT-3" with a slope of -0.170 percent relative humidity per month. Both of these trends are weak, and continued drying in the control arch is not expected, but more drying may be seen at 5-S-WT with continued monitoring.

This is a good place to compare the results measured in the field to the drying behavior of the arches that Warnock (2012) estimated with the use of finite element analysis. The predicted drying curves for the 3-inch and 12-inch depths are presented again in Figure 6.33. From looking at this graph, the 3-inch depth measurements on the bottom of the arch should be getting very close to falling below the 80 percent relative humidity mark at this time, but they are still in the upper 80 and lower 90 percent ranges. Also from looking at Figure 2.24 (B) and assuming the concrete at the measurement location is close to 3,250 psi, the 3-inch measurement locations on the top should have approximately 7 percent higher humidity than the bottom locations and be around 90 percent humidity. The actual 3-inch top readings are in the upper 80 percent humidity range, and several of the bottom locations have higher humidity than the top locations. This behavior is opposite of what was predicted by the model and further confirms that the mitigation procedure has not been effective thus far. The fact that several of the bottom locations have higher humidities than the top also leads to the

conclusion that not only is the top releasing moisture through the epoxy layer, but water may also be penetrating into the section through new cracks and migrating toward the bottom of the arch.

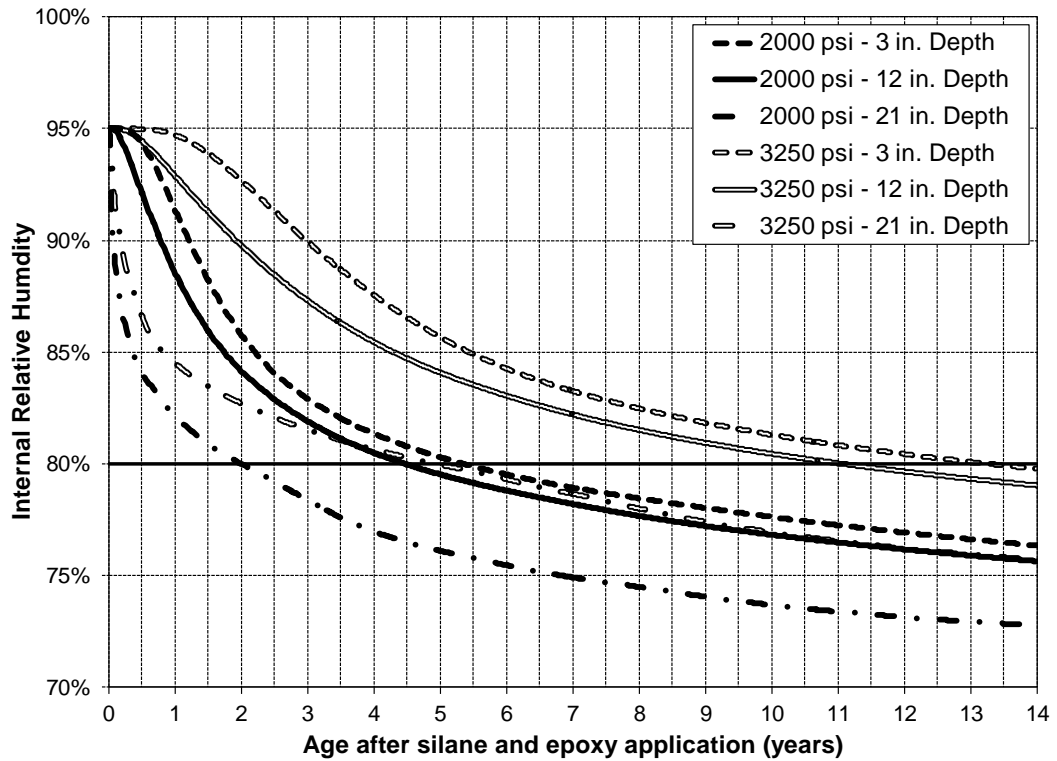


Figure 6.33. Drying time predictions for silane and epoxy treated arch section
(Adapted from Warnock 2012)

In order to compare the raw average relative humidity data and the 3-inch relative humidity data, an average of the data was taken over the 34 months of monitoring to see how similar the humidity levels were at the outer three inches of concrete versus at the 3-inch depth only. These data averages are shown in Table 6.2. It is important to note that this table is not indicative of any drying trends; it only compares the average of all of the humidity data for the two analysis types.

Table 6.2. 34-month average for 3-inch RH data and average RH data

34-Month RH Averages (%) for Average and 3-inch Data								
Arch Location	Measurement Location							
	WB		WT		EB		ET	
	Avg.	3"	Avg.	3"	Avg.	3"	Avg.	3"
4-N	82.2	83.2	86.5	90.8	80.6	80.8	87.7	89.4
4-S	87.2	87.3	84.0	86.7	82.8	83.3	86.7	88.7
5-N	75.2	75.4	90.1	90.0	91.2	92.1	89.6	86.5
5-S	91.7	92.3	90.8	90.6	92.4	93.7	91.7	90.4

For the majority, the 3-inch data are within a percent or two of the average humidity at each respective location when looking at Table 6.2, but 4-S-ET-3", 4-S-WT-3", and 4-N-WT-3" had 2.0, 2.7, and 4.3 percent, respectively, higher 34-month averages than the average data. Due to the fact that the 3-inch depth requires more time to dry than the outer couple inches of concrete, it makes sense that 12 of the 16 locations have higher 34-month averages for the 3-inch data. The only anomaly where the 34-month average of the 3-inch data was significantly lower than the average data was at the 5-N-ET location, the 3-inch data was 3.1 percent lower than the average data.

The conclusion can be drawn from the overall analysis of the raw 3-inch data that there is not enough evidence after 34 months of monitoring to claim that the ASR mitigation procedure has been effective thus far. As with the average data, a difference analysis was also performed in the next section with the 3-inch data to look for any drying trends relative to the control locations.

6.3.3.1 Relative Humidity Difference Analysis of 3-inch Data

The relative humidity difference analysis for the 3-inch data compares the treated arches to the span 4 north just like the relative humidity difference analysis for the average data. The difference plots for the 3-inch data are shown in Figure 6.34 through Figure 6.37.

5-N-WB-3", plotted in Figure 6.34, has the highest r^2 value of any of the difference plots, same as the difference analysis for the average data. 5-S-WB-3" appears to be experiencing a little drying compared to the control, but this trend is very weak at this time.

All of the west top locations presented in Figure 6.35 have negative sloping trend lines that indicate drying relative to 4-N-WT-3", but none of their trends are statistically strong enough to support the conclusion that the mitigation procedure is effective here. It is worth noting here that the 4-N-WT-3" data were quite a bit different and higher than the 4-N-WT-AVG data as previously discussed. There may be an irregularity in the concrete or the humidity tube installation at this 3-inch location that could bring into question the validity of the data in Figure 6.35.

The east bottom difference analysis data for the 3-inch location plotted in Figure 6.36 are very similar to the average relative humidity difference data at the east bottom, plotted in Figure 6.27. There are no strong trends of relative drying in Figure 6.36 for the treated arches that suggest that the mitigation procedure has been effective at the east bottom locations.

None of the east top data for the treated arches shown in Figure 6.37 have any signs of drying relative to 4-N-ET-3". However, 4-N-ET-3" did have a trend of drying in Figure 6.32 for some unknown reason, and this makes it difficult to compare it with the treated 3-inch east top locations.

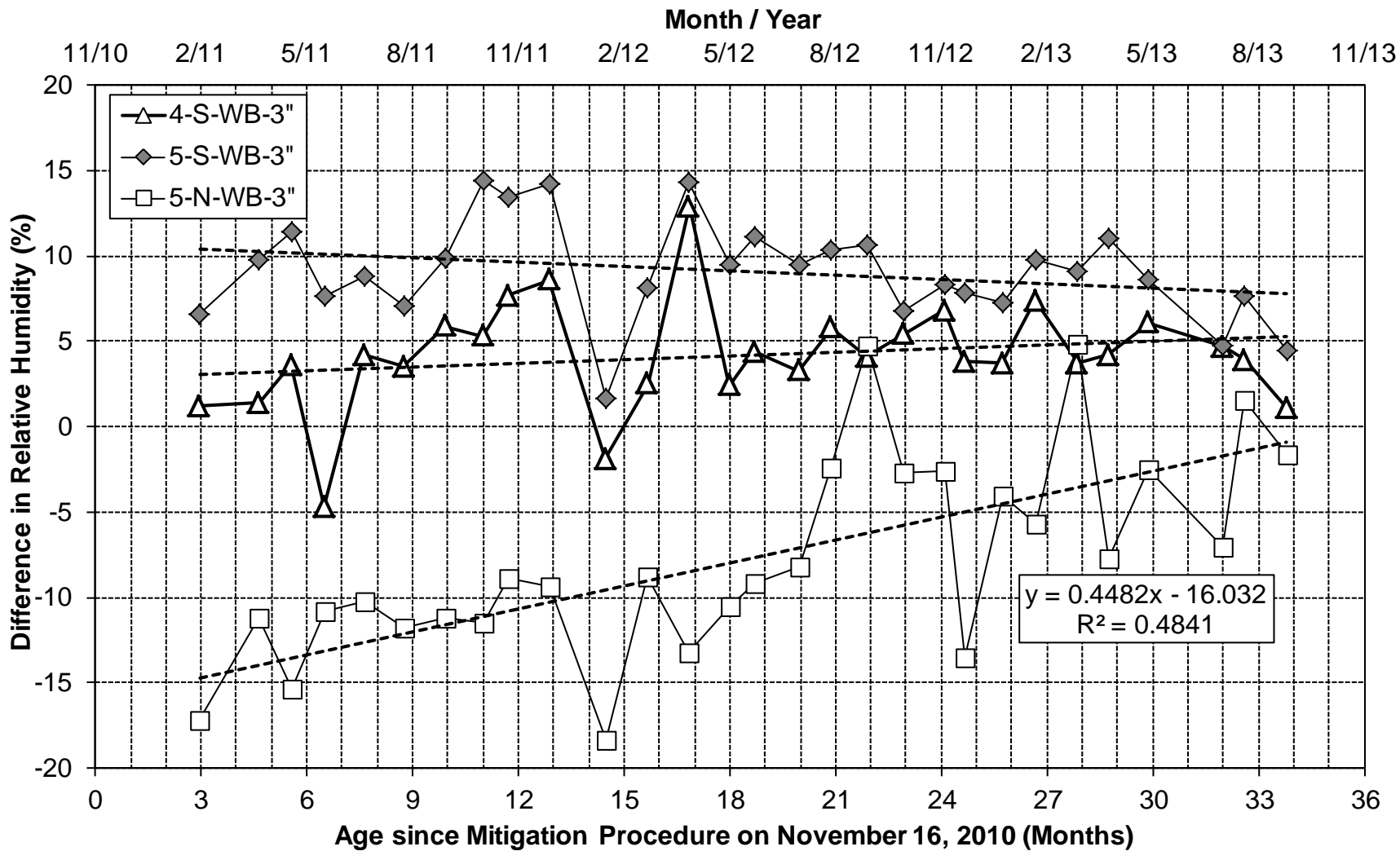


Figure 6.34. RH difference for West Bottom 3-inch depth

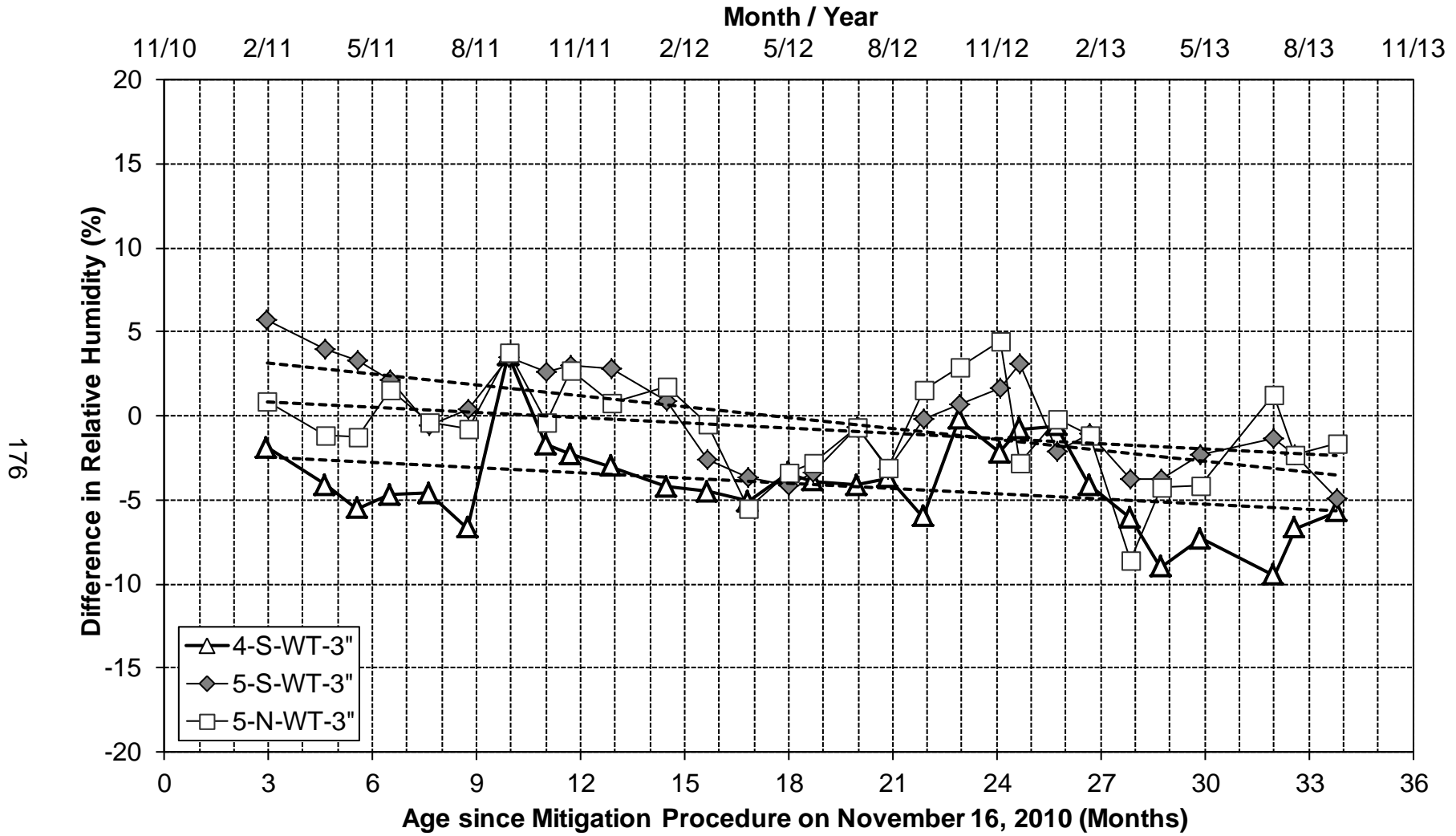


Figure 6.35. RH difference for West Top 3-inch depth

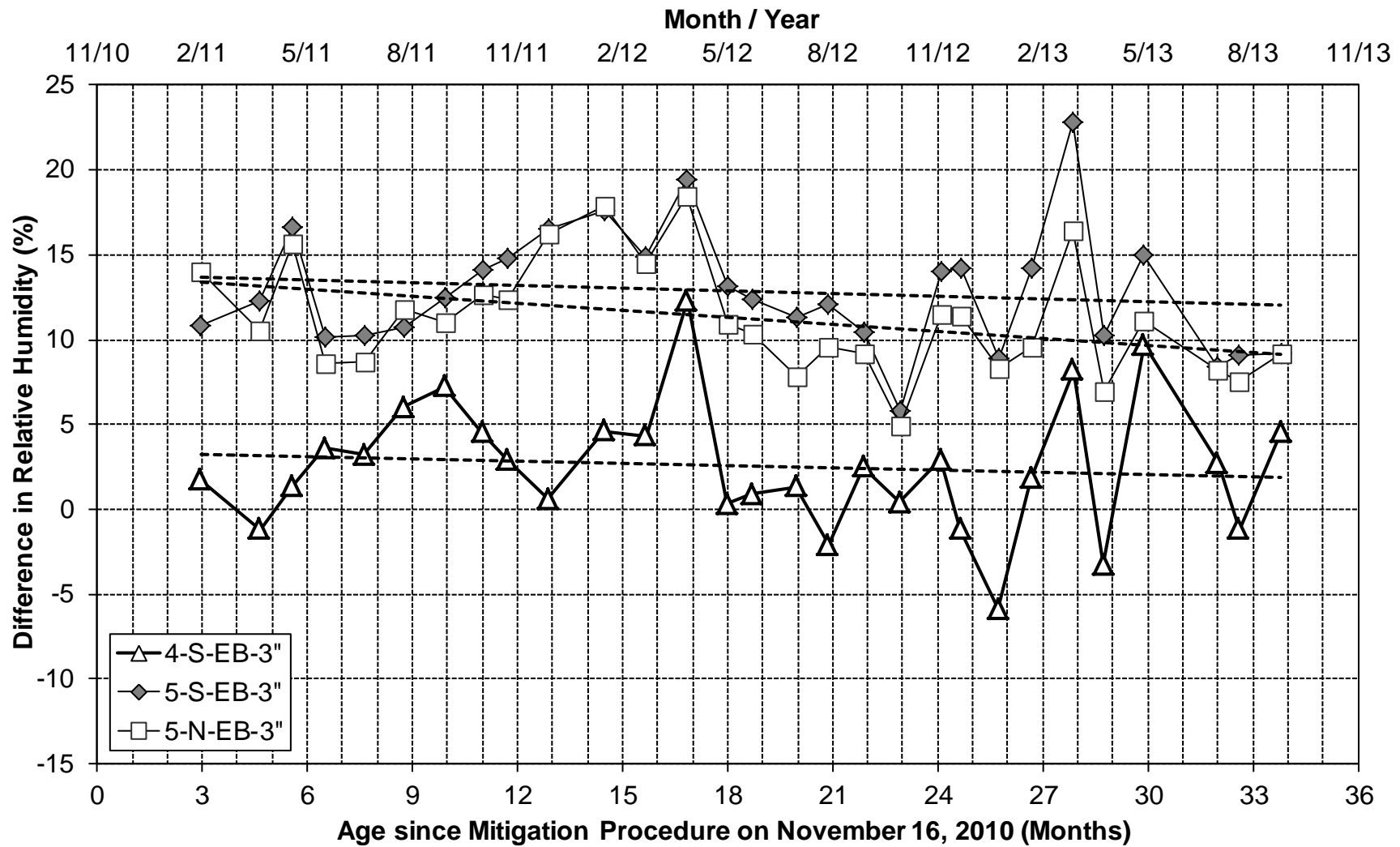


Figure 6.36. RH difference for East Bottom 3-inch depth

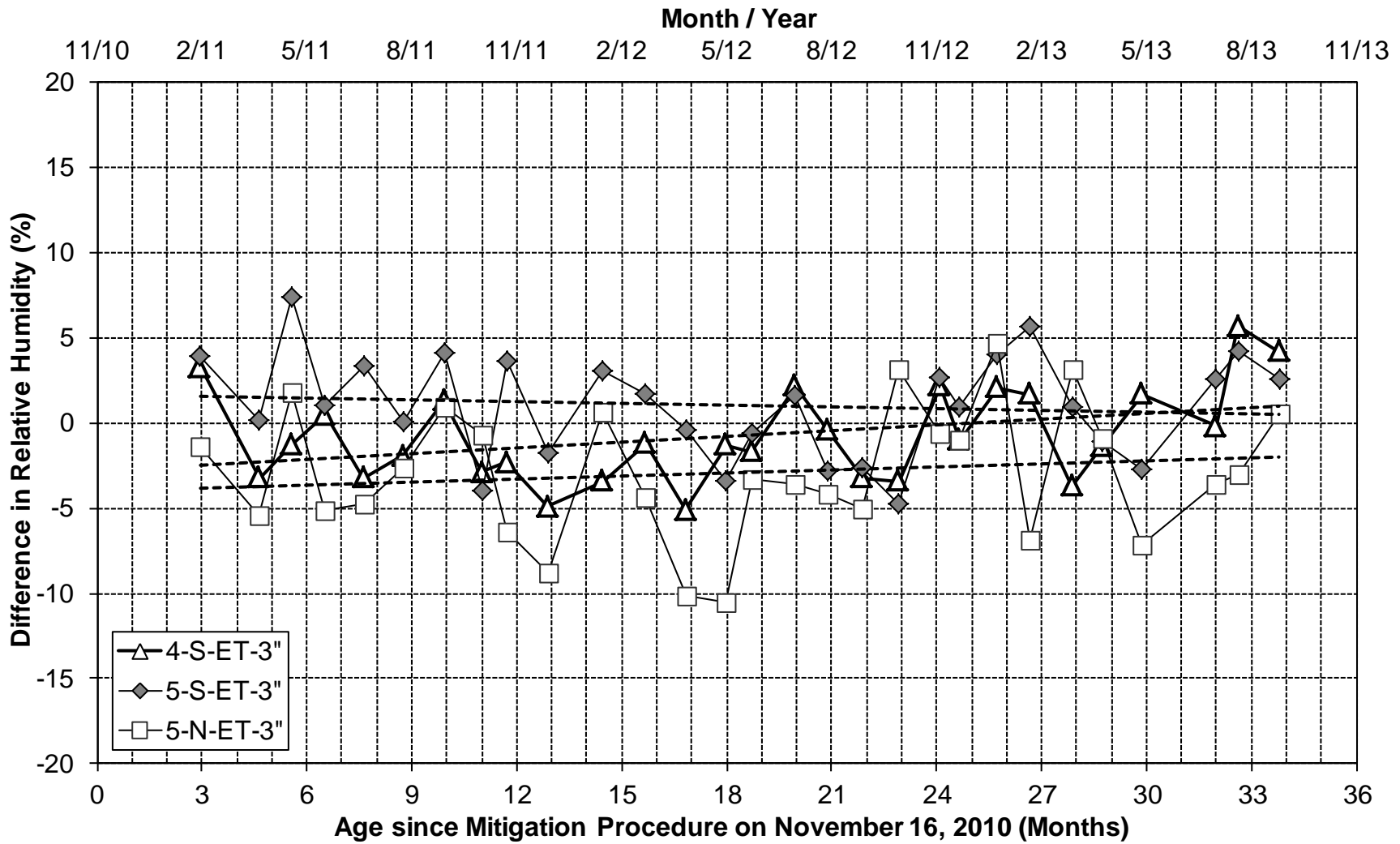


Figure 6.37. RH difference for East Top 3-inch depth

6.3.4 Relative Humidity Data Analysis Summary

After reviewing all of the results from the raw data and the relative humidity difference analysis, for the average data and the 3-inch data alone, it can be concluded with confidence that the ASR mitigation procedure as a whole has shown very little effect on drying out the concrete. All of the raw data and difference analysis data were analyzed for linear trends of drying, but only 1 of the 36 treated locations had a strong trend of drying with an r^2 value of greater than 0.5. This trend was for the plot of the raw data for 5-S-WT-3", and it had an r^2 of 0.548 with a slope of -0.170 percent humidity per month.

6.4 Concrete Strain Measurements

A summary of the concrete strain measurement survey dates along with the corresponding time since the first measurement in December 2005 and the time since the application of the ASR mitigation procedure, in mid-November of 2010, is given in Table 6.3.

Table 6.3. Concrete strain measurement survey dates

Concrete Strain Measurement Survey Dates					
Survey Date	Months from 12/05	Months After Mitigation	Survey Date	Months from 12/05	Months After Mitigation
12/16/05	0	-	05/17/12	77.1	18.0
12/09/09	47.8	-	06/08/12	77.8	18.7
11/17/10	59.1	0	07/16/12	79.0	20.0
02/02/11	61.6	2.5	08/13/12	80.0	20.9
04/07/11	63.7	4.7	09/13/12	81.0	21.9
05/05/11	64.6	5.6	10/14/12	82.0	22.9
06/03/11	65.6	6.5	11/19/12	83.2	24.1
07/07/11	66.7	7.7	12/06/12	83.7	24.7
08/10/11	67.8	8.8	01/08/13	84.8	25.8
09/15/11	69.0	10.0	02/05/13	85.7	26.7
10/18/11	70.0	11.0	03/14/13	87.0	27.9
11/08/11	70.8	11.7	04/09/13	87.8	28.8
12/14/11	72.0	12.9	05/14/13	89.0	29.9
01/31/12	73.5	14.5	07/17/13	91.1	32.0
03/08/12	74.8	15.7	08/05/13	91.7	32.6
04/12/12	75.9	16.8	09/10/13	92.9	33.8

6.4.1 Strain Measurement Identification

Concrete strain measurements were taken from 46 locations on spans 4 and 5. These locations are summarized in Table 5.1 and Figure 5.12. Just like with the relative humidity data, an identification system for the stain locations has been developed as follows:

Span Number – Arch Location – Arch Side – Measurement Location

4	South (S)	West (W)	Abutment (AB)
5	North (N)	East (E)	Side Horizontal (SH)
			Side Perpendicular (SP)
			Bottom Low (BL)
			Bottom High (BH)
			Top Low (TL)
			Top High (TH)

Example: 4-N-W-BL is the bottom low measurement location on the west side of the northern arch of span 4.

6.4.2 Strain Adjustment for Temperature

Because the goal of this analysis is to determine the ASR-related strains, the concrete expansion and contraction due to thermal effects was reduced by normalizing the strains to a temperature of 73 °F. If the average recorded concrete temperature at the 3-inch depth was less than 73 °F, the measured strain was increased, and vice versa for concrete temperatures above 73 °F.

Strains were adjusted for temperature using the following procedure:

- Strain Adjustment = $(73\text{ }^{\circ}\text{F} - T_c) \cdot \alpha_t$

Where:

- T_c = Average concrete temperature of all 3-inch depths (°F)
- α_t = Coefficient of thermal expansion (/°F)

The following assumption was used for the coefficient of thermal expansion:

- $\alpha_t = 6.95 \times 10^{-6} / ^\circ\text{F}$, which is a typical value for concrete made with Alabama river gravel (Schindler et al. 2010).

An example of using the previous concrete strain adjustment procedure would be subtracting 118 microstrains from the measured strain at each location on a day where the average concrete temperature measured at the 3-inch depths is 90 °F. This 118 microstrains represents the strain attributed solely to the temperature difference between 73 °F and 90 °F. This is obtained from the following:

- $(73 - 90) * 6.95 \times 10^{-6} = -118 \times 10^{-6} \text{ in./in.}$

6.4.3 Concrete Strain Data

This section contains all of the concrete strain data in graphical form with change in strain versus time. There are two different time frames used with the graphs in the following figures. The FHWA installed DEMEC studs at 10 points in 2005 at three different typical locations: side perpendicular, bottom low, and top low. The graphs with these data dating back to 2005 are shown in Figure 6.38, Figure 6.40, and Figure 6.42, and there is a bold vertical line plotted on these graphs in November 2010 that represents the time of the ASR mitigation procedure application. Because there were not any relative humidity readings taken before 2011 from which the concrete temperature could be obtained, the temperature used to adjust the 2005 and 2009 strain measurements was the average temperature on record for those dates at Maxwell Air Force Base. The other figures in this section present the concrete strains for all of the locations after the mitigation procedure was applied in November of 2010; even the locations that

date back to 2005 are re-plotted in these figures. All of the graphed data in the concrete strain sections of this chapter have expansion data running up to 09/10/2013. The recorded field measurements along with the calculated change in strain values are displayed in Appendix E.

Only a few general notes will be made about the strain plots in this section; more detailed discussion of the results will be presented in the linear regression analysis section that follows. The highest change in strain values in all of these plots are for the ASR-affected arches of span 5, which is expected. Another quick observation to take away from the following plots is how much overall expansion the east side of the northern arch in span 5 is experiencing; approximately 1,350 microstrain has developed over the 34 months of monitoring.

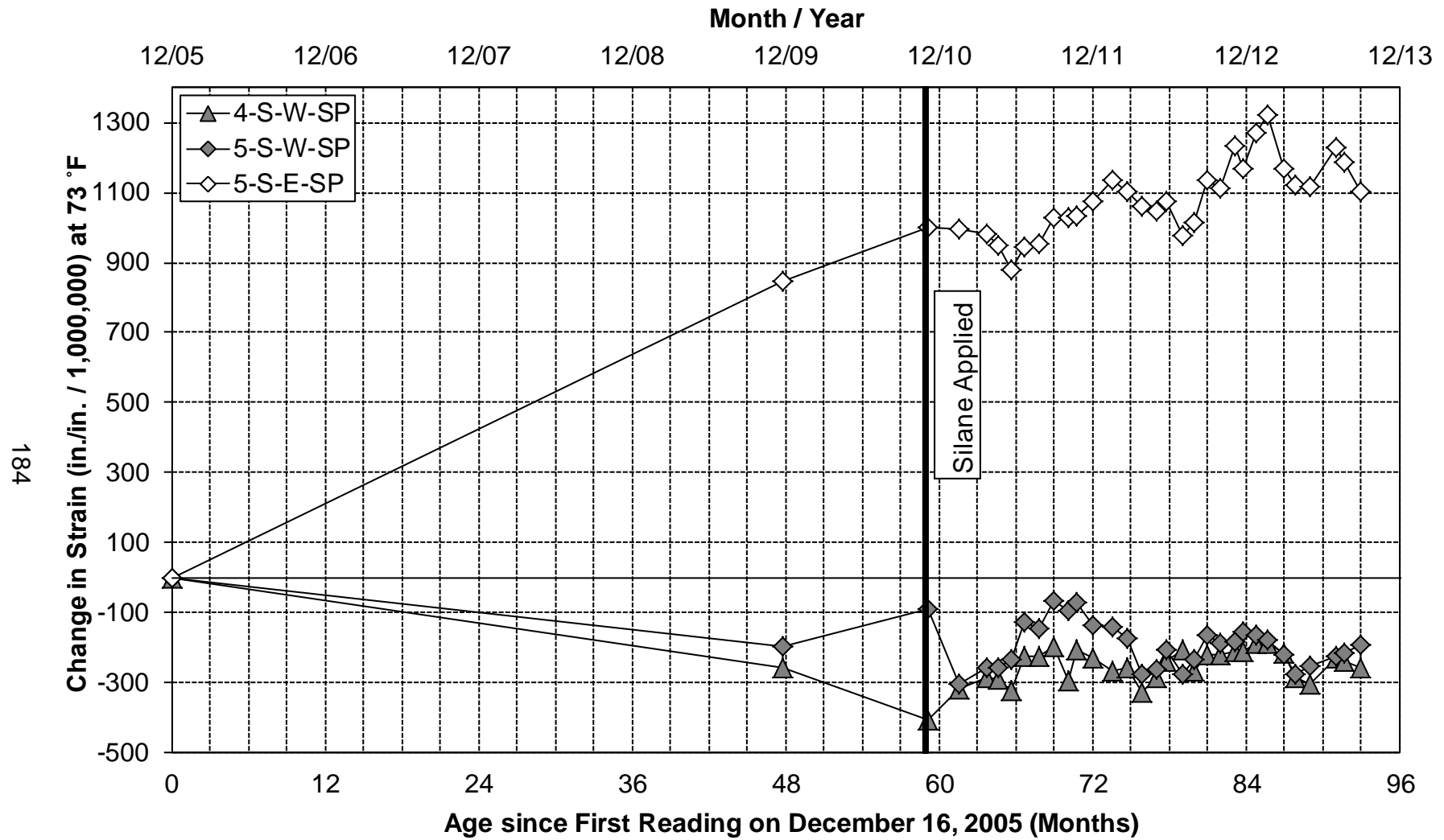


Figure 6.38. Change in concrete strain for Side Perpendicular since 2005

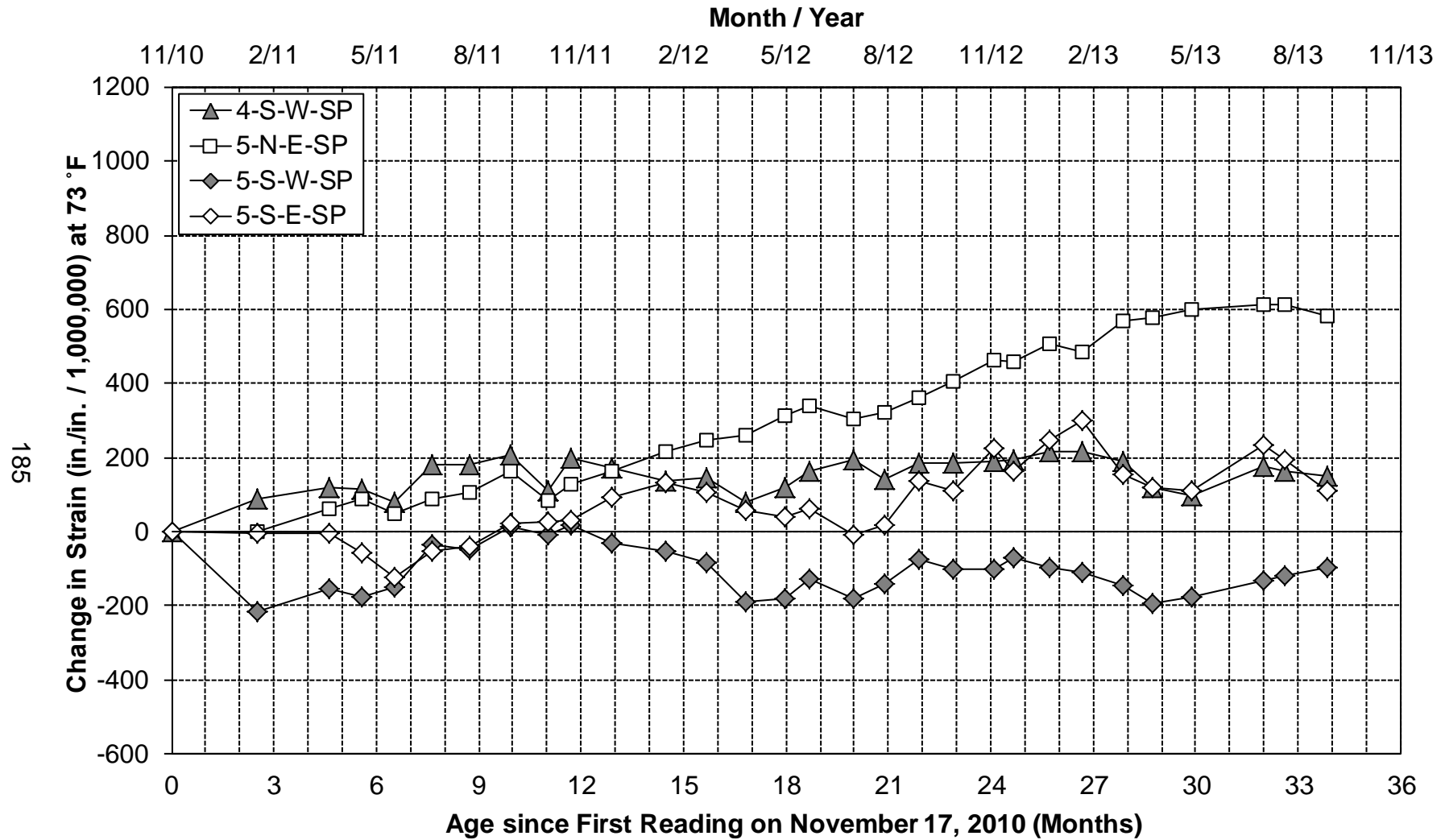


Figure 6.39. Change in concrete strain for Side Perpendicular since 2010

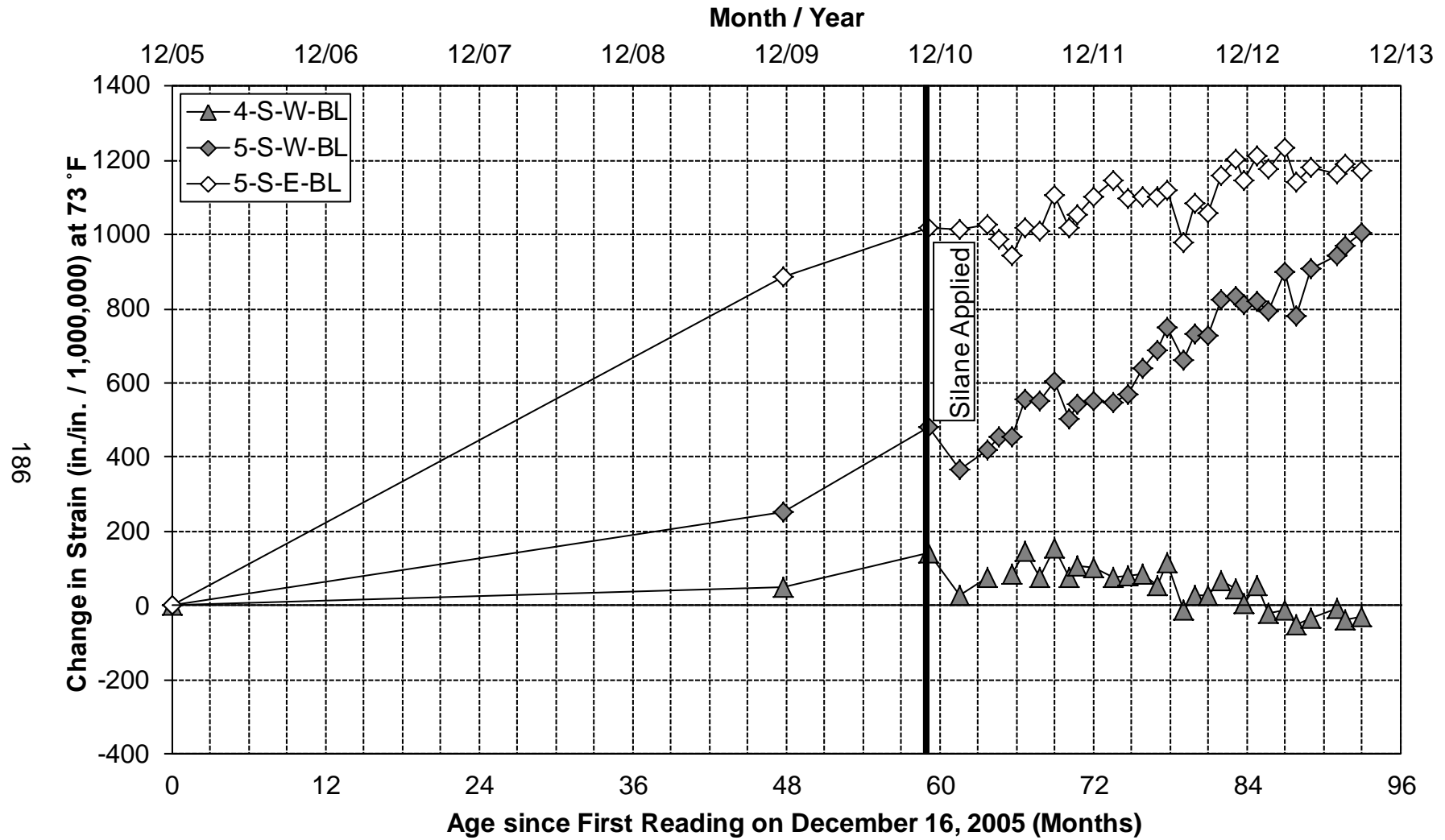


Figure 6.40. Change in concrete strain for Bottom Low since 2005

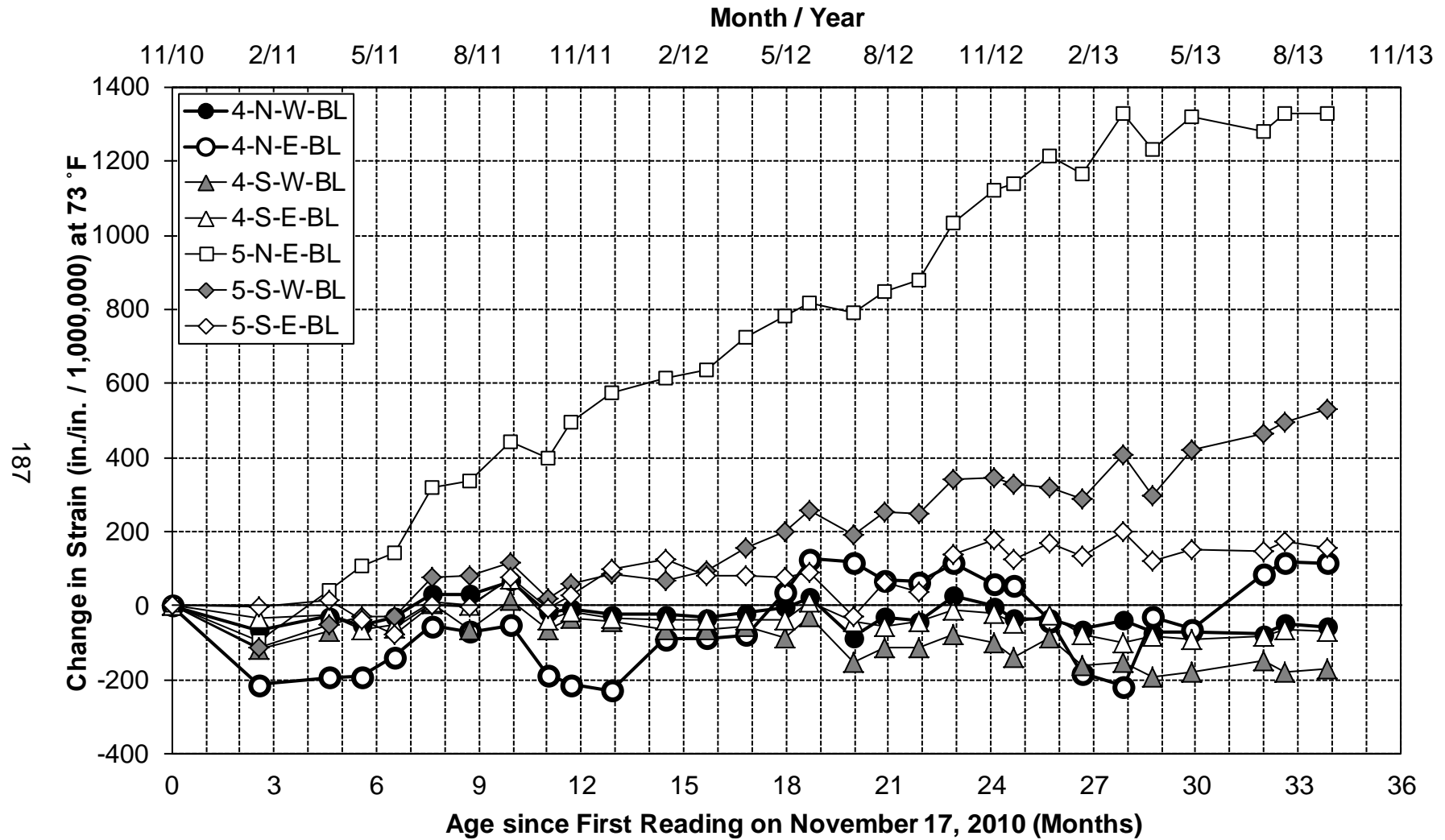


Figure 6.41. Change in concrete strain for Bottom Low since 2010

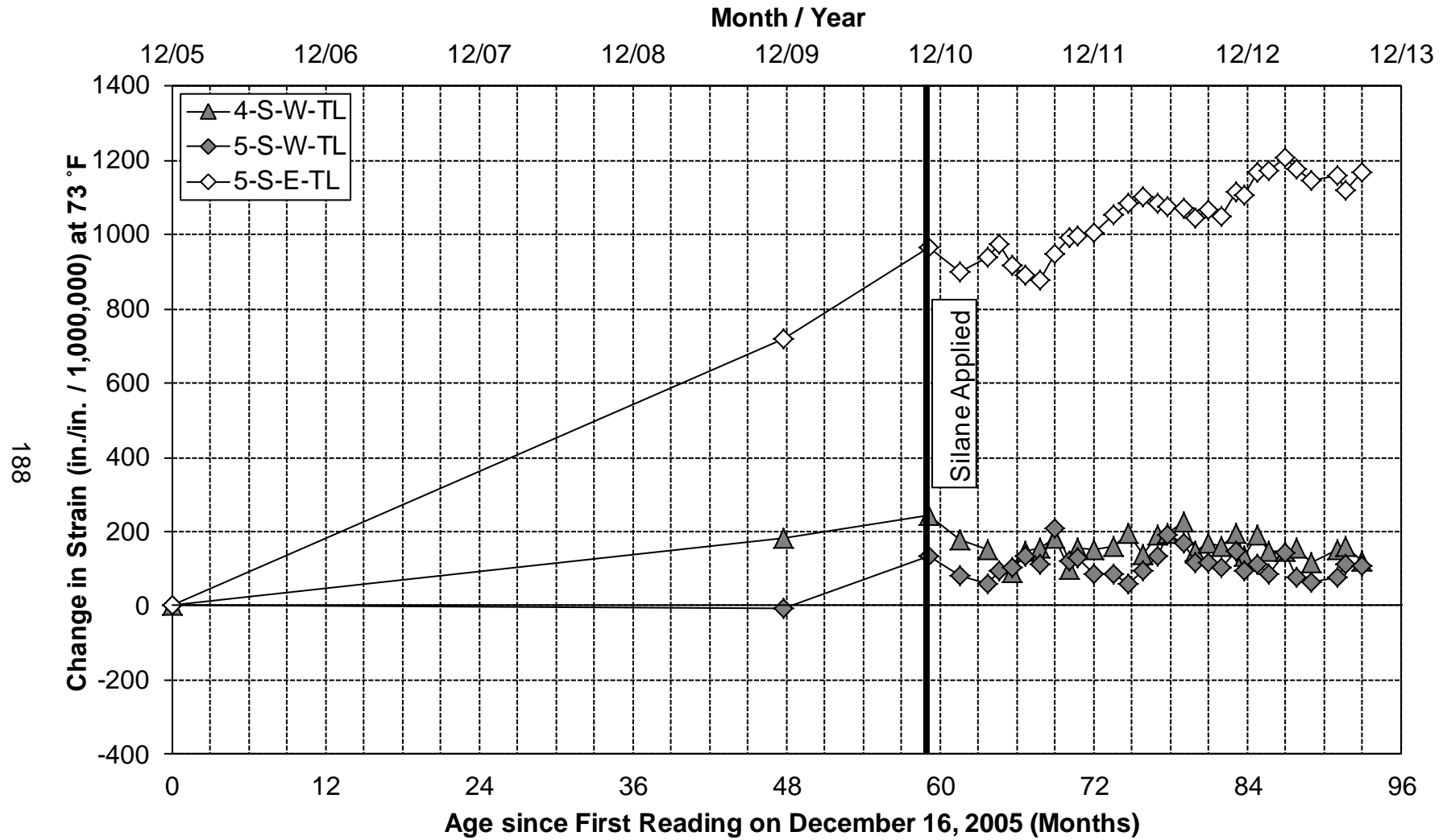


Figure 6.42. Change in concrete strain for Top Low since 2005

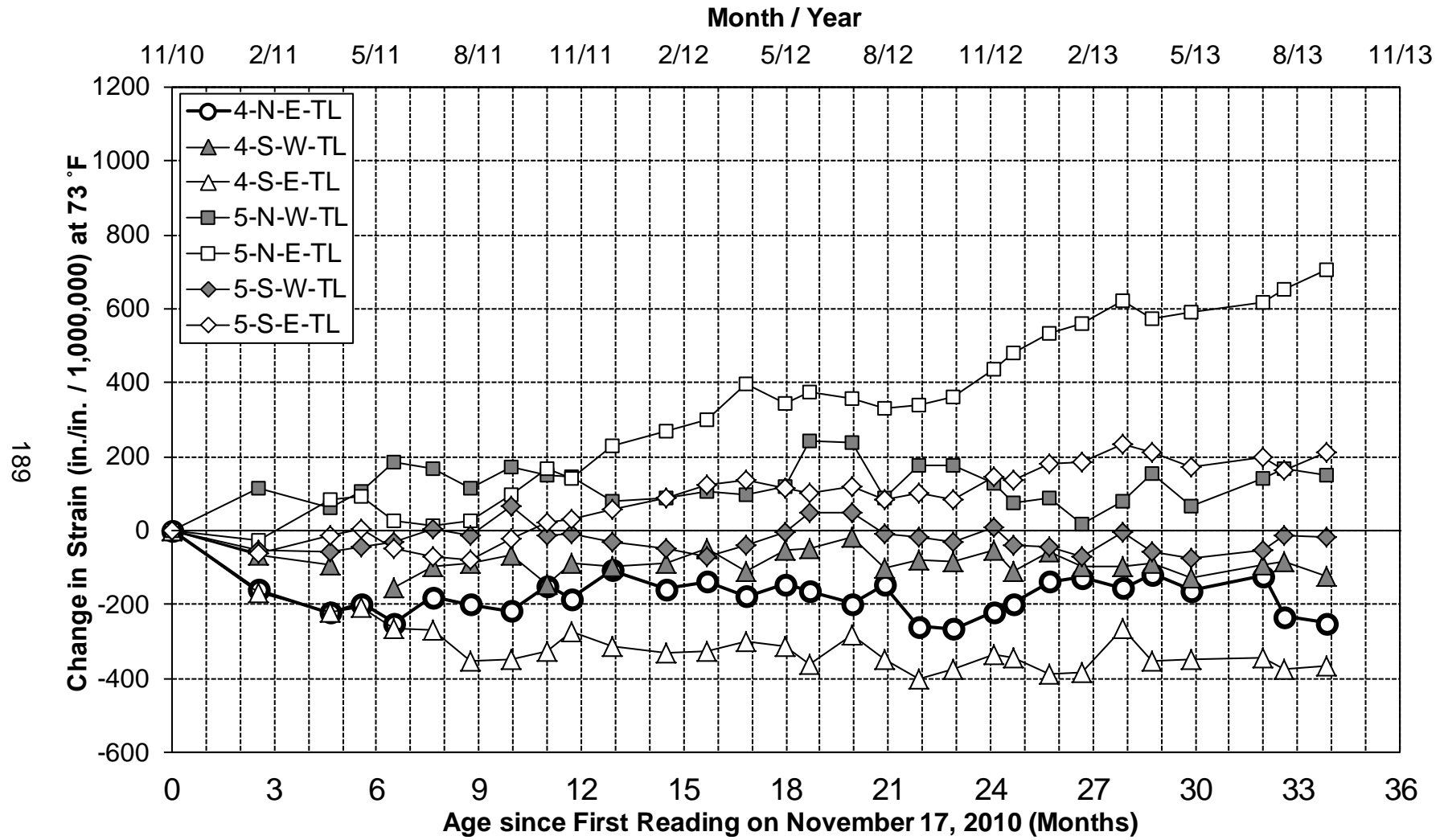


Figure 6.43. Change in concrete strain for Top Low since 2010

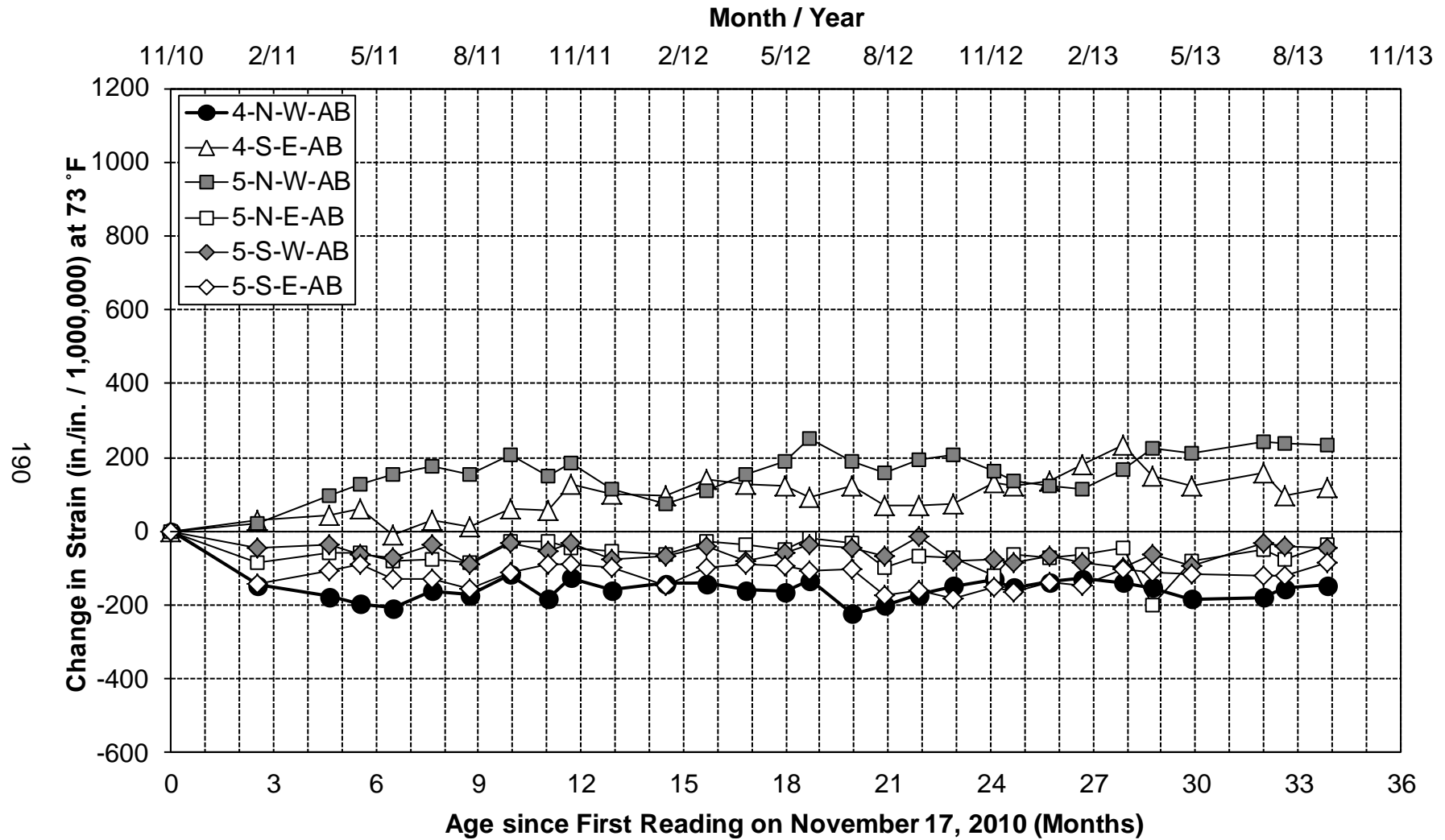


Figure 6.44. Change in concrete strain for Abutment since 2010

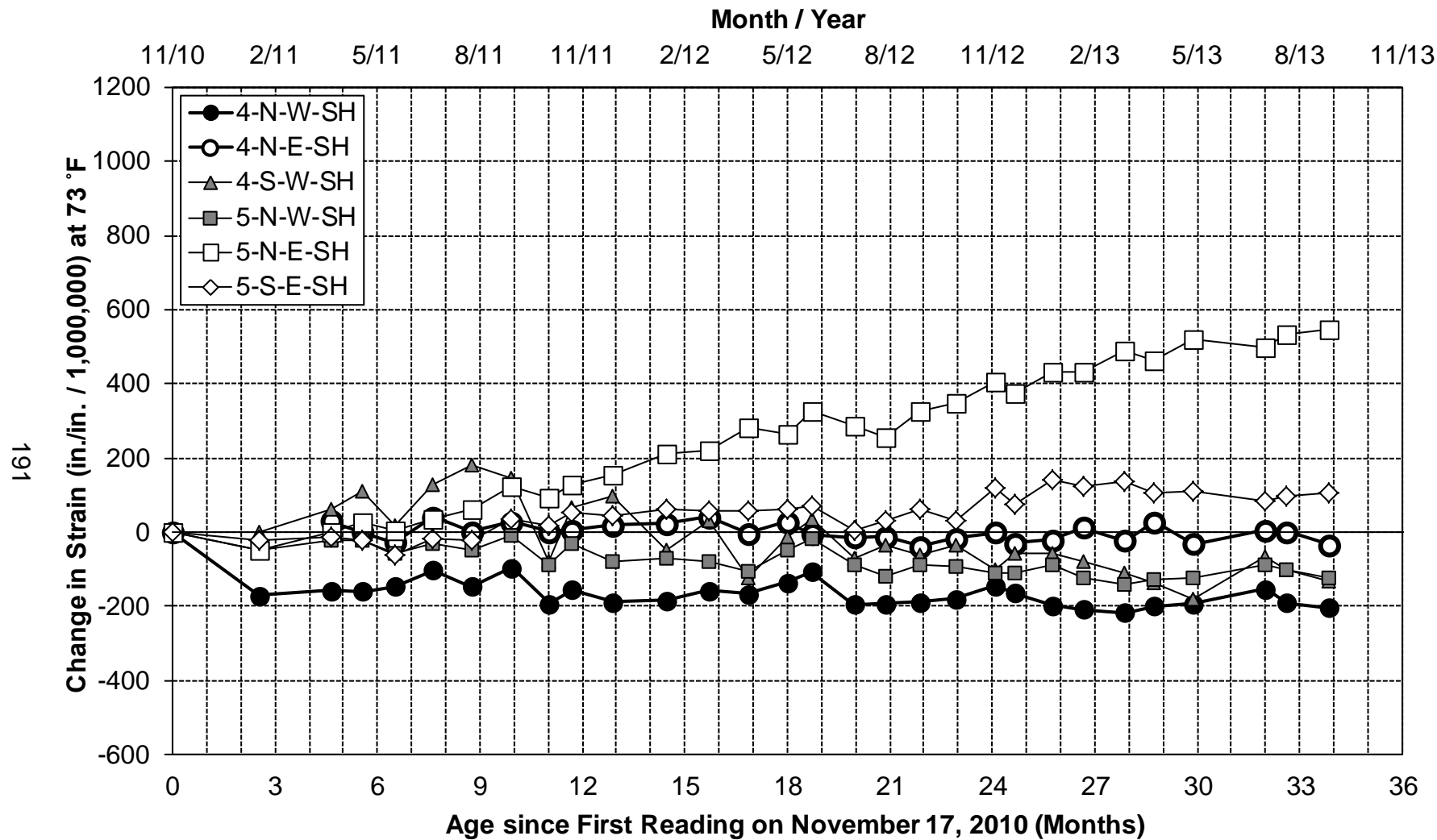


Figure 6.45. Change in concrete strain for Side Horizontal since 2010

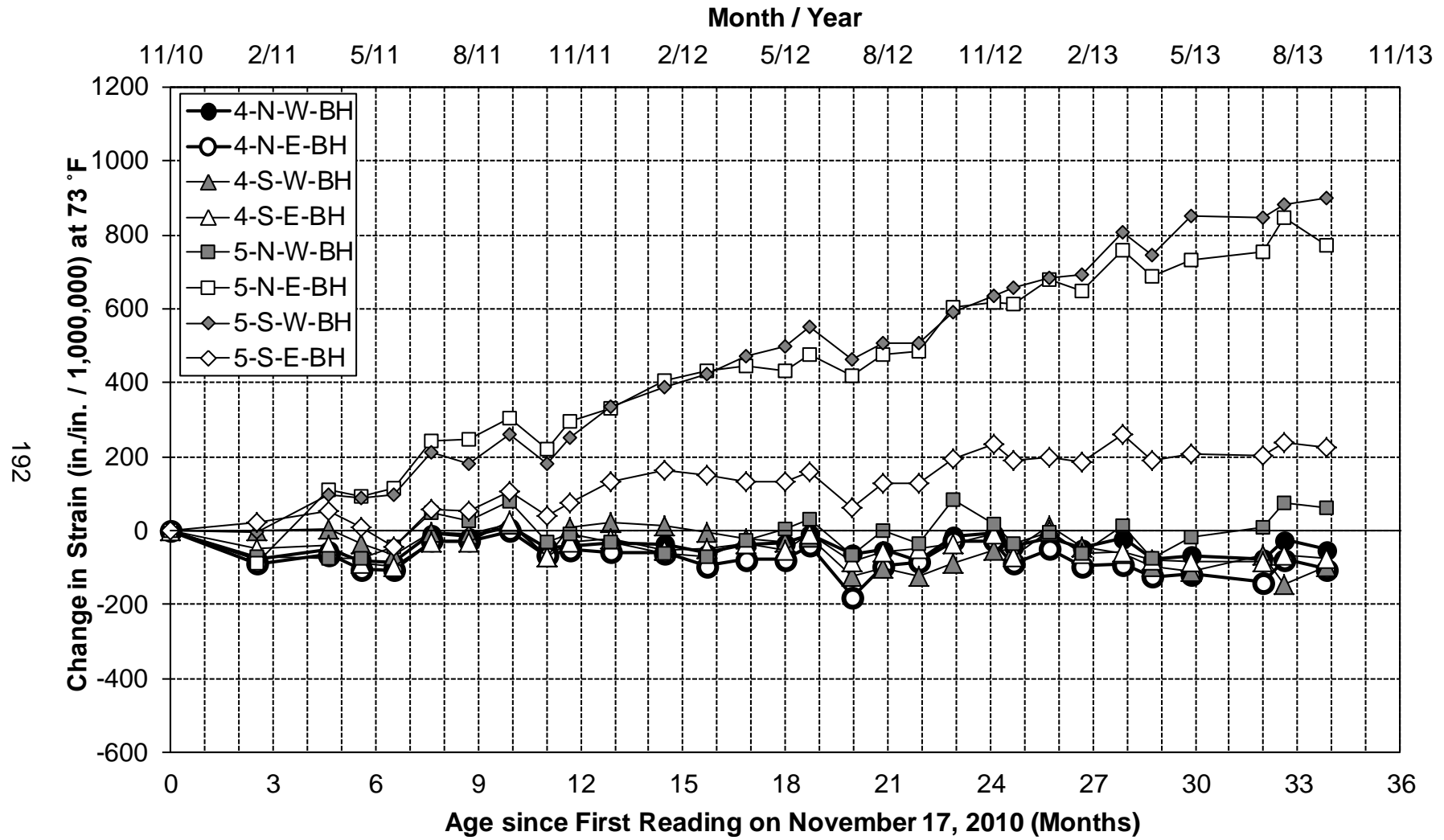


Figure 6.46. Change in concrete strain for Bottom High since 2010

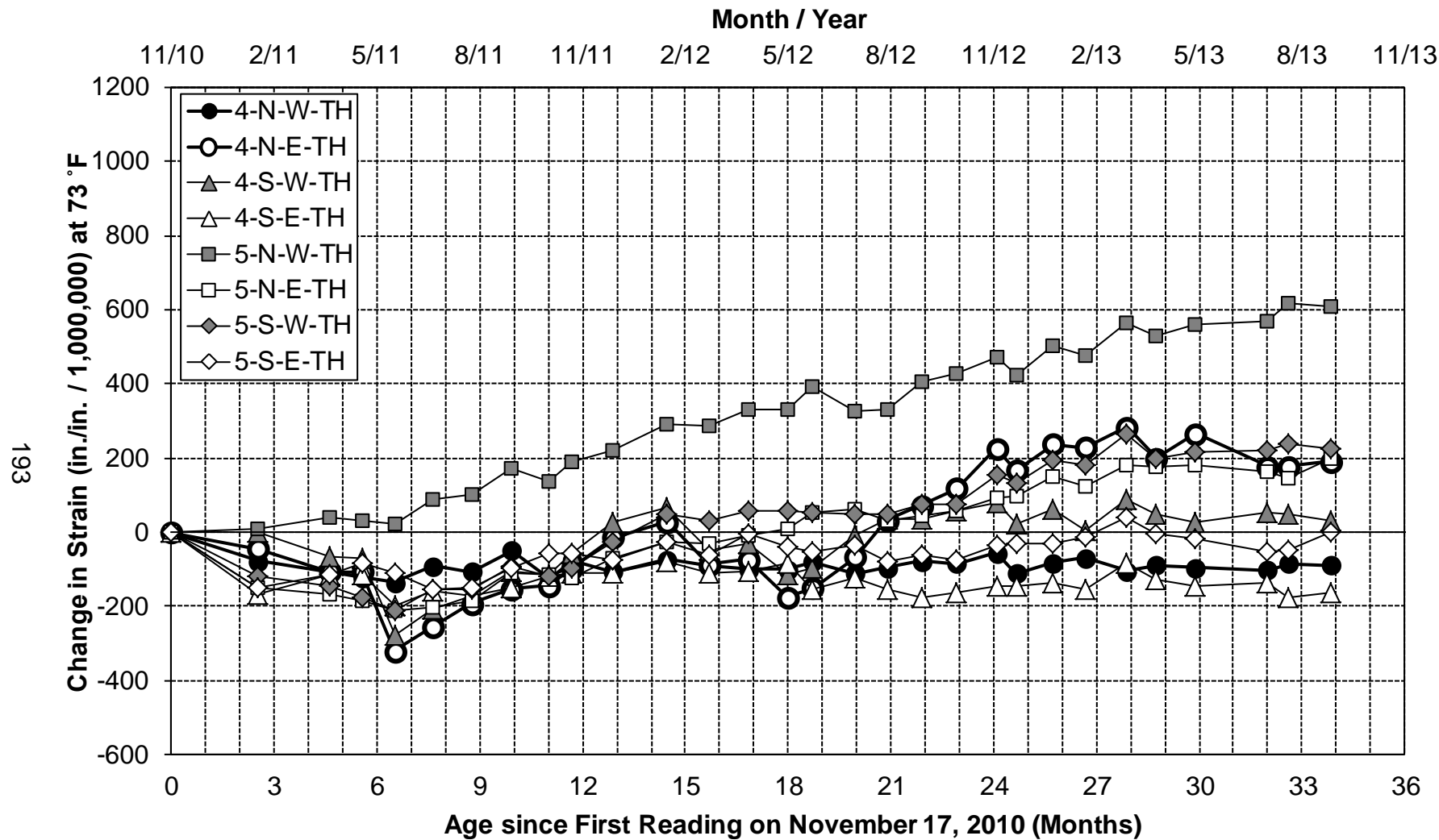


Figure 6.47. Change in concrete strain for Top High since 2010

6.4.3.1 Linear Regression Analysis of Strain Data

It is important to monitor the expansion in an ASR-affected structure because it will give an accurate prediction for the rate of future expansion. Wood (2008) says "Unless there is a change in the water availability to the structure, the rate of AAR damage and crack growth, once cracking has initiated, is steady and roughly linear with time." Examination of the expansion data alone is not enough to say whether or not the ASR mitigation procedure is showing signs of drying because as long as there are sufficient amounts of moisture in the concrete, ASR-related expansion will occur. However, once all ASR-related expansion has ceased in the concrete, it may be inferred that one or more of the three essential ingredients for ASR (alkali, reactive forms of silica, and sufficient moisture) is no longer present.

As with the linear regression for the relative humidity data, only data with coefficients of determination (r^2) above 0.5 are considered to have strong trends and are discussed in this section. The results of the linear regression analysis for the concrete strain data are presented in Table 6.4, and only trends with an r^2 above 0.5 are shown. This table gives the following information about the trends: location, r^2 , slope, and the figure in which the data is plotted.

It is evident from the data shown in Table 6.4 that span 5 is suffering from ASR much more than span 4. When looking at span 5, 15 of the 25 locations have strong expansion trends, but only two locations have strong expansion trends on span 4. One of the expansive locations on span 4 is 4-S-E-AB, and it

has very little structural implications and is only expanding at a rate of 51.2 microstrains per year.

Table 6.4. Summary of prominent strain trends after mitigation

Prominent Linear Trends in Concrete Strain Data			
Location	Coefficient of Determination, r^2	Trend Line Slope (10^{-6} in./in./month)	Figure
5-N-E-SP	0.971	21.4	Figure 6.39
5-S-E-SP	0.593	8.00	Figure 6.39
4-S-W-BL	0.607	-4.78	Figure 6.41
5-N-E-BL	0.973	46.1	Figure 6.41
5-S-W-BL	0.925	17.5	Figure 6.41
5-S-E-BL	0.667	6.3	Figure 6.41
5-N-E-TL	0.952	22.6	Figure 6.43
5-S-E-TL	0.829	8.70	Figure 6.43
4-S-E-AB	0.556	4.27	Figure 6.44
4-S-W-SH	0.585	-7.71	Figure 6.45
5-N-E-SH	0.974	19.0	Figure 6.45
5-S-E-SH	0.706	4.65	Figure 6.45
5-N-W-SH	0.647	-3.34	Figure 6.45
5-S-W-BH	0.981	28.5	Figure 6.46
5-N-E-BH	0.963	25.3	Figure 6.46
5-S-E-BH	0.799	7.48	Figure 6.46
4-N-E-TH	0.628	14.0	Figure 6.47
5-N-W-TH	0.976	20.3	Figure 6.47
5-S-W-TH	0.845	13.6	Figure 6.47
5-N-E-TH	0.832	12.4	Figure 6.47

The only other expansive location on span 4 besides 4-S-E-AB is 4-N-E-TH. This location is plotted in Figure 6.47 and has an expansion rate of 170 microstrains per year. The high expansion rate suggest that ASR could be occurring at the 4-N-E-TH location, but more field and laboratory investigations would be required to confirm this. The eastern side of span 5 north had the most expansion with six of its seven expansion measurement locations having strong trends of growth as shown in Table 6.4, the abutment is the only location that did not show expansion. 5-N-E-BL is plotted in Figure 6.41 and has the highest expansion rate of any location with 550 microstrains per year, and the average of the 5-N-E trend data is 290 microstrains per year.

Other locations with very high expansion rates include: 5-N-W-TH, shown in Figure 6.47, with an expansion rate of 245 microstrains per year; 5-S-W-BH, shown in Figure 6.46, with an expansion rate of 340 microstrains per year; 5-S-W-BL, shown in Figure 6.41, with an expansion rate of 210 microstrains per year; and 5-S-W-TH, shown in Figure 6.47, with an expansion rate of 165 microstrains per year. There are also three strong trends of contraction, two of which are in the treated control arch, but it is not understood what this could mean in terms of ASR suppression.

6.4.3.2 Concrete Strain Difference Analysis

A strain difference analysis was performed by taking the difference in the control arch and the ASR mitigation treated arches. Figure 6.48 through Figure 6.53 are the plots for the strain difference analysis, but span 4 north does not have data for east and west side perpendicular, west top low, and east abutment.

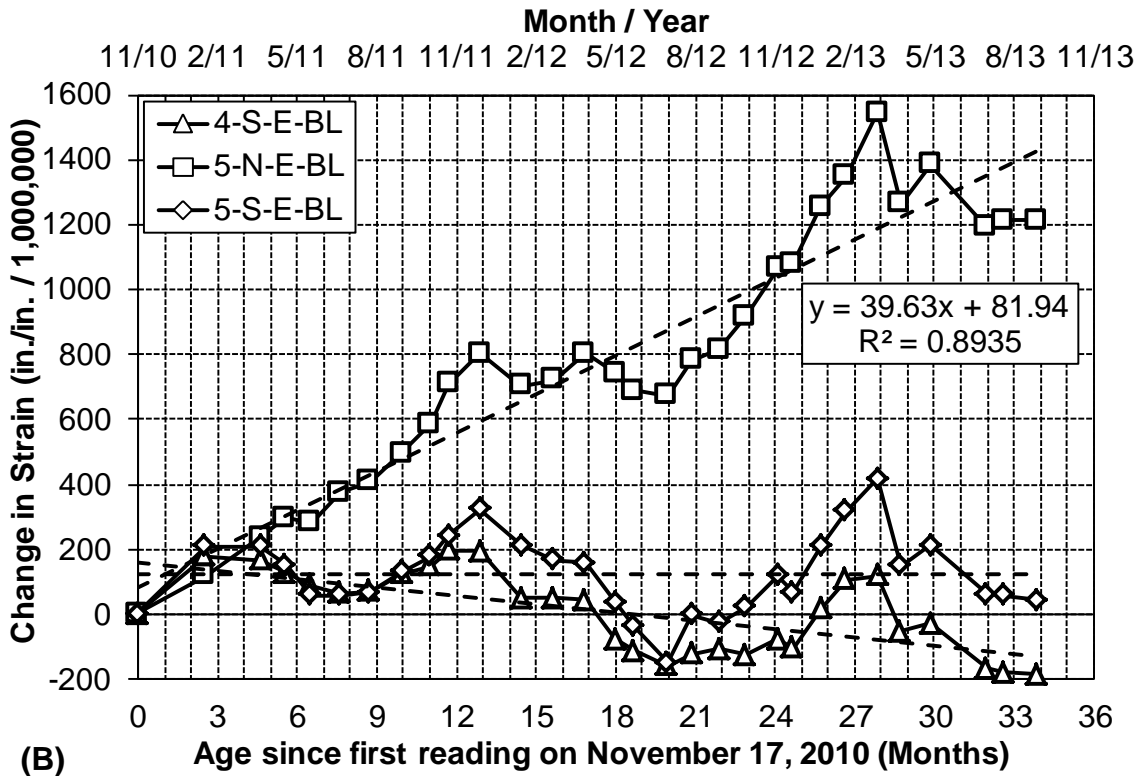
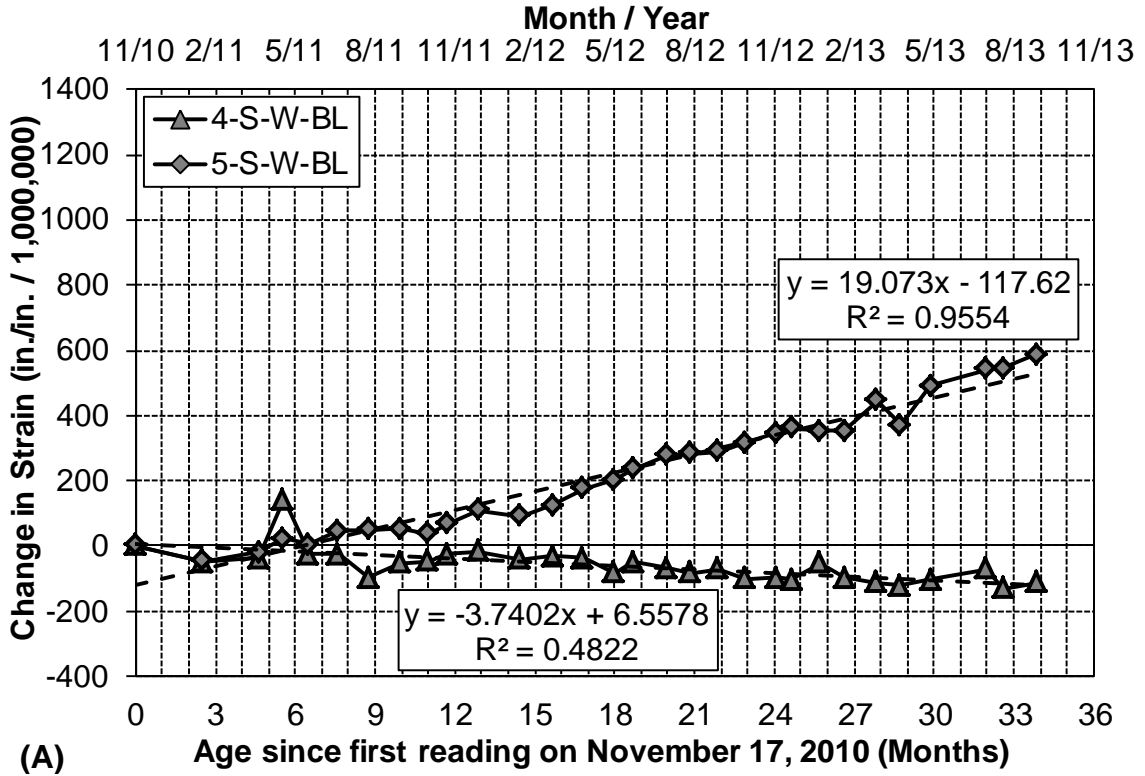


Figure 6.48. Strain difference for Bottom Low at (A) west and (B) east

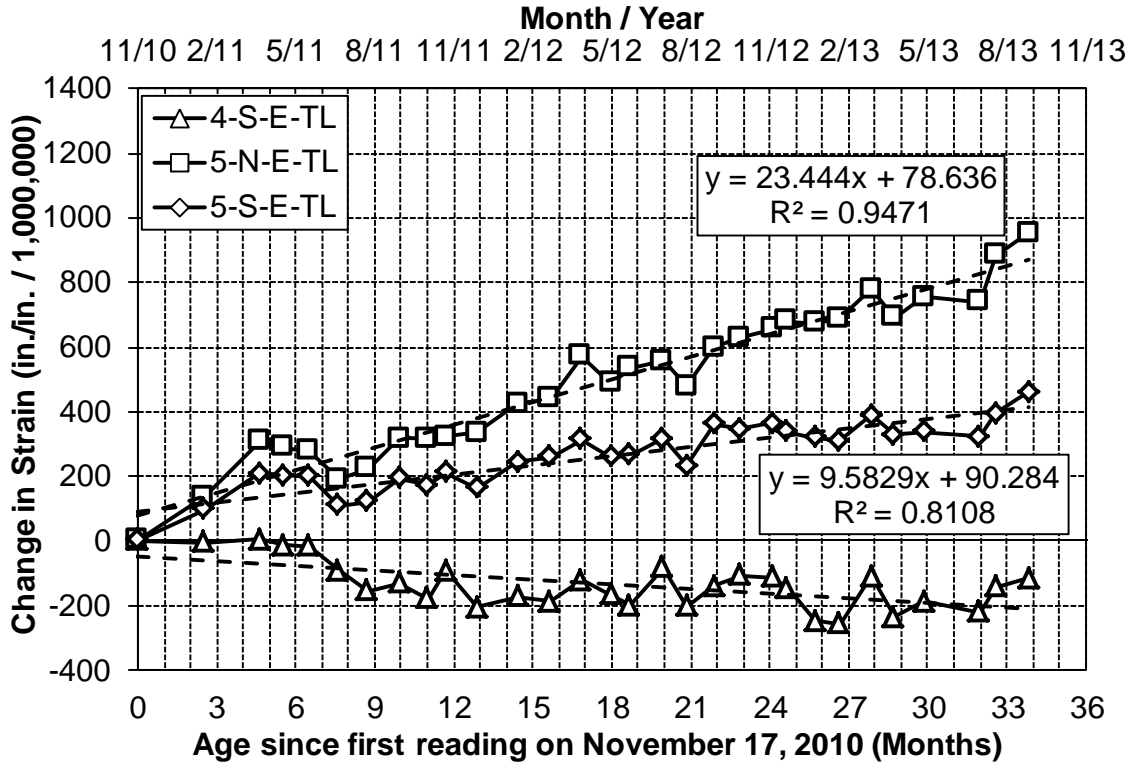


Figure 6.49. Strain difference for east, Top Low locations

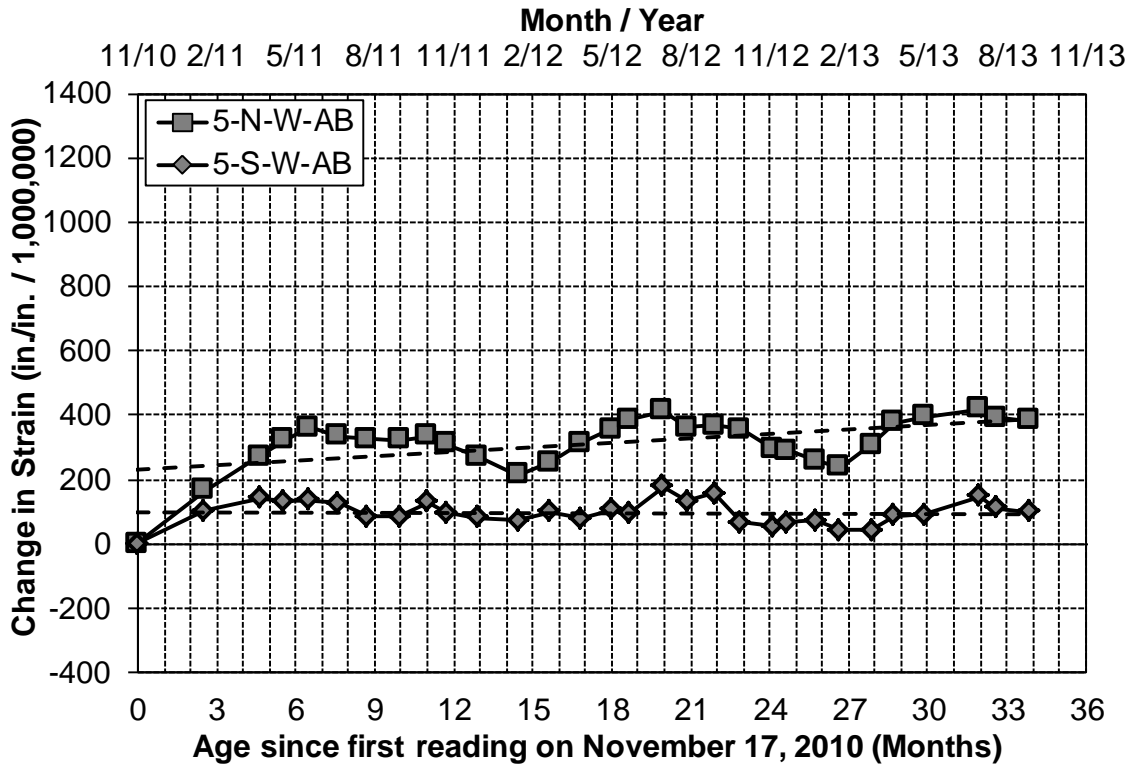


Figure 6.50. Strain difference for west, Abutment locations

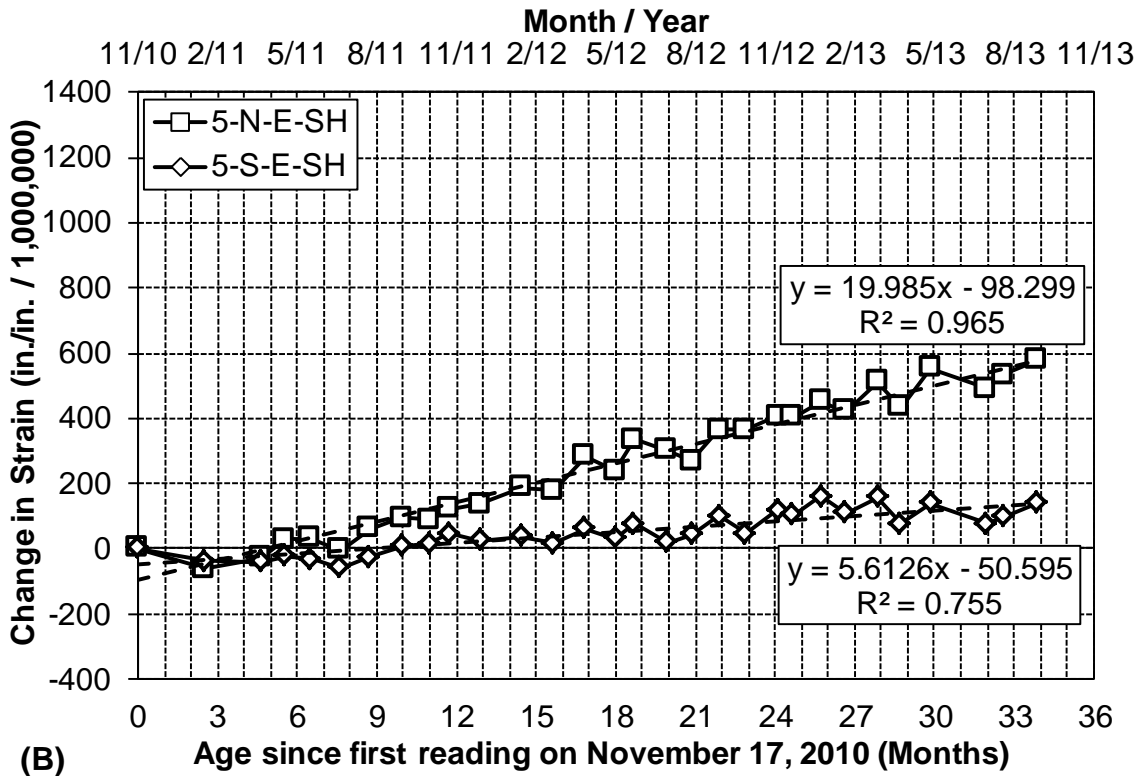
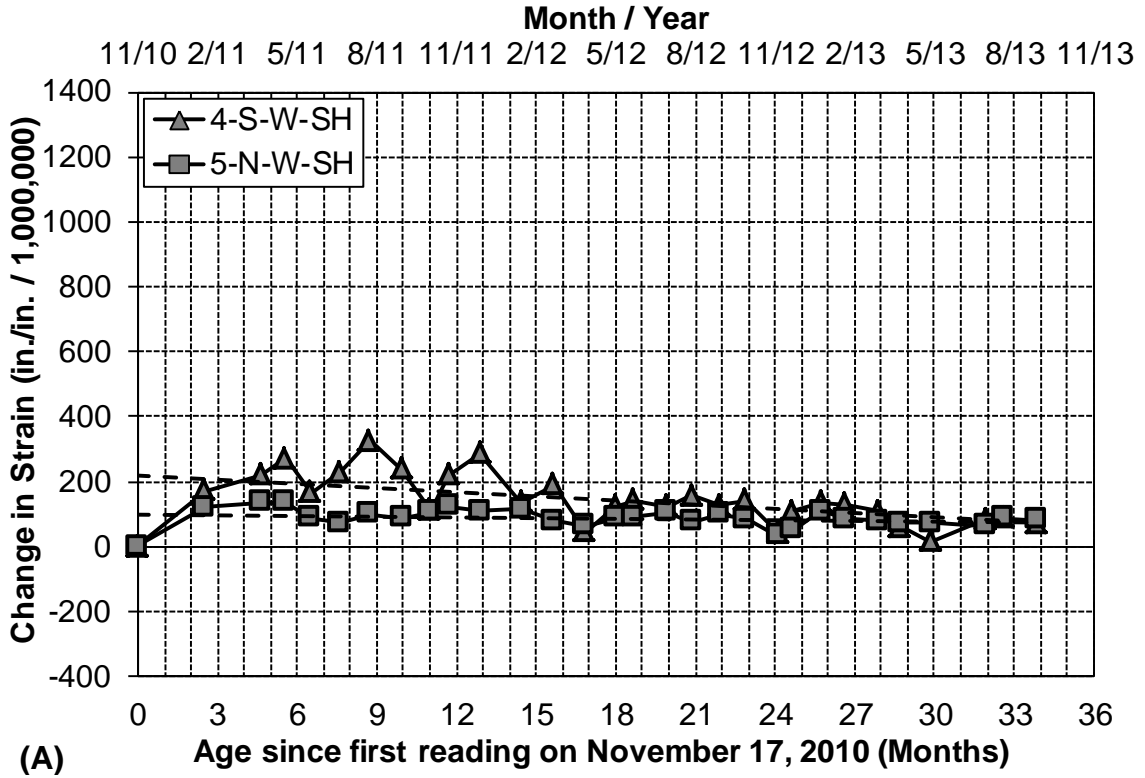


Figure 6.51. Strain difference for Side Horizontal at (A) west and (B) east

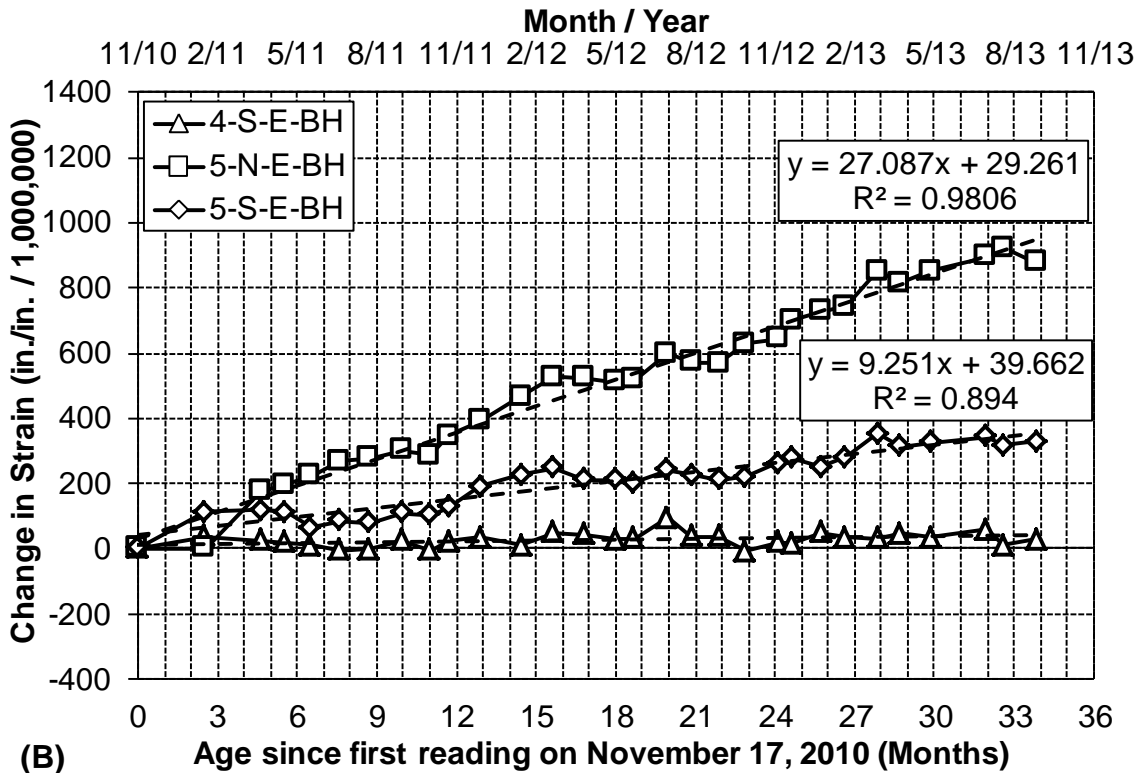
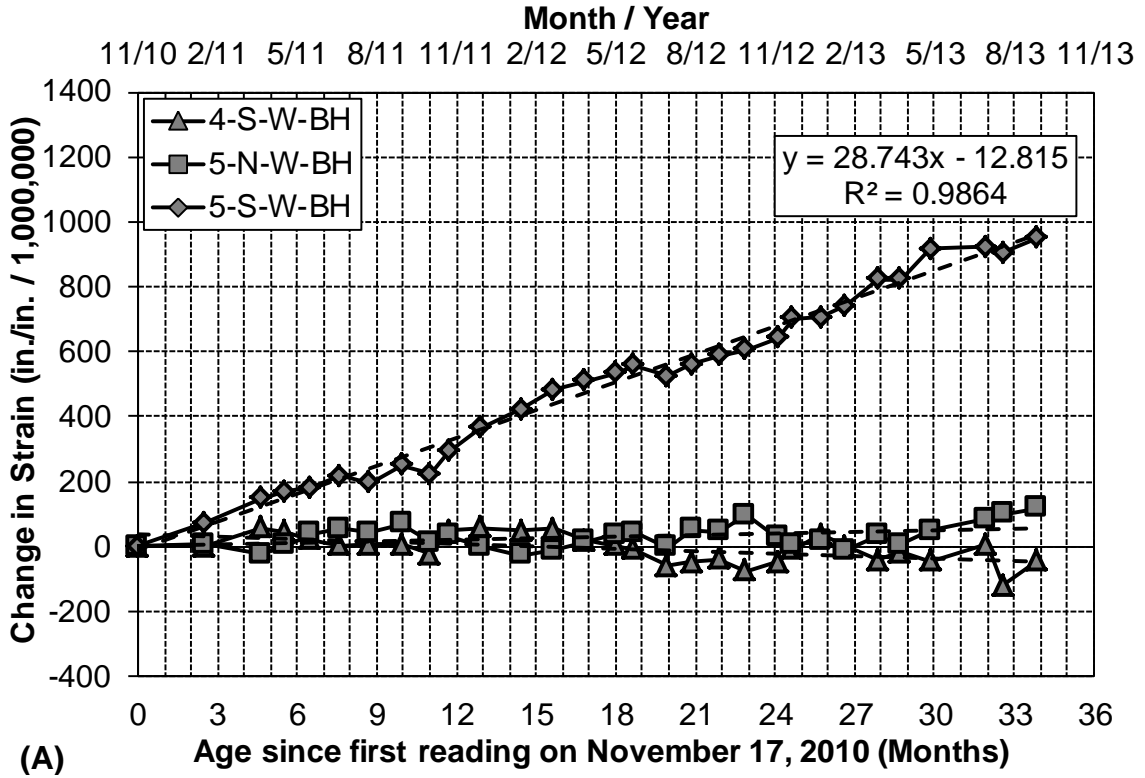


Figure 6.52. Strain difference for Bottom High at (A) west and (B) east

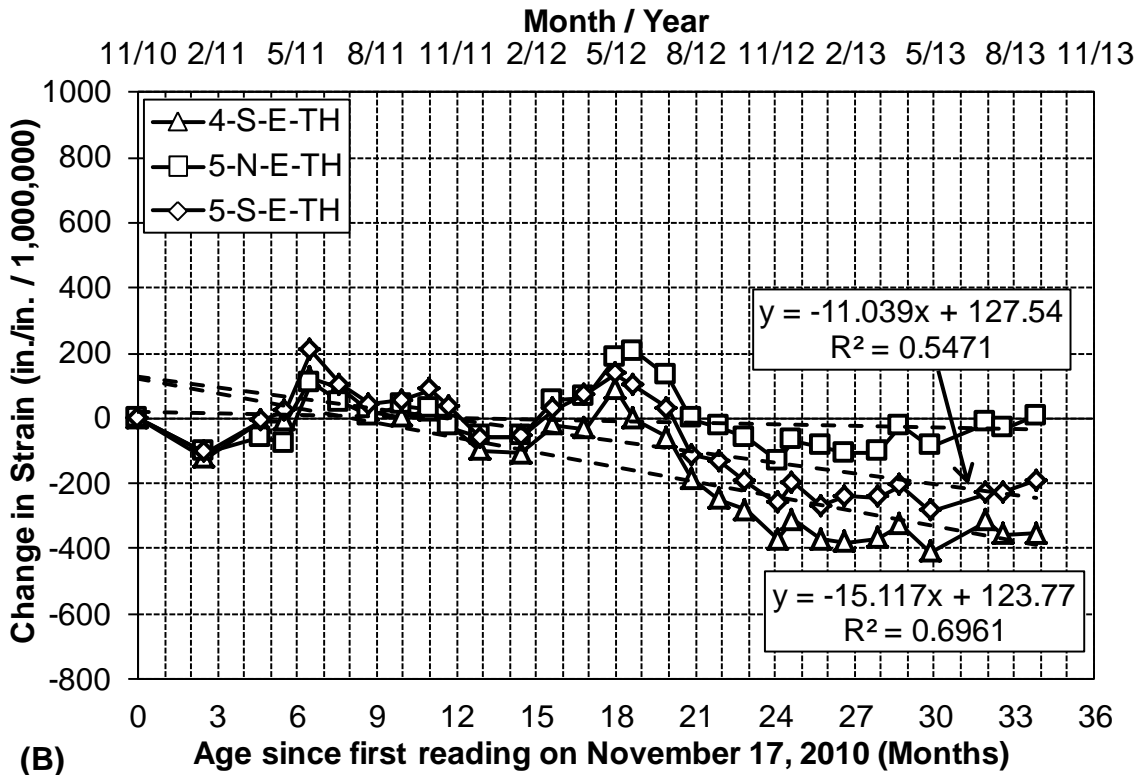
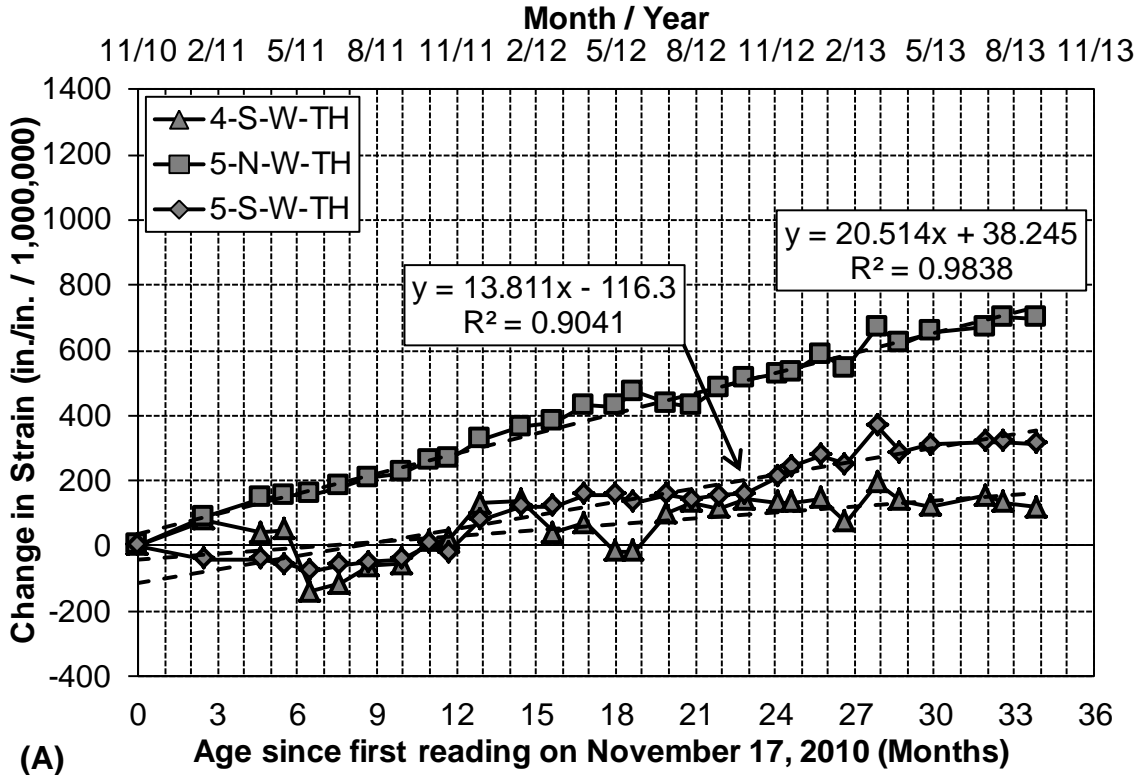


Figure 6.53. Strain difference for Top High at (A) west and (B) east

The benefits of using the strain difference analysis are the same as the benefits of the relative humidity difference analysis. The strain difference analysis reduces the environmental effects on strain, such as temperature and moisture, as much as possible and gives a better comparison for ASR-related expansions.

The strength of the expansion difference trends were quantified with the r^2 values as previously done; r^2 values greater than 0.5 represent strong trends. The trend data for the expansion difference analysis are presented in Table 6.5 and include location, r^2 , slope, and which figure the data are plotted.

Table 6.5. Summary of prominent strain difference trends

Prominent Linear Trends for Strain Difference Analysis			
Location	Coefficient of Determination, r^2	Trend Line Slope (10^{-6} in./in./month)	Figure
5-S-W-BL	0.955	19.1	Figure 6.48
4-S-W-BL	0.482	-3.74	Figure 6.48
5-N-E-BL	0.894	39.6	Figure 6.48
5-N-E-TL	0.947	23.4	Figure 6.49
5-S-E-TL	0.811	9.58	Figure 6.49
5-N-E-SH	0.965	20.0	Figure 6.51
5-S-E-SH	0.755	5.61	Figure 6.51
5-S-W-BH	0.986	28.7	Figure 6.52
5-N-E-BH	0.981	27.1	Figure 6.52
5-S-E-BH	0.894	9.25	Figure 6.52
5-N-W-TH	0.984	20.5	Figure 6.53
5-S-W-TH	0.904	13.8	Figure 6.53
5-S-E-TH	0.547	-11.0	Figure 6.53
4-S-E-TH	0.696	-15.1	Figure 6.53

There are only two locations with trends of a difference in expansion relative to span 4 north in Table 6.5 that were not in Table 6.4 for the raw data trends. These locations are 5-S-E-TH and 4-S-E-TH, but 4-N-E-TH (which was previously discussed for having a large expansion trend) is expanding at rates of 130 and 180 microstrains faster than 5-S-E-TH and 4-S-E-TH, respectively. The downward expansion difference trends for 5-S-E-TH and 4-S-E-TH can be seen Figure 6.53.

All of the data locations that were in both prominent strain trend tables, Table 6.4 and Table 6.5, have very similar trend line slopes and do not require any further explanation beyond what was stated in the raw data discussion. The assumed coefficient of thermal expansion value of $6.95 \times 10^{-6} / ^\circ\text{F}$ for the concrete arches is also validated based on the assumption that span 4 north does not have any ASR-related expansions, except for maybe at 4-N-E-TH, and the slopes for the raw data trends are similar to the strain difference trends.

6.4.4 Strain Data Analysis Summary

Strong trends of continued ASR-related expansion are present at 15 of the 25 strain measurement locations on span 5 as seen in Table 6.4. These trends help confirm the conclusion that was already made from the relative humidity data analysis that the ASR mitigation procedure has not been effective thus far in lowering the relative humidity to a sufficient level to suppress ASR. Expansion rates as high as 550 microstrains per year were seen in span 5 north, and one strong expansion trend of 170 microstrains per year was even seen in the untreated control arch, span 4 north.

When comparing the prominent trends from the strain data and the strain difference analysis, Table 6.4 and Table 6.5 respectively, 11 of the 13 strong expansive trends from the strain data were also present in the strain difference analysis. There were actually 17 strong expansion trends seen in the raw data, but 4 of them were either on span 4 north or at a location on a treated arch that did not have a counterpart for comparison on span 4 north.

Chapter 7

Future Mitigation Considerations

7.1 Introduction

It is first recommended that a structural analysis of the ASR-affected arches in the Bibb Graves Bridge be carried out to evaluate the load carrying capacity of the distressed concrete. This analysis should also account for future concrete expansion. Future expansions can be predicted with the use of expansion trends, discussed in Chapter 6, that were determined through 34 months of monitoring.

Mitigating the severely cracked arches with confining wraps or a post-tensioning system may be very effective at strengthening the arches and/or suppressing ASR-related expansion, but these techniques are very costly and require temporary closing of the bridge. Therefore, structural repair options should only be pursued if a structural analysis reveals a lack of structural integrity, insufficient strength of arches, or if future mitigation attempts to lower the relative humidity in the concrete fail.

Mitigation methods targeted at lowering the relative humidity in the concrete are highly recommended in lieu of confining and strengthening the arches, provided that the current strength and integrity of the arches are sufficient. Therefore, mitigation methods such as wrapping the arches with a waterproof fabric or installing a ventilated cladding will be discussed first in this

chapter. Physical restraining methods will be discussed later in this chapter, and they should only be used in the event that the cross sections of the arches do need to be confined in order to prevent any further ASR expansion. Confining methods that will be discussed include wrapping the arches with a carbon fiber reinforced polymer (CFRP) and post-tensioning with the use of through bolts and plates.

A mitigation option for applying penetrating sealers to the entire bridge will also be discussed at the end of this chapter. There are several signs of possible ASR in portions of the bridge other than the arches of span 5. These signs of ASR are only surface discoloration in some of the affected areas at this time; therefore, the use of penetrating sealers may be effective.

7.2 Covering Arches for Protection from Rain

While applying a cover over the arch is not as aesthetically pleasing as using a penetrating sealer such as silane, it will keep water out of the concrete much more effectively. The advantage to using a covering instead of a sealer is that it protects all rain-exposed surfaces of the concrete and future expansion and cracking will have no effect on it; whereas future cracking will give direct routes for water to enter a sealed concrete. Covering the arch would also require less maintenance than a sealer, because future cracks would not have to be sealed every few months when using a cover.

Covering the arches also has advantages over confining them. Not only is confining expensive and requires temporary closing of the bridge to install, but it also permanently changes the pleasing aesthetics of the Bibb Graves Bridge.

Applying a cover to the bridge will affect its appearance just as much as confining the arches will, but the cover is only temporary. Finite element analysis on the moisture diffusion times for the arches was performed by Warnock (2012), and these results, presented in section 2.7, predict that it could take anywhere from 5.4 to 13.9 years for the concrete to fully meet the desired relative humidity of 80 percent. Once 80 percent relative humidity is met and the cover is removed, the severely ASR-affected arches will once again look similar to the other arches.

Shielding the concrete from rain with a cover does have its difficulties though. The goal of this mitigation option is still to lower the internal relative humidity of the concrete to below the 80 percent threshold required for ASR to occur. This means that any type of cover applied to the arches must not only prevent rainwater from reaching the concrete, but it must also allow some of the moisture vapor already present in the concrete to escape. In order to dry the concrete, there must be sufficient breathability in the cover and enough space for airflow between the concrete and the cover to prevent the buildup of condensation and allow moisture to escape the shielding system. There are two types of covers discussed in this chapter; one is a waterproof fabric and the other is a ventilated cladding.

7.2.1 Waterproof Fabric Cover

The first type of covering presented is the use of a heavy duty, waterproof fabric that is wrapped around the arches. A section of the arch with this fabric on it is shown in Figure 7.1. Note that the contrasting colors used are for visual purposes only; color selection should be done to match the existing concrete. There are

two different types of fabric used in this covering system; one is waterproof and breathable, and the other is waterproof and extremely durable. The breathable fabric is represented by the gray squares and the durable non-breathable material is the brown fabric shown in Figure 7.1. If only one material is used for this system, it must be the waterproof and breathable fabric. Otherwise, moisture would be trapped under the fabric and excess condensation would buildup. However, it could be advantageous to use two materials based on economic and durability concerns. Whether one or two materials are used, it is essential that they be rated for continuous outdoor use and UV exposure. Otherwise, this system will not have a lifespan long enough for the arches to dry.

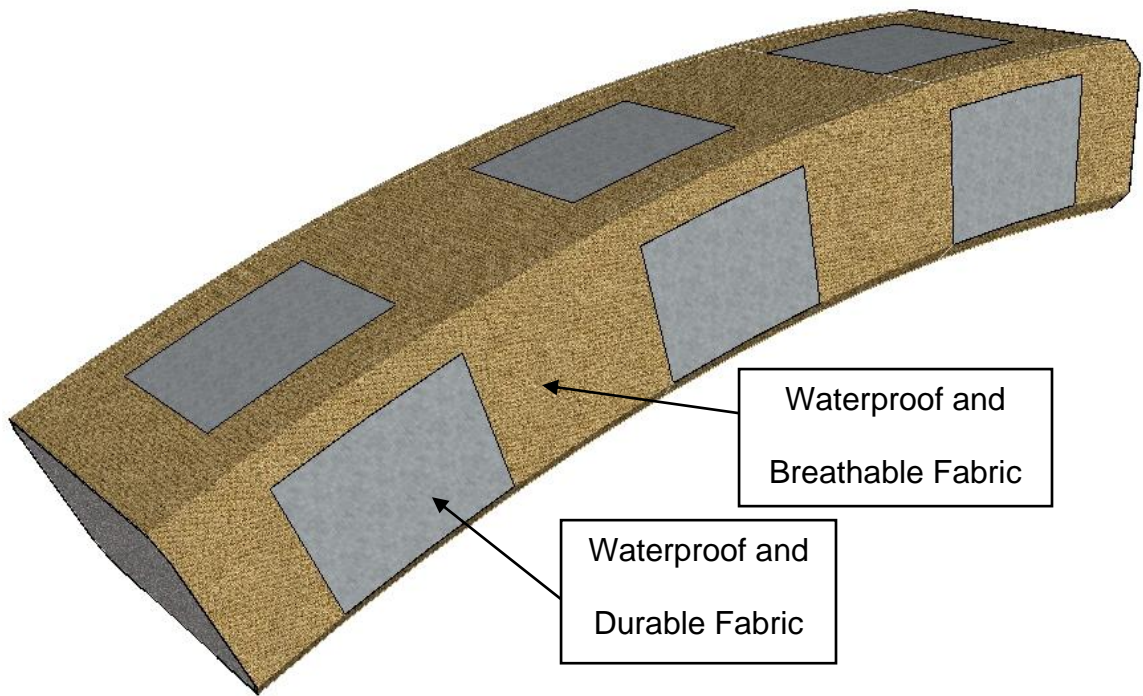


Figure 7.1. Fabric covered arch; top and side view

A cross sectional view of what the fabric system would look like is presented in Figure 7.2. The spacers that would be used to create a space for airflow between the fabric and concrete can be seen in Figure 7.2 along with an opening left between fabric panels on the underside of the arch for increased airflow. A variety of materials could be used for the spacers including: pressure-treated wood, composite decking, etc. These spacers would also only be a few feet long and not placed end-to-end so that airflow between different sides of the arch is achievable. The opening between the fabric panels on the bottom of the arch is also where the fabric could be secured around the arch. To secure the fabric and keep it taut, a cable could be tightly laced through grommet holes at the edge of the material as shown in Figure 7.3.

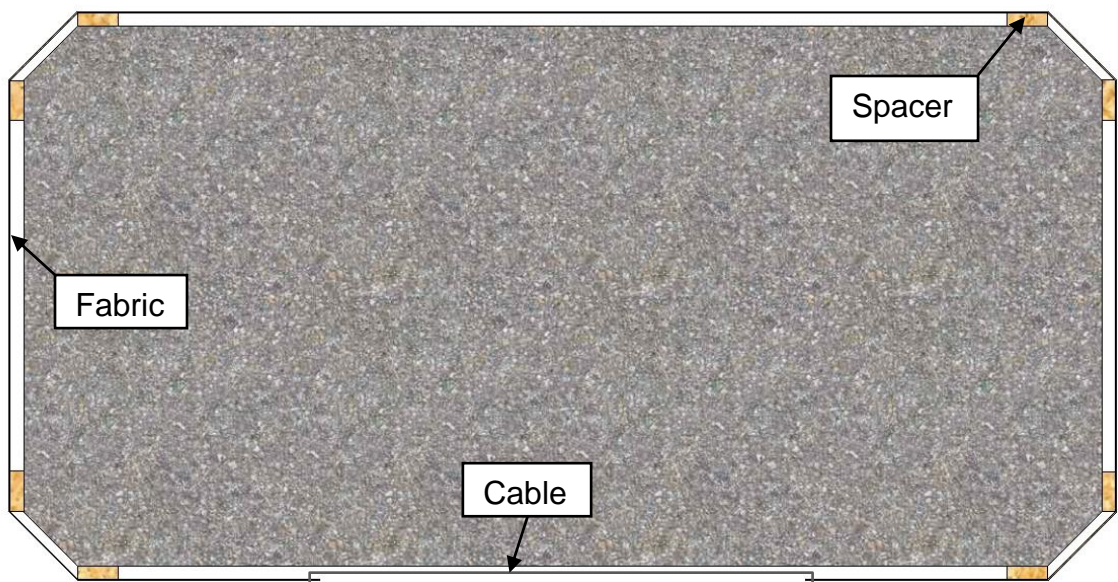


Figure 7.2. Cross section view of fabric covering

As previously mentioned, continued monitoring of the ASR-affected concrete should be done after the application of another mitigation procedure; therefore, it is important that the fabric covering be fabricated in such a way that

allows for access to the relative humidity tubes. The fabric must also be fabricated in a way that accounts for the cross braces that connect the north and south arches of each span; there are four cross braces per span. Details will need to be developed to ensure that water does not enter the fabric at the intersections of the arch and cross braces.

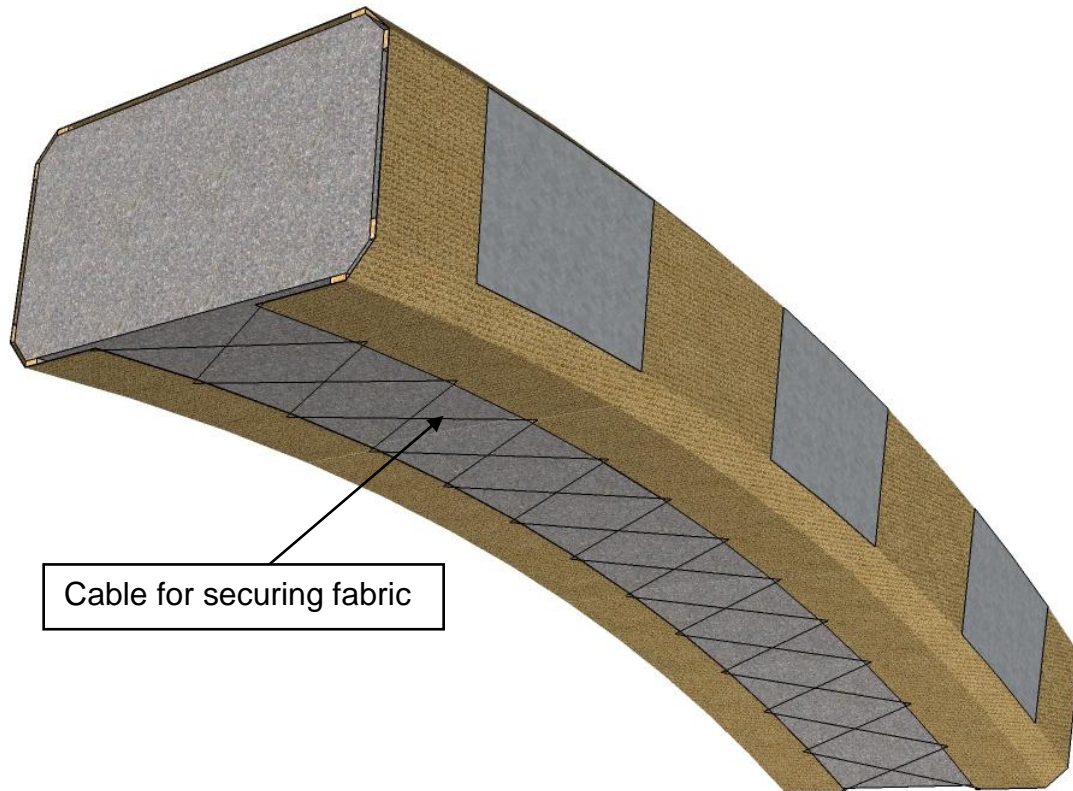


Figure 7.3. Bottom view of fabric secured around arch

7.2.2 Ventilated Cladding

The other type of covering discussed in this chapter for mitigating ASR in the Bibb Graves Bridge is a ventilated cladding. The use of a ventilated cladding was one of the measures taken to mitigate ASR in the Montrose New Bridge in Scotland. However, this bridge was removed ten years after it was repaired due to continued internal decay. This section contains several figures that illustrate

the different layers of the cladding system that are necessary for installation and to allow airflow. The first image, Figure 7.4, is a small segment of the arch to illustrate how the cladding would look once installed, and the cladding would be colored prior to installation.

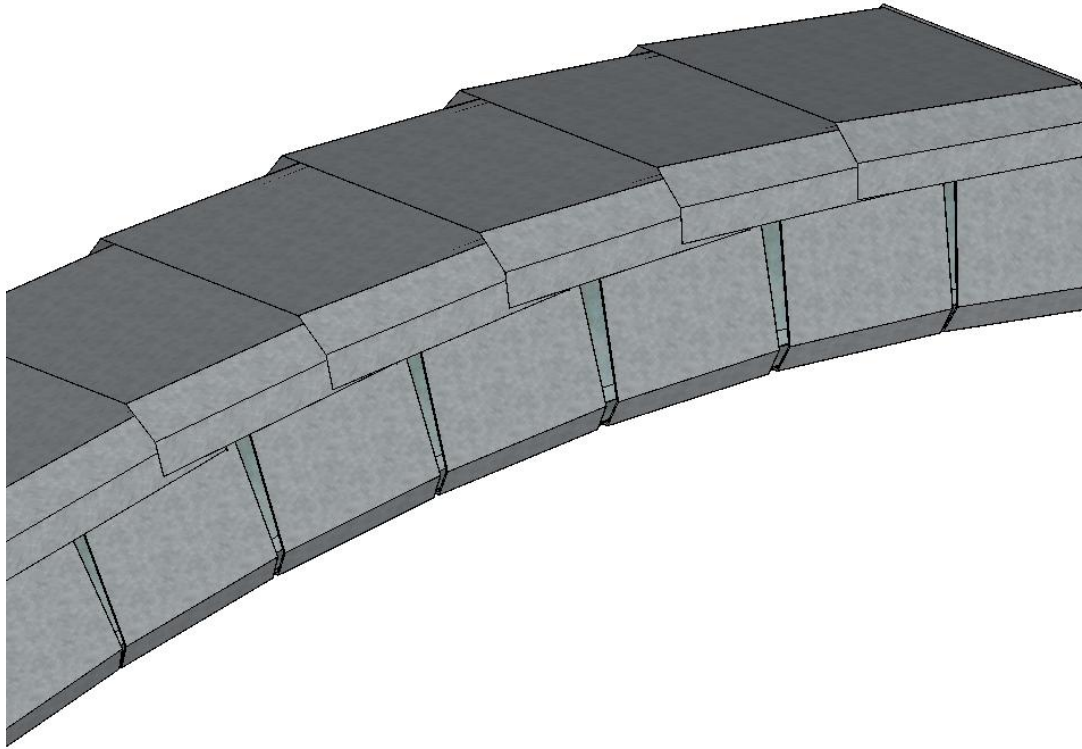


Figure 7.4. Ventilated cladding layout on arch

The first step for installing the cladding to the arch would be applying the innermost layer to the sides of the arches, as shown in Figure 7.5. Notice how all of the edges of each “inner” panel have 90 degree bends to the outside; this can be seen on the enlarged view of a panel in Figure 7.5. The purpose of the bent edges is to prevent rain from being blown off the sides of the panel and directly onto the concrete. These panels would be installed to a spacer on the concrete in order to anchor them to the arch and so that air can flow behind them. The

spacers do not have to be continuous as depicted in Figure 7.5; discontinuities and gaps between the ends of the spacers would allow more airflow between the sides of the arch. One can also see how the panel bends all the way around the bottom edge of the concrete in Figure 7.5 to cover any surfaces potentially exposed to rainwater.

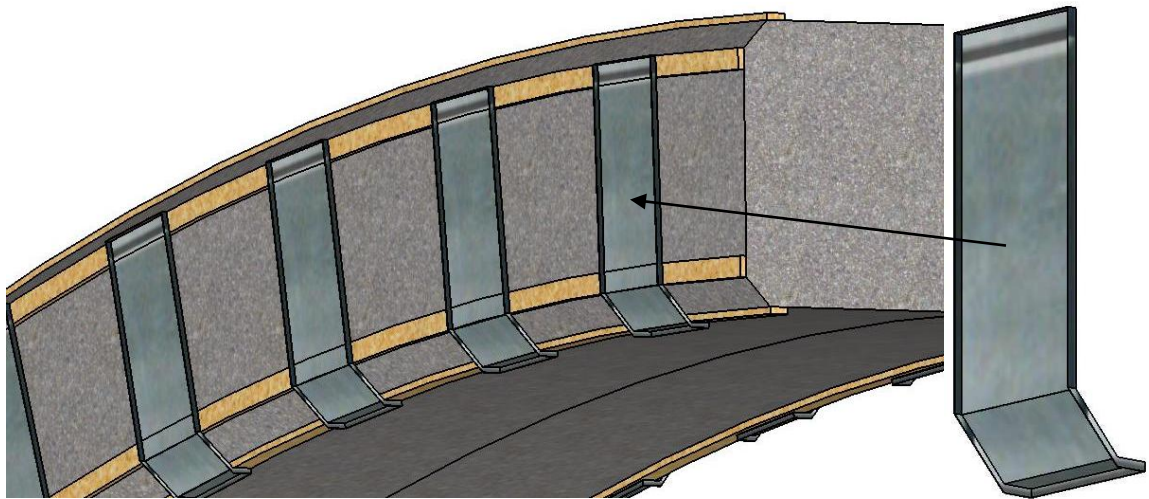


Figure 7.5. First layer of side cladding

The second layer of panels is shown in Figure 7.6 with an enlarged view of the panel as well, and these panels fit over the inner layer of paneling to shield the rest of the exposed concrete on the side of the arch from rain. The edges of this “outer” panel are also bent to control where water can and cannot go. The sides of the panel have their edges bent in to help prevent water from being blown between the inner and outer panels. Whereas the top and bottom of the outer panel have their edges bent out to keep water from being blown above the panel and to create a drip edge at the bottom of the panel, respectively.

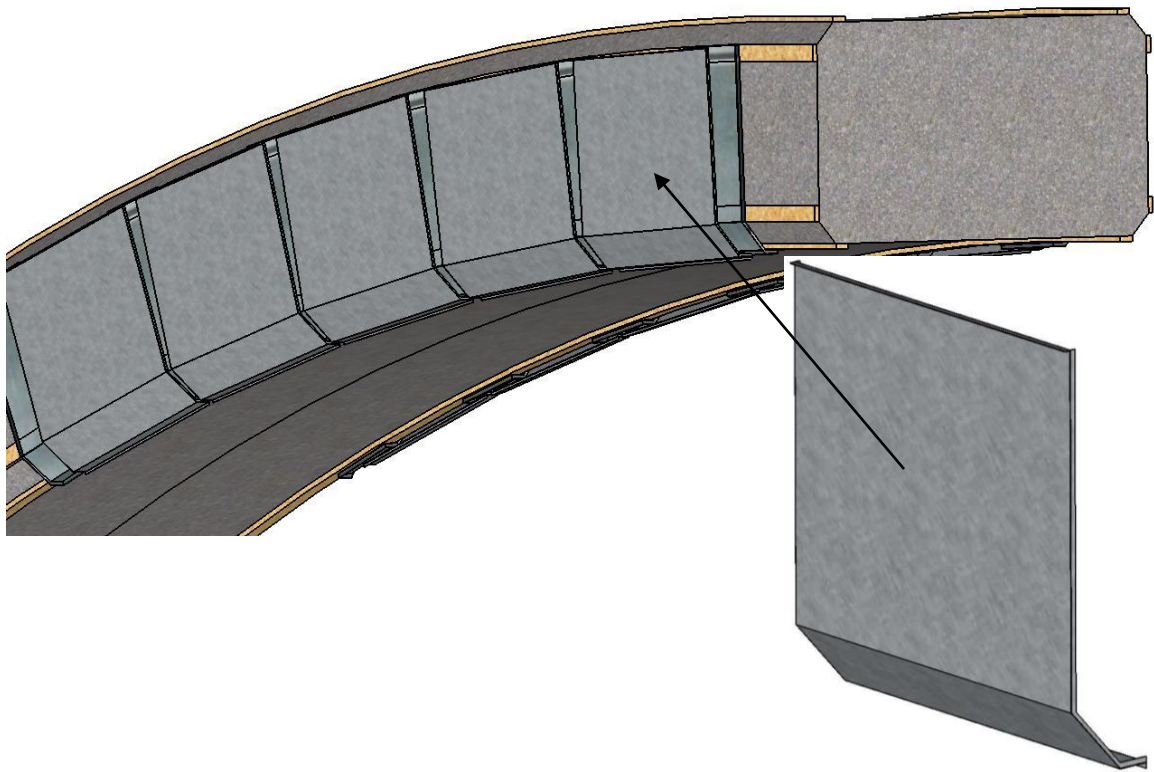


Figure 7.6. Outer side panels of cladding

The next couple of images are close-up views of how the inner and outer panels align with each other. Figure 7.7 is a close-up view of the top of the side paneling system. In this figure, one can see that the top of the outer panel sits just below the top of the inner panel, and there is a little space all the way down the side between the inner and outer panels for airflow. Figure 7.8 is a close-up view of the bottom of the side panels. The drip edges on the inner and outer panels can be seen in Figure 7.8, as well as how the bottom of the outer panel ends just short of the bottom of the inner panel.

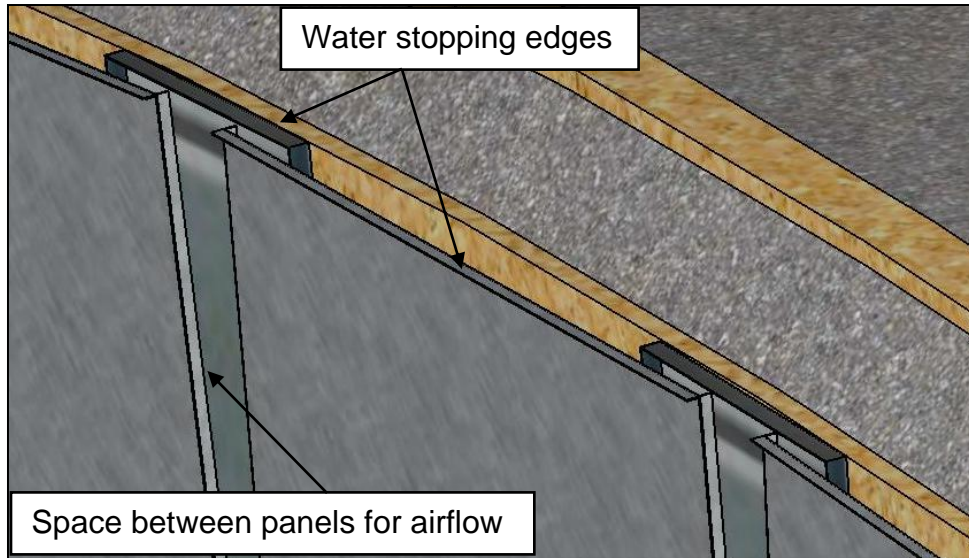


Figure 7.7. Close-up view at the top of side panels

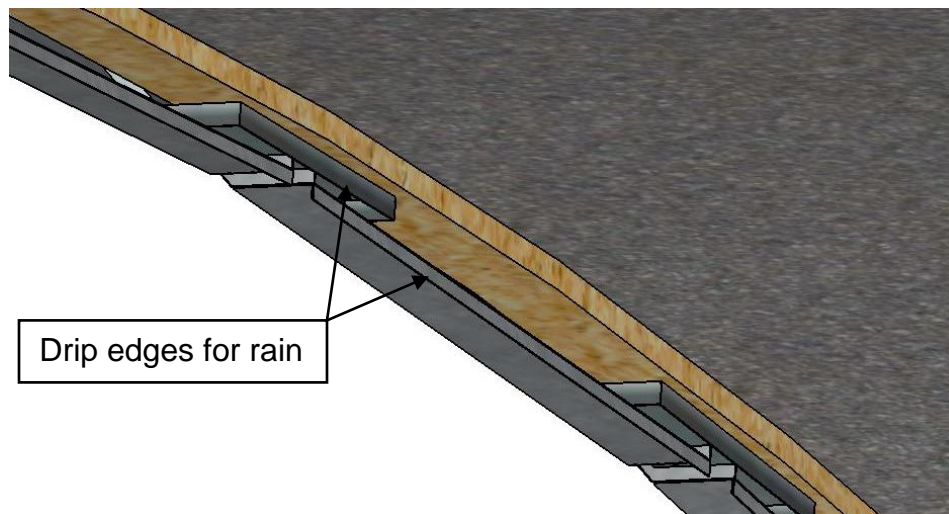


Figure 7.8. Close-up view at the bottom of side panels

The last layer of paneling is applied to the top of the arches. Figure 7.4 is a top view of the entire cladding system and Figure 7.9 is a side view of all of the paneling with an enlarged view of the “top” panel. The top panels are layered over one another like shingles and overhang the tops of the side panels to direct water down the paneling and away from the concrete. Notice in Figure 7.9 that

the upper end of the top panel also has its edge bent out to prevent water from being blown to the inside of the cladding system.

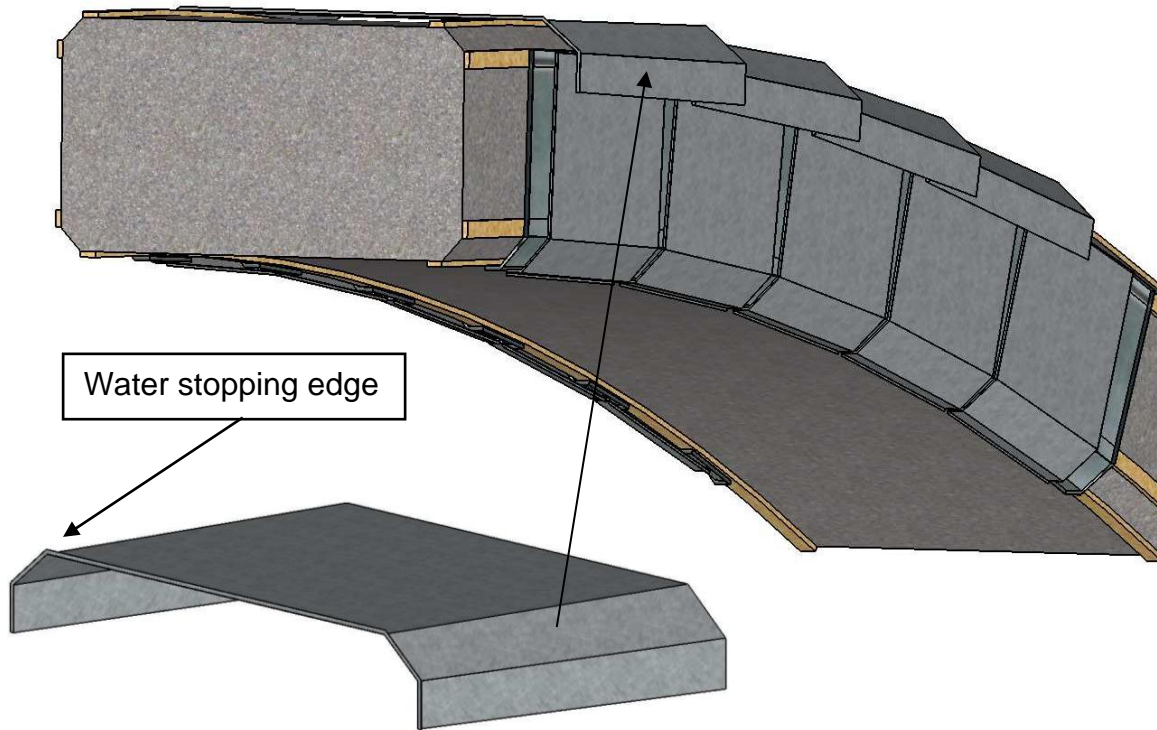


Figure 7.9. Layered top panels

There is very little to no information available about the use of ventilated cladding or fabric covers to dry out concrete suffering from ASR, and it is unclear at this time which option would be best for the Bibb Graves Bridge. The cladding would be far more durable and less susceptible to damage through vandalism, but fabrication costs and effectiveness of the two recommended mitigation systems compared to each other are unknown at this point. It is recommended that both mitigation options be investigated and small scale testing be done with them to assess rainwater resistance and drying potential. The ideas and designs presented in this chapter for the two mitigation procedures are preliminary

suggested options that may be viable. The design of these two coverings should be further engineered and evaluated before applying them to this bridge.

7.3 Cross-Sectional Confinement

There are several cases presented in section 2.6.6 of this thesis where the application of confining stress or restraint to a cross section that is expanding due to ASR will suppress the expansion process. A challenge to providing confinement to the arches for the Bibb Graves Bridge is that they are rectangular in shape, which is not ideal for this strengthening technique. This is not a simple process though. All ASR-affected concrete will have different swelling stress potentials; therefore, petrographic examination and testing should be performed on core samples from the structure to determine how much stress is needed to restrain expansion. From the three studies discussed in section 2.6.6, two of which were of field structures, confining stresses of 500, 725, and 1160 psi were required to overcome the expansion due to ASR. The 500 and 725 psi values were for the field structures, bridge columns and bridge piers, respectively. The emphasis on applying confinement in all three dimensions is also discussed in these studies. If confinement is only provided in one direction, the non-confined directions experience more expansion and deterioration than if there was no confinement at all (Rigden et al. 1992).

Once a value for the stress needed to restrain expansion in the Bibb Graves Bridge is known, structural engineers can design appropriate confining systems to meet the needs of the structure. This chapter presents two types of confining systems that may be applicable to the bridge if confining is deemed

necessary in the future. These two methods are wrapping the arches with carbon fiber reinforced polymer (CFRP) and post-tensioning with plates and through bolts. No matter what method of confinement is selected, it is recommended that all of the cracks be injected with epoxy and instrumentation be installed to monitor the development of confining stresses over time. Epoxy injection will help restore the integrity of the concrete, and allow the concrete to better withstand the high confining stresses.

7.3.1 CFRP Wrap

Mitigating and repairing the Bibb Graves Bridge with a CFRP wrap would be the preferred confining method over post-tensioning. CFRP has several benefits when compared to post-tensioning including faster application time resulting in less bridge closure, CRFP is easily applied to any shape of concrete element, and CFRP will be less noticeable after installation; whereas post-tensioning would have bulky steel plates and potentially exposed anchorage hardware.

It is well known that CFRP performs best on circular cross sections because there are uniform pressures all the way around the element, but it may still be able to provide sufficient confinement to rectangular sections if designed properly. CFRP would not be pretensioned at the time of application; therefore, the confining stress needed to counter the ASR expansion would be generated over time from the CFRP restraining continued expansion of ASR. The best way to predict how well CFRP would work on the rectangular sections of the Bibb Graves Bridge arches would be with the use of a finite element model. This model would have to simulate restrained expansion in the concrete and

determine the level of stress concentrations at the corners of the cross section due to the CFRP confinement. There is a possibility that the stress in the concrete at the corners of the cross section could exceed the compressive strength of the concrete before the concrete on the outer edges near the centerlines of the cross section reach a sufficient stress to suppress ASR expansion.

7.3.2 Post-Tensioned Confinement

The other type of confinement that may be able to be used on the Bibb Graves Bridge is post-tensioning. This is the least desirable possible mitigation method presented in this chapter; however, if attempts to dry out the arches fail and if it is determined that CFRP will crush the corners of the concrete, this may be the next best option. For the post-tensioning system to work, it must be capable of providing confining stresses on all sides of the arch that are higher than the potential expansive stresses generated by ASR. Post-tensioning the arches is an active confining system, meaning the arch is subjected to confining stresses at the time of installation. On the other hand, wrapping the arches with CFRP is a form of passive confinement, confining stress is only generated as expansion continues.

This post-tensioning system would consist of thick, flat plates that are attached to all faces of the arch with tensioned through bolts. These bolts would be threaded post-tensioning bars that go all the way through the concrete's cross section and the steel plates. The bars would then be tensioned by creating a reaction force against the plates on each side of the concrete. In order to achieve

a uniform stress distribution across the surface of the concrete, a sufficient number of bars and a stiff enough plate must be used. The ASR-affected elements must be confined in all three dimensions to effectively suppress ASR expansion (Pantazopoulou and Thomas 1999); therefore, the plates would be installed on all four sides of the arch cross section, and the bars will pass through the cross section in both perpendicular directions. This system would take a lot of time and money to install because of the large amount of holes that must be drilled through the arches for the post-tensioning bars.

7.4 Possible ASR in Locations other than Span 5

All of the research presented so far in this thesis has been about mitigating ASR in span 5, but there are also signs of ASR in other spans of the bridge that should be dealt with. These other signs are typically more isolated and do not cover the entire arch, but to be proactive, now is the time to start mitigating these areas before they are cracked as severely as parts of span 5. Figure 7.10 and Figure 7.11 have a couple examples each of possible signs of ASR in spans 3 and 4, respectively. All of these pictures have surface discoloration, and some of them even have surface deposits and cracking. There are also many other locations with signs of possible ASR besides the four locations in the pictures presented here.

The examples of possible ASR shown in Figure 7.10 and Figure 7.11 are some of the more visually distressed areas other than span 5. Cores should be taken from these locations for petrographic analysis to confirm if ASR is present. If it is ASR, mitigating the entire bridge with a surface treatment similar to what

was done on span 5 would be recommended before it has the chance to severely crack. This mitigation procedure is explained in section 4.3, but a modification for the next ASR mitigation strategy would be to seal all cracks with a flexible sealant, not only the ones wider than 0.04 inches.

Mitigation through application of surface sealers would be recommended because the vast majority of the concrete is not cracked, and the locations that are cracked are isolated and small. Sealing the surface may work here even though it did not work on span 5 because the relative humidity is already lower and there is much less expansion in the non-distressed arches, as seen in the results for span 4 presented in Chapter 6. There were also a couple locations in the silane treated arch of span 4 that had weak trends of drying. Routine inspection of the bridge should be done multiple times a year after mitigating with a surface sealer in order to seal any new cracks that appear; unsealed cracks are direct routes for water to enter the concrete.



Figure 7.10. Examples of possible ASR in span 3



Figure 7.11. Examples of possible ASR in span 4

7.5 Summary

The next ASR mitigation method should focus on applying a covering to the arches in span 5 of the Bibb Graves Bridge or adding confinement to them based on the results of a structural evaluation from a strength and durability perspective. If it is determined that the bridge is structurally adequate, mitigation options such as covering the arches with a waterproof and breathable fabric or applying a ventilated cladding to shield the arches from rainwater should be considered. But if the bridge already has strength concerns or if the arches cannot safely expand anymore, mitigation methods should focus on confining the concrete so that ASR will be suppressed. Methods of confining include wrapping the arches with CFRP or post-tensioning them with plates and through bolts.

Chapter 8

Summary, Conclusions, and Recommendations

8.1 Project Summary

8.1.1 ASR Overview

ASR is a detrimental reaction in concrete that can cause severe expansion and cracking in structures. There are three essential ingredients that must be present in concrete for the onset and continuation of ASR: (1) sufficient alkali, primarily from the cement, (2) reactive forms of silica in the aggregate, and (3) sufficient amounts of moisture in the concrete (Fournier and Bérubé 2000). Once any of these three ingredients are no longer in the concrete, the ASR expansion process will cease. Moisture is by far the least difficult of the three ingredients to remove from an existing structure, but removing moisture is not an easy task. Bérubé et al. (2002a) and Stark (1991), among others, have found that an internal relative humidity of greater than 80 percent is necessary for alkali-silica gel to expand; therefore, the goal of the mitigation procedure chosen for the Bibb Graves Bridge is to get the relative humidity in the ASR-affected arches below this threshold. The topical application of silane was selected as the ASR mitigation procedure applied to the Bibb Graves Bridge because the use of silane has proven to effectively lower the relative humidity in concrete in previous studies. For a couple of these studies, silane was applied to laboratory cylinders

and highway barriers, and it lowered the relative humidities in the test specimens to below 80 percent (Bérubé et al. 2002a; 2002b).

8.1.2 Bibb Graves Bridge Overview

The Bibb Graves Bridge is a reinforced concrete bridge that was constructed in 1931, and it spans 700 feet across the Coosa River in Wetumpka, Alabama. The bridge consists of seven arched spans that support the road deck. Other than the span at each end of the bridge, the deck is suspended at midheight of the arches.

Both arches of span 5 have severe cracking and surface deposits on all sides of them. Petrographic examination by two independent laboratories concluded that ASR was the main cause of the severe concrete distress in span 5. It is unknown why only the arches in span 5 are severely distressed due to ASR.

8.1.3 ASR Mitigation Procedure

An ASR mitigation procedure targeted at lowering the internal relative humidity of the concrete to below 80 percent was developed for the Bibb Graves Bridge by the FHWA, ALDOT, and Auburn University. The mitigation procedure consisted of the following five steps:

1. Water-blast all concrete surfaces to clean concrete surfaces and remove loose impediments, efflorescence, alkali-silica gel, algae, etc.
2. Apply silane to all surfaces.
3. Seal all cracks with widths of 0.04 inches and wider with a UV-resistant, flexible sealant.

4. Apply an epoxy flood coat to the top arch surface to seal the narrow cracks on this surface.
5. Install instrumentation for monitoring.

The ASR mitigation was applied to spans 4 and 5 of the Bibb Graves Bridge during October and November of 2010. Both arches of span 5 and the southern arch of span 4 received the full mitigation procedure, but the northern arch of span 4 was left as a control and only received the instrumentation for monitoring. Both arches of span 4 have very limited cracking along with little to no signs of ASR.

8.1.4 Monitoring the Effectiveness of the Mitigation Procedure

There were three types of in-situ monitoring carried out on the Bibb Graves Bridge to evaluate the effectiveness of the ASR mitigation procedure. The first was crack mapping of span 5 and the southern arch of span 4. This was done prior to the application of the mitigation procedure and again 33 months after mitigation. The second type of monitoring was measuring the internal relative humidity in all four arches, at a total of 48 locations. And the last type of in-situ monitoring was taking DEMEC strain gauge readings on the four arches, at a total of 46 locations. The DEMEC readings were converted into changes in concrete strain over time. Both the relative humidity and the concrete strain measurements were taken monthly, weather permitting, for 34 months beginning after the application of the mitigation procedure. However, the FHWA installed ten of the now 46 concrete strain locations in 2005; therefore, data for these ten locations date back to this time.

8.2 Conclusions

The following conclusions can be made about the effectiveness of the silane-based ASR mitigation procedure after 34 months of monitoring:

1. Based on analysis of the relative humidity results, it has been determined that the silane-based ASR mitigation procedure has not yet been effective on span 5. There were no signs of decreasing relative humidity in the ASR-affected arches of span 5, and there were very little signs of possible reduction in the relative humidity in the top of the non-distressed arch compared to the control arch. Continued monitoring may reveal that silane can be effective when applied in the early stages of ASR before cracking has initiated or when applied as a preventative measure.
2. Analysis of the in-situ concrete strain data indicates that the ASR expansion in span 5 is continuing at the same pace as it was before mitigation. This was shown by the onset of new cracking and strong, linear trends with high expansion rates in a majority of the span. Some of the highest expansion rates in the two arches of span 5 range from 340 to 550 microstrains per year.

8.3 Recommendations

The following are recommended for the Bibb Graves Bridge based on the 34 months of data collection and analysis:

1. The reliable structural capacity of the bridge in its deteriorated state should be estimated. This will also help in selecting the next ASR mitigation procedure.

2. In-situ monitoring should be continued. The best way to predict the future behavior of the bridge, all things being equal, is to look at the past behavior.
3. Develop a new ASR mitigation procedure for the Bibb Graves Bridge as soon as possible. Chapter 7 discusses four different options that may be applicable to the severely distressed arches of span 5.
 - a. If the structural capacity of the bridge is judged to be adequate, a mitigation procedure that physically covers the arches in an attempt to lower the internal relative humidity is recommended. Proposed examples are shown and discussed in section 7.2.
 - b. If the structural capacity of the bridge is inadequate or will be inadequate with continued expansion for a few years, a mitigation procedure that confines the cross sections of the arches is recommended. The addition of confinement will suppress ASR expansion if designed properly, and it can add to the structural capacity of the arches. Proposed examples are discussed in section 7.3. If installed, a confinement system should be instrumented to monitor the confining stresses developed over time.
 - c. It is also recommended that cores be extracted for petrographic analysis in locations other than span 5 in the bridge that are showing signs of ASR. If ASR is found in several other portions of the bridge, the development and application of a surface treatment mitigation procedure for the entire bridge is recommended. Pictures of potential

ASR in locations other than span 5 and a proposed mitigation treatment with the use of surface sealers are presented in section 7.4.

References

- ALDOT. 2010. "Presentation on the Coring of the Bibb Graves Bridge."
Montgomery, Alabama: Alabama Department of Transportation.
- ASTM Standard C856. 2011. "Standard Practice for Petrographic Examination of Hardened Concrete." C856-11. West Conshohocken, Pennsylvania: ASTM International,
- Bérubé, M.A., D. Chouinard, M. Pigeon, F. Jean, R. Michel, and D. Vézina. 2002a. "Effectiveness of sealers in counteracting alkali–silica reaction in plain and air-entrained laboratory concretes exposed to wetting and drying, freezing and thawing, and salt water." *Canadian Journal of Civil Engineering*: 289-300.
- Bérubé, M.A., D. Chouinard, M. Pigeon, F. Jean, R. Michel, and D. Vézina. 2002b. "Effectiveness of sealers in counteracting alkali-silica reaction in highway median barriers exposed to wetting and drying, freezing and thawing, and deicing salt." *Canadian Journal of Civil Engineering (NRC)* : 329-337.
- BCA. 1988. *The Diagnosis of Alkali-Silica Reaction – Report of a working party*. Wexham Springs, Slough, United Kingdom: British Cement Association, SL3 6PL.
- Blackburn, P. 1997. "Wetumpka's Bridges." The River Region Online (Reprinted from Wetumpka Herald's Historic Elmore County Magazine, 1996-97). Accessed August 10, 2013.
http://www.theriverregiononline.com/pages/history/wetumpka_historic_bridges.htm

- Canmore. 2013. "Site Record for Montrose, New Bridge Montrose Bridge; River South Esk; Montrose Basin; Ferryden; Temporary BridgeDetails Details." Accessed October 31, 2013.
<http://canmore.rcahms.gov.uk/en/site/36270/details/montrose+new+bridge/>
- Courtier, R.H. 1990, "The Assessment of ASR-Affected Structures." *Cement & Concrete Composites* 12 (3): 191-210.
- CSA. 2000. *Guide to the Evaluation and Management of Concrete Structures Affected by Alkali-Aggregate Reaction*. Ontario, Canada: Canadian Standards Association (CSA).
- Engstrom, G.M. 1994. *Field Performance of High Molecular Weight Methacrylate Monomers and Silanes on a D-Cracked, Jointed Reinforced Concrete Pavement*. MN/RD-94/07, Maplewood, Minnesota: Minnesota Department of Transportation.
- Folliard, K.J., M.D.A. Thomas, J.H. Ideker, B. East, and B. Fournier. 2009. *Case Studies of Treating ASR-Affected Structures with Lithium Nitrate*. Transportation Research Board Annual Meeting 2009 Paper #09-2685.
- Fournier, B., M.A. Bérubé, M.D.A. Thomas, N. Smaoui, and K.J. Folliard. 2004. *Evaluation and Management of Concrete Structures Affected by Alkali-Silica Reaction - A Review*. MTL 2004-11 (OP), Ottawa, Canada: Natural Resources Canada.
- Fournier, B., M.A. Bérubé. 2000. "Alkali-Aggregate Reaction in Concrete: A Review of Basic Concepts and Engineering Implications." *Canadian Journal of Civil Engineering* 27 (2): 167-191.
- Fournier, B., M.A. Bérubé, K.J. Folliard, and M.D.A. Thomas. 2010. *Report on the Diagnosis, Prognosis, and Mitigation of Alkali-Silica Reaction (ASR) in Transportation Structures*. Final Report, Washington D.C.: Federal Highway Administration.

- Hobbs, D.W. 1988. *Alkali-silica reaction in concrete*. London, United Kingdom: Thomas Telford Ltd, p. 83.
- Holth, N. 2010. "Historic and Notable Bridges of the U.S." BridgeHunter.com. Accessed August 11, 2013. <http://bridgehunter.com/al/elmore/928/>
- Institution of Structural Engineers. 2010. "Structural effects of alkali-silica reaction. Technical guidance on the appraisal of existing structures." London, United Kingdom: Institution of Structural Engineers. Addendum (April).
- Le Roux, A., E. Massieu, and B. Godart. 1992. "Evolution Under Stress of a Concrete Affected by AAR – Application to the Feasibility of Strengthening a Bridge by Prestressing." Proceedings of *The Ninth International Conference on Alkali-Aggregate Reaction in Concrete*, London 2 (July 27-31): 599-606
- Mayes Instruments Limited. n.d. "User's Guide to the Mayes DEMEC Demountable Mechanical Strain Gauge." Berkshire, UK: Mayes Instruments Limited
- Pantazopoulou, S.J., and M.D.A. Thomas. 1999. "Modeling Stress-Strain Behavior of Concrete Damaged by Alkali-Aggregate Reaction (AAR)." *ACI Structural Journal* 96 (5): American Concrete Institute: 790-799.
- Rigden, S.R., J.M. Salam, and E. Burley. 1992. "Influence of Stress Intensity and Orientation upon Mechanical Properties of ASR-Affected Concrete." Proceedings of *The Ninth International Conference on Alkali-Aggregate Reaction in Concrete*, London 2 (July 27-31): 865-876.
- Schindler, A.K., M.L. Hughes, R.W. Barnes, and B.E. Byard. 2010. *Evaluation of cracking of the US 331 bridge deck*. FHWA/ALDOT 930-645. Alabama Department of Transportation. 87p.
- Selley, David B. 2010. "Making Low-VOC Silicon-based Water Repellents." *Coatings Tech*. Midland, Michigan: Dow Corning Corporation: 26-35.

- Stark, D. 1991. "The Moisture Condition of Field Concrete Exhibiting Alkali-Silica Reactivity." ACI SP-126-52: American Concrete Institute: 973-988.
- Taylor, V.L. 1930. "A New Type of Highway Bridge." *The Auburn Engineer*, November: 34-35.
- The City of Wetumpka Alabama. 2013. "Photo Gallery." Accessed August 11, 2013. <http://www.cityofwetumpka.com/Default.asp?ID=527>
- The Transtec Group. 2010. *Evaluation of Bibb Graves Bridge in Wetumpka, Alabama*. Austin, Texas: The Transtec Group.
- Thomas, M.D.A. 2010. "The Damage Rating Index: A Useful Tool for Determining Damage Caused by ASR in Concrete." Reactive Solutions – An FHWA Technical Update on Alkali-Silica Reactivity (Winter 2010).
- Vaisala. 1998. *HM44 Set For Measuring Humidity in Concrete Operating Manual*.
- Warnock, Robert L. 2012. *Mitigation of Alkali-Silica Reaction in the Bibb Graves Bridge*. Masters Thesis, Auburn, Alabama: Auburn University.
- Wikimedia Commons. 2006. "Map of Alabama NA.png." Wikimedia.org. Accessed October 13, 2013. http://commons.wikimedia.org/wiki/File:Map_of_Alabama_NA.png
- WJE. 2010. *Bibb Graves Bridge Petrographic Studies of Concrete Cores*. Northbrook, Illinois: Wiss, Janney, Elstner Associates, Inc.
- Wood, J.G.M. and Angus, E.C. 1995. "Montrose Bridge: Inspection, Assessment and Remedial Work to a 65 Year Old Bridge with AAR." Proceedings of *Sixth International Conference on Structural Faults and Repair*. London, United Kingdom (July 3rd): 103-108.

Wood, J.G.M. 2008. "Improving Guidance for Engineering Assessment and Management of Structures with AAR." Proceedings of *The 13th International Conference on Alkali-Aggregate Reaction in Concrete*. Trondheim, Norway (June 16-20).

Yang, D., B.D. Merrill, and T.E. Bradberry. 2010. "Texas' Use of CFRP to Repair Concrete Bridges." In *Recent Advances in Maintenance and Repair of Concrete Bridges*. Chicago: ACI SP 277: American Concrete Institute: 39-57.

Appendix A

Coring Procedure and Samples

All of the figures and tables in this appendix are from ALDOT (2010); which is a presentation for the coring of Bibb Graves Bridge. The coring process, which involved locating reinforcement, drilling, extracting, labeling, wrapping, packing, and shipping to Illinois and Canada, is shown through pictures in Figures A.1, A.2-A.4, A.5 and A.6, A.7, A.8, A.9, and A.10, respectively.



Figure A. 1. Use of ground penetrating radar to locate reinforcement



Figure A. 2. Close up of drilling set up



Figure A. 3. Drilling core sample



Figure A. 4. Close up of drilling process



Figure A. 5. Core holes left after drilling



Figure A. 6. Extraction of core samples



Figure A. 7. Labeling of core samples



Figure A. 8. Wrapping of core samples



Figure A. 9. Packing of core sample for (A) W.J.E. in Illinois and (B) Laval University in Canada

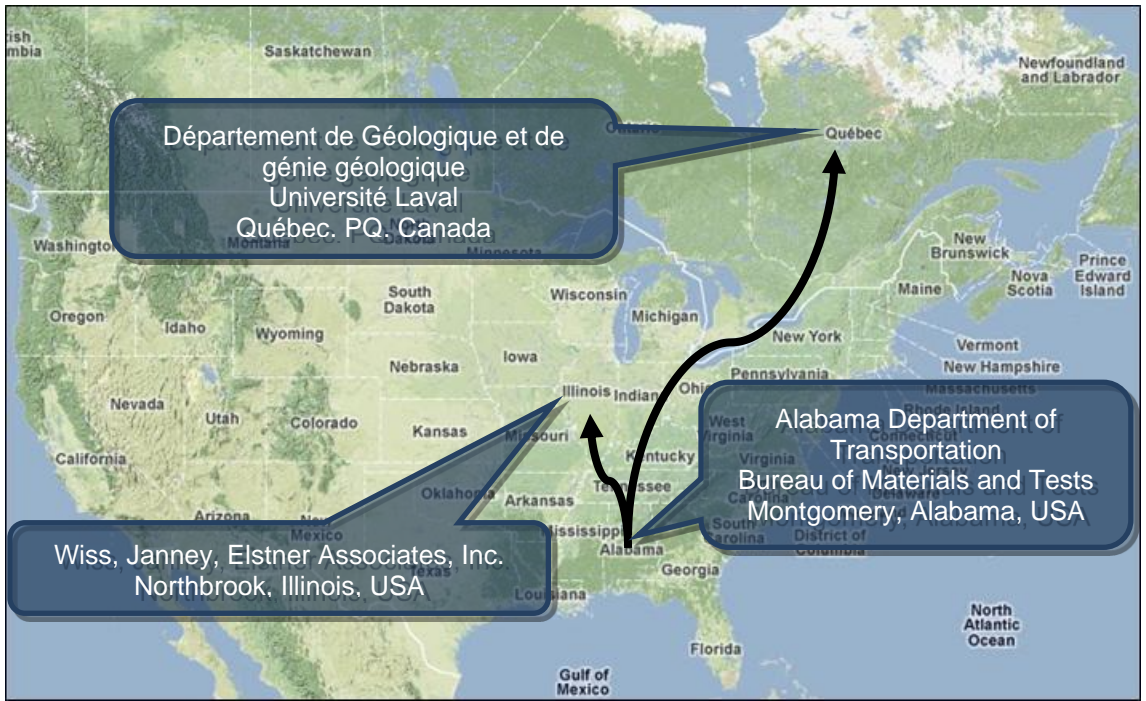


Figure A. 10. Map of core shipping

Figure A. 11 is a schematic of the core extraction locations on the Bibb Graves Bridge. Each of the four locations show here had two three-inch diameter cores taken from them, one for The Transtec Group and one for WJE. Figures A. 12 through A. 19 show all 8 of the cores and the extraction locations as identified in Figure A. 11. The details about each of the core samples are presented in Tables A. 1 through A. 8, located below each core's picture.

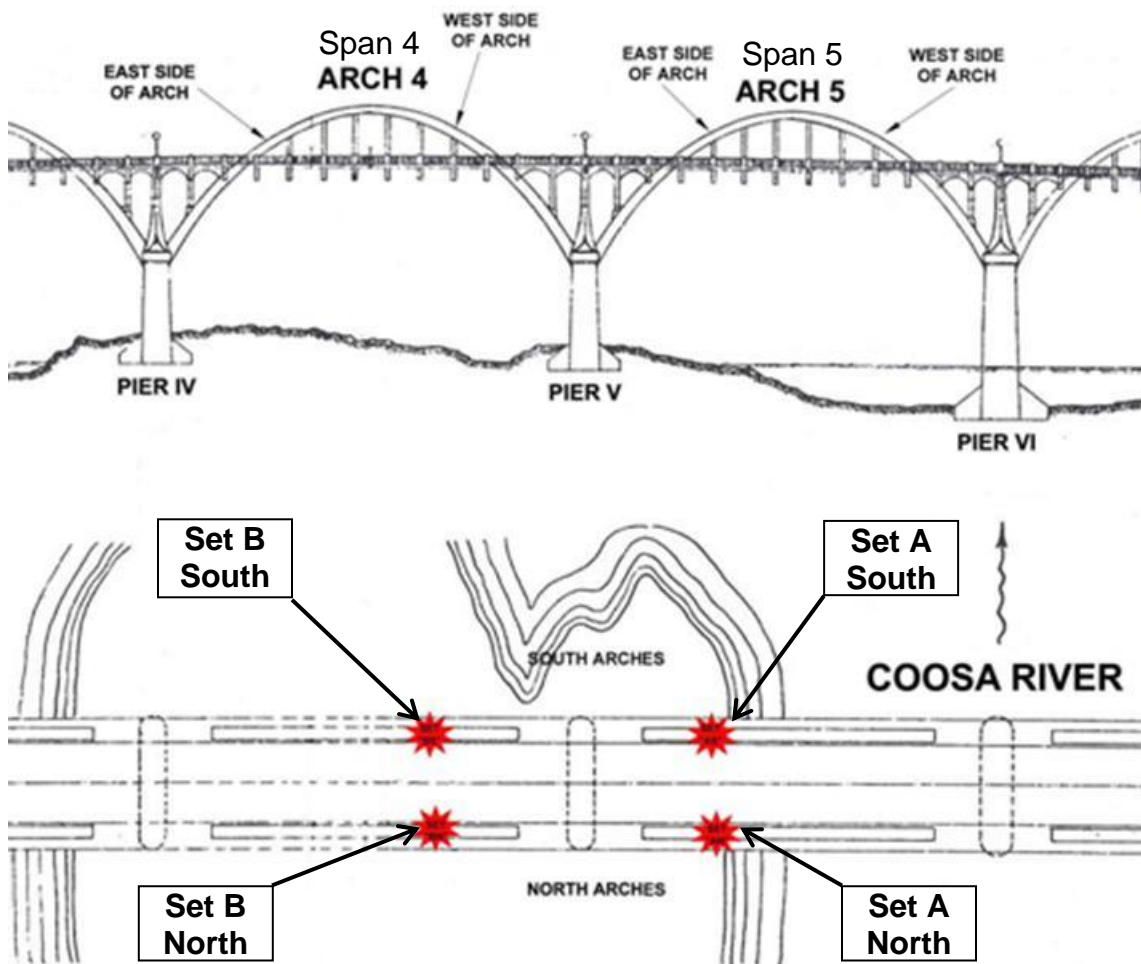


Figure A. 11. Core extraction layout



Figure A. 12. Core 1A – South

Table A. 1. Information for 1A – South

Core Details	Core Information
ID	1A – South
Location	South arch - Span 5. East side of arch. Approximately 17' 11" from top of pedestal.
Remarks	Full core extracted in two sections on 01/14/2010: 4. Section 1: Approximately 4 ¼" 5. Section 2: Approximately 4 ¾" Red discoloration, if any, from labeling marker.



Figure A. 13. Core 2A – South

Table A. 2. Information for Core 2A – South

Core Details	Core Information
ID	2A - South
Location	South arch - Span 5. East side of arch. Approximately 17' 11" from top of pedestal.
Remarks	Full core extracted in three sections on 01/14/2010: <ul style="list-style-type: none"> • Section 1: Approximately 3" • Section 2: Approximately 6 ½" • Section 3: Approximately 1" Red discoloration, if any, from labeling marker.



Figure A. 14. Core 1B – South

Table A. 3. Information for Core 1B – South

Core Details	Core Information
ID	1B - South
Location	South arch - span 4. West side of arch. Approximately 3' 6" from top of pedestal.
Remarks	Full core extracted in one section on 01/14/2010: <ul style="list-style-type: none"> • Section 1: Approximately 10 ½" Red discoloration, if any, from labeling marker.



Figure A. 15. Core 2B – South

Table A. 4. Information for Core 2B – South

Core Details	Core Information
ID	2B - South
Location	South arch - span 4. West side of arch. Approximately 3' 6" from top of pedestal.
Remarks	Full core extracted in one section on 01/14/2010: <ul style="list-style-type: none"> • Section 1: Approximately 10" Red discoloration, if any, from labeling marker.



Figure A. 16. Core 1A – North

Table A. 5. Information for 1A – North

Core Details	Core Information
ID	1A – North
Location	North arch - Span 5. East side of arch. Approximately 16' 3" from top of pedestal.
Remarks	Full core extracted in two sections on 01/14/2010: <ul style="list-style-type: none"> • Section 1: Approximately 5 ¼" • Section 2: Approximately 5 ½" Red discoloration, if any, from labeling marker.



Figure A. 17. Core 2A – North

Table A. 6. Information for 2A – North

Core Details	Core Information
ID	2A – North
Location	North arch - Span 5. East side of arch. Approximately 16' 3" from top of pedestal.
Remarks	Full core extracted in two sections on 01/14/2010: <ul style="list-style-type: none"> • Section 1: Approximately 7" • Section 2: Approximately 3 ¼" Red discoloration, if any, from labeling marker.



Figure A. 18. Core 1B – North

Table A. 7. Information for Core 1B – North

Core Details	Core Information
ID	1B – North
Location	North arch - Span 4. West side of arch. Approximately 3' 10" from top of pedestal.
Remarks	Full core extracted in one section on 01/14/2010: <ul style="list-style-type: none"> • Section 1: Approximately 11 ¼" Red discoloration, if any, from labeling marker.



Figure A. 19. Core 2B – North

Table A. 8. Information for Core 2B – North

Core Details	Core Information
ID	2B – North
Location	North arch - Span 4. West side of arch. Approximately 3' 10" from top of pedestal.
Remarks	Full core extracted in one section on 01/14/2010: <ul style="list-style-type: none"> • Section 1: Approximately 10" Red discoloration, if any, from labeling marker.

Appendix B

Petrographic Analysis Report by The Transtec Group

(Extracted from The Transtec Group 2010)

1 Introduction

This report presents the findings of the petrographic examination of concrete cores extracted from two arches of the Bibb Graves Bridge (AL Route 111 over Coosa River) in Wetumpka, Alabama. The evaluation mainly consisted of the Damage Rating Index (DRI), a method that provides a semi-quantitative assessment of the damage in concrete based on a count of petrographic features of deterioration generally associated with alkali-silica reaction (ASR).

2 Field Work - Extraction of Cores

Coring was conducted by ALDOT in January 2010. Cores were extracted from the arches no. 4 and 5 of the bridge, as indicated in Table 1 and illustrated in the Appendix A.

Table 1. Cores provided for petrographic examination (ALDOT 2010)

Core number	Location	Condition
2A-South	South arch # 5; East side of arch	Core in 3 sections
2A-North	North arch # 5; East side of arch	Core in 2 sections
2B-South	South arch # 4; West side of arch	Core in 1 section
2B-North	North arch # 4; West side of arch	Core in 1 section

3 Laboratory Testing of Cores

The concrete cores were sent to Dr. Benoit Fournier at Laval University, Québec, Canada in February 2010. The four cores were first cut in two axially and polished, then examined under the stereomicroscope to determine the Damage Rating Index (DRI).

3.1 Damage Rating Index (DRI)

Grattan-Bellew (1992) and Dunbar and Grattan-Bellew (1995) described a method to evaluate the condition of concrete by counting the number of typical petrographic features of ASR on polished concrete sections (18x magnification) (Table 2). A grid is drawn on the polished concrete section, which includes a minimum of 150 grid squares, 1 cm by 1 cm in size. The *Damage Rating Index* represents the normalized value (to 100 cm²) of the presence of these features after the count of their abundance over the surface examined has been multiplied by weighing factors representing their relative importance in the overall deterioration process (Table 2).

Table 2. Petrographic Features and Weighing Factors for the DRI (Grattan-Bellew and Mitchell 2006)

Petrographic feature	Abbreviation	Weighing factor
Coarse aggregate with cracks	CrCA	x 0.75
Open crack in coarse aggregate	OCrCA	x 4.0
Coarse aggregate with cracks and reaction products	Cr + RPCA	x 2.0
Coarse aggregate debonded	CAD	x 3.0
Reaction rims around aggregate	RR	x 0.5
Cement paste with cracks	CrCP	x 2.0
Cement paste with cracks and reaction products	Cr+RPCP	x 4.0
Air voids lined or filled with reaction products	RPAV	x 0.50

4 Results of the Petrographic Examination

The four polished sections examined as part of this investigation are illustrated in Figure 1, while the results of the DRI are summarized in Figure 2. Table 3 gives a summary of the petrographic observations (in terms of the typical crack width observed in the cement paste of the cores) and a rating of the extent of ASR in the concrete. The detailed results of DRI, including micrographs of the petrographic features in the cores examined, are given in the Appendix B.

There is currently no rating system for the DRI values that correspond to concrete affected to a low, moderate or severe degree by ASR. However, our experience is such that values below 200-250 are indicative of a low degree of reaction / deterioration, DRIs in excess of about 500-600 represent a high to very high (DRI > 1000) degree of ASR. It is important to mention, however, that since the DRI is not a standardized method, values can vary significantly from one petrographer to another.

Table 3. Summary of the petrographic observations on the cores from Alabama (Gibb Graves Bridge)

Sample	DRI	Typical crack width in the concrete (mm)	Extent of ASR	Reactive aggregates in the polished sections
2A-South	1430	Extensive cracking in the cement paste and the aggregate particles; cracks were found to reach 1mm in width (mainly 0.1 to 0.3mm)	Very high degree of ASR	Quartzite and chert
2A-North	1081	Extensive cracking in the cement paste and the aggregate particles; cracks were found to reach 1mm (mainly 0.1 to 0.2mm; several very fine cracks of < 0.05mm in size are filled with compacted ettringite)	High degree of ASR	Quartzite and chert
2B-South	141	No significant cracking in the cement paste (i.e. at the 16x magnification used for the DRI)	No significant ASR	Same type of aggregates as in 2A series but no signs of ASR
2B-North	205	No significant cracking in the cement paste (i.e. at the 16x magnification used for the DRI)	No significant ASR	

4.1 Core 2A-South

Globally, the polished concrete section 2A-South shows several large cracks (up to 1mm in size) that run through the cement paste and the coarse aggregate particles (Figures 1 and B1). The core had

actually to be glued with epoxy to allow the cutting and polishing processes to take place (blue color on the polished section of Figure 1).

The DRI value of **1430** is the highest for the set of cores obtained from the Bibb Graves Bridge (Figures 2 and B1). It is indicative of a very high degree of damage in the concrete. The micrographs in Figure B2 show extensive cracking in the coarse aggregate particles and in the cement paste. As indicated in Figure 2, the highest contributor to the DRI for this core is *Cracks in the cement paste with reaction products* (67% - 964/1430; Figure B2), followed by *Open cracks within the aggregate particles* (12% - 173/1430; e.g. Figure B2-E) and *Cracks with reaction products in the coarse aggregate particles* (7% - 100/1430; Figure B2-B). The coarse aggregates mainly consist of quartzite (Qtz) and chert (Ch) (sometimes partially leached/weathered) particles. Several quartzite aggregate particles show extensive internal cracking and/or grain joints, thus giving a sort of “mosaic” macrotexture (e.g. Figures B2-B and F). Dark reaction rims are observed around some of the above coarse aggregate particles (Figures B2-C and F). The fine aggregate mainly consist of angular to sub-angular quartz grains, with possible fragments of quartzite; it probably has a fairly low modulus of fineness.

Cracks in the cement paste are often filled with whitish/powdery, glassy and/or clear (with a “waxy” luster) secondary reaction products. The examination of concrete fragments under the stereomicroscope (Figure B3) and the scanning electron microscope (SEM) (Figure B4) indicates that the reaction products consist of ettringite (present as clear and “waxy” secondary products under the stereomicroscope as well as in whitish powdery deposits) (Figures B3, B4-B and C; B4-I to K) and alkali-silica gel (Figure B3) that closely co-exist in the deteriorated concrete. Fractured surfaces of the concrete cores reveal a typical arrangement of ASR products (Figures B3-A to C) (i.e. cracks within the aggregate particles and that extend into the cement paste are often filled with alkali-silica gel that gives the typical “mud-crack” texture on such fractured surfaces (Figures B3-G to J)) along with large deposits of ettringite (Figures B3-D to F). Concrete is not air entrained but some voids are filled with ettringite with a clear but “waxy” luster (*ett* on Figures B2-A and D).

4.2 Core 2A-North

Similar to the Core 2A-South, the polished concrete section 2A-North shows several large cracks (up to 1mm in size) that run through the cement paste and the coarse aggregate particles (Figures 1 and B5). The core had also to be glued with epoxy to allow the cutting and polishing processes to take place.

The DRI value of **1081** is the second highest for the set of cores obtained from the Bibb Graves Bridge (Figures 2 and B5). It is indicative of a very high degree of damage in the concrete. The micrographs in Figure B6 show extensive cracking in the coarse aggregate particles and in the cement paste. As indicated in Figures 2 and B5, the highest contributor to the DRI for this core is *Cracks in the cement paste with reaction products* (61% - 664/1081; Figure B6), followed by *Open cracks within the aggregate particles* (11% - 114/1081; e.g. Figure B6-D) and *Cracks in the cement paste (without reaction products)* (10% - 112/1081; Figure B6). The coarse aggregate particles are similar to that in the Core 2A-South and mainly consist of quartzite (Qtz) (possibly some quartzitic sandstone) and chert (Ch) (sometimes partially leached/weathered) particles (Figures B6-A and D). Several quartzite aggregate particles show extensive internal cracking and/or grain joints, thus giving a sort of “mosaic” macrotexture (e.g. Figure B6-F). Dark reaction rims are observed around some of the above coarse aggregate particles (Figures B6-A and B). The fine aggregate mainly consist of angular to sub-angular quartz grains, with possible fragments of quartzite; it probably has a fairly low modulus of fineness.

Similar to Core 2A-South, cracks in the cement paste are often filled with whitish/powdery, glassy and/or clear (with a “waxy” luster) secondary reaction products; some of those cracks are very fine (~0.02-0.03mm). Examination of concrete fragments under the stereomicroscope (Figure B7) indicate that the reaction products consist of ettringite (present as clear and “waxy” secondary products under the stereomicroscope as well as in whitish powdery deposits) (Figure B7-D) and alkali-silica gel (Figures B7-A to C) that co-exist in the deteriorated concrete. Concrete is not air entrained but some voids are filled with ettringite (*ett* in Figures B6-A, B and D).

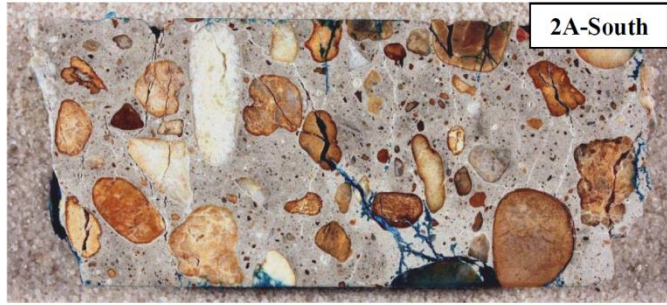


Figure 1. Polished concrete sections from the Gibb Graves Bridge, Wetumpka, Alabama.

Sample	CrCA	OCrCA	Cr+RPCA	CrCP	Cr+RPCP	CAD	RR	RPAV	DRI
2B-North	155	31	1	7	0	0	11	0	205
2B-South	103	31	0	0	0	2	5	1	141
2A-North	78	114	61	112	664	8	14	31	1081
2A-South	96	173	100	29	964	20	10	39	1430

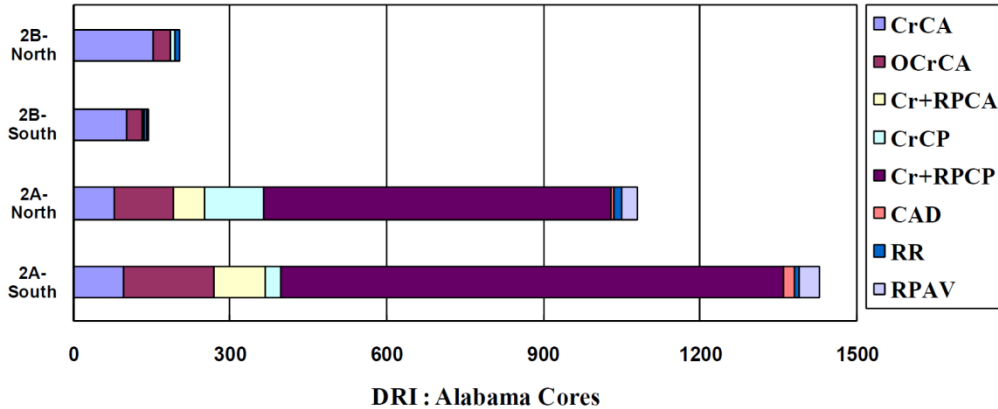


Figure 2. Results of the Damage Rating Index (DRI) for the Alabama cores

4.3 Core 2B-South

The polished concrete section 2B-South shows neither significant cracking nor deterioration (Figures 1 and B8). The DRI value of **141** is the lowest for the set of cores obtained from the Bibb Graves Bridge (Figures 2 and B8). It is indicative of a very low degree of damage in the concrete. As indicated in Figure 2, the highest contributor to the DRI for this core is *Cracks in the aggregate particles (without reaction products)* (73% - 103/141; Figure B9), followed by *Open cracks within the aggregate particles* (22% - 31/141). The coarse aggregate is similar to that of the set of 2A cores and mainly consist of quartzite (Qtz) (also possibly quartzitic sandstone) and chert (Ch) (sometimes partially leached/weathered) particles (Figure B9-D). Several quartzite aggregate particles show extensive internal cracking and/or grain joints, thus giving a sort of “mosaic” macrotecture (e.g. Figures B9-B and C). Dark reaction rims were observed around only a few of the above coarse aggregate particles (~4% of the DRI value). The fine aggregate mainly consist of angular to sub-angular quartz grains, with possible fragments of quartzite; the sand is however coarser than in the cores of the 2A series. No significant cracking, at least at the magnification used for the DRI (16X), was observed in the cement paste. Concrete is not air entrained and the few voids observed are generally empty (no secondary/reaction products).

4.3 Core 2B-North

Similar Core 2B-South, the polished concrete section 2B-North shows neither significant cracking nor deterioration (Figures 1 and B10). The DRI value of **205** is the second lowest for the set of cores obtained from the Bibb Graves Bridge (Figures 2 and B10). It is indicative of a very-low to low degree of damage in the concrete. As indicated in Figure 2, the highest contributor to the DRI for this core is *Cracks in the aggregate particles (without reaction products)* (76% - 155/205; Figure B11), followed by *Open cracks within the aggregate particles* (15% - 31/205). The coarse aggregate is similar to that

of the set of 2A cores and mainly consist of quartzite (Qtz) (also possibly quartzitic sandstone) and chert (Ch) particles (Figure B11). Several quartzite aggregate particles show extensive internal cracking and/or grain joints (e.g. Figures B11-B and E). Dark reaction rims were observed around a few of the above coarse aggregate particles (~5% of the DRI value). The fine aggregate mainly consist of angular to sub-angular quartz grains, with possible fragments of quartzite; the sand is coarser than in the cores of the 2A series. No significant cracking, at least at the magnification used for the DRI (16X) was observed in the cement paste. Concrete is not air entrained but the few voids observed are generally empty (no secondary products).

5 Conclusion - Summary of Findings

Two sets of cores were obtained from the Bibb Graves Bridge (AL Route 111 over Coosa River), Wetumpka, and Alabama. Cores extracted from the arch # 4 (2B-South and 2B-North) are in very good condition and the concrete shows no significant signs of deterioration, as indicated by the low DRI values of 141 and 205. On the other hand, cores extracted from the arch # 5 (2A-South and 2A-North) show several large cracks (up to 1mm in size) that run through the cement paste and the coarse aggregate particles. The DRI values of 1430 and 1081 are indicative of a very high degree of damage in the concrete.

For all concrete core examined (2A and 2B series), the coarse aggregate particles mainly consist of a variety of whitish to brownish quartzite (possibly some quartzitic sandstone) particles, as well as chert particles. The sand is mainly composed of angular to sub-angular quartz and seems to be finer in the set of 2A cores (deteriorated concrete) than for the cores of the 2B series (concrete in good condition).

Concrete cores 2A-South and 2A-North show extensive cracking in the coarse aggregate particles and in the cement paste. Dark reaction rims are observed around several chert and quartzite coarse aggregate particles. Cracks in the cement paste are often filled with whitish/powdery, glassy and/or clear (with a “waxy” luster) secondary reaction products. Further examination of concrete fragments under the stereomicroscope and the SEM confirm the presence of large amounts of ettringite and alkali-silica gel. Thus, the highest contributor to the DRI for those cores correspond to *Cracks in the cement paste with reaction products*, followed by *Open cracks within the aggregate particles* and *Cracks in the aggregate particles with reaction products*.

6 Recommendations

It is first recommended that a detailed structural analysis is performed on the arch affected by ASR. We understand that such an analysis was conducted recently, but that the analysis was based on the assumption that the concrete was undamaged by ASR. The authors of this report are not qualified to comment on the effect of the ASR damage on the structural integrity of the arch.

With regards to suppressing future expansion it is our recommendation that the damaged portions of the arch be treated with a suitable hydrophobic sealer such as a silane. Before application of the silane it is recommend that the concrete surface be cleaned by sand blasting and that the larger cracks be filled with a suitable flexible sealant.

7 References

- Alabama Department of Transportation. 2010. Powerpoint document illustrating the coring and sample preparation processes for the project.
- Dunbar, P.A. and Grattan-Bellew, P.E. 1995. Results of damage rating evaluation of condition of concrete from a number of structures affected by AAR. *In Proceedings of CANMET/ACI International Workshop on AAR in Concrete*, Dartmouth, Nova Scotia, CANMET, Department of Natural Resources Canada, pp. 257-265.
- Grattan-Bellew, P.E. 1992. Comparison of laboratory and field evaluation of alkali-silica reaction in large dams. *In Proceedings of the First International Conference on Concrete Alkali-Aggregate Reactions in Hydroelectric Plants and Dams*, September-October 1992, Fredericton, NB, Canada, 23p.
- Grattan-Bellew, P.E. and Mitchell, L.D. 2006. Quantitative petrographic analysis of concrete – the damage rating index (DRI) method, a review. *Proceedings of Marc-André Bérubé Symposium on Alkali-Aggregate Reaction (AAR) in Concrete*, Montréal (Canada), May 2006, edited by B. Fournier, CANMET-MTL, 45-70.

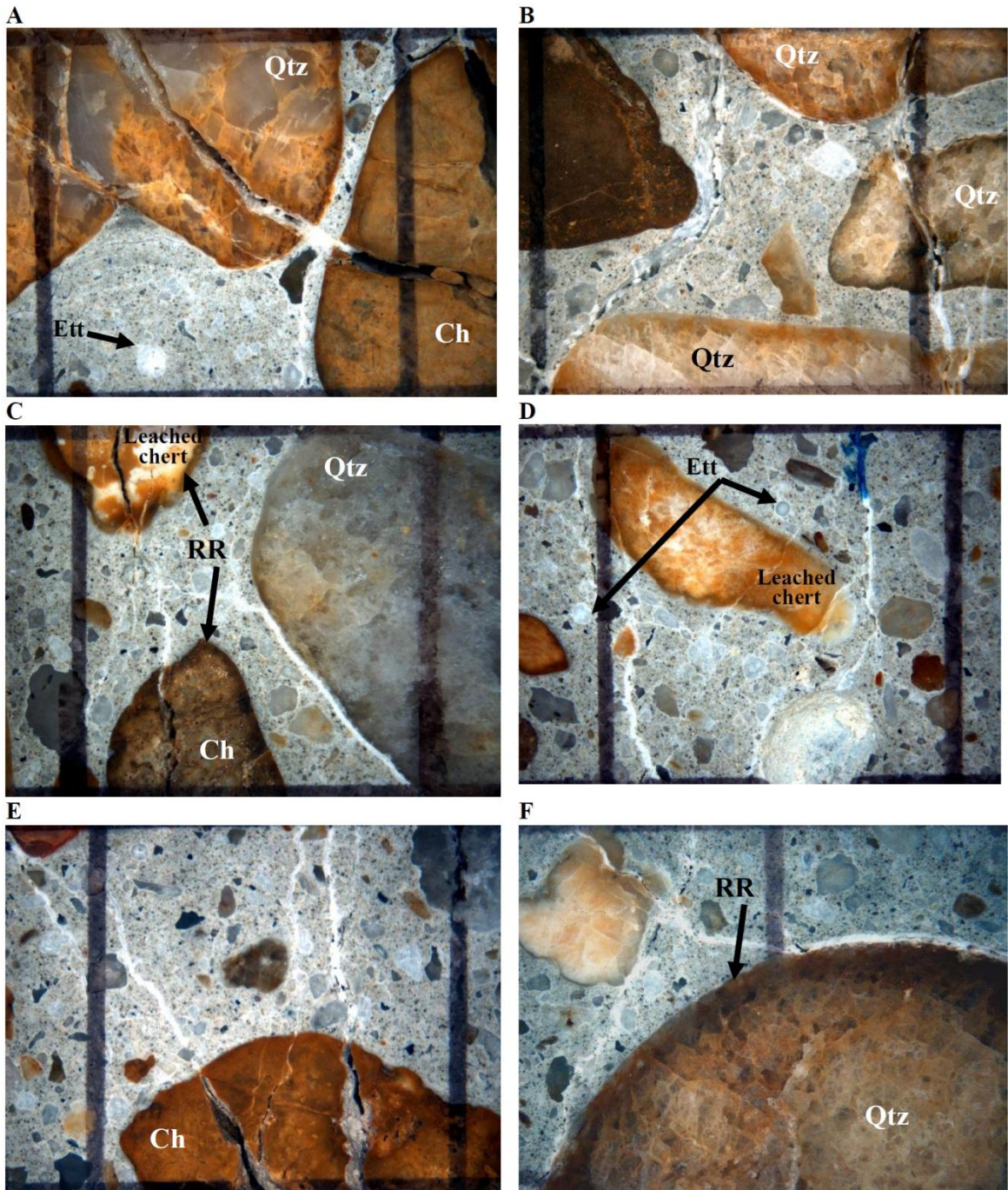
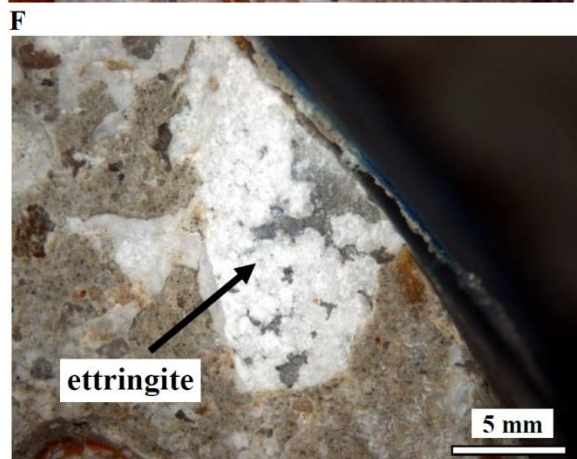
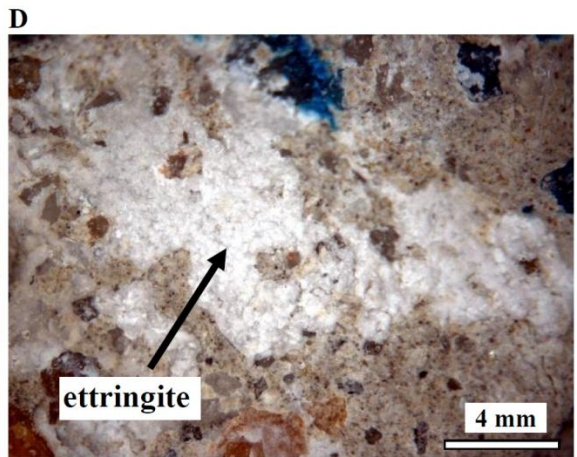
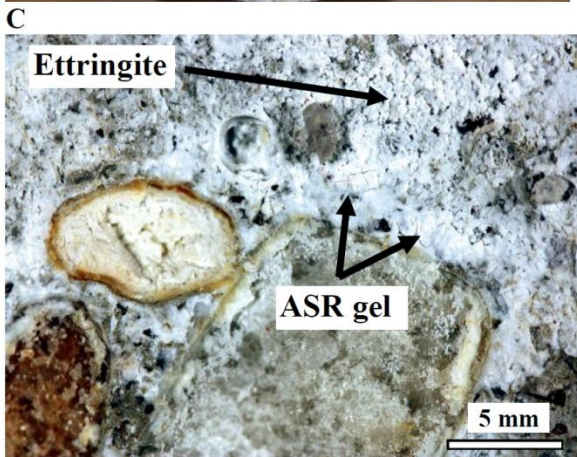


Figure B2: Micrographs of the polished core section 2A-South (distance between vertical lines = 1 cm)
 The micrographs show extensive cracking in the coarse aggregate particles and in the cement paste. The coarse aggregates mainly consist of chert (Ch) (sometimes partially leached/weathered) and quartzite particles (Qtz). Dark reaction rims (RR) are observed around some coarse aggregate particles. Concrete is not air entrained but some air voids are filled with ettringite (ett) (e.g. D). Cracks in the cement paste are often filled by ettringite (whitish and powdery deposits; also clear and waxy in luster) and alkali-silica reaction products, as illustrated in more details in Figure B3.



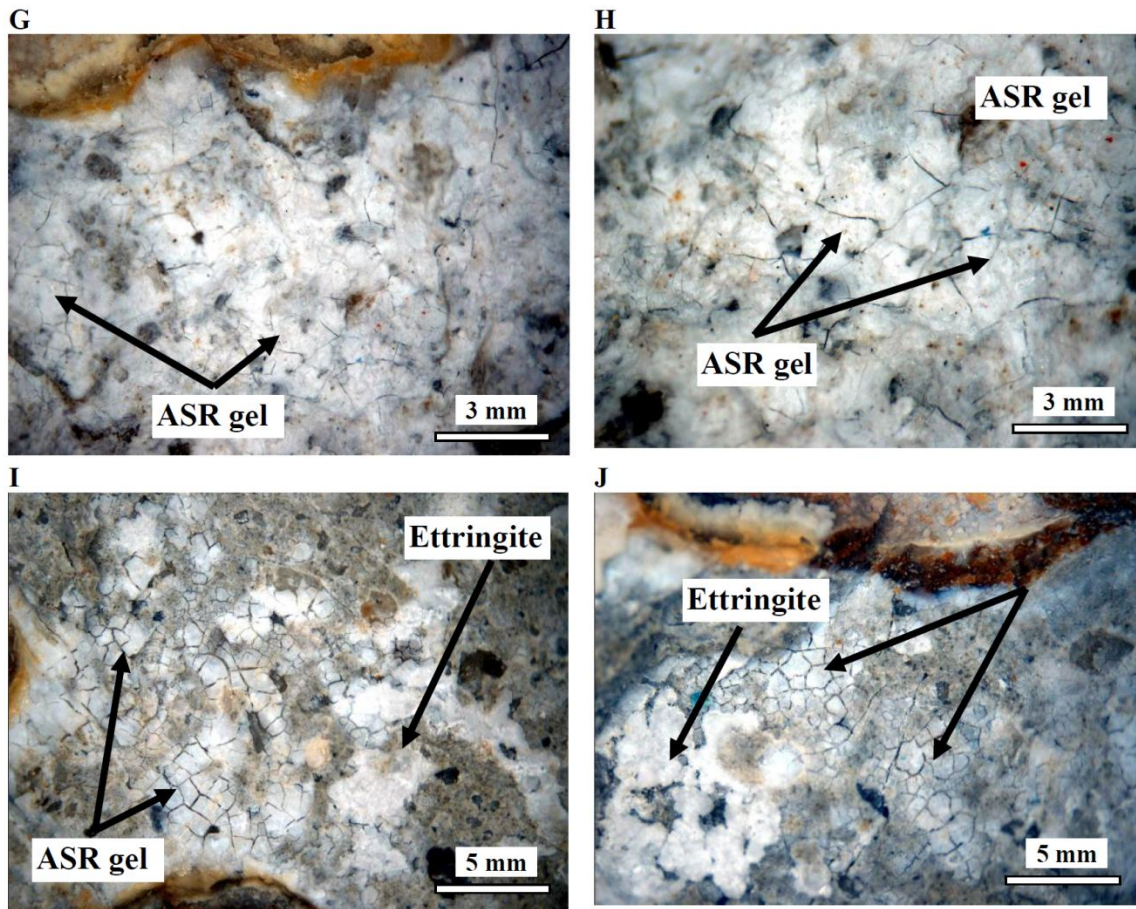


Figure B3: Micrographs of broken surfaces of the core 2A-South, as examined under the stereomicroscope. Figures B3-A and B3-B. Concrete surfaces broken along major cracks in the cement paste (core diameter = 3 inches (75mm)). Figure B3-C. The core broke along large cracks in the cement paste, thus exposing surfaces, both along cracks in the aggregates and the cement paste, largely covered by whitish secondary reaction products. Such products consist of ettringite and ASR gel (18x magnification). Figure B3-D. Whitish (powdery) reaction products (ettringite) covering large areas of the cement paste (20x magnification). Figure B3-E: Magnification (30x) of the reaction products illustrated in B3-D showing the needle-type microtexture of ettringite. Figure B3-F. Deposit of ettringite covering an aggregate particle. The deposit was found at the interface between an aggregate particle and the cement paste (as in Figure B2-C) and caused debonding of the aggregate particle when the concrete was broken for petrographic examination (20x magnification). Figures B3-G and B3-H. Deposits of ASR gel (showing typical “mud-crack” microtexture) covering large areas of the cracked cement paste (25x magnification). Figures B3-I and B3-J. Deposits of ASR gel and ettringite co-existing in the deteriorated concrete sample (18x magnification).

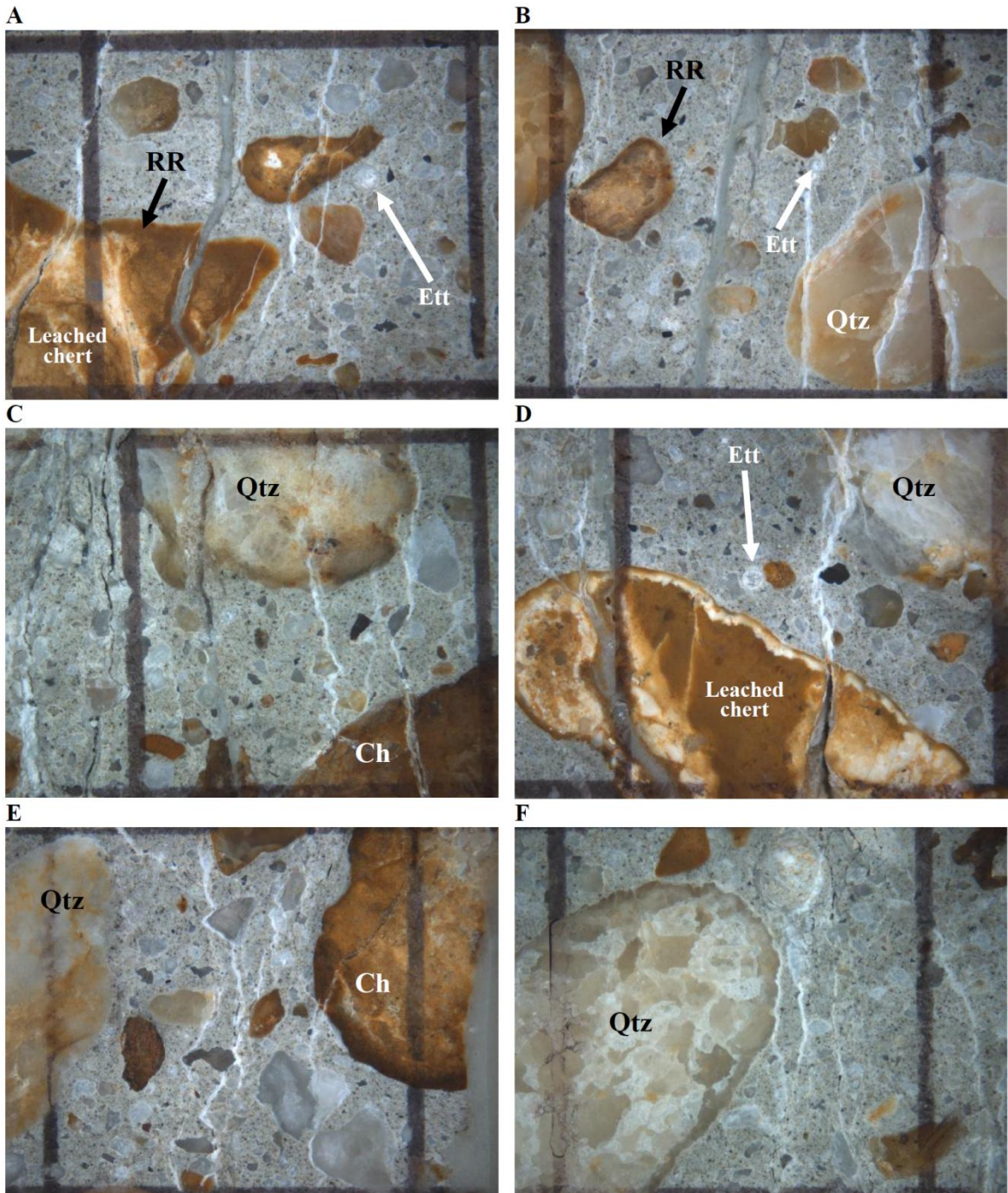


Figure B6: Micrographs of the polished core section 2A-North (distance between vertical lines = 1 cm). The micrographs show extensive cracking in the coarse aggregate particles and in the cement paste. The coarse aggregates mainly consist of chert (Ch)(sometimes partially leached/weathered) and quartzite particles (Qtz). Dark rims (RR) are observed around some coarse aggregate particles. Concrete is not air entrained but some air voids are filled with ettringite (ett) (e.g. B6-A, B6-B and B6-D). Cracks in the cement paste are often filled by ettringite (whitish and powdery deposits; also clear and waxy in luster) and alkali-silica reaction products, as illustrated in more details in Figure B7.

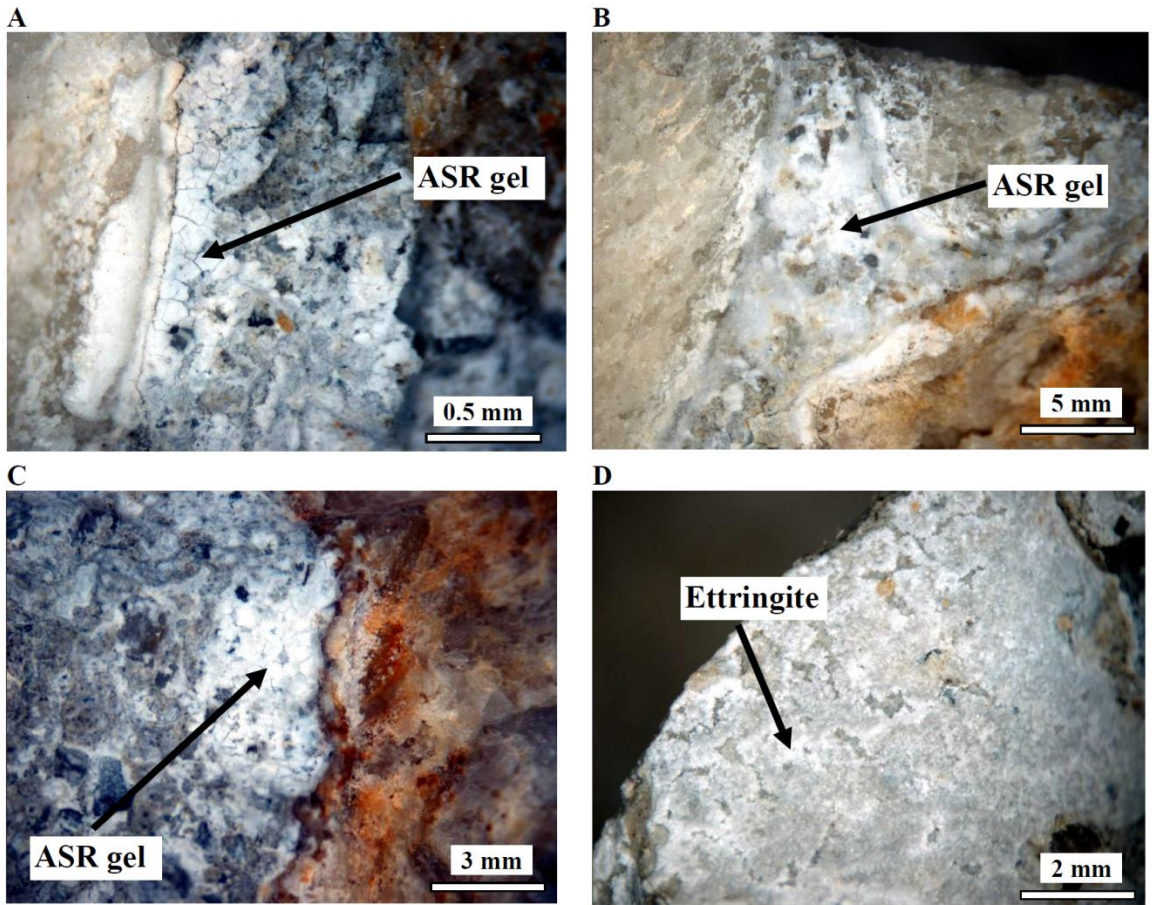


Figure B7: Micrographs of broken surfaces of the core 2A-North, as examined under the stereomicroscope. Figure B7-A to B7-C. Deposits of ASR gel (showing typical “mud-crack” microtexture) covering large areas of the cracked cement paste between aggregate particles. Figure B7-D. Deposit of ettringite in the mold of a debonded aggregate particle. The deposit was found at the interface between the aggregate particle and the cement paste (as in Figure B2-C) and caused debonding of the aggregate particle when the concrete was broken for petrographic examination.

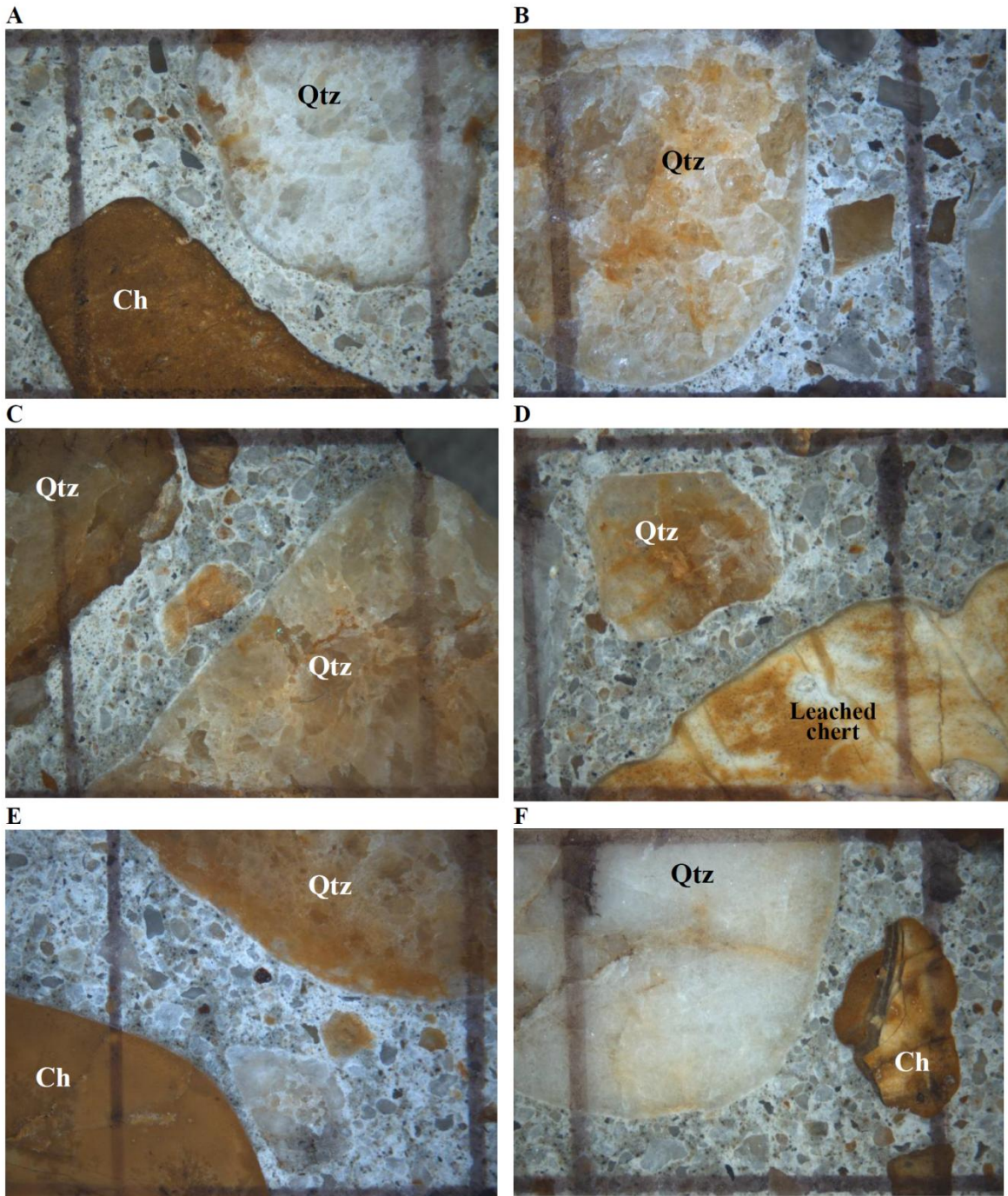


Figure B9: Micrographs of the polished core section 2B-South (distance between vertical lines = 1 cm). The micrographs show coarse aggregate particles that mainly consist of chert (Ch)(sometimes partially leached/weathered) and quartzite particles (Qtz). Very limited cracking is noticed in the cement paste.

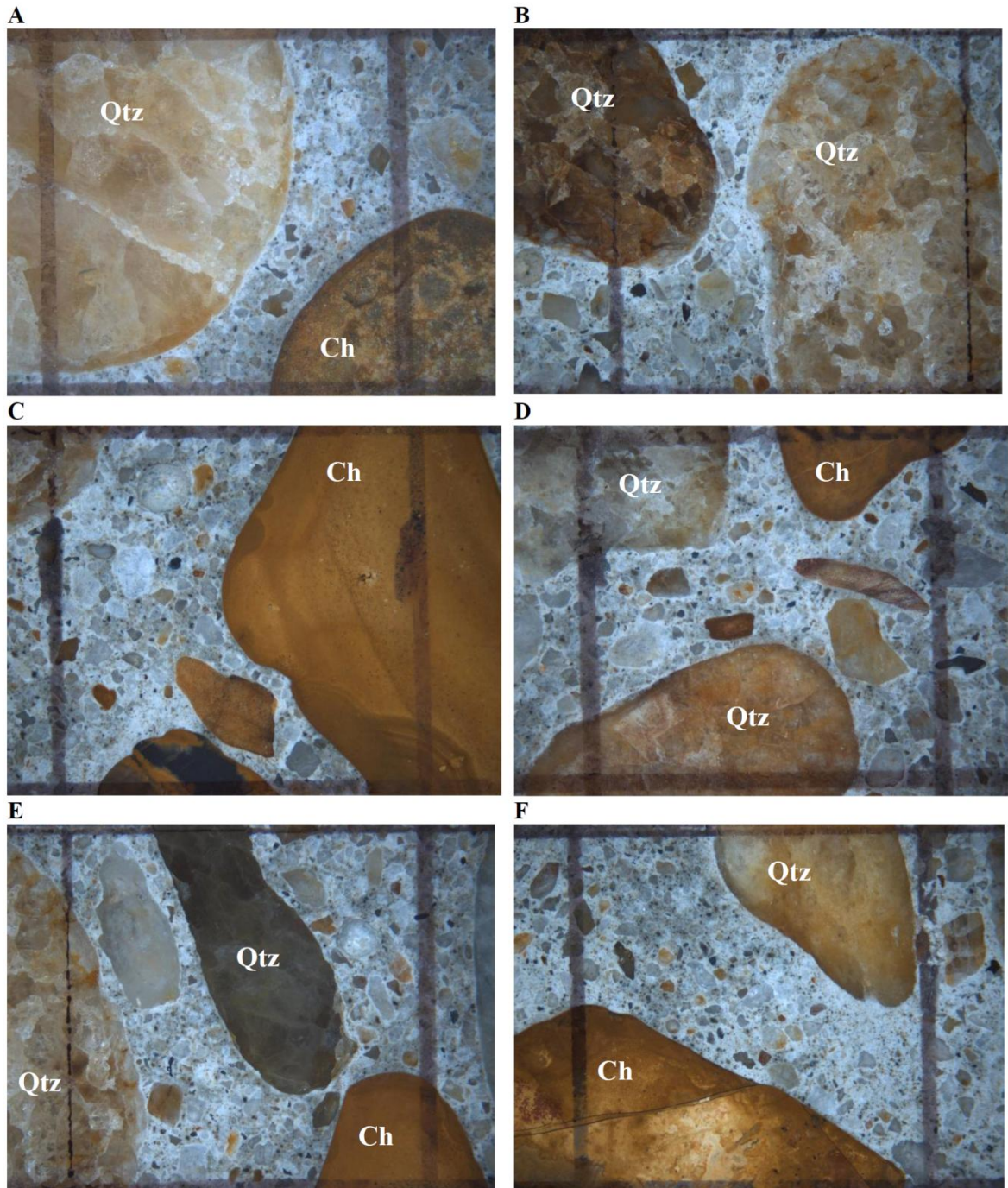


Figure B11: Micrographs of the polished core section 2B-North (distance between vertical lines = 1 cm).The micrographs show coarse aggregate particles that mainly consist of chert (Ch)(sometimes partially leached/weathered) and quartzite particles (Qtz). Very limited cracking is noticed in the cement paste.

Appendix C
Petrographic Analysis Report by WJE
(Extracted from WJE 2010)

BIBB GRAVES BRIDGE **Petrographic Studies of Concrete Cores**

Wetumpka, Alabama

INTRODUCTION

Petrographic studies have been conducted on four concrete cores received on June 21, 2010 from the Alabama Department of Transportation. The cores were taken from the historic Bibb Graves Bridge. The bridge is a reinforced concrete arch structure that spans the Coosa River in Wetumpka, Alabama, and was completed in 1931. The concrete is reportedly exhibiting unspecified distress. The petrographic studies were requested to describe the general condition of the concrete and in particular to investigate distress mechanisms.

Samples

Four 3-inch diameter cores were received for the studies. Petrographic observations and photographs of the as-received cores are included in Appendix 1. Sample identifications, dimensions, and general characteristics for each core are summarized in Table 1. Typically, concrete in all the samples was well consolidated. None of the cores contained steel reinforcement.

Table 1. Bibb Graves Bridge Samples

Core ID	Location	Core Length	General Description
1A-S	South Arch #5, East Side 17' 11" from top of pedestal	9.1 inches	<ul style="list-style-type: none"> • Weathered outside surface • Received diagonally broken at depth of 4.2 inches • Two cracks from outside end to 1 and 1.5 inches • Internal cracking of aggregates is common • Well consolidated
1A-N	North Arch #5, East Side 16' 3" from top of pedestal	10.8 inches	<ul style="list-style-type: none"> • Weathered outside surface • Received diagonally broken at 5.1 to 5.8 inches • Many narrow cracks throughout core • Internal cracking of aggregates is common • Well consolidated
1B-S	South Arch #4, West Side 3' 6" from top of pedestal	10.7 inches	<ul style="list-style-type: none"> • Weathered outside surface • No major cracks • Well consolidated
1B-N	North Arch #5, West Side 3' 10" from top of pedestal	11.6 inches	<ul style="list-style-type: none"> • Weathered outside surface • No major cracks • Well consolidated

PETROGRAPHIC STUDIES

Petrographic studies were conducted in accordance with the applicable methods of ASTM C 856 *Standard Practice for Petrographic Examination of Hardened Concrete*. Cracked samples were stabilized with epoxy resin. The samples were cut in half perpendicular to the outside end. One half of each core

was lapped using progressively finer grinding media to produce a smooth, semi-polished surface suitable for examination with a stereomicroscope. Lapped cross sections of the cores are shown in Figures 1 through 4. Immersion mounts and thin sections were prepared from selected areas of each core to study aggregate and paste characteristics using a petrographic (polarized-light) microscope.

General Characteristics of the Concrete

Cores 1A-S, 1A-N, 1B-S and 1B-N represent similar concrete made with similar aggregates and visually similar cements. Lapped longitudinal cross sections of the cores are shown in Figures 1 through 4. The concrete consists of siliceous gravel coarse aggregate and predominantly siliceous natural sand fine aggregate dispersed in a non-air-entrained portland cement paste. The concrete is well consolidated. Total air content in each core was estimated at 1 to 2 percent. Paste-aggregate bond is judged to be tight. Paste properties are generally good.

The outer surface of the each concrete core is eroded exposing the aggregate particles in relief. Black discoloration that appears to be accumulations of airborne particulates was observed on the outer surfaces of all the cores except 1B-S. The concrete surface was sound beneath the discoloration. The conditions in the outer surface region of the concrete are shown in Figures 5 through 8.

Cores 1A-S and 1A-N exhibit major distress caused by alkali-silica reaction (ASR) throughout the depth represented by the cores. Cores 1B-S and 1B-N did not exhibit distress caused by ASR; however, evidence that alkali-silica reaction has occurred was observed in both cores.

Concrete Composition

Aggregates

The coarse aggregates are hard, fairly dense to dense siliceous gravel that is mainly composed of white to yellow quartzite and yellow to brown chert. The aggregate particles are rounded to sub-angular, mostly oblong in shape, and are typically poorly graded, except in Core 1B-S. Nominal top size ranges from 3/4 inch to 1-1/2 inch. Coarse aggregate distribution is non-uniform. Aggregate volume is generally normal, but Core 1A-N appeared to be deficient in coarse aggregate particles.

The fine aggregate is a natural siliceous sand that is mainly composed of quartz, quartzite, chert, iron oxides, mica, and traces of other rocks and minerals, including occasional particles of limestone. The fine aggregate also contains small amounts of dark-colored slag-like material.

Thin, dark glassy rims were commonly observed on coarse aggregate particles and on some fine aggregate particles. Examples of typical rims are shown in Figures 9 and 10.

Paste-aggregate bond is tight; fresh fractures induced in the laboratory pass through the aggregate particles.

Paste

Paste properties are good except in locations where the concrete is distressed. In general, the paste in 1A-N and 1A-S is light to medium beige gray, locally moderately soft and absorptive to moderately hard and non-absorptive. The paste in these cores exhibits extensive microcracking that influences determination of the paste properties. The paste in 1B-N and 1B-S is predominantly moderate hard and contains patches that are moderately soft and porous. In Core 1B-S, the paste is dark gray and hard in the outer 1.2 inch.

In all the cores, paste volume is somewhat high, estimated at greater than 30 percent. Unhydrated and partially hydrated portland cement particles are estimated at 2 to 4 percent in 1A-N and 1A-S and 3 to 5 percent in 1B-N and 1B-S, but abundance of residual cement varies above and below the estimated range. The residual cement particles are large, but the size is typical of the coarsely ground portland cement of the era. The relative abundance and size of cement particles are shown in Figures 11 and 12. The extent of cement hydration is far advanced. Multiple broad hydration rims were frequently observed and cement relics are common. Portlandite crystals are non-uniformly distributed and moderate in size. The abundance of portlandite was estimated at 6 to 8 percent. Portlandite is absent or depleted adjacent to some chert and quartzite aggregate particles, suggesting incipient ASR. Minor depletion of portlandite from the paste surrounding chert and quartzite particles was commonly observed in cores 1B-S and 1B-N.

Overall, paste characteristics are consistent with concrete placed with a moderate water-cement ratio. The interpreted water-cement ratio is 0.55 +/- 0.03, based on paste characteristics. Water-cement ratio may be overestimated to the extent that the cement has experienced substantial continued hydration since setting.

Paste carbonation ranged from 0.04 to 0.1 inch at the outside end of cores 1A-S and 1A-N and 0.02 to 0.15 inch in cores 1B-S and 1B-N. The depth of paste carbonation is shallow considering the age of the concrete.

Air-Void System

The concrete is not purposefully air entrained, nor is air entrainment expected; air-entraining agents had only just been introduced in the 1930's. The concrete is well consolidated and contains an estimated 1 to 2 percent entrapped air. The air voids are typically sub-spherical to irregular in shape and occur scattered throughout the concrete.

Secondary Deposits

Cores 1A-S and 1A-N contain major amounts of secondary deposits in voids and coating fracture surfaces. ASR gel fills portions of transverse to diagonal narrow cracks that pass through reactive coarse aggregate particles. ASR gel was most commonly observed in cracks within the outer portion of aggregate particles (Figures 13 and 14). Occasional patches of crystalline material (Figure 15) were observed in the ASR gel. Microscopical characteristics suggest that some of the crystallized material may be okenite, a calcium silicate hydrate often reported in aged ASR gel. White deposits of ettringite (calcium sulfoaluminate hydrate) were most commonly observed in the portions of cracks within the paste (Figure 16 and 17). Overall, ASR gel is less common than ettringite. Cloudy gel-impregnated paste (Figure 18) partially surrounds a few chert and quartzite particles in Core 1B-N, but deposits of gel (Figure 19) were observed only in a few air voids adjacent to chert particles. No secondary deposits were observed in Core 1B-S.

Cracking Distress

Cores 1A-S and 1A-N were each received broken transversely into two segments. Core 1A-S exhibits narrow transverse cracks at intervals of approximately 0.5 to 1 inch from the outside end of the core to the inside end. Core 1A-N contains narrow cracks sub-parallel to the existing fractures at depths of 2.8, 3.8, 6.2, 6.8, 7.5, 8.0, 9.5, and 9.8 inches from the outside surface. In both cores, cracks pass through quartzite and chert coarse aggregate particles and extend outward into the paste. The body of the concrete also contains numerous microcracks that are sub-parallel to the outside surface of the concrete. Large

quantities of ettringite were observed on crack surfaces. Relatively smaller amounts of alkali-silica gel were observed in the peripheral region of cracks passing through aggregates.

Core 1A-S contained two vertical cracks that extended from the outside surface to depths of 1 and 1.5 inches, respectively. These cracks resemble normal shrinkage cracks.

Cores 1B-S Core and 1B-N did not exhibit visible distress. Depletion of portlandite (calcium hydroxide) in the paste adjacent to some chert and quartzite particles was observed in both cores. Cloudy, gel-saturated paste and small amounts of ASR gel were observed adjacent to chert aggregate particles in Core 1B-N.

Discussion of Distress

Cracking distress in the concrete represented by cores 1A-S and 1A-N is attributed to alkali-silica reaction involving quartzite and chert aggregate particles. ASR distress was possibly exacerbated by the formation of major amounts of ettringite. Cracks resulting from ASR allowed the ingress of water, which interacted with the cementitious paste locally removing calcium, aluminum, and sulfur. Ettringite was deposited in open spaces such as cracks and voids when conditions were suitable for its formation.

Alkali-silica reaction (ASR) is a secondary reaction (post concrete hardening) involving alkali hydroxides in the cement paste and certain susceptible siliceous rocks in the aggregate. The reaction product is a gel composed of silica, calcium, potassium, sodium and water. The gel imbibes water and expands causing cracking. The presence of water or a relative internal humidity higher than 80 percent is considered necessary to cause the gel to expand and induce cracking. Cracks form and propagate as the tensile strength of the concrete is exceeded.

Aggregates that contain reactive microcrystalline silica such as chert and chalcedony may cause cracking within 10 years of construction. ASR distress may develop over 20 years or more for less susceptible rock types such as quartzite.

SUMMARY AND CONCLUSIONS

Petrographic studies were conducted on four cores from the historic Bibb Graves Bridge to determine the general condition of the concrete and to determine the cause of cracking distress.

The condition of concrete represented by the two cores from west side of the bridge is non-distressed. The condition of concrete represented by the two cores from the east side of the bridge is severely distressed throughout the depth of the cores.

The cores represent visually similar concrete that consists of siliceous gravel coarse aggregate and predominantly siliceous natural sand fine aggregate dispersed in a non-air-entrained portland cement paste. The aggregate is poorly graded. Aggregate top size was 3/4 inch in some cores and 1 1/2 inches in others. Coarse aggregate volume was low in one core. The coarse aggregates were typically non-uniformly distributed. Overall, the concrete was well consolidated and appeared to have been placed with a moderate (Cores 1B-N and 1B-S) to moderately high (Core 1A-N and 1A-S) water-cement ratio. Paste volume was somewhat high, suggesting that the cement content was also moderate.

The outside surface of the concrete is eroded and aggregate particles are exposed. Dark colored particulates were observed in the surface depressions. Paste carbonation is minimal, typically less than 0.1 inch, and the underlying concrete surface is sound. The condition of the exterior region of the concrete is considered to be good considering the age of the structure.

Cores 1A-S and 1A-N exhibit significant cracking and microcracking attributed to alkali-silica reaction involving quartzite and chert coarse aggregate particles. Cracks caused by ASR were observed throughout the depth represented by these cores. ASR gel was most commonly observed in cracks within the outer portion of aggregate particles. Occasional patches of crystalline material, possibly okenite, were observed within the gel suggesting that the gel is relatively old. Overall, ASR gel is less common than ettringite, which is abundant on all crack surfaces. ASR distress was possibly exacerbated by the formation of major amounts of ettringite.

Cores 1B-S and 1B-N did not exhibit visible distress although minor evidence of alkali-silica reaction was observed. It is possible that this concrete was made with cement that had lower alkali content than the cement used in the concrete represented by cores 1A-S and 1A-N. Comparison of the alkali contents of these cores could be conducted with further analysis.

Storage: Thirty days after completion of our studies, the samples will be discarded unless the client submits a written request for their return. Shipping and handling fees will be assessed for any samples returned to the client. Any hazardous materials that may have been submitted for study will be returned to the client and shipping and handling fees will apply. The client may request that WJE retain samples in storage in our warehouse. In that case, a yearly storage fee will apply.



Figure 1. Lapped longitudinal cross section of Core 1A-N. Outside end of core is on left.



Figure 2. Lapped longitudinal cross section of Core 1A-S. Outside end of core is on left.

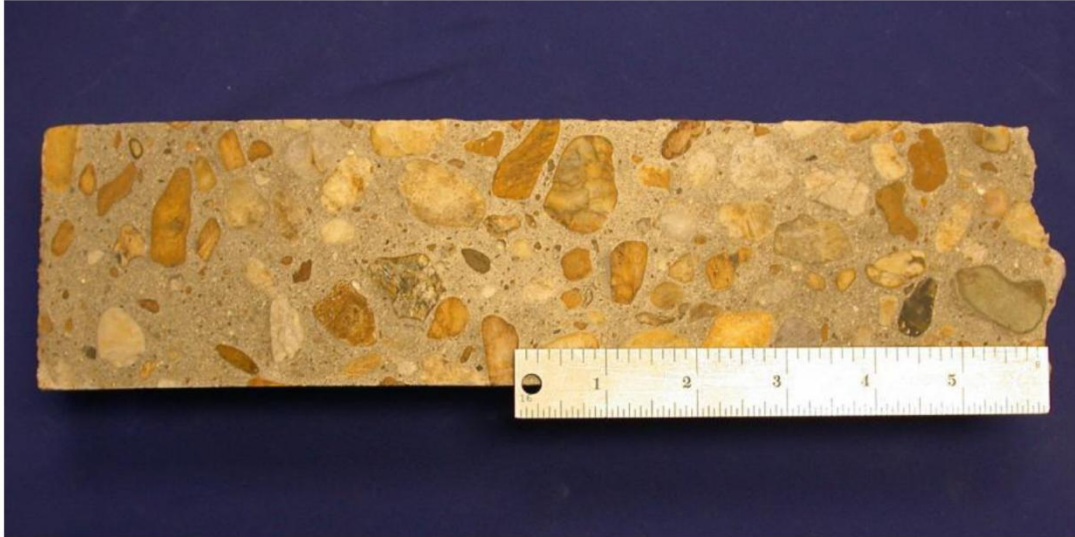


Figure 3. Lapped longitudinal cross section of Core 1B-N. Outside end of core is on left.



Figure 4. Lapped longitudinal cross section of Core 1B-S. Outside end of core is on left.

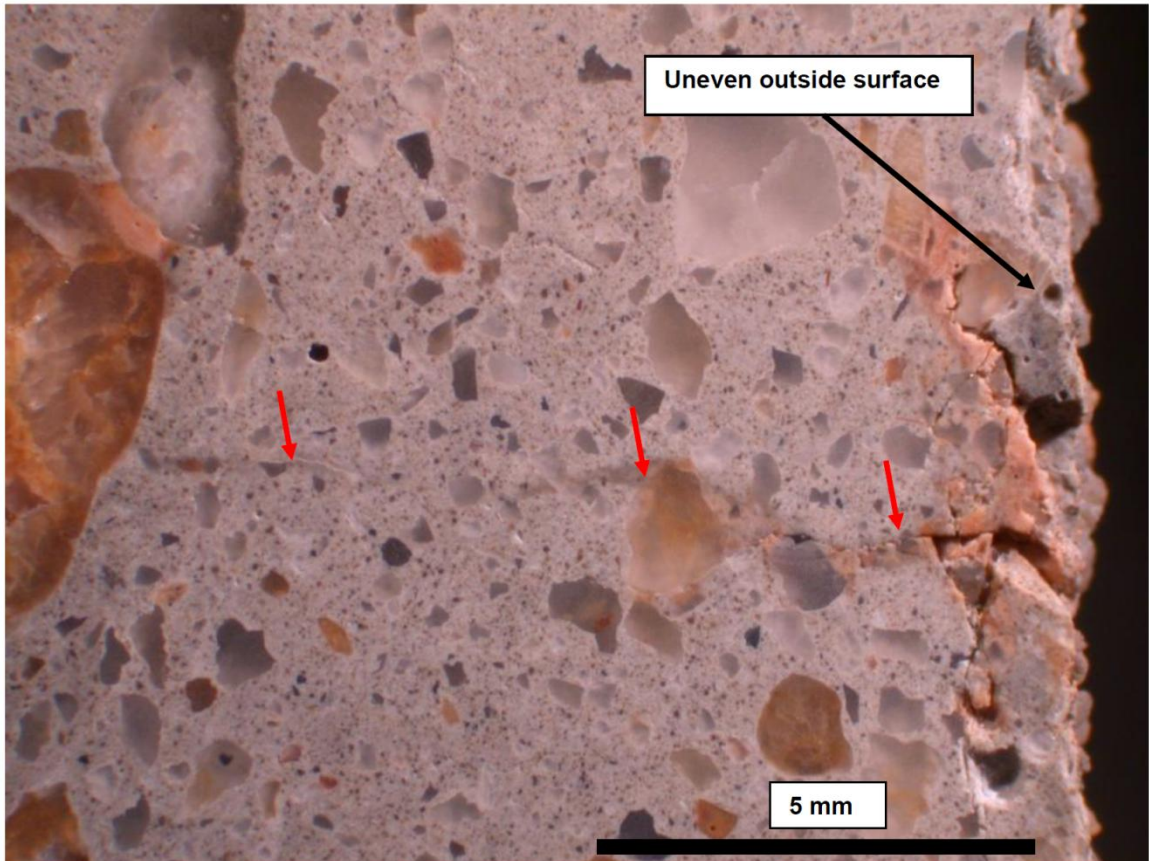


Figure 5. Core 1A-N - Narrow crack (arrows) and local paste carbonation in the outer region of the concrete. Outside surface is on the right. Carbonated paste is orange.

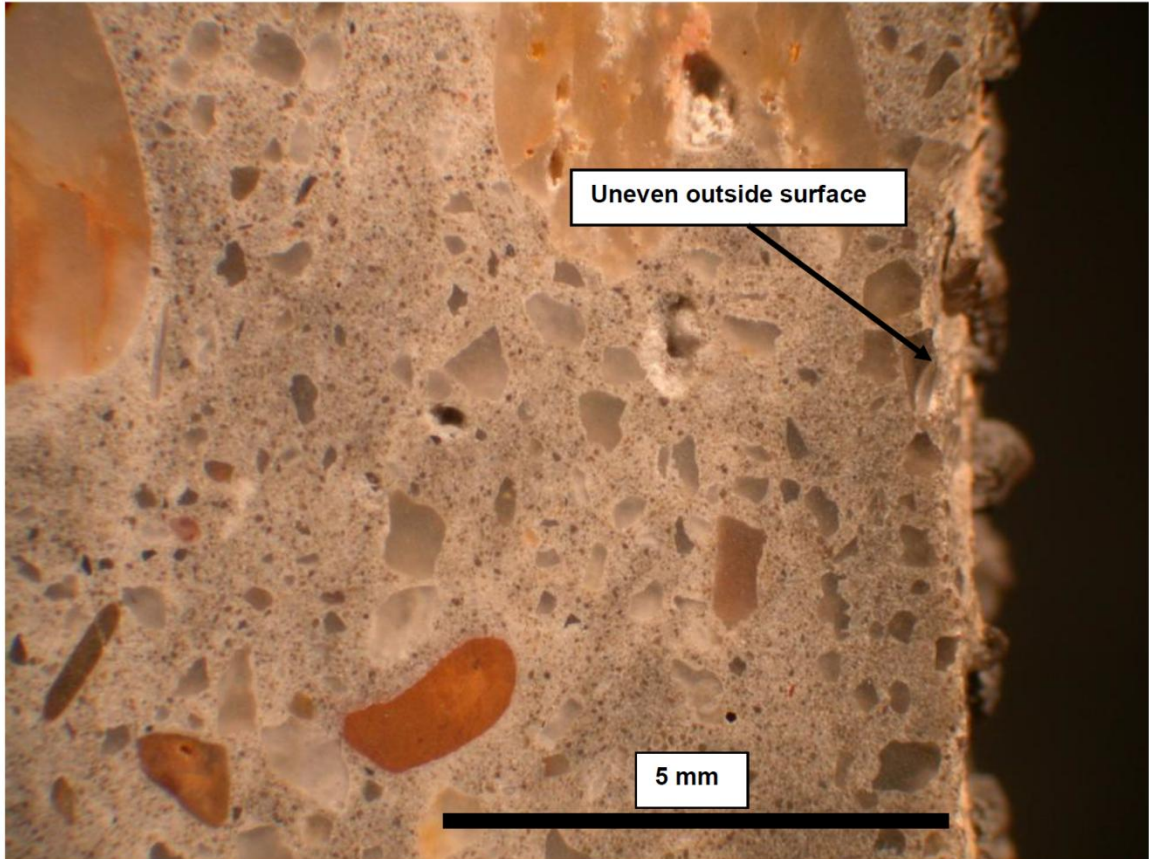


Figure 6. 1A-S - Mottled light gray to dark gray paste in the outer region of the concrete. Outside surface is on the right.

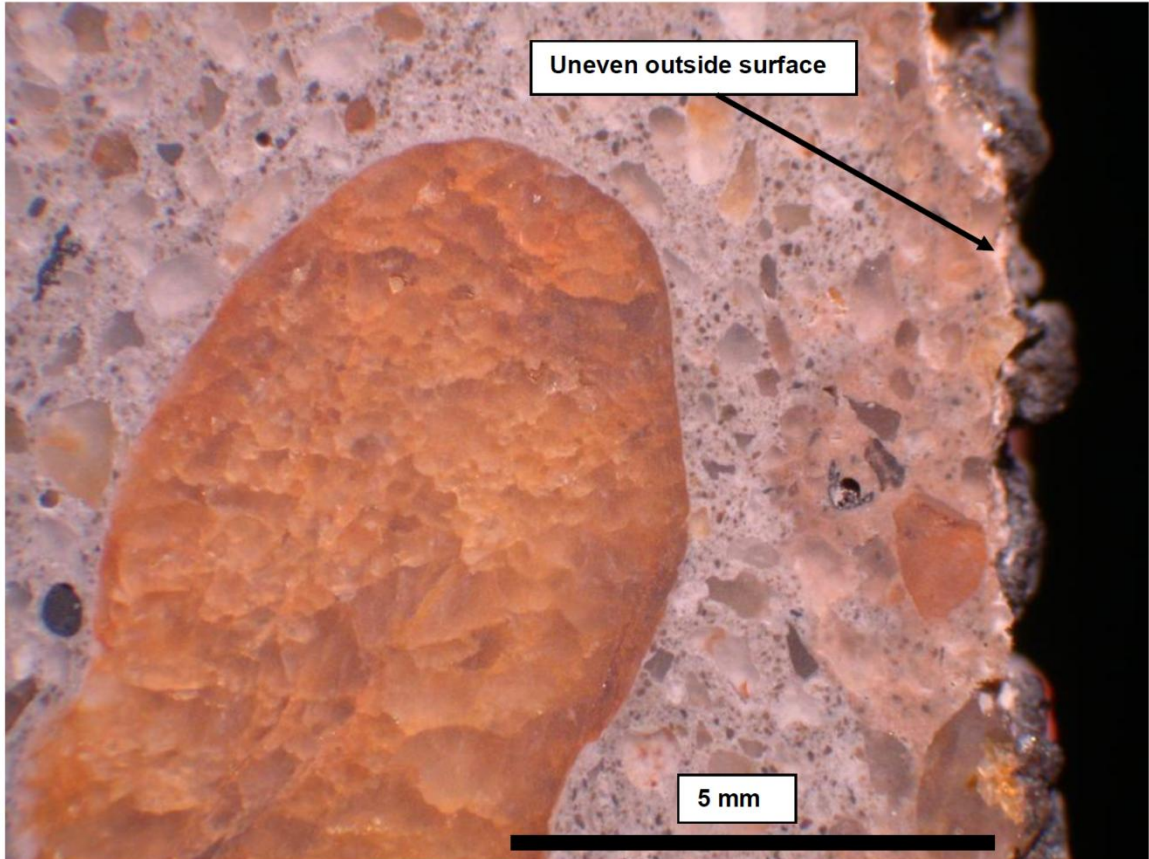


Figure 7. 1B-N - Pinkish orange carbonation in the region of the concrete.

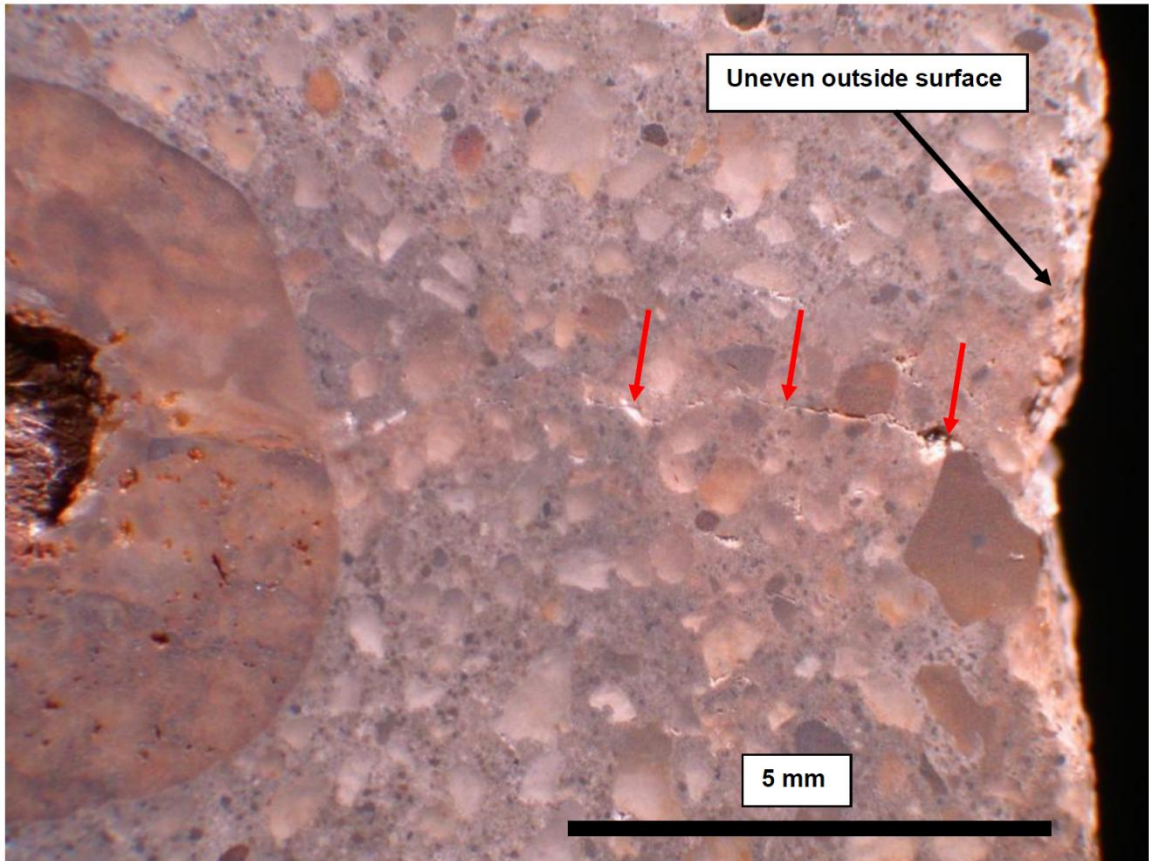


Figure 8. 1B-S - Narrow crack (arrows) in the outer region of the concrete. The crack extends from the outside surface to the aggregate particle on the left, but requires higher magnification to be seen. Outside surface is on the right. Patches of carbonated paste are pinkish orange.

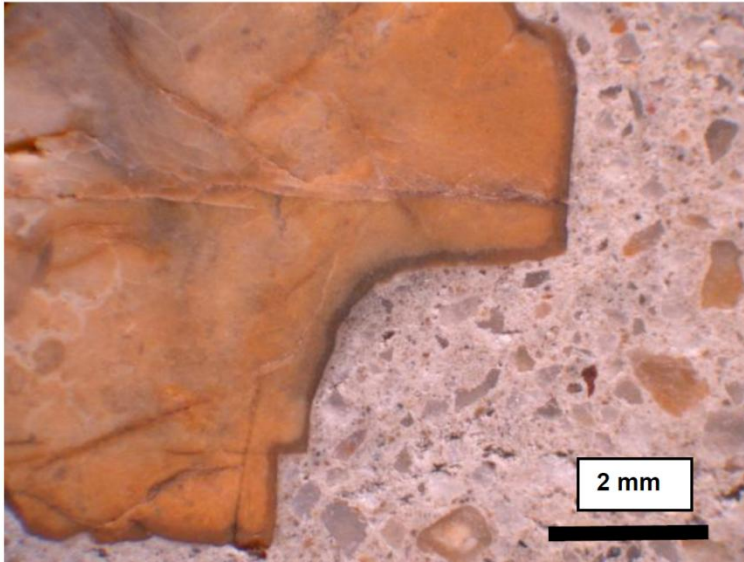


Figure 9. 1B-S - Typical dark rim on chert coarse aggregate particle.

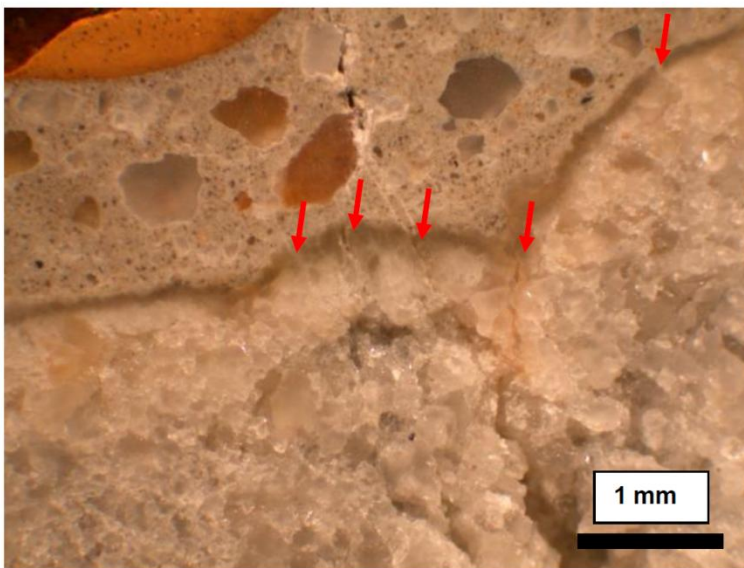


Figure 10. 1A-S - Typical dark glassy rim on white friable quartzite coarse aggregate particle. Arrows show ASR cracks in aggregate periphery.

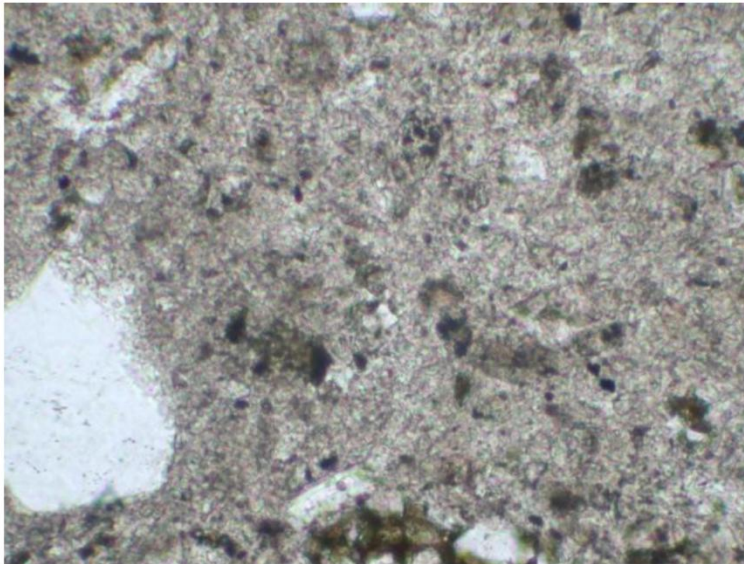
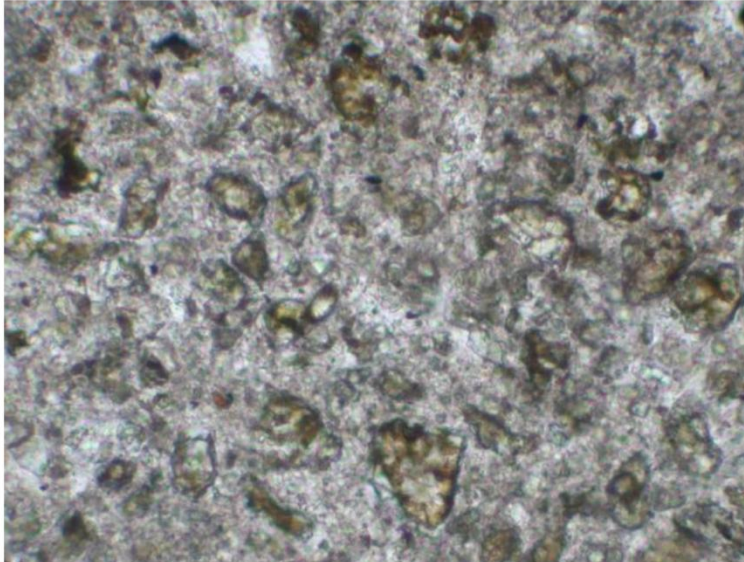


Figure 11. Core 1B-S - Variability in the abundance of portland cement particles in two nearby regions of the paste is shown. Plane-polarized light. Field width is 0.6 mm.

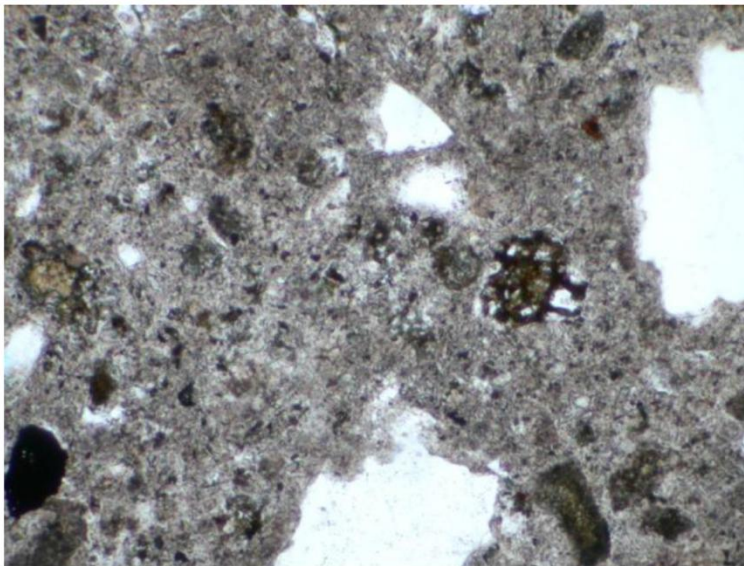
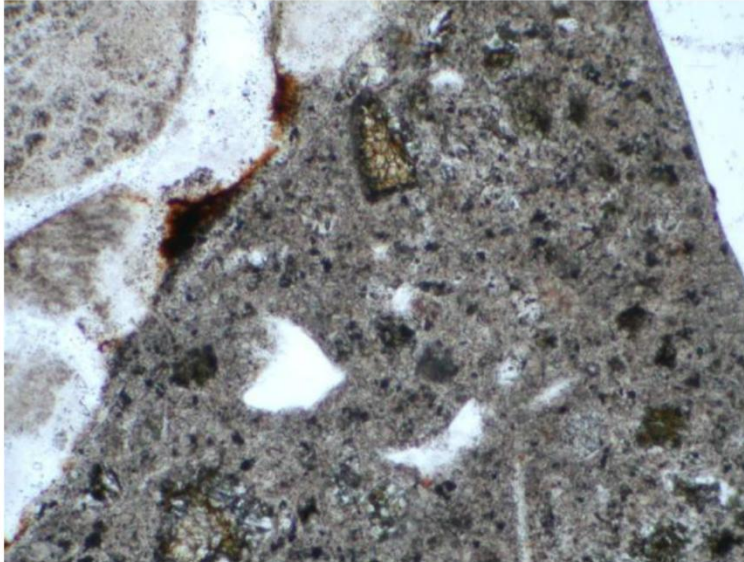


Figure 12. Core 1A-N - Variability in the abundance of portland cement particles in two nearby regions of the paste is shown. Plane-polarized light. Field width is 0.6 mm.

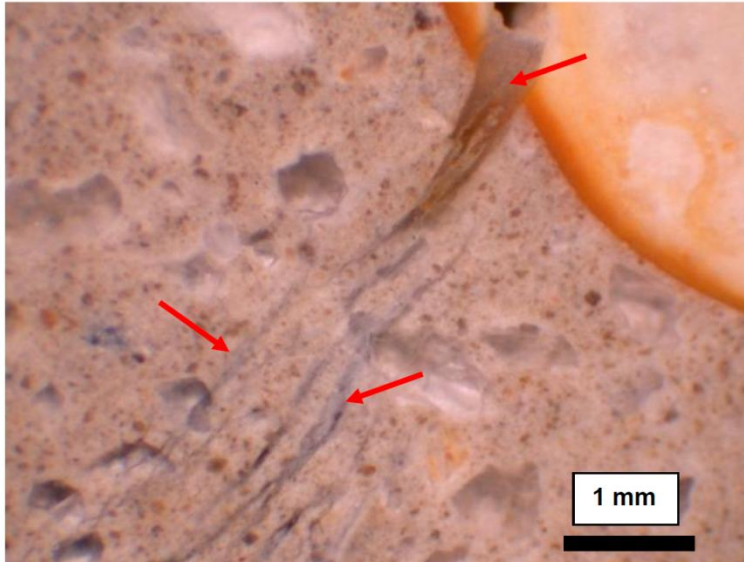


Figure 13. Crack at periphery of quartzite aggregate particle (top right) and multiple veinlets (gray) filled with ASR gel. The sample was photographed after the lapped surface was coated with acrylic to show the finer microcrack more clearly.



Figure 14. Wider cracks in chert particle are filled with ASR gel in peripheral region of particle. Cracks in paste contain white ettringite deposits.

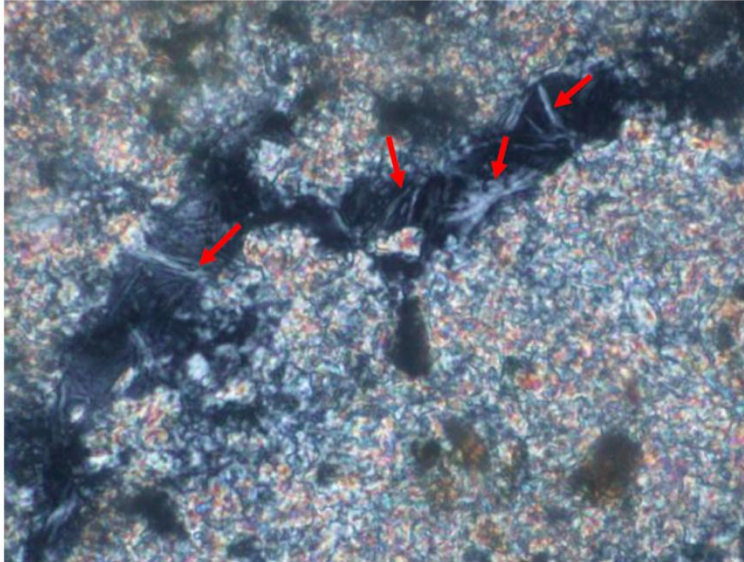


Figure 15. 1A-S - Platy crystals (arrows) in crack filled with ASR gel. Cross-polarized light with upper polar slightly rotated. Field width is 0.3 mm.

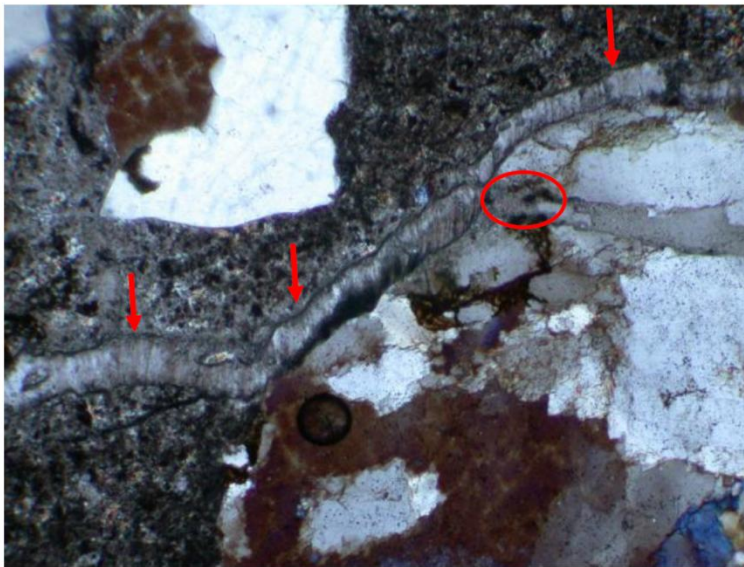


Figure 16. 1A-S - Microcrack filled with ettringite. Small amount of gel at outside edge of crack in aggregate is circled. Cross-polarized light with upper polar slightly rotated. Field width is 1.2 mm.

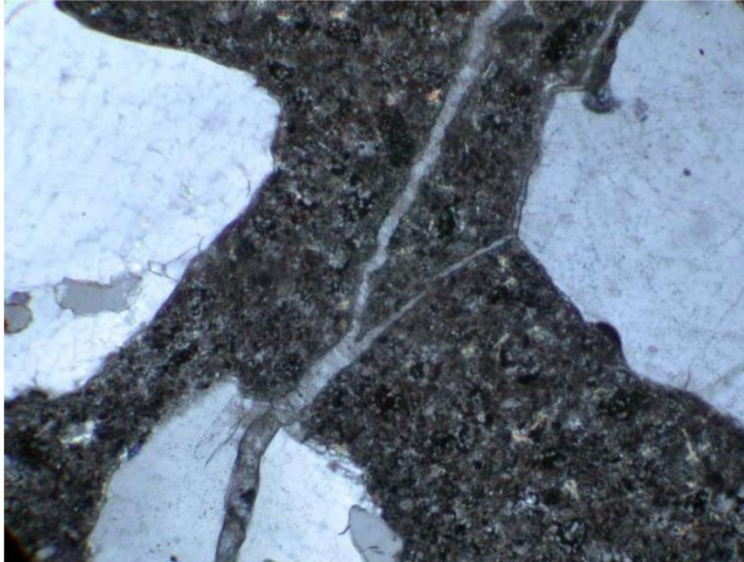


Figure 17. 1A-S - Microcracks filled with ettringite. Cross-polarized light with upper polar slightly rotated. Field width is 1.2 mm.

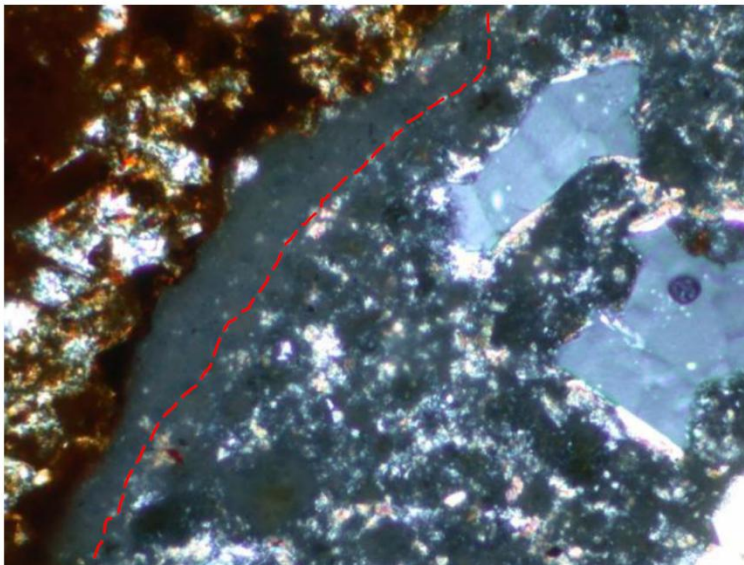


Figure 18. Cloudy, gel-impregnated paste (outlined in red) adjacent to chert aggregate particle in 1B-N. Cross-polarized light. Field width is 0.6 mm.

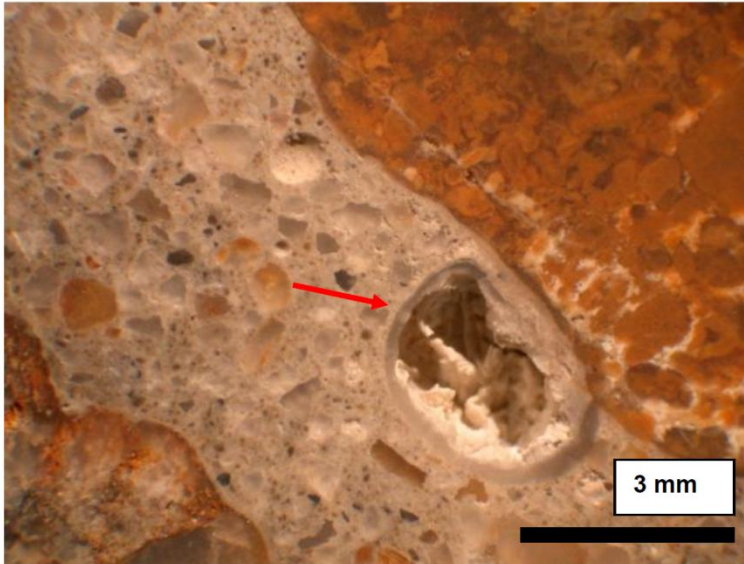


Figure 19. Air void lined with ASR gel adjacent to a chert aggregate particle in 1B-N.

Appendix D

Relative Humidity Survey Data

This appendix contains all of the relative humidity data collected from the Bibb Graves Bridge between February 2011 and September of 2013, which is 34 months after the application of the mitigation procedure.

Tables D. 1 through D. 16 contain the relative humidity data as it was collected from the bridge for the 1, 2, and 3-inch depths at each location. These tables also show which probe was used to collect the data and the concrete's temperature at the measurement depth.

This appendix also shows all of the relative humidity data averaged for all there depths at each location per month in Table D. 17, and Table D. 18 shows all of the relative humidity data for the 3-inch depths at each location per month.

Table D. 1. 4-S-WB monthly RH survey data

Span 4 South – West Bottom											
Date	Time In	Time Out	Depth: 1"			Depth: 2"			Depth: 3"		
			PN	°C	RH%	PN	°C	RH%	PN	°C	RH%
2/15/2011	3:10	4:10	4	18.5	83	2	16.8	89.4	7	16.4	86.9
4/7/2011	1:50	2:50	9	22.2	85.4	5	20.6	92.2	10	20.5	88.3
5/5/2011	12:55	1:55	9	19.7	87.9	2	18.7	91.5	6	18.7	89.6
6/3/2011	1:40	2:30	7	35.4	81.7	5	34.7	84.9	6	34.5	82.4
7/7/2011	10:30	11:35	5	31.7	91.2	7	31.3	92.3	3	31.4	90
8/10/2011	10:40	11:40	9	29.2	87.8	1	28.2	90.3	8	28	90.1
9/15/2011	12:30	1:20	10	25.2	92.5	9	26.2	92.9	2	26.4	90.8
10/18/2011	2:15	3:15	1	26.2	84.3	6	24.9	89.9	7	24.7	83.6
11/8/2011	12:20	1:15	9	23	86.5	8	21.9	91.3	4	21.8	84.8
12/14/2011	10:30	11:30	3	16.8	79.5	7	15.1	84.7	7	16.1	83.4
1/31/2012	1:30	2:30	3	17.7	80	1	15.5	85.5	8	15.1	82.6
3/8/2012	2:10	3:10	3	24.6	85.6	5	23.1	88.1	9	23.1	85.8
4/12/2012	2:40	3:30	1	19.7	83.7	2	18.6	91.9	7	18.3	92.5
5/17/2012	12:10	1:25	9	28.8	84.6	7	27.8	87.1	2	27.7	85.6
6/8/2012	11:25	12:25	5	27.7	85.8	6	27.3	88.3	9	27.1	87.5
7/16/2012	2:20	3:35	7	34.7	83.9	6	33.9	88.1	2	33.8	87.3
8/13/2012	3:15	4:10	2	27.7	89.3	3	28.6	88.5	9	28.6	89
9/13/2012	1:30	2:25	6	26.6	87.6	10	26.4	88.6	5	26.3	87.2
10/14/2012	1:55	3:00	5	25.9	86.7	2	25.4	87.4	9	25.3	89.3
11/19/2012	1:25	2:30	4	16.1	87.2	5	14.3	87.8	6	14.1	87.7
12/6/2012			UT 1.4	20.9	82.3	UT 1.1	20	83.4	UT 1.5	19.9	88
1/8/2013	2:05	3:00	7	14.2	84.7	4	12.7	86.4	2	12.4	85
2/5/2013	1:08	2:12	10	16.4	82.2	5	14.1	86.5	4	13.8	87.4
3/14/2013	12:40	1:40	4	11.8	86.6	7	10.9	83.7	10	10.8	85.1
4/9/2013	2:40	3:40	6	27.5	81.7	5	26.4	85.6	1	26.3	84.6
5/14/2013	2:15	3:05	6	24.8	87	2	23.8	88.5	7	23.5	89
7/17/2013	1:33	2:20	3	32.1	90.6	2	31.5	88.6	6	31.5	91.2
8/5/2013	2:45	3:35	9	30.9	90.4	10	30.9	95.2	4	31.1	89
9/10/2013	1:40	2:40	1	31.4	90.5	10	31	88.6	4	31.1	89

PN = Probe Number

UT = University of Texas Probe

Table D. 2. 4-S-WT monthly RH survey data

Span 4 South – West Top											
Date	Time In	Time Out	Depth: 1"			Depth: 2"			Depth: 3"		
			PN	°C	RH%	PN	°C	RH%	PN	°C	RH%
2/15/2011	1:55	3:00	1	24.2	94.5	2	23	81.2	6	21.6	87.3
4/7/2011	12:50	1:45	3	29.8	95.1	9	28.2	85.4	5	27	87.8
5/5/2011	2:00	3:00	2	31.7	95.8	9	31.9	85.5	10	30.6	84.4
6/3/2011	1:45	2:35	3	47.6	94.9	8	46.7	88.1	4	46.3	85.3
7/7/2011	11:40	12:40	7	40.9	91.4	5	39.9	90	3	38.8	87.5
8/10/2011	11:50	12:40	8	39.1	93.7	1	38.2	85.9	9	36.9	85.7
9/15/2011	1:30	2:30	9	25.7	92.5	2	27.7	90.1	10	28.8	92.9
10/18/2011	1:20	2:10	3	33	76.7	9	30.6	82	10	29	88.5
11/8/2011	1:20	2:10	5	28.2	78.2	6	27.3	81.4	3	26.4	84.6
12/14/2011	3:00	4:00	3	20.7	78.4	9	19	79.7	1	17.7	86.4
1/31/2012	2:20	3:20	1	22.3	78.5	6	20.3	81	4	19.8	84.8
3/8/2012	2:10	3:10	7	28.8	89.1	1	27.8	84.1	4	27.4	87.7
4/12/2012	2:40	3:30	10	28.2	88	4	29.1	86	6	28	88
5/17/2012	9:45	10:40	3	31.4	80.1	5	29.8	79.4	1	28.6	89
6/8/2012	9:10	10:05	5	28	81	9	27.7	79.9	6	27.2	89.2
7/16/2012	10:30	11:25	7	39	78.2	2	37.6	79	10	36.1	85.4
8/13/2012	10:45	11:45	1	35.5	78	4	32.9	77.8	5	31.4	86.7
9/13/2012	11:30	12:25	9	30.8	80.2	2	30	77.5	7	29.1	83.4
10/14/2012	10:20	11:20	7	27	84.5	3	26	75.7	9	25	89.9
11/19/2012	10:10	11:10	2	15.7	74.1	7	14.1	79.9	3	13.1	85.8
12/6/2012	12:30	1:55	7	23.7	70.6	4	22.8	80.7	10	21.7	87.2
1/8/2013	10:35	11:35	3	13.5	80.4	7	12.3	72.2	4	11.2	92.1
2/5/2013	10:52	11:52	2	18.7	74.1	5	16	89.5	4	14	88.2
3/14/2013	11:13	12:10	9	15.2	78.8	5	13.1	74.4	2	11.5	87
4/9/2013	10:55	11:55	5	30.7	78	3	29.4	73.4	2	27.8	83.3
5/14/2013	10:50	11:45	6	28.2	86.4	2	27	76.8	7	25.4	84.4
7/17/2013	10:25	11:15	1	35	82.3	6	34.3	90.1	2	33.6	81.6
8/5/2013	10:55	11:50	10	36.2	84.2	9	36.2	83.4	4	35.8	84.3
9/10/2013	10:30	11:20	4	36.1	77.1	1	33.3	88.7	10	32.1	86.5

PN = Probe Number

Table D. 3. 4-S-EB monthly RH survey data

Span 4 South – East Bottom											
Date	Time In	Time Out	Depth: 1"			Depth: 2"			Depth: 3"		
			PN	°C	RH%	PN	°C	RH%	PN	°C	RH%
2/15/2011	3:15	4:15	6	19.8	80.1	3	17.8	84.7	5	17	84.7
4/7/2011	1:50	2:50	2	22.3	86.2	6	21.2	86.5	4	20.6	84
5/5/2011	12:05	1:55	8	20.1	77.4	5	19.3	83.1	10	18.9	82
6/3/2011	12:30	1:30	4	35	86.1	8	334	91	3	34	88.7
7/7/2011	10:30	11:35	10	32.2	79.8	4	31.7	84.2	8	31.5	87.9
8/10/2011	10:45	11:45	4	29.8	84.7	2	28.9	90.8	3	28.5	89.2
9/15/2011	12:30	1:25	8	25.1	92.9	7	26.3	92.9	1	26.8	89.6
10/18/2011	2:15	3:15	5	26.3	74.3	8	25.8	83.5	4	25.3	80.8
11/8/2011	12:20	1:15	3	23	74	5	22.1	85	10	21.8	80.6
12/14/2011	11:30	12:40	2	18.5	68.8	6	16.7	75.4	4	16.3	74.8
1/31/2012	1:30	2:30	9	18.1	73.3	5	15.6	77.7	10	14.7	78.4
3/8/2012	3:20	4:20	3	25	80.3	5	23.9	83.1	9	23.6	82.3
4/12/2012	3:40	4:30	1	20.5	77.2	7	19.8	90.4	2	19.6	87.6
5/17/2012	12:15	1:25	5	28.8	76.9	1	28.2	80.8	4	27.9	80.6
6/8/2012	11:25	12:25	2	27.8	80.5	3	27.4	81.8	4	27	81.8
7/16/2012	2:15	3:30	5	34.3	87	9	34.1	86	10	33.8	84
8/13/2012	2:30	3:30	10	29.1	80.9	6	29.7	82.4	7	29.7	79.8
9/13/2012	12:35	1:25	6	26.5	81.1	10	26.2	83.1	5	26.1	84.6
10/14/2012	1:55	3:00	3	26.2	90	10	25.7	87	7	25.5	88.5
11/19/2012	1:25	2:20	2	16.1	81.6	3	14.7	85.1	7	14	83.8
12/6/2012			UT 1.3	21.5	77.3	UT 1.8	20.3	78.7	UT 1.7	20.1	78.3
1/8/2013	2:10	3:05	10	14.3	86.1	9	12.9	80.8	3	12.2	77.8
2/5/2013	1:05	2:10	2	16.4	79.4	1	14.4	81.7	6	13.7	80.6
3/14/2013	1:45	2:50	7	13.1	76.7	10	12.2	79.1	4	11.9	80.4
4/9/2013	2:35	3:30	2	27.8	75.4	7	26.7	78.1	3	26.3	79.3
5/14/2013	2:20	3:10	9	25	89.9	10	24	82.5	3	23.7	89.1
7/17/2013	1:38	2:25	7	32	88.3	1	31.7	86.5	5	31.4	87.1
8/5/2013	2:50	3:40	2	31.2	85.3	3	31.4	88.7	5	31.2	83.4
9/10/2013	1:45	2:50	6	32.3	85.2	2	31.8	80.5	7	31.3	87.3

PN = Probe Number

UT = University of Texas Probe

Table D. 4. 4-S-ET monthly RH survey data

Span 4 South – East Top											
Date	Time In	Time Out	Depth: 1"			Depth: 2"			Depth: 3"		
			PN	°C	RH%	PN	°C	RH%	PN	°C	RH%
2/15/2011	2:00	3:05	9	25.1	96.3	9	22.8	95.5	1	22.7	94.3
4/7/2011	12:50	1:45	1	31.5	96.4	3	32.6	95	1	31.6	90.2
5/5/2011	2:00	3:00	4	32.4	96.1	1	32.2	92.4	6	32	88.1
6/3/2011	1:45	2:40	10	45.8	92.9	2	47.1	93.7	1	47.3	90.4
7/7/2011	11:40	12:40	8	43.6	90.5	4	43.8	88.8	10	42.7	88.2
8/10/2011	11:50	12:40	7	41.8	92.2	3	43.1	85.2	6	41.5	91.1
9/15/2011	1:30	2:30	7	27.2	94.7	8	28.8	92.2	1	29.6	93.1
10/18/2011	1:20	2:10	2	34.5	80.2	2	34.4	87.3	3	34.1	86.8
11/8/2011	1:20	2:10	5	29.2	78.6	9	28.5	87.2	2	28.2	87.3
12/14/2011	11:30	12:40	9	25	83.1	5	23.8	83.8	3	22.7	85.5
1/31/2012	2:30	3:30	9	21.7	82.4	5	20.3	85.7	3	19.4	85.6
3/8/2012	2:10	3:10	10	29.5	82.4	6	27.6	88.6	2	27.4	89.3
4/12/2012	2:40	3:30	3	30.3	86.7	9	30.2	83.5	5	29.7	84.8
5/17/2012	9:45	10:40	6	34.8	83.5	10	35.1	83.8	4	34.5	88
6/8/2012	9:10	10:05	2	30	78	3	30.8	84.4	4	30.1	89.3
7/16/2012	10:25	11:25	9	41.5	84.4	6	42.6	86.7	5	41.3	89.9
8/13/2012	10:45	11:50	2	36.4	81.3	9	36.9	84.1	3	35.9	89.6
9/13/2012	11:30	12:20	4	31.4	79.9	1	31.8	84.8	3	31.4	86.4
10/14/2012	10:20	11:15	5	30.3	82.8	10	30.4	84.2	2	29.4	86.7
11/19/2012	10:10	11:05	6	17.1	80.7	5	16.2	81.7	4	15.6	91.5
12/6/2012	12:35	2:00	6	25.8	78.9	2	25.4	80.7	5	25.1	88.1
1/8/2013	10:35	11:35	2	15	77.5	1	14.1	82.5	10	13.4	90
2/5/2013	10:48	11:50	1	21.3	80.8	10	20.3	81.3	6	19.2	88.5
3/14/2013	11:20	12:15	3	19.8	94.9	6	20.6	77.9	1	19.5	86.7
4/9/2013	10:50	11:50	7	33.5	85.1	1	34.5	81.6	6	33.2	84.5
5/14/2013	10:50	11:40	3	31	90.3	9	32.2	84.9	10	31.3	89.1
7/17/2013	10:20	11:09	7	38.2	85.9	5	38.7	90.6	3	38.1	88.8
8/5/2013	10:55	11:50	2	38	77.5	3	39.1	83	5	38.3	91.3
9/10/2013	10:20	11:20	6	39.2	84.7	2	40.2	80.7	7	38.9	88.6

PN = Probe Number

Table D. 5. 4-N-WB monthly RH survey data

Span 4 North – West Bottom											
Date	Time In	Time Out	Depth: 1"			Depth: 2"			Depth: 3"		
			PN	°C	RH%	PN	°C	RH%	PN	°C	RH%
2/15/2011	10:10	1:10	4	13.7	87.5	8	12.4	88.7	9	12.2	85.7
4/7/2011	9:30	10:30	1	17.5	89.1	6	17.1	88.2	8	17	86.9
5/5/2011	9:45	10:50	6	16.6	81.2	2	16.4	85.1	3	16.5	86
6/3/2011	9:30	10:25	7	31.8	82.3	3	32	86.4	2	31.9	87.1
7/7/2011	7:15	8:15	9	29.8	84.7	7	30.1	85.3	6	30.2	85.8
8/10/2011	7:30	8:30	5	25.3	84.1	1	25.7	85.5	7	25.7	86.6
9/15/2011	9:30	10:25	2	26.5	79.8	9	26.9	84.2	8	27	84.9
10/18/2011	9:40	10:30	6	22.6	76.2	4	22	81	5	21.8	78.3
11/8/2011	9:20	10:10	9	20.6	74.8	8	20	81.7	3	20	77.1
12/14/2011	12:55	1:45	5	18.5	68.8	6	16.7	75.4	4	16.3	74.8
1/31/2012	10:00	11:00	10	11.8	73.1	2	10.5	76.1	1	10.1	84.5
3/8/2012	9:45	10:45	3	20.6	78.5	4	19.8	81.7	5	19.5	83.3
4/12/2012	10:00	10:50	3	15.5	74.5	2	15.5	76	7	15.6	79.6
5/17/2012	2:40	3:35	5	29.1	84.4	1	28.8	82.6	4	28.8	83.2
6/8/2012	12:35	1:35	5	28.6	76.9	6	28.2	81.6	9	28.1	83.1
7/16/2012	1:00	2:25	4	33.9	82.1	1	33.6	82.9	3	33.6	84
8/13/2012	12:05	1:05	10	29.7	81.7	6	29.1	81.5	7	28.9	83.2
9/13/2012	3:15	4:05	3	27.2	83.7	4	27	83.1	1	26.9	83.1
10/14/2012	3:05	4:00	9	26.2	84.6	5	25.6	83.7	2	25.5	83.9
11/19/2012	2:25	3:20	3	15.8	80.5	7	14.3	82.2	2	14.1	80.9
12/6/2012			UT 1.4	20.9	77.5	UT 1.1	20.1	78.3	UT 1.5	19.5	84.2
1/8/2013	2:55	3:45	1	14.1	80.9	5	12.8	84.4	6	12.5	81.3
2/5/2013	3:25	4:20	2	17	79.7	1	15.1	84	4	14.7	80
3/14/2013	3:45	4:40	2	14.3	79.5	9	13.1	83	1	12.8	81.4
4/9/2013	3:35	4:20	3	27.7	75.2	7	26.7	78.2	2	26.6	80.4
5/14/2013	3:15	4:05	10	25.6	81.7	3	24.9	87.5	2	24.6	82.9
7/17/2013	2:15	3:00	9	32.3	84.7	4	32.1	85.3	10	31.9	86.5
8/5/2013	3:30	4:20	7	31.3	80.6	1	31.6	85.4	6	31.7	85.1
9/10/2013	2:45	4:00	10	31.5	82.7	4	31.7	87.6	1	31.7	87.9

PN = Probe Number

UT = University of Texas Probe

Table D. 6. 4-N-WT monthly RH survey data

Span 4 North – West Top											
Date	Time In	Time Out	Depth: 1"			Depth: 2"			Depth: 3"		
			PN	°C	RH%	PN	°C	RH%	PN	°C	RH%
2/15/2011	10:25	11:25	6	21.7	84	1	17.5	87.6	6	14.1	89.2
4/7/2011	9:30	10:30	3	21.1	92.1	2	19.7	90.2	10	18.7	91.9
5/5/2011	9:45	10:45	4	21.7	88.8	4	22.3	92.4	1	21	89.9
6/3/2011	9:30	10:30	8	36.4	84	5	35.2	89.2	1	34.7	90
7/7/2011	7:15	8:15	1	31.2	83.3	2	32.6	88.6	1	31.2	92.1
8/10/2011	7:30	8:30	9	27.1	80.3	9	28.4	86.3	8	26.8	92.4
9/15/2011	9:30	10:25	3	27.7	83.9	3	28.6	90.2	5	28.8	89.3
10/18/2011	9:50	10:50	2	26.1	77.2	2	25.2	85.8	9	23.9	90.2
11/8/2011	9:20	10:10	6	24.8	75	6	23.1	83.8	2	22.3	86.9
12/14/2011	3:00	4:00	10	21.1	77.4	7	19.1	87.4	6	18	89.4
1/31/2012	10:00	11:00	3	16.5	81.3	9	14.2	86.2	9	10.9	89
3/8/2012	11:00	12:00	3	25.6	84.8	5	24.4	88.3	6	23.2	92.2
4/12/2012	10:00	10:50	9	20.9	79.3	5	18	90.4	4	17	93.1
5/17/2012	8:40	9:35	3	30.8	78.9	4	28	89.9	1	26.8	92.4
6/8/2012	8:00	9:00	6	27.5	78.9	9	26.8	89.5	5	26.2	93.1
7/16/2012	9:20	10:20	5	37	84.3	6	34.7	89.8	9	33.6	89.5
8/13/2012	9:40	10:40	1	31.1	84	5	30.6	86.4	9	29.7	90.4
9/13/2012	10:35	11:25	4	31.1	79.8	1	29.7	85.9	3	28.4	89.4
10/14/2012	9:20	10:20	5	26.3	86.3	2	26.7	86.7	10	26.5	90.1
11/19/2012	9:10	10:05	4	14.4	80.6	2	12.7	82.5	7	11.4	88
12/6/2012			UT 9	25.5	83.8	UT 6	23.8	85.6	UT 3	22.9	88
1/8/2013	9:30	10:30	1	13.1	78.5	2	11.2	80.6	4	9.7	92.7
2/5/2013	9:45	10:40	4	17.3	74	2	13.9	77.9	5	11.2	92.3
3/14/2013	10:05	11:05	1	11.9	79.8	6	9.9	79.3	3	8.8	93.1
4/9/2013	9:50	10:40	2	28	81.1	3	25.7	79.8	5	24.3	92.3
5/14/2013	9:50	10:40	2	25.9	87.6	7	24.3	89.3	6	23	91.7
7/17/2013	9:30	10:14	2	33.7	79.3	1	32.9	85.4	6	31.9	91.1
8/5/2013	10:00	10:50	10	35.6	85.9	4	35.2	87.4	9	34.4	91
9/10/2013	9:20	10:15	10	32.4	83.9	4	30.7	92.4	1	30	92.2

PN = Probe Number

UT = University of Texas Probe

Table D. 7. 4-N-EB monthly RH survey data

Span 4 North – East Bottom											
Date	Time In	Time Out	Depth: 1"			Depth: 2"			Depth: 3"		
			PN	°C	RH%	PN	°C	RH%	PN	°C	RH%
2/15/2011	10:15	11:15	3	15	82.8	1	13.3	85	5	12.7	83
4/7/2011	9:30	10:25	9	17.6	86.7	5	17	83.9	4	16.9	85.2
5/5/2011	9:40	10:40	10	17	85.5	5	16.5	78.7	9	16.3	80.7
6/3/2011	9:30	10:25	6	31.6	84.4	4	31.6	82.2	10	31.5	85.1
7/7/2011	7:15	8:15	5	29.2	88.4	4	29.7	82.5	8	29.7	84.7
8/10/2011	7:30	8:30	3	25.3	88.1	4	26	83.2	2	26.1	83.2
9/15/2011	9:30	10:25	7	25.9	86.2	1	26.8	78.2	10	27	82.4
10/18/2011	9:40	10:30	7	23.5	78.5	8	22.7	74.7	1	22.5	76.3
11/8/2011	9:20	10:12	10	21.3	78.4	4	20.6	76.1	5	20.1	77.7
12/14/2011	12:55	1:45	7	19.6	73.3	8	17.6	75	2	16.7	74.2
1/31/2012	10:00	11:00	4	12.6	75	5	11.2	71.9	6	10.7	73.8
3/8/2012	9:40	10:40	1	21	80.3	7	20.1	77.6	2	19.7	78
4/12/2012	10:00	10:50	6	16	84.3	10	16.1	68	1	16	75.3
5/17/2012	1:30	2:45	9	29	82.3	10	28.6	75.1	3	28.5	80.3
6/8/2012	12:35	1:35	2	28.8	80.9	3	28.1	74.2	4	27.7	80.9
7/16/2012	11:45	12:55	3	33.6	82.9	4	33.1	76.7	1	32.8	82.7
8/13/2012	1:10	2:20	7	30.7	80.9	6	30	74.5	10	29.6	81.9
9/13/2012	2:25	3:25	10	27.3	84	6	26.9	76	5	26.7	82.1
10/14/2012	2:05	3:10	4	26.3	84.9	6	26	79.8	1	25.7	88.1
11/19/2012	1:35	2:30	9	16.4	81.8	10	14.9	90.8	1	14.1	80.9
12/6/2012			UT 1.3	22	81.3	UT 1.7	20.9	75.1	UT 1.8	20.5	79.5
1/8/2013	1:55	2:55	6	14.6	81	1	13	86.5	5	12.3	83.7
2/5/2013	2:30	3:30	9	17.6	77.3	3	15.4	83.4	7	14.4	78.8
3/14/2013	2:55	4:00	4	14	79.4	10	13.1	72.1	7	12.5	72.2
4/9/2013	2:45	3:50	4	27.7	82.2	10	26.9	78.8	9	26.4	82.6
5/14/2013	2:25	3:20	4	25.3	81.8	1	24.3	75.9	5	23.7	79.4
7/17/2013	1:25	2:15	10	31.8	87	4	31.5	81.4	9	31.1	84.4
8/5/2013	2:35	3:25	6	30.5	87.3	7	30.9	77.5	1	31.1	84.6
9/10/2013	1:55	2:55	5	32	85.2	9	31.8	81.5	3	31.8	82.8

PN = Probe Number

UT = University of Texas Probe

Table D. 8. 4-N-ET monthly RH survey data

Span 4 North – East Top											
Date	Time In	Time Out	Depth: 1"			Depth: 2"			Depth: 3"		
			PN	°C	RH%	PN	°C	RH%	PN	°C	RH%
2/15/2011	10:20	11:20	2	23.5	86.1	7	22.9	93.2	10	22.5	91
4/7/2011	9:30	10:35	7	23	86.6	7	26	96	3	25.4	93.4
5/5/2011	9:40	10:45	1	24.3	89.3	8	25.6	96.5	7	25.5	89.4
6/3/2011	9:30	10:30	9	40.4	87	9	47	91.5	1	46.4	89.9
7/7/2011	7:15	8:15	10	33.9	83.7	3	32.9	92.3	2	32.5	91.4
8/10/2011	7:30	8:30	6	27.7	76.8	8	27.2	93.2	10	27	93
9/15/2011	9:30	10:25	5	29.7	84.6	4	29.5	92.5	6	29.5	91.8
10/18/2011	9:50	10:40	3	31.9	80.5	10	31.1	92.5	9	30.6	89.7
11/8/2011	9:20	10:10	7	27.3	81.6	2	26.7	86.1	1	26.3	89.6
12/14/2011	11:30	12:40	6	24.9	81.5	10	24.3	86.7	1	23.6	90.4
1/31/2012	10:00	11:00	3	16.5	76.4	8	16.4	84.4	7	15.8	89
3/8/2012	11:00	12:00	1	27.2	85.2	2	27.3	87.6	7	26.7	90.5
4/12/2012	11:00	12:00	4	26.2	88.6	5	28.6	90.1	9	29	89.9
5/17/2012	8:40	9:35	5	32.8	87.3	10	33	88.3	6	32.7	89.3
6/8/2012	8:00	9:00	3	29	94.1	2	28.8	87.6	4	28.8	91
7/16/2012	9:10	10:15	10	39.3	87.6	2	39.9	92.2	7	39.6	87.7
8/13/2012	9:40	10:40	4	34	86.9	3	34.7	93.2	2	34.3	90
9/13/2012	10:35	11:28	7	31.6	77.6	2	32.3	86.4	9	31.9	89.6
10/14/2012	9:20	10:20	5	26.3	86.3	2	26.7	86.7	10	26.5	90.1
11/19/2012	9:10	10:00	6	16.4	84.1	3	15.6	84.6	5	14.8	89.3
12/6/2012			UT 1	26.7	79.4	UT 7	25.7	87.2	UT 8	25.4	89.1
1/8/2013	9:30	10:30	7	15.3	70.1	10	14.6	88.2	3	14.1	87.9
2/5/2013	9:50	10:45	10	21.6	84.2	6	20.4	88.2	1	19.8	86.8
3/14/2013	10:10	11:10	2	16	86.7	9	17.5	88.7	5	17.2	90.4
4/9/2013	9:55	10:45	1	31.2	88.9	7	31.7	81.4	6	31.5	85.9
5/14/2013	9:55	10:45	9	29.3	93.5	3	30.7	87	10	30.3	87.4
7/17/2013	9:30	10:15	5	36.3	88	3	37.5	86.8	7	37.2	89
8/5/2013	10:00	10:53	5	38.2	84.2	2	38.3	83.4	3	38.1	85.6
9/10/2013	9:25	10:20	7	36.6	91.9	6	37.7	83.4	2	37.5	84.4

PN = Probe Number

UT = University of Texas Probe

Table D. 9. 5-S-WB monthly RH survey data

Span 5 South – West Bottom											
Date	Time In	Time Out	Depth: 1"			Depth: 2"			Depth: 3"		
			PN	°C	RH%	PN	°C	RH%	PN	°C	RH%
2/15/2011	1:50	2:50	5	17.8	88.1	4	16.1	91.2	7	14.8	92.3
4/7/2011	12:45	1:40	0:00	21.1	93.2	6	19.9	96.2	7	19	96.7
5/5/2011	11:45	12:46	1	18.6	96	4	18.1	94.8	7	17.6	97.4
6/3/2011	11:30	12:35	7	33.3	93.8	6	32.9	92.2	5	32.5	94.8
7/7/2011	9:30	10:20	7	30.6	94.2	5	30.4	95.1	3	30.5	94.6
8/10/2011	9:40	10:30	1	28	91.3	8	27.4	94.1	9	27.1	93.7
9/15/2011	11:20	12:30	9	26.1	94.7	10	26.6	94	7	26.8	94.8
10/18/2011	1:15	2:05	7	25.2	87.8	8	24.4	94	4	23.8	92.7
11/8/2011	11:20	12:20	9	22.4	90.6	5	21.5	91.1	3	21	90.6
12/14/2011	10:15	11:15	10	16.8	86.7	4	15.5	89.1	1	14.3	89
1/31/2012	12:00	1:00	6	16.7	85.1	10	14.5	89.5	4	13.5	86.2
3/8/2012	1:10	2:10	9	23.6	89.4	3	22.5	90.6	5	21.5	91.4
4/12/2012	12:00	1:20	6	17.6	93.4	10	17.3	94.4	3	17.8	93.9
5/17/2012	12:05	1:20	10	28.5	90.9	6	27.7	93.1	3	27.3	92.7
6/8/2012	10:30	11:30	7	26.4	90.6	10	26.2	93.9	1	26	94.2
7/16/2012	12:50	2:05	2	33	92.4	7	32.6	90.5	6	32.4	93.5
8/13/2012	12:55	2:10	3	30.6	91.4	2	29.8	91.7	9	29.2	93.6
9/13/2012	1:20	2:15	1	26.6	92.6	3	26.5	92.8	4	26.2	93.8
10/14/2012	12:25	1:50	5	25.6	91.7	10	25.1	93.1	7	24.6	90.7
11/19/2012	12:10	1:20	3	15.2	88.7	2	13.8	90.9	7	12.8	89.2
12/6/2012			UT 2.2	21.4	89.1	UT 2.3	20.8	91.2	UT 2.4	20.1	92.1
1/8/2013	12:55	2:00	2	13.9	87.8	4	12.2	89.2	7	11.1	88.6
2/5/2013	2:20	3:20	1	16.5	86.6	6	14.8	91.4	2	13.6	89.8
3/14/2013	1:35	2:35	1	13	91	6	12.1	91.5	3	11.4	90.5
4/9/2013	1:25	2:40	9	26.8	90.1	10	25.6	92.7	4	24.8	91.4
5/14/2013	1:15	2:15	7	24.1	89.6	2	23.3	90.7	6	22.6	91.5
7/17/2013	12:06	1:27	5	31.4	91.5	1	31.1	92.2	7	30.7	91.3
8/5/2013	1:35	2:40	2	30.6	90.8	5	30.9	92.1	3	31.2	92.8
9/10/2013	12:30	1:35	10	31.2	90.8	4	30.8	92.1	1	30.4	92.4

PN = Probe Number

UT = University of Texas Probe

Table D. 10. 5-S-WT monthly RH survey data

Span 5 South – West Top											
Date	Time In	Time Out	Depth: 1"			Depth: 2"			Depth: 3"		
			PN	°C	RH%	PN	°C	RH%	PN	°C	RH%
2/15/2011	12:45	1:40	10	23	89	7	21.1	91.6	9	20.6	94.9
4/7/2011	11:40	12:40	1	27.7	92.7	9	26	91.7	6	25.4	95.9
5/5/2011	11:45	12:46	6	27.6	93.9	2	27	91.7	3	26.9	93.2
6/3/2011	11:30	12:45	2	46	97	10	45.4	92.7	10	43.1	92.1
7/7/2011	10:30	11:40	9	39.7	93	9	39.9	92.3	2	40	91.5
8/10/2011	10:35	11:30	6	35.5	92.8	10	33.6	90.8	7	33.3	92.8
9/15/2011	12:30	1:30	6	27.9	96	3	28.9	94.4	5	29.4	92.8
10/18/2011	12:05	12:55	1	29.5	91.3	7	28.4	87.7	8	27.4	92.8
11/8/2011	12:20	11:15	1	20.9	93.1	6	26.2	91.9	2	26.4	89.9
12/14/2011	9:00	10:00	9	16.8	85.5	2	13.9	90.8	6	13.4	92.2
1/31/2012	1:20	2:20	4	21.4	88.3	6	19.9	89.1	7	18.6	89.9
3/8/2012	12:05	1:05	6	26.9	91.5	3	25.7	91.1	2	25.6	89.6
4/12/2012	1:30	2:30	3	27.8	94.3	10	27.3	92.5	9	27.4	89.4
5/17/2012	10:50	11:55	5	34.4	91.2	10	32.7	90.4	6	32.4	88.3
6/8/2012	10:15	11:10	3	32.2	89.6	9	29.7	91.4	4	30	89.7
7/16/2012	11:35	12:40	7	41.8	90.8	10	40.9	90.6	5	40.5	88.8
8/13/2012	11:55	12:55	9	37.8	91.3	2	36.4	89	3	36.1	87.2
9/13/2012	12:25	1:15	3	32.9	92	4	32.2	89.3	1	31.6	89.2
10/14/2012	11:25	12:20	2	30.3	87.8	10	28	89.9	5	27.5	90.8
11/19/2012	11:10	12:05	3	16.6	89.9	7	15.2	86.7	2	14.9	89.7
12/6/2012			UT 8	23.2	90.5	UT 6	22.7	89.7	UT 1	22.3	91.1
1/8/2013	11:40	12:40	7	14.8	88.2	4	14.1	91.3	2	13.6	90.6
2/5/2013	12:00	1:00	10	19	89.9	2	17.4	88.9	1	16.7	91.3
3/14/2013	12:30	1:27	5	19	89	9	16.9	92.9	2	16.8	89.3
4/9/2013	12:05	1:05	1	32.6	91.2	7	31.7	87.1	6	31.6	88.5
5/14/2013	11:50	1:10	9	32	92.7	3	31.5	89.7	10	31.3	89.4
7/17/2013	11:20	12:00	7	37.4	91.6	5	36.5	91.3	1	36.5	89.8
8/5/2013	12:00	1:30	3	36.9	93.1	5	37	92.8	2	37.5	88.7
9/10/2013	11:30	12:20	6	36.6	88.3	7	35.6	90.9	2	35.5	87.3

PN = Probe Number

UT = University of Texas Probe

Table D. 11. 5-S-EB monthly RH survey data

Span 5 South – East Bottom											
Date	Time In	Time Out	Depth: 1"			Depth: 2"			Depth: 3"		
			PN	°C	RH%	PN	°C	RH%	PN	°C	RH%
2/15/2011	1:55	2:55	8	18.4	89.5	3	16.6	96.2	10	15.9	93.8
4/7/2011	12:45	1:40	8	21.5	92.3	4	20.4	96.6	2	19.9	97.5
5/5/2011	12:50	1:50	7	20.1	95.5	1	19.5	96.1	4	19.2	97.3
6/3/2011	12:35	1:30	6	34.9	90.8	7	34	94.9	5	33.7	95.2
7/7/2011	9:30	10:20	4	31	93.6	8	30.8	95.2	10	30.8	94.9
8/10/2011	9:45	10:40	4	28.7	93.4	3	28.2	93.3	2	27.9	93.9
9/15/2011	11:20	12:30	2	26.2	93.8	1	27.1	94.5	8	27.3	94.9
10/18/2011	1:15	2:05	1	26.1	90.8	6	25.4	93.4	5	24.9	90.4
11/8/2011	11:20	12:20	4	22.6	89.2	8	21.8	94.4	10	21.3	92.5
12/14/2011	10:15	11:15	8	17.2	88.1	6	16.4	89.3	2	15	90.7
1/31/2012	12:00	1:10	1	16.9	87.2	8	17	82	2	13.9	91.4
3/8/2012	1:10	2:10	10	23.7	90.5	1	23.3	90.9	7	22	92.9
4/12/2012	1:30	2:30	1	19.3	92.8	7	18.8	94.2	2	18.7	94.7
5/17/2012	11:05	12:00	9	28	91.5	7	27.3	92.1	2	27.1	93.4
6/8/2012	11:35	12:40	1	27.8	92.1	10	27.2	94.2	7	26.9	93.3
7/16/2012	12:45	2:10	10	33.3	91.5	5	33.1	93.2	9	33	94
8/13/2012	12:55	2:05	5	30.7	91.1	1	30	93.3	4	29.6	94
9/13/2012	1:20	2:10	9	26.8	93.1	7	26.6	92.1	2	26.5	92.5
10/14/2012	12:25	1:45	2	26	90.9	9	25.7	93.5	3	25.4	93.9
11/19/2012	12:10	1:25	5	15.7	90	6	14.3	93.5	4	13.6	94.9
12/6/2012			UT 2.1	21.5	90.1	UT 2.6	21.8	85.9	UT 2.5	20.6	93.7
1/8/2013	12:50	2:00	3	13.9	86.7	10	12.2	93.3	9	11.7	92.6
2/5/2013	2:17	3:17	4	17.3	87	5	15	90.9	10	14.2	93
3/14/2013	1:32	2:30	2	13.4	89.3	9	12.6	93.9	5	12.2	95
4/9/2013	12:20	1:20	4	26.2	89.3	10	25.1	94.7	9	24.8	92.8
5/14/2013	1:15	2:10	10	24.6	90.5	3	23.7	92.5	9	23.3	94.4
7/17/2013	12:07	1:30	2	31.7	89.3	6	31.3	91.9	3	31.2	92.8
8/5/2013	1:35	2:45	4	31	92.8	10	31.2	95.8	9	31.4	93.7
9/10/2013	12:25	1:30	2	32	88.4	6	31.5	90	7	31.2	92

PN = Probe Number

UT = University of Texas Probe

Table D. 12. 5-S-ET monthly RH survey data

Span 5 South – East Top											
Date	Time In	Time Out	Depth: 1"			Depth: 2"			Depth: 3"		
			PN	°C	RH%	PN	°C	RH%	PN	°C	RH%
2/15/2011	12:50	1:45	6	26.3	93.5	8	26.2	90.3	1	26.1	94.9
4/7/2011	11:40	12:40	7	31.1	94.1	2	30.6	93.1	8	31.1	93.6
5/5/2011	12:50	2:00	3	32.7	95.2	7	32.9	93.9	3	33.3	96.8
6/3/2011	12:50	1:45	1	47.9	97	9	48.3	92	9	48.8	90.9
7/7/2011	10:30	11:45	6	41.5	96.1	2	43	92.1	1	42.6	94.8
8/10/2011	10:40	11:30	5	39.2	95.3	5	42.2	94.1	10	42.1	93.1
9/15/2011	12:30	1:30	1	30.1		3	30	95.4	6	30	95.9
10/18/2011	12:05	12:55	6	33.4	93.5	4	33.2	92.3	5	33.4	85.7
11/8/2011	12:20	11:10	7	27.9	93.1	7	28	92.6	1	28.2	93.2
12/14/2011	9:00	10:00	1	20	89.6	5	18.6	89.9	4	19.3	88.6
1/31/2012	1:20	2:20	2	22.2	88.1	2	20.1	92.4	7	20.1	92.1
3/8/2012	1:10	2:10	6	27.7	93.3	2	26.9	92.8	4	27.3	92.2
4/12/2012	1:30	2:30	6	29.2	95	5	30.4	92.1	4	30.7	89.5
5/17/2012	10:50	11:50	1	36.2	93.6	3	36.9	88.2	4	37	85.9
6/8/2012	10:15	11:10	2	32.7	95.2	6	33.9	90.3	5	33.4	90.4
7/16/2012	11:30	12:35	2	45.1	95.3	9	45.4	87.9	6	45	89.3
8/13/2012	11:50	12:50	5	37.9	94.1	1	38.9	93.6	4	38.8	87.2
9/13/2012	12:25	1:15	9	33.2	94.8	2	33.2	90.3	7	33.2	87
10/14/2012	11:20	12:20	3	31.8	90	9	31.8	89.4	7	31.5	85.4
11/19/2012	11:15	12:10	4	19.3	88.5	5	17.1	92.1	6	17	92
12/6/2012			UT 7	25.4	92.2	UT 9	25.6	92.1	UT 3	25.7	90
1/8/2013	11:40	12:40	10	16	93.4	1	15	91.9	3	14.9	91.9
2/5/2013	11:55	12:55	4	21.2	92.7	5	20.3	92	6	20.3	92.5
3/14/2013	12:23	1:23	6	22.1		1	23.1	91.5	3	23.8	91.3
4/9/2013	12:00	1:00	2	35.2	92.4	3	36.6	84.7	5	36.2	84.8
5/14/2013	11:45	1:10	7	34	92.8	2	35	88.8	6	35.1	84.7
7/17/2013	11:15	12:00	3	39.6	93.7	6	40.2	92.2	2	40.3	91.6
8/5/2013	12:00	1:30	10	39	94.7	4	39.7	92.1	9	39.8	89.8
9/10/2013	11:25	12:20	1	40.3		4	41.6	92.1	10	41.7	87

PN = Probe Number

UT = University of Texas Probe

Table D. 13. 5-N-WB monthly RH survey data

Span 5 North – West Bottom											
Date	Time In	Time Out	Depth: 1"			Depth: 2"			Depth: 3"		
			PN	°C	RH%	PN	°C	RH%	PN	°C	RH%
2/15/2011	11:35	12:30	4	15.1	76.2	5	13.2	74.3	9	12.6	68.5
4/7/2011	11:40	12:40	4	20	73.2	5	18.5	76.7	3	18.2	75.7
5/5/2011	10:50	11:45	9	17.8	68.7	5	17.2	69.3	10	17	70.6
6/3/2011	10:45	11:20	5	32.7	73.1	3	32.5	75.3	8	32.2	76.3
7/7/2011	8:25	9:25	8	30.5	71.8	4	30.4	74.4	5	30.3	75.6
8/10/2011	8:35	9:30	2	26.9	70.7	3	26.6	74	4	26.5	74.8
9/15/2011	10:30	11:20	1	26.3	69.6	2	26.8	71.7	8	26.9	73.7
10/18/2011	11:00	11:50	1	24.1	61.4	8	22.7	66.5	7	22.2	66.8
11/8/2011	10:20	11:10	3	21.5	61.2	9	20.4	67.5	8	20.1	68.2
12/14/2011	9:00	10:00	3	14.8	60.2	8	13.2	65.7	7	12.3	65.4
1/31/2012	11:00	11:50	8	14.2	77.9	4	11.6	79	6	10.6	66.1
3/8/2012	11:00	12:00	9	22.1	81.6	4	20.7	82.5	10	20	74.5
4/12/2012	11:00	12:00	3	16.2	72.9	6	16.1	80.3	10	16	66.4
5/17/2012	1:30	2:30	4	29.2	70.4	5	28.2	78.4	1	27.9	72.7
6/8/2012	12:50	1:50	10	28.6	82.7	1	27.8	78	7	27.4	73.9
7/16/2012	2:30	3:25	1	34.5	71.2	3	33.8	76.4	4	33.4	75.8
8/13/2012	2:15	3:10	9	30.5	75.5	3	30	80.7	2	29.5	80.8
9/13/2012	2:15	3:10	4	26.8	81.5	1	26.4	79.5	3	26.3	87.9
10/14/2012	11:30	12:30	4	24.4	78.3	1	23.8	77.2	6	23.6	81.2
11/19/2012	11:15	12:15	9	13.9	76.7	10	12.2	80.4	1	11.6	78.3
12/6/2012			UT 2.3	21.7	66.7	UT 2.4	21.5	72.1	UT 2.2	19.8	70.7
1/8/2013	11:45	12:45	9	12.9	76.4	5	10.7	77.7	6	10	77.3
2/5/2013	1:15	2:25	7	16	80.7	3	13.8	87.2	9	12.9	74.3
3/14/2013	2:40	3:37	3	13.7	80.7	6	12.3	78.4	5	11.7	86.3
4/9/2013	1:15	2:25	3	26.8	62.7	7	25.3	70.1	2	24.8	72.7
5/14/2013	1:20	2:20	5	24.6	79.2	1	23.4	74.3	4	22.9	80.4
7/17/2013	12:13	1:20	9	31.4	79.6	4	31	84.5	10	30.7	79.5
8/5/2013	1:25	2:30	1	30.4	80.3	7	30.9	79.8	6	31.1	86.7
9/10/2013	11:40	12:35	5	30.2	84.5	3	29.9	76	9	29.7	86.3

PN = Probe Number

UT = University of Texas Probe

Table D. 14. 5-N-WT monthly RH survey data

Span 5 North – West Top											
Date	Time In	Time Out	Depth: 1"			Depth: 2"			Depth: 3"		
			PN	°C	RH%	PN	°C	RH%	PN	°C	RH%
2/15/2011	11:40	12:35	3	21.8	89.1	3	18.7	88.1	2	16.9	90.1
4/7/2011	10:40	11:40	8	24.5	91.7	10	21.3	94	10	23.4	90.8
5/5/2011	11:45	12:46	5	26.3	96.3	10	25.8	91.3	9	25.1	88.7
6/3/2011	10:40	11:30	4	42.1	95.1	4	38.7	91.9	2	37.8	91.6
7/7/2011	8:30	9:30	9	33.3	92.3	6	31.9	90.9	6	33.2	91.7
8/10/2011	8:4	9:35	10	30	91.1	6	28.4	90.4	6	29.4	91.6
9/15/2011	11:20	12:30	5	28	93.2	3	28.9	93.5	4	29.1	93.1
10/18/2011	11:10	12:00	2	29.1	88.1	10	25.6	91.2	3	34.2	89.8
11/8/2011	10:20	11:10	6	27.6	87.5	7	23	89.8	1	22.3	89.6
12/14/2011	1:50	2:50	9	20.2	88.7	3	17.8	89.8	8	17.1	90.2
1/31/2012	12:00	1:00	3	18.4	87.5	9	15.8	90.5	7	14.6	90.8
3/8/2012	12:05	1:05	1	25.5	91.8	4	24.6	90.7	10	24.1	91.7
4/12/2012	12:00	1:15	2	23.8	93.7	7	23.7	89.2	1	23	87.6
5/17/2012	9:55	11:00	2	31.8	86.9	7	29.6	88	9	29	89
6/8/2012	9:20	10:20	7	28.5	89.3	10	27.7	90.1	1	27.4	90.3
7/16/2012	10:45	11:40	1	39	89.9	4	37.1	88.4	3	36.2	88.8
8/13/2012	10:55	11:55	10	34.3	88.3	6	32	89.4	7	31.1	87.3
9/13/2012	11:35	12:35	5	30.4	90.2	10	29.4	90.2	6	29	91
10/14/2012	10:30	11:30	6	26.7	91	1	25.4	91	4	24.4	93
11/19/2012	10:10	11:10	1	14.7	87.8	10	13	91.7	9	12.5	92.5
12/6/2012	2:05	3:10	6	23.6	89.2	5	22.3	91.5	7	21.4	85.2
1/8/2013	10:35	11:40	6	13.3	89.8	5	11.4	91.4	9	10.8	92.5
2/5/2013	11:00	12:05	3	17.8	86.9	7	15	85.5	9	14.1	91.2
3/14/2013	11:28	12:35	10	16.7	88.8	4	13.7	91.2	7	12.1	84.5
4/9/2013	11:05	12:05	9	30.3	88.9	10	28.3	90.2	4	27.4	88.1
5/14/2013	10:50	11:50	4	27.5	89.9	1	25.9	88.7	5	25.1	87.6
7/17/2013	10:25	11:20	4	34.6	92.3	9	33.6	91.5	10	33.1	92.4
8/5/2013	11:00	12:00	6	36.2	89.9	7	35.9	87	1	35.7	88.7
9/10/2013	10:35	11:35	9	36.4	89.3	3	33.1	86.6	5	31.9	90.6

PN = Probe Number

Table D. 15. 5-N-EB monthly RH survey data

Span 5 North – East Bottom											
Date	Time In	Time Out	Depth: 1"			Depth: 2"			Depth: 3"		
			PN	°C	RH%	PN	°C	RH%	PN	°C	RH%
2/15/2011	11:30	12:25	7	16	87.1	8	14.4	92.3	10	13.7	97
4/7/2011	10:35	11:30	5	19.1	91.5	9	18.2	95	4	17.8	95.7
5/5/2011	10:50	11:40	2	18	93.2	6	17.6	93.3	3	17.3	96.4
6/3/2011	10:40	11:25	6	32.8	88.3	7	32.4	92.4	10	32.2	93.7
7/7/2011	8:25	9:25	10	30.1	92.5	3	30.3	94.3	7	30.1	93.4
8/10/2011	8:35	9:30	5	27.1	93.2	1	27	93.6	7	26.9	95
9/15/2011	10:30	11:20	10	26.1	94.2	9	26.9	94	7	27.1	93.4
10/18/2011	11:00	11:50	4	24.9	87.7	6	24	91.6	5	23.4	89
11/8/2011	10:20	11:10	10	21.7	88.1	4	20.9	90.7	5	20.5	90.1
12/14/2011	9:00	10:00	10	15.5	87.9	9	16	90.5	5	15.2	90.4
1/31/2012	11:00	11:50	10	14.4	85.3	2	12.5	89.1	1	11.5	91.7
3/8/2012	9:50	10:50	9	21	88.8	10	20	92	6	19.6	92.5
4/12/2012	11:00	12:00	2	16.4	91.5	7	16.9	93.1	1	17	93.8
5/17/2012	1:30	2:35	2	29.1	87.8	7	28.4	90.7	6	28.1	91.2
6/8/2012	1:40	2:40	2	29	88.2	5	28.3	93.1	4	27.9	91.2
7/16/2012	3:25	4:20	4	34.3	90.2	1	34	92.2	3	33.9	90.5
8/13/2012	2:20	3:20	4	30.5	90.9	5	29.9	92.3	1	29.7	91.5
9/13/2012	2:20	3:15	9	27.1	91.7	2	26.7	91.8	7	26.4	91.3
10/14/2012	12:30	2:00	6	26.1	91.6	1	25.6	93.4	4	24.4	93
11/19/2012	12:20	1:30	1	15.4	87.6	10	14	93	9	13.4	92.4
12/6/2012			UT 2.6	22.4	89.4	UT 2.1	22.3	92.2	UT 2.5	20.8	90.9
1/8/2013	12:50	1:50	6	13.6	88.5	1	12.3	91.9	5	11.3	92
2/5/2013	12:10	1:10	9	15.8	86.8	3	13.9	91.7	7	12.9	88.4
3/14/2013	2:45	3:40	1	14	88.8	9	13.1	92.4	2	12.6	88.6
4/9/2013	1:10	2:20	1	26.9	88.1	6	25.8	89.7	5	25.1	89.6
5/14/2013	11:50	1:20	1	23.9	88.7	4	22.9	91	5	22.2	90.5
7/17/2013	11:25	12:10	10	30.9	92.2	9	30.4	92.2	4	30.1	92.6
8/5/2013	12:00	1:20	7	30.9	88.8	6	31.2	89.9	1	31.3	92.1
9/10/2013	12:40	1:50	3	31.7	88.5	5	31.4	90.1	9	31.2	92

PN = Probe Number

UT = University of Texas Probe

Table D. 16. 5-N-ET monthly RH survey data

Span 5 North – East Top											
Date	Time In	Time Out	Depth: 1"			Depth: 2"			Depth: 3"		
			PN	°C	RH%	PN	°C	RH%	PN	°C	RH%
2/15/2011	12:40	1:35	5	25	97.7	2	25.4	95	4	24	89.6
4/7/2011	10:35	11:35	6	25.9	95.8	1	25.8	92.9	2	24.1	88
5/5/2011	10:50	11:45	8	28.1	97.8	8	27.9	95.9	7	27.3	91.2
6/3/2011	11:30	12:30	8	43.9	95.8	3	45.4	91.7	2	44.9	84.8
7/7/2011	9:30	10:30	9	37.1	93.5	2	38.4	92.1	1	37.4	86.7
8/10/2011	9:40	10:30	7	34.7	93.3	10	34.5	91.7	5	33.5	90.4
9/15/2011	10:30	11:20	6	29.4		6	29.8	93.7	4	29.7	92.7
10/18/2011	12:00	12:50	3	33.1	91	9	32.5	92	10	32.8	89
11/8/2011	11:20	12:30	2	28	92.7	1	27.9	91.7	7	27.7	83.2
12/14/2011	1:50	2:50	6	22.2	89.4	7	21	91.1	10	21.3	81.6
1/31/2012	11:00	12:00	5	17.2	90.2	7	16.4	84.2	5	17.5	89.7
3/8/2012	12:05	1:05	5	26.5	92.7	9	26.5	88.4	7	26.3	86.1
4/12/2012	12:00	1:15	5	26.5	94.7	4	28.6	88.4	9	29.1	79.8
5/17/2012	8:50	9:50	9	31.8	89.9	7	32.1	85.6	2	31.8	78.8
6/8/2012	8:05	9:20	7	27.3	89.4	10	28.2	91.4	1	28.1	87.7
7/16/2012	9:20	10:35	3	38.6	92	4	39.3	88.2	1	39	84.1
8/13/2012	9:40	10:55	7	32.6	87.8	10	32.9	89.6	6	32.6	85.8
9/13/2012	10:35	11:35	6	29.8	92.9	10	30.3	89.8	5	30	84.6
10/14/2012	9:25	10:25	4	25.3	92.2	1	25.9	91.2	6	25.4	93.3
11/19/2012	9:10	10:10	9	15.1	91.5	10	14.6	90.7	1	14.1	88.7
12/6/2012	2:00	3:05	4	25.1	92.5	10	24.8	89	2	24.8	88.1
1/8/2013	9:30	10:35	9	13.6	92.1	5	13.4	91.3	6	12.5	92.6
2/5/2013	9:55	10:55	9	18.5	91.5	3	18.7	85.2	7	16.9	79.9
3/14/2013	10:15	11:20	7	15.5	82.6	4	16.8	88.6	10	15.9	93.6
4/9/2013	10:00	11:00	4	29.8	89.4	10	30.5	87.8	9	29.6	85
5/14/2013	9:50	10:50	5	27.7	89.9	1	29	90.5	4	29	80.2
7/17/2013	9:35	10:25	10	34.9	94.7	4	35.8	91.1	9	36.3	85.4
8/5/2013	10:00	11:00	1	37.7	90.7	6	37.6	83.7	7	36.9	82.6
9/10/2013	9:35	10:35	5	35.3	93.1	9	36.2	90.4	3	35.7	85

PN = Probe Number

Table D. 17. Average RH data for all readings

Date	Months	Average RH%															
		West Bottom				West Top				East Bottom				East Top			
		4 – S	4 – N	5 – S	5 – N	4 – S	4 – N	5 – S	5 – N	4 – S	4 – N	5 – S	5 – N	4 – S	4 – N	5 – S	5 – N
2/15/2011	3.0	86.4	87.3	90.5	73.0	87.7	86.9	91.8	89.1	83.2	83.6	93.2	92.1	95.4	90.1	92.9	94.1
4/7/2011	4.6	88.6	88.1	95.4	75.2	89.4	91.4	93.4	92.2	85.6	85.3	95.5	94.1	93.9	92.0	93.6	92.2
5/5/2011	5.6	89.7	84.1	96.1	69.5	88.6	90.4	92.9	92.1	80.8	81.6	96.3	94.3	92.2	91.7	95.3	95.0
6/3/2011	6.5	83.0	85.3	93.6	74.9	89.4	87.7	93.9	92.9	88.6	83.9	93.6	91.5	92.3	89.5	93.3	90.8
7/7/2011	7.6	91.2	85.3	94.6	73.9	89.6	88.0	92.3	91.6	84.0	85.2	94.6	93.4	89.2	89.1	94.3	90.8
8/10/2011	8.7	89.4	85.4	93.0	73.2	88.4	86.3	92.1	91.0	88.2	84.8	93.5	93.9	89.5	87.7	94.2	91.8
9/15/2011	9.9	92.1	83.0	94.5	71.7	91.8	87.8	94.4	93.3	91.8	82.3	94.4	93.9	93.3	89.6	95.7	93.2
10/18/2011	11.0	85.9	78.5	91.5	64.9	82.4	84.4	90.6	89.7	79.5	76.5	91.5	89.4	84.8	87.6	90.5	90.7
11/8/2011	11.7	87.5	77.9	90.8	65.6	81.4	81.9	91.6	89.0	79.9	77.4	92.0	89.6	84.4	85.8	93.0	89.2
12/14/2011	12.9	82.5	73.0	88.3	63.8	81.5	84.7	89.5	89.6	73.0	74.2	89.4	89.6	84.1	86.2	89.4	87.4
1/31/2012	14.5	82.7	77.9	86.9	74.3	81.4	85.5	89.1	89.6	76.5	73.6	86.9	88.7	84.6	83.3	90.9	88.0
3/8/2012	15.7	86.5	81.2	90.5	79.5	87.0	88.4	90.7	91.4	81.9	78.6	91.4	91.1	86.8	87.8	92.8	89.1
4/12/2012	16.8	89.4	76.7	93.9	73.2	87.3	87.6	92.1	90.2	85.1	75.9	93.9	92.8	85.0	89.5	92.2	87.6
5/17/2012	18.0	85.8	83.4	92.2	73.8	82.8	87.1	90.0	88.0	79.4	79.2	92.3	89.9	85.1	88.3	89.2	84.8
6/8/2012	18.7	87.2	80.5	92.9	78.2	83.4	87.2	90.2	89.9	81.4	78.7	93.2	90.8	83.9	90.9	92.0	89.5
7/16/2012	20.0	86.4	83.0	92.1	74.5	80.9	87.9	90.1	89.0	85.7	80.8	92.9	91.0	87.0	89.2	90.8	88.1
8/13/2012	20.9	88.9	82.1	92.2	79.0	80.8	86.9	89.2	88.3	81.0	79.1	92.8	91.6	85.0	90.0	91.6	87.7
9/13/2012	21.9	87.8	83.3	93.1	83.0	80.4	85.0	90.2	90.5	82.9	80.7	92.6	91.6	83.7	84.5	90.7	89.1
10/14/2012	22.9	87.8	84.1	91.8	78.9	83.4	87.7	89.5	91.7	88.5	84.3	92.8	92.7	84.6	87.7	88.3	92.2
11/19/2012	24.1	87.6	81.2	89.6	78.5	79.9	83.7	88.8	90.7	83.5	84.5	92.8	91.0	84.6	86.0	90.9	90.3
12/6/2012	24.7	84.6	80.0	90.8	69.8	79.5	85.8	90.4	88.6	78.1	78.6	89.9	90.8	82.6	85.2	91.4	89.9
1/8/2013	25.7	85.4	82.2	88.5	77.1	81.6	83.9	90.0	91.2	81.6	83.7	90.9	90.8	83.3	82.1	92.4	92.0
2/5/2013	26.7	85.4	81.2	89.3	80.7	83.9	81.4	90.0	87.9	80.6	79.8	90.3	89.0	83.5	86.4	92.4	85.5
3/14/2013	27.9	85.1	81.3	91.0	81.8	80.1	84.1	90.4	88.2	78.7	74.6	92.7	89.9	86.5	88.6	91.4	88.3
4/9/2013	28.7	84.0	77.9	91.4	68.5	78.2	84.4	88.9	89.1	77.6	81.2	92.3	89.1	83.7	85.4	87.3	87.4
5/14/2013	29.9	88.2	84.0	90.6	78.0	82.5	89.5	90.6	88.7	87.2	79.0	92.5	90.1	88.1	89.3	88.8	86.9
7/17/2013	32.0	90.1	85.5	91.7	81.2	84.7	85.3	90.9	92.1	87.3	84.3	91.3	92.3	88.4	87.9	92.5	90.4
8/5/2013	32.6	91.5	83.7	91.9	82.3	84.0	88.1	91.5	88.5	85.8	83.1	94.1	90.3	83.9	84.4	92.2	85.7
9/10/2013	33.8	89.4	86.1	91.8	82.3	84.1	89.5	88.8	88.8	84.3	83.2	90.1	90.2	84.7	86.6	89.6	89.5

D-18

Table D. 18. 3-inch RH data for all readings

Date	Months	3 in. Depth RH%															
		West Bottom				West Top				East Bottom				East Top			
		4 – S	4 – N	5 – S	5 – N	4 – S	4 – N	5 – S	5 – N	4 – S	4 – N	5 – S	5 – N	4 – S	4 – N	5 – S	5 – N
2/15/2011	3.0	86.9	85.7	92.3	68.5	87.3	89.2	94.9	90.1	84.7	83.0	93.8	97.0	94.3	91.0	94.9	89.6
4/7/2011	4.6	88.3	86.9	96.7	75.7	87.8	91.9	95.9	90.8	84.0	85.2	97.5	95.7	90.2	93.4	93.6	88.0
5/5/2011	5.6	89.6	86.0	97.4	70.6	84.4	89.9	93.2	88.7	82.0	80.7	97.3	96.4	88.1	89.4	96.8	91.2
6/3/2011	6.5	82.4	87.1	94.8	76.3	85.3	90.0	92.1	91.6	88.7	85.1	95.2	93.7	90.4	89.9	90.9	84.8
7/7/2011	7.6	90.0	85.8	94.6	75.6	87.5	92.1	91.5	91.7	87.9	84.7	94.9	93.4	88.2	91.4	94.8	86.7
8/10/2011	8.7	90.1	86.6	93.7	74.8	85.7	92.4	92.8	91.6	89.2	83.2	93.9	95.0	91.1	93.0	93.1	90.4
9/15/2011	9.9	90.8	84.9	94.8	73.7	92.9	89.3	92.8	93.1	89.6	82.4	94.9	93.4	93.1	91.8	95.9	92.7
10/18/2011	11.0	83.6	78.3	92.7	66.8	88.5	90.2	92.8	89.8	80.8	76.3	90.4	89.0	86.8	89.7	85.7	89.0
11/8/2011	11.7	84.8	77.1	90.6	68.2	84.6	86.9	89.9	89.6	80.6	77.7	92.5	90.1	87.3	89.6	93.2	83.2
12/14/2011	12.9	83.4	74.8	89.0	65.4	86.4	89.4	92.2	90.2	74.8	74.2	90.7	90.4	85.5	90.4	88.6	81.6
1/31/2012	14.5	82.6	84.5	86.2	66.1	84.8	89.0	89.9	90.8	78.4	73.8	91.4	91.7	85.6	89.0	92.1	89.7
3/8/2012	15.7	85.8	83.3	91.4	74.5	87.7	92.2	89.6	91.7	82.3	78.0	92.9	92.5	89.3	90.5	92.2	86.1
4/12/2012	16.8	92.5	79.6	93.9	66.4	88.0	93.1	89.4	87.6	87.6	75.3	94.7	93.8	84.8	89.9	89.5	79.8
5/17/2012	18.0	85.6	83.2	92.7	72.7	89.0	92.4	88.3	89.0	80.6	80.3	93.4	91.2	88.0	89.3	85.9	78.8
6/8/2012	18.7	87.5	83.1	94.2	73.9	89.2	93.1	89.7	90.3	81.8	80.9	93.3	91.2	89.3	91.0	90.4	87.7
7/16/2012	20.0	87.3	84.0	93.5	75.8	85.4	89.5	88.8	88.8	84.0	82.7	94.0	90.5	89.9	87.7	89.3	84.1
8/13/2012	20.9	89.0	83.2	93.6	80.8	86.7	90.4	87.2	87.3	79.8	81.9	94.0	91.5	89.6	90.0	87.2	85.8
9/13/2012	21.9	87.2	83.1	93.8	87.9	83.4	89.4	89.2	91.0	84.6	82.1	92.5	91.3	86.4	89.6	87.0	84.6
10/14/2012	22.9	89.3	83.9	90.7	81.2	89.9	90.1	90.8	93.0	88.5	88.1	93.9	93.0	86.7	90.1	85.4	93.3
11/19/2012	24.1	87.7	80.9	89.2	78.3	85.8	88.0	89.7	92.5	83.8	80.9	94.9	92.4	91.5	89.3	92.0	88.7
12/6/2012	24.7	88.0	84.2	92.1	70.7	87.2	88.0	91.1	85.2	78.3	79.5	93.7	90.9	88.1	89.1	90.0	88.1
1/8/2013	25.7	85.0	81.3	88.6	77.3	92.1	92.7	90.6	92.5	77.8	83.7	92.6	92.0	90.0	87.9	91.9	92.6
2/5/2013	26.7	87.4	80.0	89.8	74.3	88.2	92.3	91.3	91.2	80.6	78.8	93.0	88.4	88.5	86.8	92.5	79.9
3/14/2013	27.9	85.1	81.4	90.5	86.3	87.0	93.1	89.3	84.5	80.4	72.2	95.0	88.6	86.7	90.4	91.3	93.6
4/9/2013	28.7	84.6	80.4	91.4	72.7	83.3	92.3	88.5	88.1	79.3	82.6	92.8	89.6	84.5	85.9	84.8	85.0
5/14/2013	29.9	89.0	82.9	91.5	80.4	84.4	91.7	89.4	87.6	89.1	79.4	94.4	90.5	89.1	87.4	84.7	80.2
7/17/2013	32.0	91.2	86.5	91.3	79.5	81.6	91.1	89.8	92.4	87.1	84.4	92.8	92.6	88.8	89.0	91.6	85.4
8/5/2013	32.6	89.0	85.1	92.8	86.7	84.3	91.0	88.7	88.7	83.4	84.6	93.7	92.1	91.3	85.6	89.8	82.6
9/10/2013	33.8	89.0	87.9	92.4	86.3	86.5	92.2	87.3	90.6	87.3	82.8	92.0	92.0	88.6	84.4	87.0	85.0

D-19

Appendix E

Concrete Expansion Survey Data

This appendix contains all of the DEMEC gauge readings that were taken from December 2005 to September 2013 and the results that were obtained from converting the gauge readings into a change in strain over time; this procedure is described in section 5.4.

Tables E. 1 to E.4 contain the DEMEC gauge readings that were taken each month from November 2010 to September 2013 and an average temperature for that day. This temperature is the average temperature from all of the 3-inch humidity measurement depths on the given survey date.

Tables E. 5 through E. 8 show the calculated changes in concrete strain between all of the survey dates and the first one. The measured concrete temperature was used in this process to normalize the concrete strains to a temperature of 73 °F. This was done in order to minimize the temperature related strain, and therefore, more accurately show the ASR-related expansion.

There are also two tables in this appendix, Tables E. 9 and E. 10, which show the DEMEC gauge data and change in strain, respectively, from 2005 to 2011 for the 10 expansion measurement locations that were installed in 2005.

Table E. 1. Span 4 South gauge readings

Span 4 South Arch (Gauge Readings)																
Date	Temp.	Ref. Bar	West							East						
			AB	SH	SP	BL	BH	TL	TH	AB	SH	SP	BL	BH	TL	TH
11/17/2010	60.5	837	CNM		1596	-2423		877		1790	CNM	DNE	-2271	1250	270	300.1
2/2/2011	63.9	849		-2262	1642	-2407	-2115	876	2676	1818.5			-2280	1254	238	267.5
4/7/2011	72.1	852		-2301.5	1673	-2442.5	-2137	887.5	2676	1843			-2303	1278	242	304
5/5/2011	72.9	859.25		-2326	1680		-2133		2683	1857			-2300	1272	254	313
6/3/2011	100.8	857		-2355	1727.5	-2512	-2182.5	935.5	2678	1894			-2362	1327	294	346
7/7/2011	93.1	857		-2372	1742	-2515	-2184	936	2682	1889			-2364	1330	276	341
8/10/2011	86.8	858		-2375.5	1729	-2480.5	-2170	926.5	2681.5	1871			-2349	1318	238	325
9/15/2011	82.6	850.75		-2348.5	1721	-2489	-2162	918	2685.5	1869.5			-2354.5	1319.5	223	315.5
10/18/2011	80.8	853		-2277.5	1690	-2463	-2134	891.5	2681.5	1867			-2319	1288	228	323
11/8/2011	74.1	850		-2305	1700	-2455	-2140	891	2681	1871			-2308.5	1283	227	308.5
12/14/2011	63.0	849		-2290	1667	-2428	-2120	864.5	2681.5	1838.5			-2278	1260	190	283
1/31/2012	58.6	846		-2232.5	1643	-2408	-2104.5	855	2682	1825			-2264	1239	173	280
3/8/2012	74.4	848		-2293.5	1682	-2444.5	-2135	902.5	2682	1874			-2300	1276	210	307.5
4/12/2012	71.7	846		-2238	1653.5	-2438.5	-2122	876	2680	1862			-2293	1272	210	300.5
5/17/2012	85.6	844.5		-2300	1694.5	-2458	-2148	921.5	2682	1890			-2320.5	1295.5	235	335
6/8/2012	82.5	845		-2309	1702	-2470	-2145	917	2682	1873			-2330	1302	213	308
7/16/2012	97	795		-2257	1693	-2412	-2094	907	2690	1865			-2295	1260	219	298
8/13/2012	88.8	787		-2243	1650	-2399	-2075	856.5	2679	1822.5			-2265	1242.5	172.5	263.5
9/13/2012	83.3	784		-2220	1649	-2384.5	-2054	848.5	2664	1807			-2254	1231.5	142	241.5
10/14/2012	78.8	781.25		-2215	1636.5	-2383.5	-2052	834	2658	1797			-2251.5	1222.5	138	233
11/19/2012	56.9	774		-2141	1584.5	-2322	-2008	790	2610	1760			-2194	1177	96	184
12/6/2012	71.4	780		-2192	1622	-2347	-2046	809	2630	1794			-2223	1194	130	222
1/8/2013	53.8	773		-2146	1584	-2318	-2022	781	2598	1754			-2185	1171	72	180
2/5/2013	59.3	773		-2152	1596	-2307	-2015	780	2591	1779			-2181	1165	85	186
3/14/2013	56.9	749		-2113	1559	-2280	-1981	751	2588	1767			-2145	1136	92	178
4/9/2013	82.3	748		-2158	1591	-2321	-2024	807	2630	1794			-2203	1184	119	219
5/14/2013	78.9	736		-2126	1565	-2307	-2000	775	2603	1766			-2181	1163	100	194
7/17/2013	92.3	734		-2187	1616	-2343	-2040	813	2638	1804			-2211	1190	129	223
8/5/2013	93.5	735		-2180	1616	-2337	-2019	819	2641	1789			-2220	1198	123	214
9/12/2013	91.8	732		-2164	1604	-2333	-2028	800	2628	1789			-2212	1189	119	212

E-2

Table E. 2. Span 4 North gauge readings

Span 4 North Arch (Gauge Readings)																
Date	Temp.	Ref. Bar	West							East						
			AB	SH	SP	BL	BH	TL	TH	AB	SH	SP	BL	BH	TL	TH
11/17/2010	60.5	837	115	-2143	DNE	103	1170	CNM	1171	CNM	219	DNE	1462	868	-2368	2671
2/2/2011	63.9	848.5	89	-2109		101.5	1165.5		1165.5				1415	859.5	-2337	2676
4/7/2011	72.1	850	98	-2132		132	1192		1176		266		1440	886	-2337	2676
5/5/2011	72.9	858.5	102	-2142		135	1193		1181		267		1451	883.5	-2355	2686
6/3/2011	100.8	856	156	-2203.5		199	1249		1235		316		1525	940.5	-2396	2677.5
7/7/2011	93.1	856.5	154.5	-2201		202	1257		1232		321		1534.5	949	-2402	2682
8/10/2011	86.8	852.75	134	-2170		185	1237.5		1210		292		1512.5	931.5	-2378.5	2684
9/15/2011	82.6	851	140	-2175		185	1235		1217		289		1507.5	929.5	-2362	2685.5
10/18/2011	80.8	849.75	114.5	-2140		154	1212.5		1188.5		276		1461	904	-2378	2683
11/8/2011	74.1	850.5	118.5	-2138		143	1200		1190		263.5		1439	895	-2354	2684
12/14/2011	63.0	847	81	-2100		111	1175		1153.5		240		1407	865	-2350	2682
1/31/2012	58.6	845	75.5	-2090		99.5	1163		1152.5		230.5		1438.5	853	-2323	2683.5
3/8/2012	74.4	850	114	-2137		136	1194.5		1185.5		274.5		1478	881	-2368	2687
4/12/2012	71.7	845	97.5	-2123.5		129	1190		1172		250		1469.5	876	-2345	2680
5/17/2012	85.6	846	127	-2164		164.5	1222.5		1203		290.5		1536.5	906.5	-2386	2679.5
6/8/2012	82.5	845.5	130	-2166		166	1223		1202		273		1557	911	-2373	2680
7/16/2012	97	792	79	-2116		110	1184		1170		248		1532	846	-2340	2684
8/13/2012	88.8	786	62.5	-2093.5		103.5	1163.5		1151		225		1493	848	-2332	2691
9/13/2012	83.3	786	59.5	-2083		88	1142.5		1144.5		205		1480	840	-2285.5	2691
10/14/2012	78.8	780	51.5	-2070		93.5	1148		1127		196		1480	842	-2268	2690
11/19/2012	56.9	775	5	-2029		33	1098		1084		149		1410	790	-2230	2671
12/6/2012	71.4	781	35	-2060		60	1124		1104		177		1447	808	-2274	2690
1/8/2013	53.8	781	2	-2012		22	1093		1075		142		1379	782	-2255	2674
2/5/2013	59.3	783	19	-2022		27	1099		1093		166		1349	782	-2272	2685
3/14/2013	56.9	755	-2482	-1986		1	1074		1049		122		1305	750	-2230	2669
4/9/2013	82.3	748.5	26	-2040		39	1104		1102		186		1411	788	-2290	2691
5/14/2013	78.9	732	-2493	-2018		15	1084		1076		144		1377	766	-2252	2688
7/17/2013	92.3	735	26	-2062		46	1113		1106		187		1455	791	-2296	2692
8/5/2013	93.5	732	33	-2050		54	1128		1111		185		1464	810	-2262	2692
9/12/2013	91.8	732	32	-2042		48	1116		1106		171		1460	798	-2253	2692

CS

Table E. 3. Span 5 South gauge readings

Span 5 South Arch (Gauge Readings)																
Date	Temp.	Ref. Bar	West							East						
			AB	SH	SP	BL	BH	TL	TH	AB	SH	SP	BL	BH	TL	TH
11/17/2010	60.5	837	1447	DNE	-2322	372	-2024	-2385	430	1215	850	1270	1052	1347	2440	502
2/2/2011	63.9	849	1453		-2275	356.5	-2042.5	-2388.5	412.5	1190.5	862	1288	1070	1373.5	2439.5	475
4/7/2011	72.1	848.5	1472		-2310	393	-2090	-2403	421	1218	883	1304.5	1093.5	1400	2472	502.5
5/5/2011	72.9	861.25	1478		-2318	413.5	-2102	-2422	426	1237.5	894	1303.5	1090.5	1400	2492.5	527.5
6/3/2011	100.8	858	1532		-2383	471	-2161	-2482.5	472	1283	939	1340	1135	1441	2532	575
7/7/2011	93.1	856	1525		-2400	485	-2178	-2475	472	1264	933	1343	1142	1454	2507	544
8/10/2011	86.8	855.75	1495		-2382	472	-2155	-2456.5	457	1242	918	1333	1126.5	1438	2491	531.5
9/15/2011	82.6	853	1500		-2389.5	472	-2168	-2469.5	465	1244	924	1340	1139.5	1444	2496	535
10/18/2011	80.8	854	1491		-2380	439	-2140	-2441	454	1248	916.5	1339	1111	1419.5	2507.5	545.5
11/8/2011	74.1	851	1480.5		-2370	433	-2145	-2426	443	1230	909	1323	1104	1414	2492	527
12/14/2011	63.0	844.75	1436		-2325	412	-2140	-2388	435	1198	877	1311	1095	1401	2470.5	492
1/31/2012	58.6	846	1431		-2310	397.5	-2148.5	-2375	450.5	1174	874.5	1316.5	1095.5	1403	2472	498.5
3/8/2012	74.4	847.5	1474.5		-2336	441	-2195.5	-2404	480	1225	908.5	1343.5	1117.5	1434	2518	524
4/12/2012	71.7	847	1456		-2297	454	-2204	-2407	482	1222	902	1322	1110.5	1422	2516	535
5/17/2012	85.6	846.5	1492		-2330	497	-2242	-2447	511.5	1249	932	1346	1139	1451.5	2539	553
6/8/2012	82.5	848	1494		-2341	510	-2252	-2458	505	1240	930	1348	1138	1455	2530	544
7/16/2012	97	792	1466		-2300	465	-2200	-2433	478	1216	885	1300	1076	1400	2510	524
8/13/2012	88.8	786	1435.5		-2287.5	460	-2190.5	-2391.5	454.5	1171.5	869	1285.5	1082	1397	2476	487
9/13/2012	83.3	784	1438		-2294.5	444.5	-2176.5	-2375.5	449	1162	865	1308.5	1060	1382.5	2467	479
10/14/2012	78.8	782	1406		-2274.5	462	-2191.5	-2359	438	1143.5	843.5	1289	1078.5	1391	2449.5	463
11/19/2012	56.9	776	1355		-2222	410	-2152	-2319	409	1100	818	1271	1038	1351	2416	422
12/6/2012	71.4	781	1388		-2268	441	-2195	-2340	439	1132	840	1288	1058	1373	2450	460
1/8/2013	53.8	780	1355		-2220	399	-2164	-2300	419	1101	822	1275	1033	1337	2425	421
2/5/2013	59.3	780	1361		-2228	402	-2179	-2304	426	1110	828	1303	1034	1345	2437	439
3/14/2013	56.9	753	1325		-2185	406	-2181	-2292	420	1091	800	1226	1022	1336	2420	423
4/9/2013	82.3	749	1386		-2221	423	-2213	-2326	450	1139	841	1265	1048	1364	2464	459
5/14/2013	78.9	739	1360		-2209	443	-2228	-2303	438	1120	825	1245	1040	1353	2435	438
7/17/2013	92.3	733	1402		-2245	480	-2250	-2333	462	1142	840	1306	1062	1374	2466	450
8/5/2013	93.5	733	1401		-2252	492	-2263	-2348	470	1144	847	1297	1073	1388	2457	454
9/12/2013	91.8	730	1393		-2252	496	-2262	-2340	460	1149	843	1264	1061	1377	2465	462

E-4

Table E. 4. Span 5 North gauge readings

Span 5 North Arch (Gauge Readings)																
Date	Temp.	Ref. Bar	West							East						
			AB	SH	SP	BL	BH	TL	TH	AB	SH	SP	BL	BH	TL	TH
11/17/2010	60.5	837	2500	171	DNE	CNM	959	0	392	387.4	60		1651	1105	557	2177
2/2/2011	63.9	849	2525.5	175			957	54.5	414.5	380	64.5	2338.5	1641	1097.5	568.5	2150
4/7/2011	72.1	851.75	2569	204			975	58	444	409.5	100	2378	1703.5	1179	623	2165.5
5/5/2011	72.9	859.75	2588	213			984.5	82	451	418.5	118	2395	1733	1182.5	634.5	2169
6/3/2011	100.8	858.5	2655	261			1053	165.5	507	470	169.5	2442.5	1803.5	1249	673	2219.5
7/7/2011	93.1	856.25	2643	251			1063	141	509	453	160	2436	1839	1269	650	2203
8/10/2011	86.8	853	2620	229			1040	108.5	496	434	152	2424	1828	1254.5	637	2192.5
9/15/2011	82.6	851	2625	230			1045.5	115	507	440	159.5	2431	1850	1260	648.5	2204
10/18/2011	80.8	850.5	2603.5	201			1006.5	103.5	491.5	435.5	145.5	2402	1831.5	1230	666	2198.5
11/8/2011	74.1	853.5	2602.5	207			1002	91	496	419	145	2405	1850	1242	646	2185
12/14/2011	63.0	847	2550	162			964.5	40	475	386	123	2385.5	1844.5	1223	642.5	2171
1/31/2012	58.6	845	2527	153.5			944	30.5	486	371.5	129	2390	1845	1234.5	643.5	2172.5
3/8/2012	74.4	849	2576	188			978.5	75	522.5	421	170	2438	1889.5	1280	691.5	2209
4/12/2012	71.7	846	2580.5	172			984.5	63	527	409.5	180	2432.5	1908	1275.5	712	2207
5/17/2012	85.6	845	2621	218.5			1022	99	555.5	433.5	204	2477.5	1954.5	1301	724.5	2241.5
6/8/2012	82.5	846.5	2635	223			1026	131	570	438	218	2481	1960	1309	729	2250
7/16/2012	97	795	2595	180			975	110	529	414	185	2450	1932	1271	704	2233
8/13/2012	88.8	787	2560	145.5			969.5	37.5	505.5	368	150	2429	1924.5	1262.5	670	2197
9/13/2012	83.3	784	2556	139.5			943.5	50	513	363	156.5	2426.5	1919	1251	657.5	2186.5
10/14/2012	78.8	776	2542.5	120.5			963	33	502	343	145.5	2422.5	1949	1269.5	647	2173.5
11/19/2012	56.9	777	2483	69			897	-2472	470	282	118	2395	1930	1228	624	2138
12/6/2012	71.4	781	2510	104			915	-2491	490	336	143	2428	1970	1262	673	2175
1/8/2013	53.8	778	2464	71			884	-2454	474	292	120	2402	1953	1241	649	2150
2/5/2013	59.3	784	2479	77			885	-2450	483	312	138	2414	1956	1250	675	2159
3/14/2013	56.9	753	2460	36			871	-2432	475	282	119	2404	1970	1248	658	2141
4/9/2013	82.3	744	2523	86			890	1	510	280	157	2451	1986	1272	688	2185
5/14/2013	78.9	734	2502	70			890	-2457	502	299	158	2441	1996	1268	676	2169
7/17/2013	92.3	733	2539	108			926	8	532	336	178	2473	2011	1303	712	2192
8/5/2013	93.5	734	2541	107			950	20	551	332	193	2476	2030	1334	726	2190
9/12/2013	91.8	731	2534	94			940	8	542	337	190	2460	2023	1305	736	2199

51

Table E. 5. Span 4 South change in strain

Span 4 South Arch $\Delta\epsilon$ (in/in / 1,000,000)														
Months	West							East						
	AB	SH	SP	BL	BH	TL	TH	AB	SH	SP	BL	BH	TL	TH
0.0	CNM		0	0		0		0	CNM	DNE	0	0	0	0
2.5		0	86	-115	0	-67	0	30			-34	-50	-166	-168
4.6		61	120	-67	5	-94	-67	42			-26	-39	-220	-117
5.6		112	114		-37		-73	59			-64	-87	-210	-116
6.5		19	80	-58	-64	-155	-276	-9			-51	-96	-267	-197
7.6		127	181	6	-5	-99	-209	29			10	-32	-272	-159
8.7		179	179	-66	-10	-90	-170	11			2	-31	-354	-170
9.9		144	206	14	16	-65	-105	59			72	26	-350	-149
11.0		-80	111	-64	-69	-145	-113	56			-38	-70	-329	-119
11.7		65	200	-34	7	-91	-58	125			-15	-30	-276	-110
12.9		97	174	-41	23	-96	24	101			-33	-24	-315	-111
14.5		-49	136	-65	12	-87	66	97			-39	-52	-330	-81
15.7		32	146	-64	-5	-49	-50	139			-38	-48	-326	-108
16.8		-122	79	-58	-22	-109	-31	126			-36	-36	-301	-106
18.0		-13	120	-86	-29	-54	-117	125			-39	-52	-312	-86
18.7		36	164	-28	-19	-49	-97	90			12	-11	-363	-153
20.0		-71	196	-154	-123	-20	-10	125			-40	-85	-283	-125
20.9		-34	140	-113	-102	-100	37	70			-54	-59	-350	-153
21.9		-60	184	-112	-122	-78	37	68			-42	-47	-401	-177
22.9		-36	184	-75	-88	-85	58	76			-10	-36	-374	-164
24.1		-100	192	-99	-55	-52	78	132			-20	-7	-334	-147
24.7		-55	193	-138	-52	-111	22	122			-47	-73	-344	-144
25.7		-59	215	-87	15	-56	64	137			-25	-2	-387	-135
26.7		-78	215	-161	-45	-98	3	180			-76	-60	-383	-154
27.9		-110	190	-154	-61	-97	88	235			-98	-59	-266	-85
28.7		-137	120	-194	-95	-89	50	149			-84	-77	-352	-126
29.9		-178	99	-177	-111	-130	25	121			-92	-83	-351	-144
32.0		-68	177	-147	-68	-94	52	157			-82	-82	-344	-137
32.6		-102	165	-178	-147	-86	50	97			-64	-68	-375	-178
33.9		-132	148	-170	-97	-126	30	119			-69	-75	-366	-163

Table E. 6. Span 4 North change in strain

Span 4 North Arch $\Delta\epsilon$ (in/in / 1,000,000)														
Months	West							East						
	AB	SH	SP	BL	BH	TL	TH	AB	SH	SP	BL	BH	TL	TH
0.0	0	0	DNE	0	0	CNM	0	CNM	0	DNE	0	0	0	0
2.5	-145	-171		-66	-76		-79				-213	-89	-161	-45
4.6	-178	-158		-29	-52		-107		29		-194	-65	-223	-107
5.6	-198	-159		-52	-81		-123		0		-191	-105	-198	-107
6.5	-209	-146		-31	-86		-135		-28		-138	-107	-251	-321
7.6	-162	-102		31	-8		-92		40		-55	-27	-180	-254
8.7	-172	-146		31	-15		-108		2		-70	-28	-200	-192
9.9	-118	-96		66	11		-50		27		-52	0	-219	-152
11.0	-184	-192		-18	-45		-126		2		-186	-66	-150	-144
11.7	-127	-155		-9	-41		-77		6		-213	-51	-184	-96
12.9	-160	-189		-24	-33		-106		18		-227	-59	-108	-14
14.5	-141	-184		-24	-36		-73		24		-89	-62	-159	27
15.7	-142	-158		-32	-60		-92		41		-87	-97	-139	-87
16.8	-160	-167		-20	-39		-101		-3		-79	-78	-178	-75
18.0	-165	-136		-5	-34		-100		28		37	-79	-145	-176
18.7	-132	-106		23	-9		-80		-6		127	-41	-164	-151
20.0	-225	-195		-85	-63		-111		-14		118	-179	-199	-66
20.9	-202	-192		-30	-53		-96		-12		69	-96	-148	33
21.9	-173	-188		-42	-82		-79		-39		65	-84	-260	71
22.9	-148	-179		26	-14		-85		-17		115	-27	-266	119
24.1	-130	-143		-1	-7		-56		-1		57	-27	-221	226
24.7	-153	-163		-34	-43		-111		-30		57	-89	-199	167
25.7	-138	-196		-34	-21		-83		-21		-41	-51	-138	237
26.7	-128	-208		-63	-47		-69		12		-183	-95	-128	228
27.9	-140	-218		-40	-20		-104		-24		-218	-91	-156	284
28.7	-153	-198		-72	-79		-88		28		-30	-124	-118	199
29.9	-183	-193		-73	-66		-96		-31		-63	-118	-163	267
32.0	-179	-153		-75	-75		-101		5		86	-140	-124	177
32.6	-155	-191		-48	-26		-84		0		117	-77	-233	178
33.9	-146	-205		-56	-53		-88		-33		116	-104	-250	190

Table E. 7. Span 5 South change in strain

Span 5 South Arch $\Delta\epsilon$ (in/in / 1,000,000)														
Months	West							East						
	AB	SH	SP	BL	BH	TL	TH	AB	SH	SP	BL	BH	TL	TH
0.0	0	DNE	0	0	0	0	0	0	0	0	0	0	0	0
2.5	-43		-215	-113	-3	-51	-119	-142	-24	-4	-4	23	-64	-150
4.6	-37		-157	-50	96	-60	-147	-108	-11	-6	16	53	-14	-116
5.6	-64		-177	-30	88	-45	-177	-92	-22	-56	-40	7	5	-82
6.5	-73		-151	-28	95	-33	-212	-128	-60	-122	-80	-44	-51	-112
7.6	-36		-36	78	210	3	-152	-129	-19	-52	3	58	-71	-152
8.7	-88		-49	80	180	-12	-156	-156	-24	-40	-3	51	-79	-148
9.9	-34		13	118	260	68	-92	-112	34	21	77	108	-25	-99
11.0	-54		-9	20	179	-15	-119	-90	19	27	-5	38	22	-56
11.7	-32		15	57	251	-7	-98	-91	51	31	28	77	28	-59
12.9	-78		-33	87	333	-33	-26	-97	45	90	97	132	56	-75
14.5	-68		-55	66	387	-49	50	-149	63	134	125	165	87	-28
15.7	-42		-85	93	424	-69	31	-98	59	107	81	151	122	-60
16.8	-81		-191	155	472	-39	58	-88	58	58	79	132	136	-3
18.0	-60		-179	199	500	-5	58	-95	60	41	76	133	115	-40
18.7	-36		-127	258	549	48	54	-108	70	64	90	161	103	-53
20.0	-47		-179	193	461	47	47	-105	5	-11	-30	63	118	-37
20.9	-69		-143	253	507	-11	48	-172	30	18	65	130	85	-80
21.9	-16		-76	248	506	-18	74	-158	61	138	39	128	100	-61
22.9	-82		-103	342	593	-33	77	-181	30	112	136	193	81	-75
24.1	-75		-101	345	636	9	154	-150	119	226	177	235	145	-36
24.7	-85		-69	329	659	-40	134	-163	73	164	125	189	138	-30
25.7	-67		-99	318	684	-44	195	-138	140	247	169	199	182	-31
26.7	-86		-111	290	694	-69	180	-147	122	299	134	186	183	-11
27.9	-98		-146	407	805	-4	264	-104	135	154	200	261	232	41
28.7	-64		-194	298	745	-58	198	-113	104	117	120	188	211	-6
29.9	-92		-176	419	849	-76	215	-118	108	108	150	209	173	-18
32.0	-30		-134	465	847	-53	219	-121	83	232	148	203	200	-53
32.6	-42		-119	495	880	-13	236	-123	97	194	175	240	162	-48
33.9	-46		-98	530	899	-17	226	-85	106	109	158	226	209	-1

Table E. 8. Span 5 North change in strain

Span 5 North Arch $\Delta\epsilon$ (in/in / 1,000,000)														
Months	West							East						
	AB	SH	SP	BL	BH	TL	TH	AB	SH	SP	BL	BH	TL	TH
0.0	0	0	DNE	CNM	0	0	0	0	0		0	0	0	0
2.5	20	-50			-69	114	10	-87	-48	0	-95	-87	-25	-150
4.6	95	-22			-77	59	40	-57	1	62	41	111	85	-166
5.6	125	-24			-77	106	31	-59	28	86	106	91	91	-185
6.5	152	-59			-46	186	22	-83	4	49	143	116	25	-212
7.6	174	-30			48	167	90	-76	35	89	319	242	12	-205
8.7	154	-47			27	116	102	-84	63	105	338	249	24	-184
9.9	205	-8			81	173	173	-29	123	163	445	302	97	-112
11.0	150	-88			-31	150	137	-29	92	83	399	219	168	-115
11.7	184	-32			-9	146	188	-46	127	130	496	295	140	-122
12.9	112	-79			-32	80	219	-54	154	165	576	332	227	-69
14.5	74	-70			-62	86	291	-64	210	216	615	406	267	-28
15.7	110	-81			-72	107	287	-27	220	249	636	431	300	-32
16.8	153	-104			-24	97	330	-35	281	260	724	445	394	-10
18.0	191	-47			3	120	329	-51	265	312	781	434	342	8
18.7	253	-15			33	240	392	-20	327	340	816	476	373	52
20.0	189	-89			-66	238	325	-32	287	306	791	419	358	63
20.9	159	-117			-1	86	332	-98	256	320	850	475	331	30
21.9	194	-89			-37	175	404	-66	325	360	880	485	338	44
22.9	208	-93			83	177	426	-74	347	405	1034	602	361	59
24.1	164	-111			19	129	471	-122	407	465	1122	617	436	93
24.7	138	-111			-37	76	422	-61	374	458	1137	613	481	99
25.7	121	-86			-5	89	503	-71	432	505	1214	677	535	150
26.7	112	-124			-60	18	474	-64	432	487	1166	649	561	122
27.9	167	-140			12	77	565	-44	488	571	1329	759	623	180
28.7	224	-126			-74	153	531	-198	463	576	1233	690	573	175
29.9	212	-121			-18	66	561	-81	522	600	1321	733	590	179
32.0	242	-88			9	141	568	-51	497	613	1280	756	617	164
32.6	236	-103			75	169	618	-75	534	611	1330	845	651	146
33.9	235	-124			64	151	611	-38	546	581	1329	772	704	197

Table E. 9. Strain gauge readings for DEMEC studs installed in 2005

Gauge Readings												
Date	Temp.	Ref. Bar	Span 4 South			Span 5 South						
			West			West			East			
			SP	BL	TL	SP	BL	TL	AB	SP	BL	TL
12/16/2005	59	850	1731	-2389	811	-2359	233	-2354	1179	971	747	2152
12/9/2009	66	850	1666	-2419	882	-2312	326	-2367	1179	1247	1035	2389
11/17/2010	60.5	837	1596	-2423	877	-2322	372	-2385	1215	1270	1052	2440

E-10

Table E. 10. Change in strain for locations dating back to 2005

$\Delta\epsilon$ (in/in / 1,000,000)										
Months	Span 4 South			Span 5 South						
	West			West			East			
	SP	BL	TL	SP	BL	TL	AB	SP	BL	TL
0.0	0	0	0	0	0	0	0	0	0	0
47.8	-258	49	181	-199	252	-8	-47	845	884	719
59.1	-404	142	246	-88	480	132	149	1000	1020	964